ACTIVATION OF SMALL MOLECULES BY PINCER IRIDIUM CATALYSTS

by

KATHLEEN DONOHUE FIELD

A dissertation submitted to the

Graduate School-New Brunswick

Rutgers, The State University of New Jersey

In partial fulfillment of the requirements

For the degree of

Doctor of Philosophy

Graduate Program in Chemistry and Chemical Biology

Written under the direction of

Alan S. Goldman

And approved by

_____

_____

_____

_____

New Brunswick, New Jersey

October 2014

ABSTRACT OF THE DISSERTATION

ACTIVATION OF SMALL MOLECULES BY

PINCER IRIDIUM CATALYSTS

By

KATHLEEN DONOHUE FIELD

Dissertation Director:

Alan S. Goldman

Since the initial report of pincer complexes in the late 1960's, much research has been undertaken to understand the reactivity and applicability of these complexes. This thesis aims to add to the rich knowledge of pincer complexes and the activation of small molecules to lead to interesting chemical transformations.

Advantageously, the pincer framework can be easily adapted by changing different aspects of the ligand. The synthesis, characterization and reactivity of (Me-PCP)$IrH_{n,}$ in which the para position on the backbone of the catalyst has been changed from a hydrogen to a methyl group is reported. Finally, attempts to isolate the highly reactive 3-coordinate 14-electron (Me-PCP)Ir species are also addressed.

Rather than isolation or observance of any active catalytic species proposed as a $14e^-$, agostic, solvated, or dimeric species, it has been found that the cyclometalation or C-H activation of the ^{t}butyl group attached to one of the phosphorous atoms occurs readily. Characterization of cyclometalated complexes and an interesting cyclometalated insertion product is described. Two different mechanisms are proposed and discussed in relation to previously cited pathways for the formation of each complex.

The knowledge of the activation and binding of oxygen as well as the reactivity of oxidants and isolation of reactive intermediates is limited. The synthesis and characterization of two (Me-PCP)Ir oxygen species is detailed via reaction with oxygen directly followed by a discussion of the reactivity with other oxidants.

A combined experimental and computational study was completed to determine the binding energies for the addition of a variety of ligands to the metal center of (PCP)IrHCl, (PCP)IrH_2, and the

(PCP)Ir fragment. The thermodynamics were determined directly through equilibrium reactions and compared to values derived from DFT calculations utilizing a variety of functionals with good agreement.

Finally, the activation of hydrazine and related compounds by the parent (PCP)IrH_2 complex is achieved and leads to both dehydrogenation and hydrogenation of hydrazine by pincer iridium (PCP) type catalysts to synthesize N_2, H_2 and NH_3. The reactivity of other pincer complexes for this reaction will be compared and a computationally calculated mechanism for both pathways will be discussed along with supporting experimental evidence.

Dedication

To my parents, Joan and Bill, my sister Jenny, and my fiancé Joe,

you inspire and guide me every day.

Acknowledgements

I would like to thank my advisor Professor Alan Goldman. He has allowed me to pursue challenging projects and grow as a scientist over the last six years; I have truly enjoyed working with him.

I would like to thank Professor Karsten Krogh-Jespersen for not only serving on my committee, but also for his collaboration. His expertise proved invaluable for many of my projects, but mostly for our work on the thermodynamic study of ligand binding energies.

I would like to thank Professor Kai Hultzsch for his valuable time and serving on my committee. His class provided a deep foundation in the area of organometallic chemistry for which I am ever thankful.

Dr. Carolyn Supplee is thanked for not only serving as my committee member but for also introducing me to my love of organometallic chemistry. Carolyn has not only been an excellent mentor and professor during my undergraduate years, she has also become a caring friend over the last six years.

I express gratitude to Dr. Nagarajan Murali for assistance with NMR spectroscopy and Dr. Tom Emge for his work with X-Ray crystallography.

I would like to thank all former and current members of the Goldman Research group. I would like to thank Drs. Jongwook Choi and Agnieszka Nawara-Hultzsch for their support and advice as I started my research here at Rutgers. I would like to thank Dr. Sabuj Kundu for his advice and the work he contributed towards the thermodynamic study. Tian Zhou was responsible for the computational component of my experimental work with hydrazine and I thank him for his contributions. Dr. Yury Kissin has not only been a valued advisor for the entire Goldman group, but I have had the pleasure of working with him while analyzing my kinetics data for hydrazine. I am very grateful for all of his assistance. Samreen Bano and Milos Cejkovmich are acknowledged for their dedicated time and effort in helping me with various experiments. I would like to thank Mike Haibach, Dr. Jason Hackenberg, and Dr. David Wang for all the discussions we have had over the years and I would like to thank Dr. David Laviska for his friendship and leadership during my time here at Rutgers.

I am grateful for my professors at Monmouth University whom fostered my knowledge of chemistry and inspired me to pursue my doctoral degree. I am also thankful for all the teachers who enabled my love of knowledge.

Finally, I would like to thanks all my friends and family who supported me not only during my pursuit of a doctoral degree, but throughout different periods of my life. Words cannot express my gratitude and love to my parents Joan and Bill and sister Jenny who supported me in all my endeavors. To Joe, thank you for keeping the smile on my face. This would not have been possible without each of you.

Table of Contents

Abstract		ii
Dedication		iv
Acknowledgements		v
Table of Contents		vii
List of Figures		x
List of Schemes		xii
List of Tables		xiv
Chapter 1	**Introduction**	1
1.2	Research Goals of This Thesis	6
	References	8
Chapter 2	**Synthesis and General Reactivity of (Me-PCP)Ir Complexes**	10
2.1	Introduction	11
2.2	Synthesis of (Me-PCP)IrH_n	14
2.3	Reactivity towards TBE, NBE, CO, Ethylene, Benzene, N_2, Benzophenone, and H_2O	15
2.4	Attempts to Synthesize (Me-PCP)Ir 14-Electron Species	18
2.5	Summary	19
2.6	Experimental	19
	References	40
Chapter 3	**Synthesis of Cyclometalated (PCP)Ir Complexes**	42
3.1	Introduction	43
3.2	Results and Discussion	48
	3.2.1 Formation of Cyclometalated (PCP)IrNBE Complexes	48
	3.2.2 Reaction of Cyclometalated (Me-PCP)IrNBE Complex with CO	49
	3.2.3 Reactions of Cyclometalated Complex, **3-2**, with H_2 and Ethylene	52
	3.2.4 Proposed Mechanisms for the Formation of Cyclometalated	53

Products

3.2.5 Synthesis of Cyclometalated (Me-PCP)IrCl, **3-4** 55

3.2.6 Synthesis of Cyclometalated (PCP)IrFBF$_3$, **3-5** 56

3.3 Conclusion 56

3.4 Experimental 56

References 71

Chapter 4 Initial Studies on the Reactivity of (PCP)Ir Towards Oxidants 72

4.1 Introduction 73

4.2 Results and Discussion 76

4.2.1 Isolation of the (Me-PCP)Ir Dioxygen Complexes 76

4.2.2 Reaction with DMDO, TMAO, Acetone, and H_2O_2 76

4.2.3 Cylometalation in the Presence of Oxidants 78

4.2.4 Reaction with N_2O 79

4.3 Summary 81

4.4 Experimental 82

References 86

Chapter 5 Determination of Metal-Ligand Bond Energies for (PCP)Ir Complexes 87

5.1 Introduction 88

5.2 Results and Discussion 89

5.2.1 Equilibrium Studies of (PCP)IrHCl, **5-1** 89

5.2.2 Equilibrium Studies of (PCP)IrH_2, **5-2** 96

5.2.3 Equilibrium Studies of (PCP)Ir, **5-3** 102

5.3 Conclusions 108

5.4 Experimental 109

5.4.1 General Methods 109

5.4.2 Chemical Equilibria 109

5.4.3 Exchange Equilibria 110

5.4.4 Dehydrogenation of Isopropanol 112
5.4.5 Synthesis of (PCP)IrHClL 113
5.4.6 Synthesis of (PCP)IrH_2L 114
5.4.7 Synthesis of (PCP)IrL 116
5.4.8 Computational Details 119
References 160
Chapter 6 Dual Reactivity of Pincer Iridium Complexes towards Hydrazine 162
6.1 Introduction 163
6.2 Results and Discussion 167
6.2.1 Synthesis of Hydrazine Complexes 167
6.2.2 Dehydrogenation of Hydrazine 170
6.2.3 Synthesis of Ammonia 171
6.2.4 Preliminary Catalytic Screening 171
6.2.5 Thermodynamic Studies 173
6.2.6 Reactivity of Other Pincer Catalysts 175
6.2.7 Kinetic Results 176
6.2.8 Discussion of Proposed Mechanism 180
6.2.9 Reaction with Hydrazine Sulfate, Azobenzene and Azo-*tert*-butane 184
6.3 Closing 185
6.4 Experimental 186
References 203

List of Figures

Figure 1.1	Mechanism for the Hydrogenation of Alkenes via Wilkinson's catalyst	2
Figure 1.2	General Reaction Scheme for Alkane Metathesis	4
Figure 1.3	General Structure of Pincer Complex	4
Figure 1.4	Activation of Small Molecules by Pincer Iridium complexes	6
Figure 2.1	Crystal Structure of (Me-PCP)IrHCl, **2-9**	24
Figure 3.1	Milstein Examples of C-H Activation Products	43
Figure 3.2	Inserted (PCP)Ir(acetate) Products	45
Figure 3.3	Examples of Cyclometalated Pincer Complexes	46
Figure 3.4	Proposed Mechanism for the Formation of Cyclometalated Complexes	48
Figure 3.5	Crystal Structure of **3-3**	50
Figure 3.6	2D gCOSY NMR spectrum of **3-3**	51
Figure 3.7	Expanded Region from 0.0 - 4.0 ppm of 2D gCOSY NMR Spectrum of **3-3**	51
Figure 3.8	Proposed Mechanism for the Formation of **3-1** and **3-2**	53
Figure 3.9	Proposed Pathways for the Formation of the Cyclometalated Insertion CO Product	54
Figure 3.10	Potential Mechanism for the Formation of **3-4**	55
Figure 4.1	Room Temperature Mass Spectrum of N_2O	81
Figure 4.2	General Schematic for the Detection of Ions from N_2O	85
Figure 5.1	Determination of Enthalpy for 2-methylpentane via Group Increment Theory	88
Figure 5.2	Graph of ΔG (kcal/mol) versus Temperature (K) for the Addition of L to **5-1**	92
Figure 5.3	Graph of Experimental ΔG Values versus Computational ΔG Values for the Addition of Ligands to **5-1**	96
Figure 5.4	Crystal Structure of (PCP)IrH_2Py, **5-23**	97
Figure 5.5	Graph of ΔG (kcal/mol) versus Temperature (K) for the	98

	Addition of L to **5-2**	
Figure 5.6	Graph of Experimental ΔG Values versus Computational ΔG Values for the Addition of Ligands to **5-2**	101
Figure 5.7	Experimental and Gepasi Fit Data for the Dissociation of Pyridine from **5-3**	104
Figure 5.8	Eyring Plot for the Dissociation of Pyridine	105
Figure 5.9	Graph of ΔG (kcal/mol) versus Temperature (K) for the Equilibrium Exchange between Pyridine and PEt_3	106
Figure 5.10	Graph of Experimental ΔG Values versus Computational ΔG Values for the Addition of Ligands to **5-3**	108
Figure 5.11	Crystal Structure of (PCP)IrHClPy, **5-8**	120
Figure 5.12	Crystal Structure of (PCP)Ir$NCCH_3$, **5-50**	130
Figure 5.13	Crystal Structure of (PCP)IrPMe_2Ph, **5-54**	139
Figure 5.14	Crystal Structure of (PCP)Ir$POEt_3$, **5-59**	149
Figure 6.1	Crystal structure of (PCP)Ir$H_2N_2H_4$, **6-2a**	169
Figure 6.2	Conversion of Hydrazine to Ammonia at 85 °C Catalyzed with (PCP)IrH_2 ([(PCP)IrH_2]° = 20 mM) and its Representation by a Linear Regression	178
Figure 6.3	Conversion of Hydrazine to Ammonia at 85 °C Catalyzed with (PCP)IrH_2 ([(PCP)IrH_2]° = 10 mM) and its Representation by a Linear Regression	179
Figure 6.4	Proposed Mechanism for the Catalytic Synthesis of Ammonia, Nitrogen and Hydrogen	181
Figure 6.5	Proposed Pathway for the Hydrogenation of Hydrazine to Form Ammonia, Nitrogen and Hydrogen	182
Figure 6.6	Proposed Pathway for the Dehydrogenation of Hydrazine to Form Nitrogen and Hydrogen	183

List of Schemes

Scheme 1.1	Oxidative Addition of H_2 to Vaska's Complex	1
Scheme 1.2	Oxidative Addition of Benzene to Cp_2WH_2	2
Scheme 2.1	General Schematic for a Pincer Ligand	11
Scheme 2.2	Hydrogenation of TBE or NBE and Formation of the Vinyl Hydride and NBE π Complexes	13
Scheme 2.3	C-H activation of Benzene by (PCP)Ir	13
Scheme 2.4	Proposed Oligomerization for (PCP)Ir Catalysts	14
Scheme 2.5	Synthesis of (Me-PCP)IrH_2	15
Scheme 2.6	Formation of the (Me-PCP)Ir Vinyl Hydride and NBE π Complexes	16
Scheme 2.7	Synthesis of Four Coordinate (Me-PCP)Ir-CO	16
Scheme 2.8	Reaction of (Me-PCP)IrH_2 and Ethylene	17
Scheme 2.9	Reaction of (Me-PCP)IrH_2 and Benzene	17
Scheme 2.10	Reaction of (Me-PCP)IrH_2 and Benzephenone	17
Scheme 2.11	Reaction of (Me-PCP)IrH_2 and Nitrogen	18
Scheme 2.12	Addition of H_2O to (PCP)Ir	18
Scheme 3.1	C-C and C-H Activation of Pincer Ligands	43
Scheme 3.2	Formation of Proposed Intermediates in the C-H and C-C Bond Activation Pathways	44
Scheme 3.3	Resonance Structures for (PCP)Ir Complexes	47
Scheme 3.4	Synthesis of Cyclometalated Norbornene Complexes, **3-1** and **3-2**	49
Scheme 3.5	Addition of CO to Cyclometalated Complex **3-2**	49
Scheme 3.6	Reaction of **3-2** with H_2	52
Scheme 3.7	Reaction of **3-2** with Ethylene	53
Scheme 3.8	Synthesis of Cyclometalated (PCP)IrCl Complex, **3-4**	55
Scheme 3.9	Synthesis of Cyclometalated (PCP)$IrFBF_3$ complex, **3-5**	56
Scheme 4.1	Reversible Binding of Oxygen to Vaska's Complex	73
Scheme 4.2	Reaction of Cationic (PCN)Pt Pincer Complex with DMDO	75

Scheme 4.3	Reaction Between the (Me-PCP)IrH_n and O_2	76
Scheme 4.4	Reaction of (Me-PCP)IrH_4 with DMDO	77
Scheme 4.5	Addition of Acetone to (PCP)IrTBE Complex	77
Scheme 4.6	Reaction of H_2O_2 with (Me-PCP)IrNBE Complex	78
Scheme 4.7	Conversion of (Me-PCP)IrO_2 into Cyclometalated Hydroxide Product **4-5**	79
Scheme 4.8	Addition of CO to Cyclometatalated Hydroxyl Species	79
Scheme 4.9	Reaction of (Me-PCP)Ir with N_2O	79
Scheme 5.1	Hydrogenation of 2-methylpropene	88
Scheme 5.2	Iridium (I) and (III) Pincer Complexes	89
Scheme 5.3	Addition of Ligands to **5-1**	89
Scheme 5.4	Exchange Equilibrium for **5-1**	95
Scheme 5.5	Equilibrium Between **5-2** and L	96
Scheme 5.6	Equilibrium Exchange Between **5-3** and L	102
Scheme 5.7	Dissociative Pathway for the Displacement of Pyridine by Acetonitrile	103
Scheme 6.1	N-H Activation of Ammonia and Aniline by ($^{t\text{Bu4}}$PCP)Ir	165
Scheme 6.2	Addition of Hydrazine Derivatives to (PCP)IrPhH	166
Scheme 6.3	Addition of $MePhNNH_2$ and Me_2NNH_2 to (PCP)Ir Fragment	167
Scheme 6.4	Addition of Hydrazine and Phenylhydrazine to (PCP)Ir Complexes to Synthesize (PCP)Ir Hydrazine Complexes **6-1** through **6-2d**	168
Scheme 6.5	Low Temperature Reactions for the Addition of Hydrazine to (PCP)Ir	169
Scheme 6.6	Formation of (PCP)IrN_2 and (PCP)IrH_2 from (PCP)$IrH_2N_2H_4$	170
Scheme 6.7	Formation of Ammonia from (PCP)$IrH_2N_2H_4$	171
Scheme 6.8	Addition of Hydrazine to ($^{i\text{Pr4}}$PCP)IrH_2 to yield ($^{i\text{Pr4}}$PCP)$IrH_2(N_2H_4)$, **6-4**	172
Scheme 6.9	Equilibrium Between (PCP)IrH_2 and NH_3	174
Scheme 6.10	Reaction with Hydrazine Sulfate	184
Scheme 6.11	Reaction with Azobenzene	185

List of Tables

Table 2.1	Crystal Data and Structure Refinement for (Me-PCP)IrHCl, **2-9**	25
Table 2.2	Atomic Coordinates and Equivalent Isotropic Displacement Parameters for (Me- PCP)IrHCl, **2-9**	26
Table 2.3	Bond Lengths (Å) and Bond Angles (˚) for (Me-PCP)IrHCl, **2-9**	28
Table 2.4	Anisotropic Displacement Parameters for (Me-PCP)IrHCl, **2-9**	33
Table 2.5	Hydrogen Coordinates and Isotropic Displacement Parameters for (Me-PCP)IrHCl, **2-9**	35
Table 2.6	Torsion angles [°] for (Me-PCP)IrHCl, **2-9**	37
Table 3.1	Retention Times for the Reaction of **3-2** with H_2 to Release Norbornene	52
Table 3.2	Crystal Data and Structure Refinement for (Me-PCP)Ir–CO Cyclometalated, **3-3**	60
Table 3.3	Atomic Coordinates and Equivalent Isotropic Displacement Parameters for (Me-PCP)Ir–CO Cyclometalated, **3-3**	61
Table 3.4	Bond lengths [Å] and angles [°] for (Me-PCP)Ir–CO Cyclometalated, **3-3**	62
Table 3.5	Anisotropic Displacement Parameters for (Me-PCP)Ir–CO Cyclometalated, **3-3**	66
Table 3.6	Hydrogen Coordinates and Isotropic Displacement Parameters for (Me-PCP)Ir–CO Cyclometalated, **3-3**	67
Table 3.7	Torsion Angles [°] for (Me-PCP)Ir–CO Cyclometalated, **3-3**	69
Table 4.1	GC Data of Reaction Before Addition of N_2O	80
Table 4.2	GC Data of Reaction After Addition of N_2O	80
Table 5.1	Thermodynamic Parameters for the Addition of L to **5-1**	92
Table 5.2	Comparison of Experimental Thermodynamic Parameters to Computational Thermodynamic Values using Various DFT functionals	94
Table 5.3	Experimental ΔG Values (kcal/mol) for the Addition of a Series of Ligands to **5-1** Compared to Computational ΔG Values (kcal/mol) Determined using M06-L and PBE Functionals	95

Table 5.4	Determination of the Thermodynamic Values for the Addition of H_2 to **5-2** via Dehydrogenation of Acetone	98
Table 5.5	Thermodynamic Parameters for the Addition of L to **5- 2**	99
Table 5.6	Comparison of Experimental Thermodynamic Parameters to Computational Thermodynamic Values using Various DFT Functionals	99
Table 5.7	Experimental ΔG Values (kcal/mol) for the Addition of a Series of Ligands to **5-2** Compared to Computational Values (kcal/mol) Determined using M06-L and PBE Functionals	100
Table 5.8	Relative Experimental ΔG values (kcal/mol) for the Addition of Ligands to **5-3** Compared to Computational Values (kcal/mol) Determined using M06-L and PBE Functionals	107
Table 5.9	Substrate Ratio and Equilibrium Constants for the Equilibria of **5-1**	110
Table 5.10	Substrate Ratio and Equilibrium Constants for the Equilibria of **5-2**	111
Table 5.11	Substrate Ratio and Equilibrium Constants for the Equilibria of **5-3**	112
Table 5.12	Crystal Data and Structure Refinement for (PCP)IrHClPy, **5-8**	121
Table 5.13	Atomic Coordinates and Equivalent Isotropic Displacement Parameters for (PCP)IrHClPy, **5-8**	122
Table 5.14	Bond Lengths [Å] and Angles [°] for (PCP)IrHClPy, **5-8**	124
Table 5.15	Torsion Angles [°] for(PCP)IrHClPy, **5-8**	128
Table 5.16	Crystal Data and Structure Refinement for (PCP)Ir$NCCH_3$, **5-50**	131
Table 5.17	Atomic Coordinates and Equivalent Isotropic Displacement Parameters for (PCP)Ir$NCCH_3$, **5-50**	132
Table 5.18	Bond lengths [Å] and Angles [°] for (PCP)Ir$NCCH_3$, **5-50**	133
Table 5.19	Torsion Angles (˚) for (PCP)Ir$NCCH_3$, **5-50**	137
Table 5.20	Crystal Data and Structure Refinement for (PCP)IrPMe_2Ph, **5-54**	140
Table 5.21	Atomic Coordinates and Equivalent Isotropic Displacement Parameters for (PCP)IrPMe_2Ph, **5-54**	141
Table 5.22	Bond Lengths [Å] and Angles [°] for (PCP)IrPMe_2Ph, **5-54**	143

Table 5.23	Torsion Angles [°] for (PCP)IrPMe$_2$Ph, **5-54**	147
Table 5.24	Crystal Data and Structure Refinement for (PCP)IrPOEt$_3$, **5-59**	150
Table 5.25	Atomic Coordinates and Equivalent Isotropic Displacement Parameters for (PCP)IrPOEt$_3$, **5-59**	151
Table 5.26	Bond Lengths [Å] and Angles [°] for (PCP)IrPOEt$_3$, **5-59**	153
Table 5.27	Torsion Angles [°] for (PCP)IrPOEt$_3$, **5-59**	158
Table 6.1	Ammonia Production for the Catalytic Reduction of Hydrazine with Varied Catalytic Conditions	173
Table 6.2	Equilibrium Constants (K, M^{-1}) and Free Energy Values (ΔG, kcal/mol) for the Addition of NH_3, H_2, Hydrazine and PEt_3 to (PCP)IrH_2 at 298 K	175
Table 6.3	Catalytic Conversion of Ammonia using Various Pincer Complexes	176
Table 6.4	Kinetic results for Hydrazine to Ammonia Conversion with 20 mM of PCPIr(H_2) at 85 °C	177
Table 6.5	Kinetic Results for Hydrazine to Ammonia Conversion with 10 mM of PCPIr(H_2) at 85 °C	177
Table 6.6	Values of k_1, the Rate Constant for the Release of NH_3 from **6-2a**	180
Table 6.7	Crystal Data and Structure Refinement for (PCP)IrH_2(N_2H_4), **6-2a**	191
Table 6.8	Atomic Coordinates and Equivalent Isotropic Displacement Parameters for (PCP)IrH_2(N_2H_4), **6-2a**	192
Table 6.9	Bond Lengths [Å] and Angles [°] for (PCP)IrH_2(N_2H_4), **6-2a**	193
Table 6.10	Hydrogen Coordinates and Isotropic Displacement Parameters for (PCP)IrH_2(N_2H_4), **6-2a**	197
Table 6.11	Torsion Angles [°] for (PCP)IrH_2(N_2H_4), **6-2a**	199

Chapter 1

Introduction

The activation of small molecules by transition metals leads to knowledge of bond reactivity, which can then be applied to functionalization for synthesis of new materials. In general, the activation of small molecules proceeds through oxidative addition. Oxidative addition and the reverse process, reductive elimination, are fundamental reaction steps in many organometallic reactions and catalytic cycles.[1,2] Oxidative addition implies a formal two electron addition to a metal center involving the cleavage of an X-Y bond and formation of M-X and M-Y bonds.

Diatomic hydrogen as the smallest molecule has a rich chemistry associated with transition metals.[3] One of the first examples of H_2 addition to an iridium center was reported by Vaska in 1962 (Scheme 1.1).[4] The unsaturated $16e^-$ complex can oxidatively add H_2 easily to give an $18e^-$ iridium hydride species. The release of H_2 from the coordinatively saturated center to regenerate the $16e^-$ species is the reductive elimination. Following, Vaska successfully reported the hydrogenation of ethylene and acetylene using this $18e^-$ complex.[5]

Scheme 1.1 Oxidative Addition of H_2 to Vaska's Complex

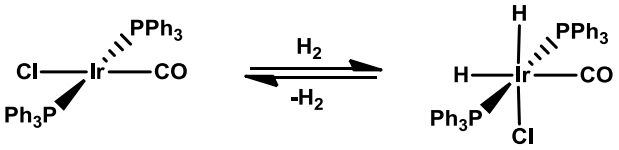

Wilkinson reports the oxidative addition of hydrogen to a square planar rhodium complex during the catalytic hydrogenation of alkenes to form alkanes (Figure 1.1).[6,7] After release of one triphenylphosphine ligand (PPh_3), the active species is generated and can undergo oxidative addition of hydrogen easily to give the dihydride complex. Addition of an olefin gives the π complex which then undergoes hydride migration to give the olefin insertion product. The final step is reductive elimination of the alkane to regenerate the active species.

Figure 1.1 Mechanism for the Hydrogenation of Alkenes via Wilkinson's Catalyst

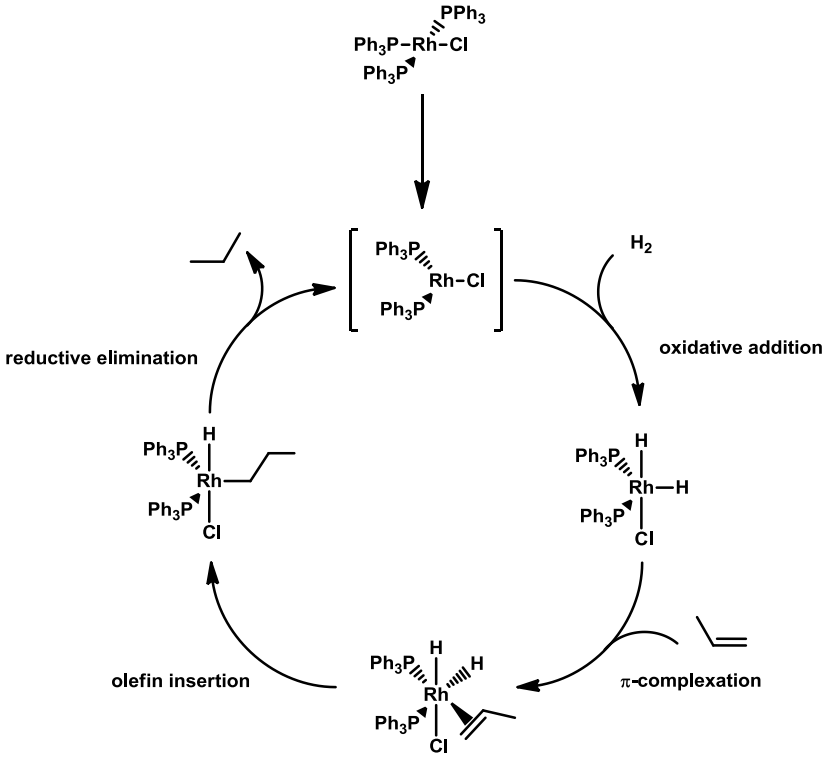

The oxidative addition of H_2 has been studied in great detail as it is not only an intermediate step in hydrogenation and hydroformylation reactions but the activation of H_2 also provides information regarding the activation of other bonds. C-H activation, similar in nature to the oxidative addition of H_2 to transition metals probably represents the most desired reactions in chemistry as it can lead to functionalization forming a wide variety of organic molecules.[8] The first report of C-H activation was published in 1965 by Chatt and Davidson in which a ruthenium catalyst activates the aryl hydrogen bonds of naphthalene to give a ruthenium aryl hydride complex.[9,10] Similarly, Green and coworkers reported the addition of benzene upon photolytic loss of H_2 from Cp_2WH_2 (Scheme 1.2).[11-13]

Scheme 1.2 Oxidative Addition of Benzene to Cp_2WH_2

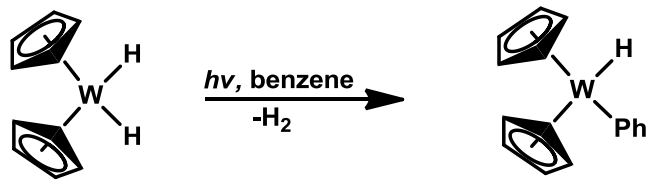

In the early 1980's the first reports for the C-H activation of alkanes appeared as Bergman,[14,15] Jones,[16] and Graham[17] each reported the oxidative addition of C-H bonds of alkanes to transition metal complexes. Surprisingly, there is high selectivity to activate the strongest primary C-H bond rather than the tertiary C-H bond.[18-20] Separate reports have also examined the kinetic and thermodynamic favorability for the C-H activation of arene C-H bonds over alkyl C-H bonds, even though arene C-H bonds are much stronger than alkyl C-H bonds. One reason is the difference between metal-aryl and metal-alkyl bond strengths versus the bond strengths of the starting molecules.[18,21,22]

The oxidative addition of C-H bonds is highly important in many transformations. The direct production of alkenes from abundant alkanes is very desirable as olefins are highly useful precursors for many chemical transformations. The first selective homogeneous dehydrogenation of alkanes was studied by Crabtree in 1979, in which a cationic $[IrH_{2(}acetone)_2(PPh_3)_2][BF_4]$ complex dehydrogenated cyclopentane or cyclooctane in the presence of *tert*-butylethylene (TBE), the hydrogen acceptor.[23] Soon after, catalytic transfer dehydrogenations were reported (Equation 1).[24-26]

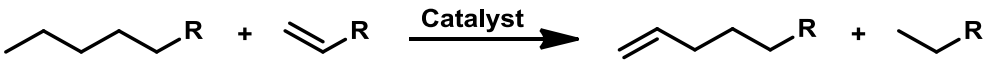

(1)

Shilov reported the reverse process, the hydrogenation of olefins using platinum catalysts.[10] The critical step in this reaction was reversible C-H activation to give a Pt(alkyl) species. Later in 1972, Shilov reported the conversion of methane to methanol via a Pt(II)/Pt(IV) system.[27] This was the first example of alkane functionalization and despite the use of stoichiometric Pt(IV) as the oxidant in this system, it still remains one of the few examples of methane conversion to methanol.

Alkane metathesis has been defined as the molecular redistribution of alkanes and has proven most promising in the area of Fischer Tropsch (FT) chemistry.[28,29] In FT chemistry, high molecular weight (MW) *n*-alkanes are cracked to lower MW alkanes generating highly useful C9-C19 fragments or diesel fuel and less desirable C3-C8 fragments. Alkane metathesis allows for conversion of the C3-C8 fragments back into the useful diesel fraction (Figure 1.2). The first example of alkane metathesis was achieved by Burnett and Hughes in 1973 with a combination of two heterogeneous catalysts.[30] In this process, platinum/alumina acted as the transfer dehydrogenation catalyst while tungsten oxide/silica acted as the olefin metathesis catalyst.

Figure 1.2 General Reaction Scheme for Alkane Metathesis

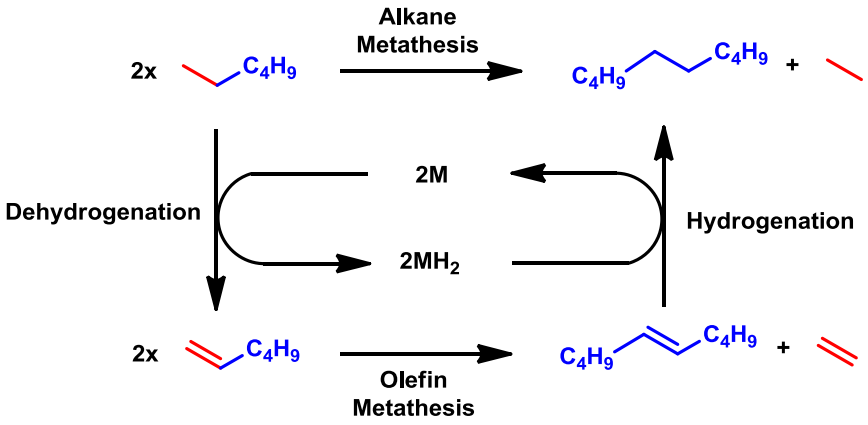

One of the most successful catalysts for dehydrogenation and alkane metathesis has been the pincer complex. The PCP ligand (where PCP = κ^3-C_6H_6-2,6-$(CH_2PR_2)_2$; R = ^{t}Bu) and first pincer complex were synthesized by Shaw in 1976 (Figure 1.3), however the term "pincer" was coined by van Koten much later.[31-34] Generally, the nomenclature abbreviation for these complexes stems from the atoms attached to the metal center, and additional denotations are only to differentiate any changes from the parent PCP complex. The wide applicability of these complexes is due in part to their high stability at a variety of temperatures as well as their extensive tunability. Adaptations to the sterics, electronics and reactivity of the pincer complex can be achieved by making subtle changes to the R-groups attached to the phosphorous atoms,[35-37] replacing the phosphorous atoms with nitrogen atoms,[38] exchanging the methylene linkers with oxygen[39] atoms, making changes to the backbone aryl ring and introducing different transition metals including Ir, Rh, Ni, Pt, and Pd.[40-50]

Figure 1.3 General Structure of Pincer Complex

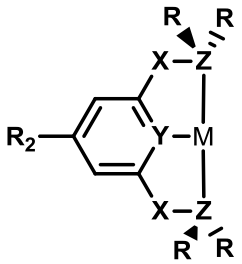

R = Me, ^{t}Bu, ^{i}Pr, Ad, CF_3
X = O, CH_2,
Y = N, C
Z = P, N
R_2 = H, Me, MeO, NH_2, CO_2Me
M = Fe, Ru, Ni, Co, Ir, Rh, Pd, Pt

Pincer complexes have achieved much attention due to their high applicability in a variety of reactions (Figure 1.4).[43] In 1996, Kaska and Jensen reported the first transfer dehydrogenation utilizing

pincer complexes.[51-53] Interestingly, the iridium pincer complex showed high activity for the cyclooctane/TBE transfer dehydrogenation while its rhodium counterpart was ineffective. The acceptorless dehydrogenation utilizing pincer complexes was also demonstrated. In 2006, Goldman and Brookhart reported the use of a pincer catalyst as the transfer dehydrogenation catalyst in combination with a Schrock molybdenum olefin metathesis catalyst for alkane metathesis.[28] In addition to the dehydrogenation of alkanes, the dehydrogenation of other substrates has been reported including cycloalkanes followed by a subsequent report by Goldman et. al. describing the C-H activation of aryl and vinyl substrates.[52,54,55] There have been reports on the use of pincer catalysts for C-C bond forming reactions including Suzuki biaryl and Heck olefin arylation coupling reactions with success.[34]

Pincer complexes can successfully activate O-H bonds, including water[56] and C-O type bonds.[57] The oxidative addition of oxygen leads to differing results, for instance, insertion of O_2 into a Pd-H bond of (PCP)PdH yields a Pd(II) hydroperoxide complex, while reaction of the (PCP)Ir fragment with O_2 leads to the mono and bis di-oxygen complexes and no evidence of oxygen insertion.[58-60] The dehydrogenation of alcohols to give aldehydes and ketones as well as the activation of esters and ethers, has also been published.[61,62] Recently, the addition of olefins across alcohols through hydroaryloxylation was developed.[63] Even the oxidative addition of C-F bonds via initial C-H activation has also been reported.[64]

Given, that N-H bonds and C-H bonds are intrinsically similar in homolytic bond strengths and the importance of bond activation of both types in hydroamination, transitioning from C-H activation to N-H activation seems only natural. The dehydrogenation of tertiary amines to give enamines, as well as the activation of other N-H bonds, has been reported with pincer catalysts.[62,65-67] The hydrogenation of amides to give amines and alcohols was also reported by Milstein using a (PNP)Ru catalyst.[68] In 2006, Goldberg and Heinekey reported the dehydrogenation of ammonia-borane occurring through a boron bound hydride intermediate rather than via N-H activation.[69,70] Unfortunately, the coordination of N_2 was found as an inhibitory reaction throughout many reactions depicted for pincer complexes.[71-73] Overall the reactions described are a sample of the high applicability and reactivity of pincer complexes.

Figure 1.4 Activation of Small Molecules by Pincer Iridium Complexes

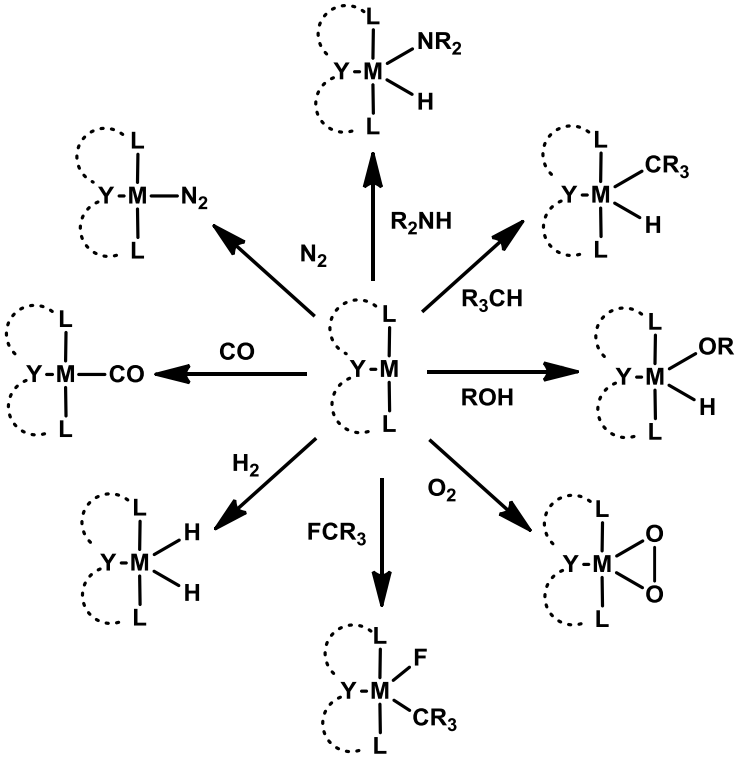

1.2 Research Goals of This Thesis

This thesis aims to add to the wealth of knowledge in the area of small molecule activation via pincer iridium catalysts. The first portion of the thesis focuses on the synthesis and reactivity of a new pincer complex [(Me-PCP)Ir] in which the para position hydrogen of the aryl backbone has been replaced with a methyl group. The second portion of this thesis focuses on studies with the parent (PCP)Ir complex. The two portions of the thesis are tied together by the discussions of the active $14e^-$ fragment.

Chapter 2 will discuss the synthesis of (Me-PCP)IrH_2, in which the hydrogen in the para position of the parent (PCP)IrH_2 complex has been replaced with a methyl group along with a discussion of its reactivity with small molecules (i.e. N_2, CO, ethylene, etc.). Comparisons will be made between the parent (PCP)IrH_2 and derivatized (Me-PCP)IrH_2 complexes. Finally, attempts to isolate the active $14e^-$ (Me-PCP)Ir species will be discussed.

Chapter 3 presents the synthesis of cyclometalated complexes in which the (R-PCP)Ir (R= H and Me) complexes undergo intramolecular C-H activation of the *tert*-butyl group rather than isolation or observance of any proposed $14e^-$, agostic, solvated, or dimeric species. Addition of CO to the cyclometalated complexes leads to an interesting insertion product in which a carbon is inserted between the backbone and iridium metal center. The characterization and proposed mechanisms are discussed in relation to previously cited pathways for the formation of these cyclometalated complexes and the cyclometalated insertion product.

Chapter 4 discusses the reactivity of (Me-PCP)Ir with different oxidants. Reaction with oxygen leads to the dioxygen monomer and dimer complexes, similar in structure to the parent (PCP)IrO_2 complexes. A reaction with DMDO leads to decyclization of the DMDO to form a (Me-PCP)Ir(acetate) complex. Next, the reaction with hydrogen peroxide leads to the mono oxygen complex which further reacts to form a cyclometalated product, similar to those described in Chapter 3. The characterization of this cyclometalated oxygen complex along with a six coordinate cyclometalated CO adduct will be detailed. Finally, the efforts to react nitrous oxide with (Me-PCP)Ir closes this chapter.

Chapter 5 presents a combined experimental and computational study of binding energy determination for the addition of a variety of ligands, which undergo C, H, O, N, S, and P heteroatom additions, to the metal center of (PCP)IrHCl, (PCP)IrH_2, and the (PCP)Ir fragment. The thermodynamics for the addition of these ligands will be discussed in detail. The experimentally determined values are compared to values derived from DFT calculations utilizing a variety of functionals with good agreement.

Chapter 6 presents the activation of hydrazine and related compounds by the parent (PCP)IrH_2 complex. Hydrazine is an important intermediate along the pathway for the synthesis of ammonia from N_2 and H_2. Both the dehydrogenation of hydrazine by pincer iridium (PCP) type catalysts to N_2 and H_2 as well as the hydrogenation to form ammonia will be discussed. Thermodynamic and kinetics experiments were used to support a computationally calculated mechanism in which hydrazine acts as the hydrogen donor and acceptor rather than promotion by an external reductant or proton source.

References

(1) Hartwig, J. F. *Organotransition Metal Chemistry*; University Science Books: Sausalito, CA, 2010.
(2) Halpern, J. *Acc. Chem. Res.* **1970**, *3*, 386.
(3) Deutsch, P. P.; Eisenberg, R. *Chem. Rev.* **1988**, *88*, 1147.
(4) Vaska, L.; DiLuzio, J. W. *J. Am. Chem. Soc.* **1962**, *84*, 679.
(5) Vaska, L.; Rhodes, R. E. *J. Am. Chem. Soc.* **1965**, *87*, 4970.
(6) Osborn, J. A.; Jardine, F. H.; Young, J. F.; Wilkinson, G. *J. Chem. Soc., A* **1966**, 1711.
(7) Osborn, J. A.; Wilkinson, G. *Inorg. Synth.* **1967**, *10*, 67.
(8) Goldman, A. S.; Goldberg, K. I. In *Activation and Functionalization of C-H Bonds*; Goldberg, K. I., Goldman, A. S., Eds. 2004; Vol. ACS Symposium Series 885, p xiii.
(9) Chatt, J.; Davidson, J. M. *J. Chem. Soc.* **1965**, 843.
(10) Shilov, A. E.; Shul'pin, G. B. *Chem. Rev.* **1997**, *97*, 2879.
(11) Green, M. L. H.; Knowles, P. J. *J. Chem. Soc., Chem. Comm.* **1970**, 1677.
(12) Green, M. L. H.; Knowles, P. J. *J. Chem. Soc., A* **1971**, 1508.
(13) Green, M. *Organometal. Chem.* **1972**, *1*, 431.
(14) Janowicz, A. H.; Bergman, R. G. *J. Am. Chem. Soc.* **1982**, *104*, 352.
(15) Janowicz, A. H.; Bergman, R. G. *J. Am. Chem. Soc.* **1983**, *105*, 3929.
(16) Jones, W. D.; Feher, F. J. *Organometallics* **1983**, *2*, 562.
(17) Hoyano, J. K.; Graham, W. A. G. *J. Am. Chem. Soc.* **1982**, *104*, 3723.
(18) Buchanan, J. M.; Stryker, J. M.; Bergman, R. G. *J. Am. Chem. Soc.* **1986**, *108*, 1537.
(19) Bryndza, H. E.; Fong, L. K.; Paciello, R. A.; Tam, W.; Bercaw, J. E. *J. Am. Chem. Soc.* **1987**, *109*, 1444.
(20) Northcutt, T. O.; Wick, D. D.; Vetter, A. J.; Jones, W. D. *J. Am. Chem. Soc.* **2001**, *123*, 7257.
(21) Janowicz, A. H.; Periana, R. A.; Buchanan, J. M.; Kovac, C. A.; Stryker, J. M.; Wax, M. J.; Bergman, R. G. *Pure and Appl. Chem.* **1984**, *56*, 13.
(22) Jones, W. D.; Feher, F. J. *J. Am. Chem. Soc.* **1984**, *106*, 1650.
(23) Crabtree, R. H.; Mihelcic, J. M.; Quirk, J. M. *J. Am. Chem. Soc.* **1979**, *101*, 7738.
(24) Burk, M. J.; Crabtree, R. H.; Parnell, C. P.; Uriarte, R. J. *Organometallics* **1984**, *3*, 816.
(25) Burk, M. J.; Crabtree, R. H. *J. Am. Chem. Soc.* **1987**, *109*, 8025.
(26) *(a)* Baudry, D.; Ephritikine, M.; Felkin, H.; Holmes-Smith, R. J. Chem. Soc., *Chem. Commun.* ***1983****, 788-789. (b)* Felkin, H.; Fillebeen-Khan, T.; Gault, Y.; Holmes-Smith, R.; Zakrzewski, J. *Tetrahedron Lett.* ***1984****, 26, 1999- 2000.(c)* Felkin, H.; Fillebeen-Khan, T.; Holmes-Smith, R.; Lin, Y. *Tetrahedron Lett.* ***1985****, 26, 1999-2000.*
(27) Muradov, N. Z.; Shilov, A. E.; Shteinman, A. A. *Kinetika i Kataliz* **1972**, *13*, 1357.
(28) Goldman, A. S.; Roy, A. H.; Huang, Z.; Ahuja, R.; Schinski, W.; Brookhart, M. *Science* **2006**, *312*, 257.
(29) Haibach, M. C.; Kundu, S.; Brookhart, M.; Goldman, A. S. *Acc. Chem. Res.* **2012**, *45*, 947.
(30) Burnett, R. L.; Hughes, T. R. *J. Catalysis* **1973**, *31*, 55.
(31) Moulton, C. J.; Shaw, B. L. *J. Chem. Soc., Dalton Trans.* **1976**, 1020.
(32) Koten, G. v. *Pure Appl. Chem.* **1989**, *61*, 1681.
(33) Choi, J.; MacArthur, A. H. R.; Brookhart, M.; Goldman, A. S. *Chem. Rev.* **2011**, *111*, 1761.
(34) Albrecht, M.; van Koten, G. *Angew. Chem., Intl. Ed.* **2001**, *40*, 3750.
(35) Punji, B.; Emge, T. J.; Goldman, A. S. *Abstracts of Papers, 236th ACS National Meeting, Philadelphia, PA, United States, August 17-21, 2008* **2008**, INOR-268.
(36) Punji, B.; Emge, T. J.; Goldman, A. S. *Organometallics* **2010**, *29*, 2702.
(37) Adams, J. J.; Lau, A.; Arulsamy, N.; Roddick, D. M. *Organometallics* **2011**, *30*, 689.
(38) Flores, J. A.; Haibach, M. C.; Goldman, A. S.; ACS: 2012, INOR 8.
(39) Göttker-Schnetmann, I.; White, P. S.; Brookhart, M. *Organometallics* **2004**, *23*, 1766.
(40) Ozerov, O. V.; Pelton, E.; Gerber, L.; Weng, W.; Parkin, S. R.; Foxman, B. M. *Abstracts of Papers, 234th ACS National Meeting, Boston, MA, United States, August 19-23, 2007* **2007**, INOR-218.

(41) Zhu, K.; Goldman, A. S., manuscript in preparation.
(42) Albrecht, M.; Morales-Morales, D. *Iridium Complexes in Organic Synthesis* **2009**, 299.
(43) van der Boom, M. E.; Milstein, D. *Chem. Rev.* **2003**, *103*, 1759.
(44) Kuznetsov, V. F.; Lough, A. J.; Gusev, D. G. *Inorg. Chim. Acta* **2006**, *359*, 2806.
(45) Bonnet, S.; Li, J.; Siegler, M. A.; von Chrzanowski, L. S.; Spek, A. L.; van Koten, G.; Klein Gebbink, R. J. M. *Chem.-Eur. J.* **2009**, *15*, 3340.
(46) Kossoy, E.; Rybtchinski, B.; Diskin-Posner, Y.; Shimon, L. J. W.; Leitus, G.; Milstein, D. *Organometallics* **2009**, *28*, 523.
(47) Boro, B. J.; Duesler, E. N.; Goldberg, K. I.; Kemp, R. A. *Inorg. Chem.* **2009**, *48*, 5081.
(48) Frech, C. M.; Shimon, L. J. W.; Milstein, D. *Organometallics* **2009**, *28*, 1900.
(49) Adams, J. J.; Lau, A.; Arulsamy, N.; Roddick, D. M. *Inorg. Chem.* **2007**, *46*, 11328.
(50) MacInnis, M. C.; MacLean, D. F.; Lundgren, R. J.; McDonald, R.; Turculet, L. *Organometallics* **2007**, *26*, 6522.
(51) Gupta, M.; Hagen, C.; Flesher, R. J.; Kaska, W. C.; Jensen, C. M. *Chem. Commun.*, **1996**, 2083.
(52) Jensen, C. M. *Chem. Commun.* **1999**, 2443.
(53) Goldman, A. S.; Renkema, K. B.; Czerw, M.; Krogh-Jespersen, K. In *Activation and Functionalization of C-H Bonds*; Goldberg, K. I., Goldman, A. S., Eds. Washington, DC, 2004; Vol. ACS Symposium Series 885, p 198.
(54) Gupta, M.; Hagen, C.; Kaska, W. C.; Cramer, R. E.; Jensen, C. M. *J. Am. Chem. Soc.* **1997**, *119*, 840.
(55) Kanzelberger, M.; Singh, B.; Czerw, M.; Krogh-Jespersen, K.; Goldman, A. S. *J. Am. Chem. Soc.* **2000**, *122*, 11017.
(56) Morales-Morales, D.; Lee, D. W.; Wang, Z.; Jensen, C. M. *Organometallics* **2001**, *20*, 1144.
(57) Lee, D. W.; Jensen, C. M.; Morales-Morales, D. *Organometallics* **2003**, *22*, 4744.
(58) Boisvert, L.; Goldberg, K. I. *Acc. Chem. Res.* **2012**, *45*, 899.
(59) Denney, M. C.; Smythe, N. A.; Cetto, K. L.; Kemp, R. A.; Goldberg, K. I. *J. Am. Chem. Soc.* **2006**, *128*, 2508.
(60) Williams, D. B.; Mayer, J.; Goldberg, K. I. *Abstracts of Papers, 232nd ACS National Meeting, San Francisco, CA, United States, Sept. 10-14, 2006* **2006**, INOR-490.
(61) Kundu, S.; Choi, J.; Wang, D. Y.; Choliy, Y.; Emge, T. J.; Krogh-Jespersen, K.; Goldman, A. S. *J. Am. Chem. Soc.* **2013**, *135*, 5127.
(62) Morales-Morales, D.; Redon, R.; Chen, W.; Yung, C.; Jensen, C. M. *Abstracts of Papers, 220th ACS National Meeting, Washington, DC, United States, August 20-24, 2000* **2000**, INOR-274.
(63) Haibach, M. C.; Guan, C.; Wang, D. Y.; Li, B.; Lease, N.; Steffens, A. M.; Krogh-Jespersen, K.; Goldman, A. S. *J. Am. Chem. Soc.* **2013**, *135*, 15062.
(64) Choi, J.; Wang, D. Y.; Kundu, S.; Choliy, Y.; Emge, T. J.; Krogh-Jespersen, K.; Goldman, A. S. *Science* **2011**, *332*, 1545.
(65) Kanzelberger, M.; Zhang, X.; Emge, T. J.; Goldman, A. S.; Zhao, J.; Incarvito, C.; Hartwig, J. F. *J. Am. Chem. Soc.* **2003**, *125*, 13644.
(66) Huang, Z.; Zhou, J.; Hartwig, J. F. *J. Am. Chem. Soc.* **2010**, *132*, 11458.
(67) Zhang, X.; Kanzelberger, M.; Emge, T. J.; Hartwig, J.; Krogh-Jespersen, K.; Goldman, A. S. In *Abstracts of Papers, 226th ACS National Meeting, New York, NY, United States, September 7-11* 2003, INOR-040.
(68) Balaraman, E.; Gnanaprakasam, B.; Shimon, L. J. W.; Milstein, D. *J. Am. Chem. Soc.* **2010**, *132*, 16756.
(69) Denney, M. C.; Pons, V.; Hebden, T. J.; Heinekey, D. M.; Goldberg, K. I. *J. Am. Chem. Soc.* **2006**, *128*, 12048.
(70) Paul, A.; Musgrave, C. B. *Angew. Chem., Int. Ed.* **2007**, *46*, 8153.
(71) Lee, D. W.; Kaska, W. C.; Jensen, C. M. *Organometallics* **1998**, *17*, 1.
(72) Ghosh, R.; Kanzelberger, M.; Emge, T. J.; Hall, G. S.; Goldman, A. S. *Organometallics* **2006**, *25*, 5668.
(73) Van der Boom, M. E.; Liou, S.-Y.; Ben-David, Y.; Gozin, M.; Milstein, D. *J. Am. Chem. Soc.* **1998**, *120*, 13415.

Chapter 2

Synthesis and General Reactivity of (Me-PCP)Ir Catalyst

Abstract

Advantageously, the pincer framework can be easily adapted by changing different aspects of the ligand. The parent (PCP)Ir complex readily activates C-H bonds of aryl rings, possibly leading to oligomerization of (PCP)Ir complexes as a potential decomposition pathway, therefore blocking the para position of the aryl backbone, would hopefully eliminate this possibility and lead to isolation of the catalytically active 14-electron "(PCP)Ir" species. The synthesis and characterization of (Me-PCP)Ir$H_{n,}$ in which the para position on the backbone of the catalyst has been changed from a hydrogen to a methyl group is reported. The reactivity of this complex in comparison to the parent (PCP)Ir complex is also discussed, for example addition of CO or ethylene leads to four coordinate (Me-PCP)Ir-CO and (Me-PCP)Ir-ethylene complexes, respectively. Finally, attempts to isolate the highly reactive 3-coordinate 14-electron (Me-PCP)Ir species are also addressed.

2.1 Introduction

The pincer ligand was first introduced by Moulton and Shaw in 1976.[1] Since that time, the term "pincer" has been applied to many tridentate ligands.[2-7] One of the advantages of this pincer framework is the ability to adapt the sterics, electronics and reactivity of this complex by making subtle changes.[8] The R-groups attached to the phosphorous atoms can be changed to methyl (Me), isopropyl (iPr), phenyl (Ph), adamantyl (Ad),[9,10] or trifluoromethyl (CF_3)[11] groups to replace one or more ^{t}butyl groups, which can dramatically change the steric environment around the metal center. One or more phosphorous atoms (Z) can be replaced with nitrogen atoms, thereby giving an NCN or a hybrid PCN motif. The methylene linkers (X) can be exchanged with oxygen[12] or nitrogen[13] atoms leading to interesting and complicated changes in both the sterics and electronics. The benzene ring can be changed to a pyridyl (PNP) type backbone (Y-position), influencing the electronics of the overall system through trans influence.[14] Substitutions made along the backbone of the pincer complex (R_2), specifically replacement of the hydrogen in the para position with OMe, CO_2Me, or NMe_2 groups have been reported, leading to a more controlled, yet less pronounced, effect on the electronics. [15]

Scheme 2.1 General Schematic for a Pincer Ligand

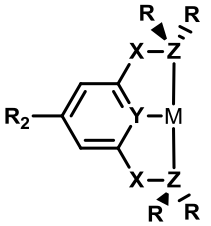

R = Me, ^{t}Bu, ^{i}Pr, Ad, CF_3
X = O, N, CH_2,
Y = N, C
Z = P, N
R_2 = H, Me, MeO, NH_2, CO_2Me
M = Fe, Ru, Ni, Co, Ir, Rh, Pd, Pt

A variety of complexes can be created via chelation of various transition metals including, Ir, Rh, Ni, Pt, Pd, and others.[2,16-23] Metalation for pincer ligands can occur through a direct process, oxidative addition to carbon halogen bonds, transmetalation, i.e. lithiation, or transcyclometalation.[7] Direct metalation of pincer ligands for PCP type systems is the preferred method, occurring through C-H or C-C bond activation. The competition between C-H activation and C-C activation to form the metalated species will be discussed in further detail in the next chapter. For NCN systems, direct cylometalation is less common and pre-coordination often occurs instead, most likely due to a weak M-N bond. Therefore, the NCN ligand motifs more readily undergo oxidative addition of an aryl halide to the metal center.

Post metalation, the active catalyst must be generated in order to achieve bond activation or catalytic transformations. The active species or intermediate for the activation of many small molecules including water,[24] carbon dioxide,[25] carbon monoxide, dinitrogen,[26] alkyls and aryls[27,28] by the parent (PCP)IrH_2, **2-1**, is thought to be the 14e$^-$ species, **2-3**. 14-electron (14e$^-$) metal complexes are generally transient species, oftentimes extremely reactive and generated by ligand dissociation in situ. Kaska and Jensen reported a solvated 14e$^-$ rhodium species formed by reaction of (PCP)Rh(H)(Cl) with a reactive base.[29] However, this 14e$^-$ species was not isolated and only short lived as it further reacts to form more stable species which will be discussed in further chapters of this thesis. Fujita et. al. report the spectroscopic evidence for a transient species generated by photoejection of various small ligands from both the aryl and alkyl (PCP)Rh pincer complexes.[30] The exact structure, agostic bonding, and solvent interactions of this transient species are unknown which only serves to emphasize the high reactivity of the catalytically active species.

Crabtree et. al reported the use of *tert*-butylethene (TBE) as an effective acceptor for early studies of dehydrogenation studies, since then the use of TBE has become standard to generate the active 14e$^-$ species.[31] It has been shown that when **2-1** is reacted with TBE or the strained cyclic molecule norbornene (NBE), the first equivalent of acceptor is hydrogenated and the second equivalent undergoes either vinylic C-H addition to form (PCP)Ir(H)($^{t\text{Bu}}$Vi), **2-2**, or in the case of norbornene, it has been proposed that a π-complex is formed (**2-4**, Scheme 2.2).[28,32,33] Both, the resulting π-complex and vinylic hydride species are in rapid equilibrium with the proposed 14e$^-$ species, **2-3**.

Scheme 2.2 Hydrogenation of TBE or NBE and Formation of the Vinyl Hydride and NBE π Complexes

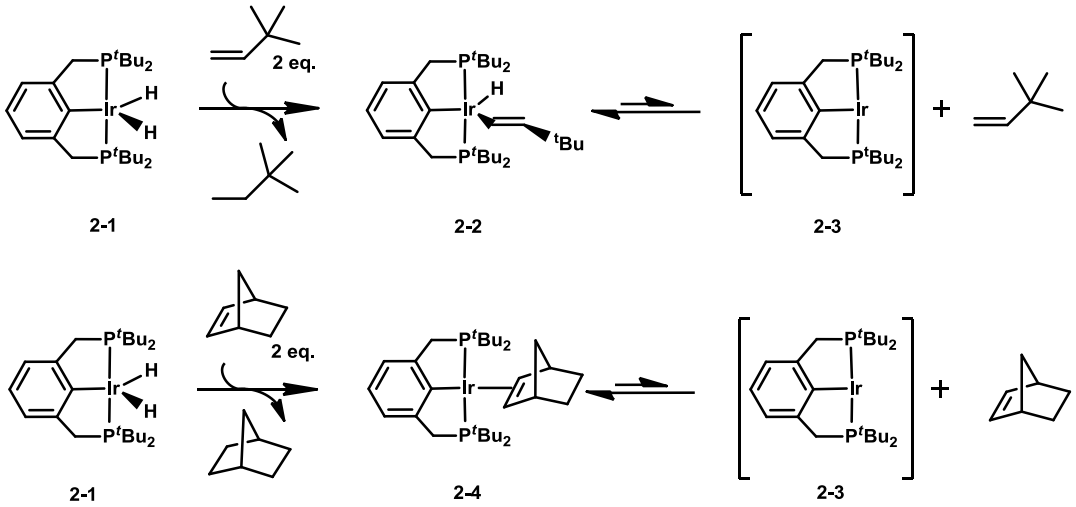

In the presence of an aryl solvent such as benzene, toluene or *m*-xylene, C-H activation of the solvent aryl ring prevails over formation of the vinyl hydride or the NBE π complex, as a result an aryl hydride complex is synthesized (Scheme 2.3).[28] Three isomers are formed in the presence of toluene while in *m*-xylene two isomers are formed. There is a preference for (PCP)IrH_n to activate the ortho position of aryls, and, since mesitylene and *p*-xylene are considerably more sterically hindered at the ortho position, these solvents are not activated by (PCP)Ir catalysts. Thus, these two solvents are ideal candidates in which to observe the active catalyst.

Scheme 2.3 C-H Activation of Benzene by (PCP)Ir

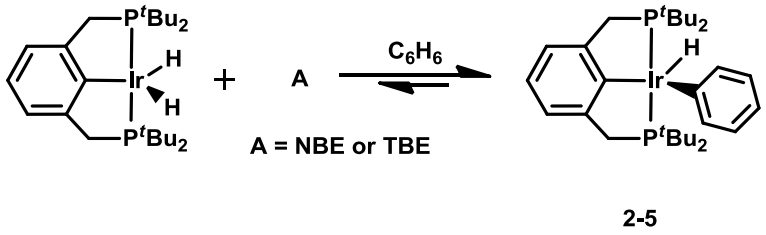

As described for **2-2** and **2-4**, species **2-5** has also been found to undergo rapid exchange via reversible loss of benzene to form the proposed that the 14e$^-$ or "naked" (PCP)Ir species, **2-3**. This equilibrium will be discussed in further detail in Chapter 5.

As often proposed the stabilization of the 14e$^-$ species can be achieved through an agostic or solvated species as described by Kaska and Jensen, and either species may act as the active catalyst.[29]

Different ruthenium pincer complexes have also been reported in which rapid aryl CH_2 activation is achieved and even aryl iridium agostic complexes have been characterized.[34] Kaska and Jensen have previously studied the elimination of TBA from the vinyl hydride species to give a very active intermediate.[33] Any attempts to characterize and isolate this intermediate proved unsuccessful, yet various possibilities were proposed for the intermediate's structure and stabilization including agostic bonding between TBE and/or solvent, an active $14e^-$ species, or even an agostic interaction between the tert-butyl groups of the pincer backbone (this scenario will be discussed in Chapter 3). The possibility that the catalyst undergoes oligomerization, where the iridium metal center activates the C-H bonds of the aryl ring of the subsequent PCP catalyst, has not been previously discussed but may also be a possibility.

Scheme 2.4 Proposed Oligomerization for (PCP)Ir Catalysts

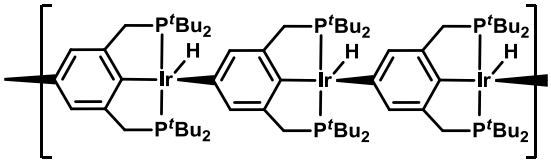

2-6

The ability to eliminate the proposed agostic interaction between subsequent catalyst molecules could possibly lead to isolation or observation of the $14e^-$ species. In this chapter, the synthesis of (Me-PCP)IrH_n, in which the hydrogen in the para position has been replaced with a methyl group will be described. Subsequently, the isolation and characterization of a variety of (Me-PCP)Ir complexes will be addressed and compared to the parent (PCP)Ir complexes. Finally, the attempts to isolate the active $14e^-$ (Me-PCP)Ir species will be discussed.

2.2 Synthesis of (Me-PCP)IrH_n

The synthesis of (Me-PCP)IrH_n, **2-10** and **2-11,** begins with the synthesis of the (Me-PCP)ligand, **2-8**. Phosphination of 3,5-bis(bromomethyl) toluene, **2-7**, with di-^{t}butyl phosphine and subsequent heating of this solution followed by workup in a sodium carbonate solution gives **2-8**, Scheme 2.5.[35] Following the procedure developed by Moulton and Shaw, treatment of **2-8** with iridium cyclooctadiene chloride dimer in toluene and then heating for 3 days yields the metalated hydridochloride species, **2-9** in 82% yield.[1] The final step is the reduction of **2-9** to a mixture of **2-10** and **2-11**. Species **2-9** is treated with super hydride or

sodium *tert*-butoxide under a hydrogen atmosphere until the color changes from orange-red to pale yellow, as described in literature.[36] The ratio of **2-10** to **2-11** is dependent upon the concentration of hydrogen gas. **2-10** can be isolated purely by repeated dissolution and reduced pressure of complex **2-11** in either hexanes or pentane. Conversely, **2-11** can be isolated in pure yield by addition of excess hydrogen to **2-10**. Species **2-8 – 11** have been characterized by ^{31}P, ^{1}H, and ^{13}C NMR spectroscopy; **2-9** was fully characterized including single crystal X-ray analysis.

Scheme 2.5 Synthesis of (Me-PCP)IrH_n

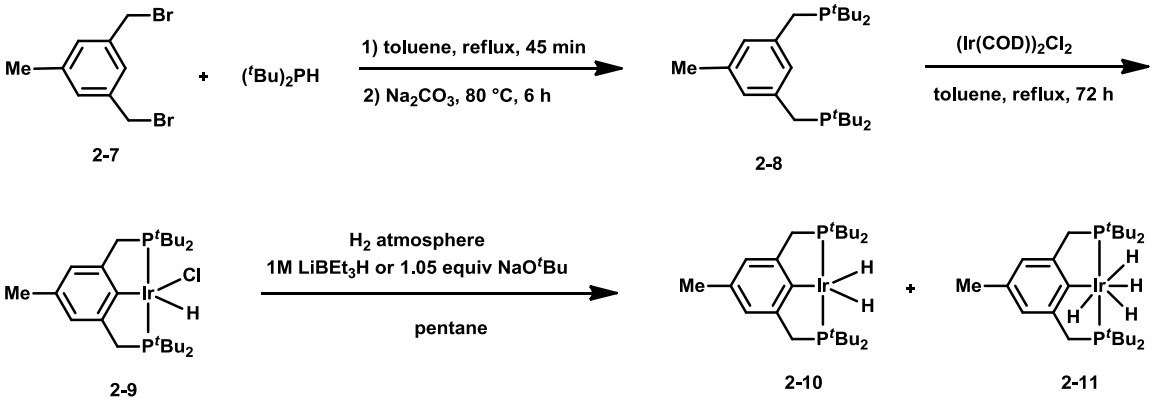

2.3 Reactivity towards TBE, NBE, CO, Ethylene, Benzene, N_2, Benzophenone, and H_2O

Addition of TBE and NBE to **2-10** yields **2-12** and **2-13** which can be observed by ^{31}P and ^{1}H NMR spectroscopy (Scheme 2.6).[28] The ^{31}P NMR shift for **2-12** is observed at 71 ppm, whereas the ^{31}P NMR shift of **2-13** is observed at 63 ppm. Species **2-13** is the proposed structure for the addition of NBE to the active species and has only been characterized by ^{31}P NMR spectroscopy. For **2-12**, a hydride signal is not observed at room temperature indicating very labile ligands and fast exchange between the active species and the coordinated species.

Scheme 2.6 Formation of the (Me-PCP)Ir Vinyl Hydride and NBE π Complexes

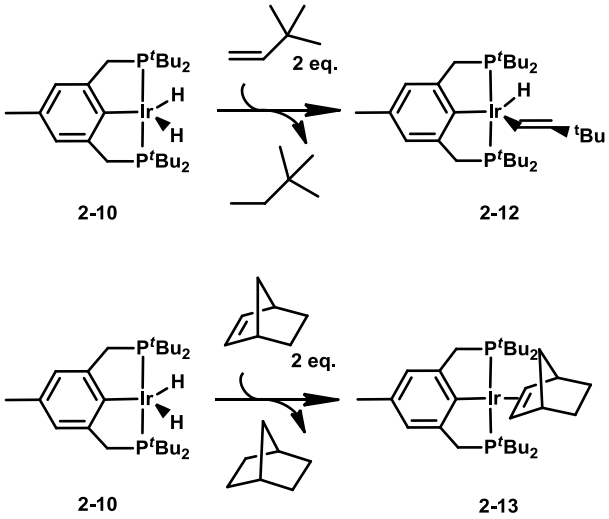

The four coordinate carbonyl complex was synthesized by reacting **2-10** with 1 atm of carbon monoxide gas at room temperature (Scheme 2.7). The addition of CO to the parent (PCP)Ir 14e$^-$ fragment proceeds to a similar complex.[25] Species **2-14** was formed in quantitative yield and has been characterized by ^{31}P, ^{1}H, ^{13}C NMR and IR spectroscopy. The iridium carbonyl stretching frequency is observed at 1926 cm^{-1}, while 1913 cm^{-1} has been reported for the parent carbonyl complex.

Scheme 2.7 Synthesis of Four Coordinate (Me-PCP)Ir-CO

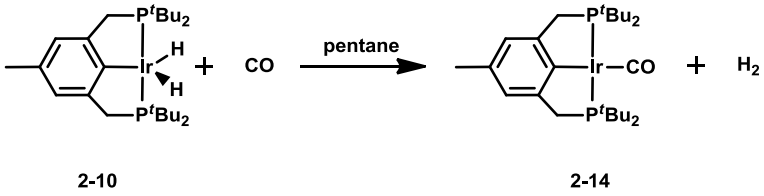

Addition of 1 atm of ethylene to the active species generates **2-15** quantitatively (Scheme 2.8).[37] The ethylene complex is generally hypothesized to be a π complex, as the hydrogen signals on the ethylene ligand are equivalent and observed as a singlet at 3.4 ppm in the ^{1}H NMR spectrum. A singlet is observed at approximately 59.6 ppm in the ^{31}P NMR spectrum. These shifts are comparable to those observed for the parent complex.

Scheme 2.8 Reaction of (Me-PCP)IrH_2 and Ethylene

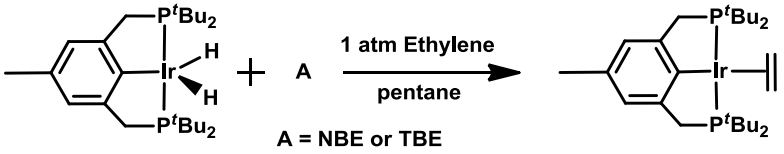

2-10 2-15

As was observed with the parent complex, when **2-10** is reacted with a hydrogen acceptor in benzene, then the C-H activation product (Me-PCP)Ir(Ph)(H), **2-16**, is synthesized quantitatively (Scheme 2.9).[28] This complex has comparative spectroscopic data to the parent complex, **2-5**, and the hydride signal is not observed at room temperature.

Scheme 2.9 Reaction of (Me-PCP)IrH_2 and Benzene

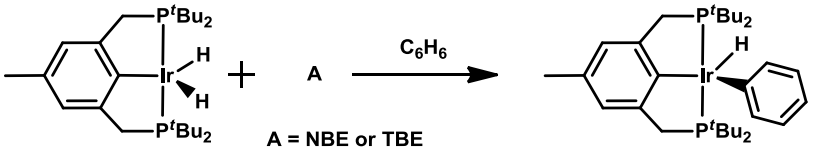

2-10 2-16

One of the most well used methods for drying a variety of alkane type solvents is the combination of sodium metal and benzephenone to produce a dibenzoketyl which then reacts with residual water and oxygen. This method was initially used to dry mesitylene in this study. In certain reactions, an unidentified signal was observed in the ^{31}P NMR spectrum at 59 ppm. It was discovered that excess benzophenone in mesitylene reacted with the active catalyst to form the C-H activation product of benzophenone, **2-17** (Scheme 2.10). The most likely position for C-H activation is para to the ketone. This species has not been previously isolated for the parent complex, but presumably similar reactivity would be observed. This method of drying was no longer utilized for the remainder of this work.

Scheme 2.10 Reaction of (Me-PCP)IrH_2 and Benzophenone

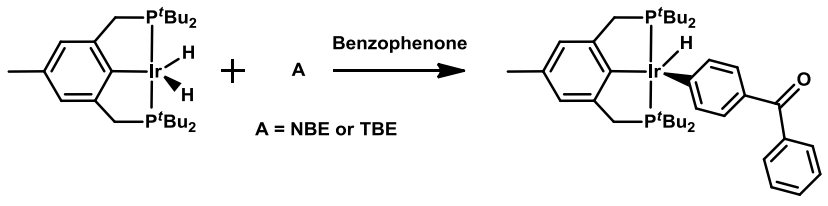

2-10 2-17

Reaction of the active species, arising from **2-10**, under a nitrogen atmosphere leads to a combination of the dinitrogen monomer, **2-18**, and dinitrogen dimer, **2-19**, in which N_2 bridges two metal centers (Scheme 2.11).[26,33] Oftentimes, the nitrogen species are described as inert and unreactive. The parent (PCP)IrN_2 monomer and dimer complexes will be discussed in more detail in Chapter 6.

Scheme 2.11 Reaction of (Me-PCP)IrH_2 and Nitrogen

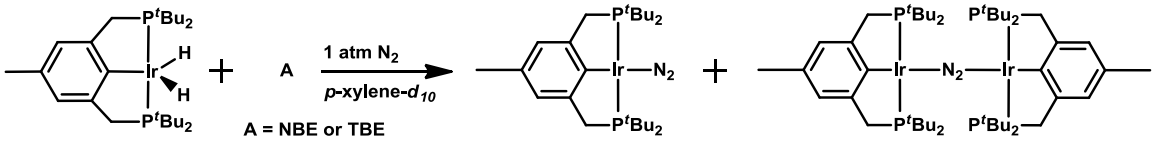

2-10 **2-18** **2-19**

Oxidative addition of water to the active species leads to formation of the hydrido hydroxyl species, **2-20** (Scheme 2.12).[24] A doublet is observed in the ^{31}P NMR spectrum at 64.87 ppm due to the coupling between the phosphorous and the hydride proton. The hydride proton is observed at -31.0 ppm and the hydroxyl proton is observed as a broad singlet at 5.28 in the ^{1}H NMR spectrum. These shifts are comparable to those observed for the parent complex.

Scheme 2.12 Addition of H_2O to (PCP)Ir

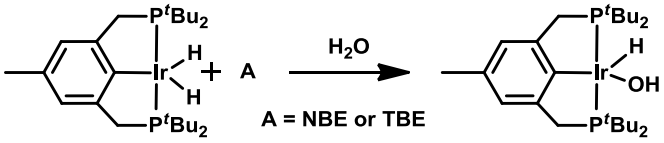

2-10 **2-20**

2.4 Attempts to Synthesize (Me-PCP)Ir 14-Electron Species

In an attempt to observe either the 14e$^-$ species or a species stabilized by agostic interactions, the **2-12** was evacuated in an attempt to remove TBE and shift the equilibrium towards the 14e$^-$ species. In a J. Young NMR tube, a solution of either **2-12** or **2-13** was placed under vacuum to remove excess volatiles and approximately half the solvent which was followed by addition of fresh solvent. The solution was monitored by NMR spectroscopy and this procedure was repeated multiple times. Instead of observing any 14e$^-$ species, the catalyst scavenges the atmosphere of the NMR tube, and other less labile ligands oxidatively add to the 14e$^-$ species, leading to observation of **2-14**, **2-18**, **2-19**, and **2-20** complexes.

Reactions were completed in *p*-xylene and mesitylene, with different solvent volumes, varying ratios of acceptor to catalyst, and in all cases multiple species were observed by ^{31}P NMR spectroscopy with the major species as complexes **2-14**, **2-18**, **2-19**, and **2-20**. The results from these experiments were inconclusive.

2.5 Summary

A new pincer complex, (Me-PCP)IrH_n was synthesized which exhibits similar reactivity as that of the parent (PCP)IrH_n species. The pincer iridium complexes with water, carbon monoxide, ethylene, benzene, benzophenone, and nitrogen have been isolated successfully. However, the active 14e$^-$ species has elusively evaded all attempts to be isolated and/or observed. The reasoning for its nonobservance will be discussed further in subsequent chapters.

2.6 Experimental

General

All reactions were performed under an argon atmosphere using standard Schlenck techniques or in an argon-filled glove box. C_6H_6, C_6D_6, TBE, and *p*-xylene-d_{10} were dried over Na/K alloy and collected via vacuum transfer. NBE was sublimed before use. All other substrates were degassed before entry to glovebox and used without further purification. ^{1}H, ^{13}C, and ^{31}P NMR spectra were obtained from either a 400 or 500 MHz Varian instrument. The residual peak of the deuterated solvent was used as a reference for all ^{1}H NMR spectra and an internal capillary standard of PMe_3 in *p*-xylene-d_{10} (-62.4 ppm) was used to reference ^{31}P NMR chemical shifts.

(Me-PCP) ligand, 2-8[35]

4.75 g (17.2 mmol) 3,5-bis(bromomethyltoluene) was refluxed with 5.0 g (34 mmol) di-^{t}butyl phosphine in 40 mL degassed acetone for 45 minutes. A white precipitate was formed after cooling to room temperature. A degassed solution of 15.3 g Na_2CO_3 in 65 mL H_2O was added. The resulting mixture was heated at 80 ˚C overnight with stirring. Upon cooling, the water layer was decanted into a clean 100 mL flask and the solvent was removed via vacuum from the resulting oil, leaving behind a tan solid. 40 mL ether was added to solid and ether layer was decanted to clean flask and the sample was pulled to dryness. The final product was a tan solid isolated in 90% yield. **^{31}P NMR (C_6D_6, 161.9 MHz):** δ 33.62

(s). **^{1}H NMR (C_6D_6, 400 MHz):** δ 7.12 (d, 2H, Ar-*H*), 2.76 (d of vt, 2H, C*H*$_2$P), 2.16 (s, 3H, Ar-C*H*$_3$), 1.08 (d, J_{PH} = 10.8 Hz, 36H, P^{t}Bu). **^{13}C NMR (C_6D_6, 100.6, MHz):** δ 127.9 (t, *C*H$_2$), 31.7 (s, *C*H$_3$), 29.8 (d, P^{t}Bu).

(Me-PCP)IrHCl, 2-9[1]

[IrCl(cyclooctadiene)]$_2$ (1.01 g, 1.5 mmol) was added to 1.18 g (3 mmol) of (Me-PCP) ligand in toluene at room temperature. Mixture was heated under reflux for 72+ hrs with stirring under H_2 atmosphere and the solvent was removed under vacuum. The resulting solid was extracted with hexane, recrystallized by slow evaporation from benzene and gave a yield of 0.790 g (82.2%) of the complex as dark red crystals. The crystal structure is shown as Figure 2.1 while X-ray crystallography refinement and structure parameters are included in Tables 2.1 through 2.6. **^{31}P NMR (C_6D_6, 161.9 MHz):** δ 68.26 (d, J_{PH} = 16.5 Hz, (Me-PCP)IrHCl), 67.52 (d, J_{PH} = 29.5, (Me-PCP)IrHBr). **^{1}H NMR (C_6D_6, 400 MHz,):** δ 7.121 (s, 2H, (Me-PCP)IrHCl Ar-*H*), 6.799 (s, 2H, (Me-PCP)IrHBr Ar-*H*), 3.067 (d of vt, J_{PH} = 3.75 , J_{HH} = 17.5, 2H, C*H*$_2$P), 2.975 (d of vt, J_{PH} = 3.75, J_{HH} = 17.5, 2H, C*H*$_2$P), 2.269 (s, 3H, Ar-C*H*$_3$), 2.250 (s, 3H, (Me-PCP)IrHBr Ar-C*H*$_3$), 1.269 (t, J_{PH} = 6.5 Hz, 18H, P^{t}Bu), 1.217 (t, J_{PH} = 6.75 Hz, 18H, P^{t}Bu), -42.818 (t, J_{PH} = 12.75, 1H, Ir-*H*).

(Me-PCP)IrH$_n$, 2-10 and 2-11

Method 1:[38] A solution of 100.1 mg (Me-PCP)IrHCl (0.157 mmol) in pentane was saturated with H_2 at room temperature. To this solution, 0.24 mL of a 1M LiBEt$_3$H in THF (0.24 mmol) was added dropwise until the solution changed from an orange red to a pale yellow and some white precipitate was formed. The solution was filtered and solvent was removed *in vacuo* leaving behind a red-brown mixture as the dihydride and tetrahydride. *Method 2*: 100.6 mg NaO^{t}Bu (1.05 mmol) and 249.5 mg (Me-PCP)IrHCl (0.392 mmol) are both added to Schlenck flask. Solids are dissolved in 60 mL benzene. Solution is stirred while H_2 was bubbled through solution for 3.5 hours. Solution turned from a dark red color to light orange. Solution was filtered and solvent was removed under vacuum and orange-red crystals are left as final product in 0.236 g (90%) yield. **^{31}P NMR (C_6D_6, 161.9 MHz):** δ 86.97 (s, Me-PCP)IrH$_2$), 73.96 (s, Me-PCP)IrH$_4$). **^{1}H NMR (C_6D_6, 400 MHz):** δ (Me-PCP)IrH$_2$: 7.17 (s, 2H, Ar-*H*), 3.54 (t, J_{PH} = 3.0 Hz, 4H, C*H*$_2$P), 2.35 (s, 3H, PCP-C*H*$_3$), 1.26 (t, J_{PH} = 6.4 Hz, 36H, P^{t}Bu), -19.38 (t, J_{PH} = 8.6 Hz, 2H, Ir*H*$_2$). (Me-

PCP)IrH$_4$: 6.91 (s, 2H, Ar-*H*), 3.29 (t, J_{PH} = 2.8 Hz, 4H, CH_2P), 2.35 (s, 3H, Ar-CH_3), 1.20 (t, J_{PH} = 6.6 Hz, 36H, P^{t}Bu), -9.10 (t, J_{PH} = 9.6 Hz, 4H, IrH_4). **^{13}C NMR (C_6D_6, 100.6 MHz):** δ 158.24 (t, aromatic C-Ir), 136.632 (s, aromatic), 128.02 (t, C_6D_6 and aromatic), 121.00 (t, Ar), 40.35 (t, *C*H$_2$P), 34.40 (q, *C*(CH$_3$)$_3$), 30.01 (t, C(*C*H$_3$)$_3$), 22.14 (s, Ar-*C*H$_3$).

(Me-PCP)Ir(TBE), 2-12

5 mg of the mixture of **2-9** and **2-10** was dissolved in *p*-xylene-d_{10} and 0.05 mL TBE (0.387 mmol) was added to the solution. After ten minutes, the solution changed from red to dark red in color. The compound was characterized *in situ*. **^{31}P NMR (*p*-xylene-d_{10}, 202.3 MHz):** δ 70.88 (s). **^{1}H NMR (*p*-xylene-d_{10}, 500 MHz):** δ 7.31(s, 2H, Ar-*H*), 6.18 (m, TBE), 5.30 (d, TBE), 5.21 (bs, TBE), 3.73 (vt, J_{PH} = 3.6 Hz, 4H, CH_2P), 2.54 (s, 3H, Ar-CH_3), 1.55 (vt, J_{PH} = 6.4 Hz, 36H, P^{t}Bu), 1.39 (t, TBE).

(Me-PCP)IrNBE, 2-13

5 mg of the mixture of **2-9** and **2-10** was dissolved in *p*-xylene-d_{10} and excess NBE was added to the solution. After five minutes, the solution changed from red to orange in color. The compound was characterized *in situ*. **^{31}P NMR (*p*-xylene-d_{10}, 161.9 MHz):** δ 63.4 (s).

(Me-PCP)Ir-CO, 2-14

To a solution of 9.5 mg (Me-PCP)IrH$_n$ (15.8 μmol) in pentane, 1 atm CO was added in a J. Young NMR tube. Solution changed from dark red to yellow in color. The solvent was removed solvent *in vacuo*, leaving a yellow solid which was dissolved in C_6D_6. (Me-PCP)IrCO was formed in 98% yield as determined by NMR spectroscopy. **^{31}P NMR (C_6D_6, 202.3 MHz):** δ 83.15 (s). **^{1}H NMR (C_6D_6, 500 MHz):** δ 7.04 (s, 2H, Ar-*H*), 3.41 (vt, J_{PH} = 3.0 Hz, 4H, CH_2P), 2.35 (s, 3H, Ar-CH_3), 1.29 (vt, J_{PH} = 6.5 Hz, 36H, P^{t}Bu). **^{13}C NMR (C_6D_6, 125.67 MHz):** δ 208.77 (s, Ir-*C*O), 156.02 (s, σ-*C*), 128.4(s, *ρ*-*C*), 121.44 (vt, J_{PC} = 6.8 Hz, *C*(CH$_3$)$_3$), 34.50 (s, *C*H$_3$), 29.84 (vt, J_{PC} = 2.2 Hz, C(*C*H$_3$)$_3$), 22.78 (s), 14.33 (s). **IR (KBr, cm^{-1}):** ν_{IrCO} = 1926.4 (s).

(Me-PCP)Ir(ethylene), 2-15

To a solution of 9.5 mg (Me-PCP)IrH$_n$ (15.8 μmol) in pentane, 1 atm ethylene was added in a J. Young NMR tube. Solution changed from dark red to brown in color. Remove solvent *in vacuo*, leaving a

brown solid which was dissolved in *p*-xylene-d_{10}. (Me-PCP)Ir-ethylene was formed in 98% yield as determined by NMR spectroscopy. **^{31}P NMR (*p*-xylene$_{d10}$, 161.9 MHz):** δ 59.62 (s). **^{1}H NMR (*p*-xylene$_{d10}$, 400 MHz):** δ 7.070 (s, 1H, Ar-*H*), 7.009 (s, 1H, Ar-*H*), 3.42 (vt, *J* = 3.4 Hz, 4H, ethylene), 3.27 (vt, *J* = 3.0 Hz, 4H, CH_2P), 3.98 (s, 3H, Ar-CH_3), 1.26 (t, *J* = 5.8 Hz, 36H, P^{t}bu).

(Me-PCP)Ir(Ph)(H), 2-16

To a solution of 9.5 mg (Me-PCP)IrH_n (15.8 μmol) in *p*-xylene-d_{10}, a solution of 90 μL C_6H_6 (1.01 mmol) in 140 μL TBE (1.09 mmol) was added in a J. Young NMR tube. Solution was mixed and NMR characterization completed. **^{31}P NMR (*p*-xylene-d_{10}, 202.3 MHz):** δ 68.06 (s). **^{1}H NMR (*p*-xylene-d_{10}, 500 MHz):** δ 6.82 (s, 2H, Ar-*H*), 2.03 (vt, 4H, CH_2P), 1.53 (s, 3H, Ar-CH_3), 0.872 (s, 36H, P^{t}Bu$_2$).

(Me-PCP)Ir(H)(Benzophenone), 2-17

To a solution of 9.5 mg (Me-PCP)IrH_n (15.8 μmol) in C_6D_6, a solution of excess benzophenone in 140 μL TBE (1.09 mmol) was added in a J. Young NMR tube. Solution was mixed and NMR characterization completed. **^{31}P NMR (C_6D_6, 202.3 MHz):** δ 58.65 (s). **^{1}H NMR (C_6D_6, 500 MHz):** δ 7.97 (d, 2H, aromatic), 7.92 (d, 2H, Ar-*H*), 7.80 (t, 4H, Ar-*H*), 7.76 (d, 2H, Ar-*H*), 7.32 (t, 8H, Ar-*H*), 7.28 (s, 1H, Ar-*H*), 3.31 (d of vt, 2H, CH_2P), 3.03 (d of vt, 2H, CH_2P), 2.40 (s, 3H, Ar-CH_3), 1.42 (t, 18H, P^{t}Bu$_2$), 1.13 (t, 18H, P^{t}Bu$_2$), -9.023 (t, 1H, Ir-*H*).

(Me-PCP)IrN_2 monomer, 2-18, and (Me-PCP)IrN_2 dimer, 2-19

In a J. Young NMR tube, a solution of 9.5 mg (Me-PCP)IrH_n (16 μmol) in *p*-xylene-d_{10} was degassed and 1 atm N_2 was added. Upon mixing the solution changed from dark red to orange. Both the monomer and dimer were observed in solution by NMR spectroscopy. **(Me-PCP)IrN_2 monomer, 2-18: ^{31}P NMR (*p*-xylene-d_{10}, 202.3 MHz):** δ 73.24 (s). **^{1}H NMR (*p*-xylene-d_{10}, 500 MHz):** δ 6.86 (s, 1H, Ar-*H*), 6.53 (s, 1H, Ar-*H*), 3.18 (vt, *J*=3.80 Hz, 4H, CH_2P), 2.31 (s, 3H, Ar-CH_3), 1.35 (t, 36H, *J* = 6.3 Hz, P^{t}bu). **(Me-PCP)IrN_2 dimer, 2-19**: **^{31}P NMR (*p*-xylene-d_{10}, 202.3 MHz):** δ 74.9 (s). **^{1}H NMR (*p*-xylene-d_{10}, 500 MHz):** δ 6.90 (s, 1H, Ar-*H*), 6.60 (s, 1H, Ar-*H*), 3.20 (vt, 4H, *J* = 2.9 Hz, CH_2P), 2.35 (s, 3H, Ar-CH_3), 1.42 (t, *J* = 6.4 Hz, 36H, P^{t}bu).

(Me-PCP)Ir(H)(OH), 2-20

5 mg of a mixture of **2-9** and **2-10** was dissolved in *p*-xylene-d_{10} and 0.05 mL TBE (0.4 mmol) was added to the solution. After ten minutes, the solution changed from red to dark red in color. 0.2 μL (11 umol) degassed, deionized water was added and solution was mixed. The compound was characterized *in situ*. **^{31}P NMR (*p*-xylene-d_{10}, 161.9 MHz):** δ 64.87 (d). **^{1}H NMR (*p*-xylene-d_{10}, 400 MHz):** δ 7.30 (s, 2H, Ar-*H*), 5.28 (bs, 1H, Ir-O*H*), 3.30 (d of vt, J_{PH} = 16 Hz, J_{HH} = 4 Hz, 2H, CH_2P), 3.19 (d of vt, J_{PH} = 16 Hz, J_{HH} = 4 Hz, 2H, CH_2P), 2.54 (s, 3H, Ar-CH_3), 1.57 (t, J_{PH} = 6 Hz, 18H, P^{t}bu), 1.48 (t, J_{PH} = 6 Hz, 18H, P^{t}bu), -31.0 (t, J_{PH} = 12 Hz, Ir-*H*).

Reaction of 2-12 under vacuum

5 mg of a mixture of **2-9** and **2-10** was dissolved in *p*-xylene-d_{10} and 0.05 mL TBE (0.4 mmol) was added to the solution. After ten minutes, the solution changed from red to dark red in color. Excess volatiles and ~50% solvent were removed followed by addition of fresh solvent. Process was repeated multiple times and NMR spectra were obtained. Multiple complexes were observed by ^{31}P NMR spectroscopy including **2-14**, **2-18**, **2-19**, and **2-20.**

Figure 2.1 Crystal Structure of (Me-PCP)IrHCl, **2-9**

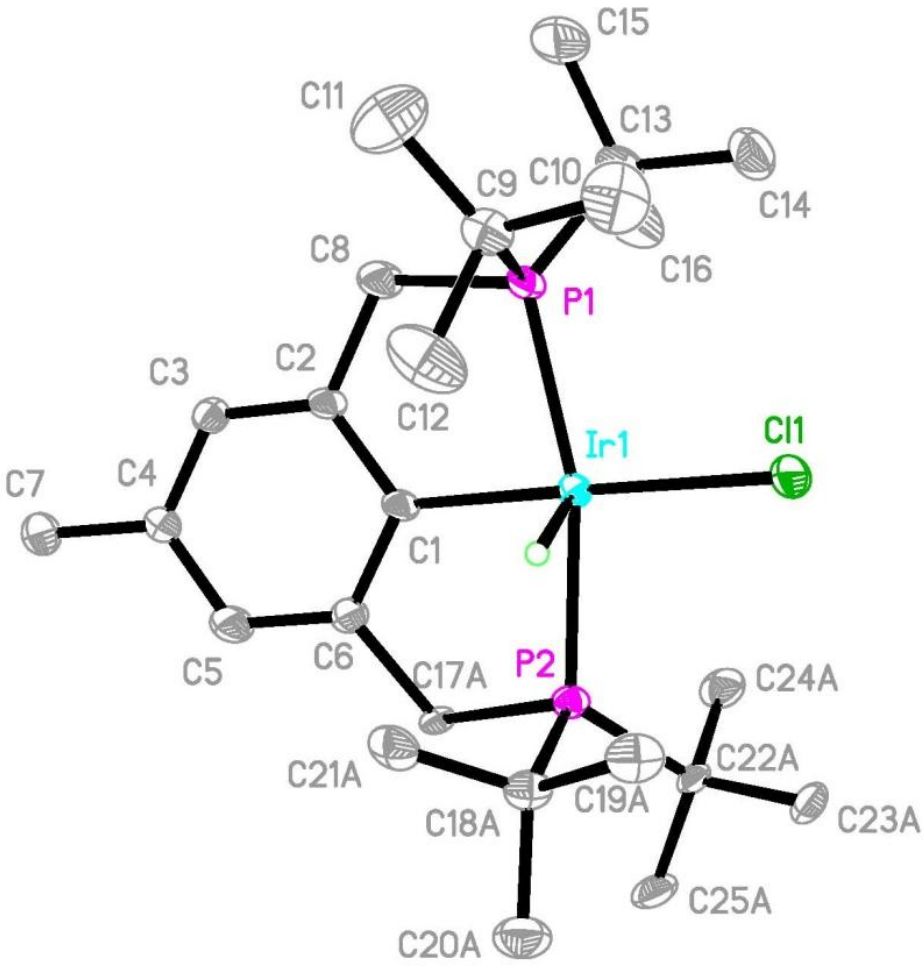

Table 2.1 Crystal Data and Structure Refinement for (Me-PCP)IrHCl, **2-9**

Identification code	me_hcl	
Empirical formula	C25 H46 Cl Ir P2	
Formula weight	636.21	
Temperature	100(2) K	
Wavelength	0.71073 Å	
Crystal system	Monoclinic	
Space group	P2(1)/n	
Unit cell dimensions	a = 7.918(4) Å	□= 90°.
	b = 24.314(12) Å	□= 98.705(9)°.
	c = 14.102(7) Å	□ = 90°.
Volume	2683(2) $Å^3$	
Z	4	
Density (calculated)	1.575 Mg/m^3	
Absorption coefficient	5.204 mm^{-1}	
F(000)	1280	
Crystal size	0.33 x 0.22 x 0.07 mm^3	
Theta range for data collection	1.68 to 30.61°.	
Index ranges	-11<=h<=11, -34<=k<=34, -20<=l<=19	
Reflections collected	35142	
Independent reflections	8225 [R(int) = 0.0470]	
Completeness to theta = 30.61°	99.4 %	
Absorption correction	Semi-empirical from equivalents	
Max. and min. transmission	0.7121 and 0.2785	
Refinement method	Full-matrix least-squares on F^2	
Data / restraints / parameters	8225 / 334 / 368	
Goodness-of-fit on F^2	1.013	
Final R indices [I>2sigma(I)]	R1 = 0.0385, wR2 = 0.0793	
R indices (all data)	R1 = 0.0479, wR2 = 0.0829	
Largest diff. peak and hole	2.468 and -1.101 $e.Å^{-3}$	

Table 2.2 Atomic Coordinates (x 10^4) and Equivalent Isotropic Displacement Parameters ($Å^2$x 10^3) for (Me-PCP)IrHCl, **2-9**. U(eq) is defined as one third of the trace of the orthogonalized U^{ij} tensor.

	x	y	z	U(eq)
Ir(1)	7425(1)	1785(1)	7592(1)	14(1)
P(1)	6343(1)	2582(1)	8156(1)	16(1)
P(2)	8478(1)	912(1)	7410(1)	15(1)
Cl(1)	8653(2)	2199(1)	6282(1)	32(1)
C(1)	6549(5)	1440(2)	8736(3)	16(1)
C(2)	5634(5)	1749(2)	9345(3)	16(1)
C(3)	5139(5)	1518(2)	10162(3)	17(1)
C(4)	5480(5)	974(2)	10412(3)	20(1)
C(5)	6322(7)	659(2)	9804(4)	32(1)
C(6)	6806(7)	884(2)	8974(3)	33(1)
C(7)	4920(6)	732(2)	11297(3)	27(1)
C(8)	5111(6)	2326(2)	9067(3)	25(1)
C(9)	8161(6)	2981(2)	8849(3)	24(1)
C(10)	9070(7)	3325(2)	8176(4)	41(1)
C(11)	7694(8)	3336(3)	9654(5)	52(2)
C(12)	9424(7)	2529(3)	9273(5)	49(2)
C(13)	4804(5)	3040(2)	7377(3)	23(1)
C(14)	5607(7)	3292(2)	6558(3)	32(1)
C(15)	4102(8)	3501(2)	7952(4)	43(1)
C(16)	3328(8)	2670(3)	6935(5)	54(2)
C(17A)	7243(10)	496(3)	8158(5)	12(1)
C(18A)	10719(10)	839(3)	8019(6)	19(1)
C(19A)	11837(11)	1270(4)	7570(7)	25(2)
C(20A)	11530(30)	275(5)	7944(11)	31(3)
C(21A)	10797(11)	951(4)	9075(6)	25(2)
C(22A)	8098(11)	564(3)	6204(5)	16(1)
C(23A)	9353(12)	757(4)	5575(6)	24(2)
C(24A)	6275(12)	750(4)	5743(7)	26(2)
C(25A)	8100(30)	-59(5)	6253(17)	26(3)
C(17B)	8160(15)	561(4)	8504(7)	32(2)
C(18B)	10880(12)	846(4)	7444(9)	36(2)
C(19B)	11344(17)	1002(6)	6429(9)	57(3)
C(20B)	11570(30)	272(6)	7670(11)	36(3)

C(21B)	11663(18)	1265(6)	8125(11)	58(3)
C(22B)	7299(14)	506(4)	6390(7)	35(2)
C(23B)	7180(20)	792(5)	5459(8)	52(3)
C(24B)	5415(14)	471(6)	6617(10)	51(3)
C(25B)	7880(30)	-86(6)	6350(20)	40(4)

Table 2.3 Bond Lengths (Å) and Bond Angles (˚) for (Me-PCP)IrHCl, **2-9**

Ir(1)-C(1)	2.031(4)	C(9)-C(12)	1.544(7)
Ir(1)-P(2)	2.3074(14)	C(10)-H(10A)	0.9800
Ir(1)-P(1)	2.3095(14)	C(10)-H(10B)	0.9800
Ir(1)-Cl(1)	2.4324(13)	C(10)-H(10C)	0.9800
Ir(1)-H(1A)	1.580(10)	C(11)-H(11A)	0.9800
Ir(1)-H(1B)	1.599(10)	C(11)-H(11B)	0.9800
P(1)-C(8)	1.835(4)	C(11)-H(11C)	0.9800
P(1)-C(13)	1.877(4)	C(12)-H(12A)	0.9800
P(1)-C(9)	1.881(4)	C(12)-H(12B)	0.9800
P(2)-C(17B)	1.815(10)	C(12)-H(12C)	0.9800
P(2)-C(17A)	1.845(7)	C(13)-C(14)	1.529(7)
P(2)-C(18A)	1.859(8)	C(13)-C(16)	1.531(7)
P(2)-C(22B)	1.873(10)	C(13)-C(15)	1.536(7)
P(2)-C(22A)	1.883(8)	C(14)-H(14A)	0.9800
P(2)-C(18B)	1.902(10)	C(14)-H(14B)	0.9800
C(1)-C(6)	1.400(6)	C(14)-H(14C)	0.9800
C(1)-C(2)	1.420(5)	C(15)-H(15A)	0.9800
C(2)-C(3)	1.390(5)	C(15)-H(15B)	0.9800
C(2)-C(8)	1.499(6)	C(15)-H(15C)	0.9800
C(3)-C(4)	1.384(6)	C(16)-H(16A)	0.9800
C(3)-H(3)	0.9500	C(16)-H(16B)	0.9800
C(4)-C(5)	1.392(6)	C(16)-H(16C)	0.9800
C(4)-C(7)	1.507(6)	C(17A)-H(17A)	0.9900
C(5)-C(6)	1.398(6)	C(17A)-H(17B)	0.9900
C(5)-H(5)	0.9500	C(18A)-C(21A)	1.507(11)
C(6)-C(17B)	1.556(11)	C(18A)-C(20A)	1.524(12)
C(6)-C(17A)	1.566(8)	C(18A)-C(19A)	1.564(12)
C(7)-H(7A)	0.9800	C(19A)-H(19A)	0.9800
C(7)-H(7B)	0.9800	C(19A)-H(19B)	0.9800
C(7)-H(7C)	0.9800	C(19A)-H(19C)	0.9800
C(8)-H(8A)	0.9900	C(20A)-H(20A)	0.9800
C(8)-H(8B)	0.9900	C(20A)-H(20B)	0.9800
C(9)-C(11)	1.515(7)	C(20A)-H(20C)	0.9800
C(9)-C(10)	1.524(7)	C(21A)-H(21A)	0.9800

C(21A)-H(21B)	0.9800	C(19B)-H(19E)	0.9800
C(21A)-H(21C)	0.9800	C(19B)-H(19F)	0.9800
C(22A)-C(23A)	1.504(11)	C(20B)-H(20D)	0.9800
C(22A)-C(25A)	1.517(12)	C(20B)-H(20E)	0.9800
C(22A)-C(24A)	1.556(12)	C(20B)-H(20F)	0.9800
C(23A)-H(23A)	0.9800	C(21B)-H(21D)	0.9800
C(23A)-H(23B)	0.9800	C(21B)-H(21E)	0.9800
C(23A)-H(23C)	0.9800	C(21B)-H(21F)	0.9800
C(24A)-H(24A)	0.9800	C(22B)-C(23B)	1.476(14)
C(24A)-H(24B)	0.9800	C(22B)-C(25B)	1.516(13)
C(24A)-H(24C)	0.9800	C(22B)-C(24B)	1.575(15)
C(25A)-H(25A)	0.9800	C(23B)-H(23D)	0.9800
C(25A)-H(25B)	0.9800	C(23B)-H(23E)	0.9800
C(25A)-H(25C)	0.9800	C(23B)-H(23F)	0.9800
C(17B)-H(17C)	0.9900	C(24B)-H(24D)	0.9800
C(17B)-H(17D)	0.9900	C(24B)-H(24E)	0.9800
C(18B)-C(21B)	1.472(14)	C(24B)-H(24F)	0.9800
C(18B)-C(20B)	1.515(13)	C(25B)-H(25D)	0.9800
C(18B)-C(19B)	1.577(14)	C(25B)-H(25E)	0.9800
C(19B)-H(19D)	0.9800	C(25B)-H(25F)	0.9800

C(1)-Ir(1)-P(2)	83.18(12)	C(17B)-P(2)-Ir(1)	103.9(3)
C(1)-Ir(1)-P(1)	83.32(12)	C(17A)-P(2)-Ir(1)	102.1(2)
P(2)-Ir(1)-P(1)	165.73(4)	C(18A)-P(2)-Ir(1)	111.9(3)
C(1)-Ir(1)-Cl(1)	176.37(11)	C(22B)-P(2)-Ir(1)	115.1(3)
P(2)-Ir(1)-Cl(1)	95.97(4)	C(22A)-P(2)-Ir(1)	120.2(3)
P(1)-Ir(1)-Cl(1)	97.21(5)	C(18B)-P(2)-Ir(1)	116.9(3)
C(1)-Ir(1)-H(1A)	90.1(8)	C(6)-C(1)-C(2)	115.7(4)
P(2)-Ir(1)-H(1A)	69.1(5)	C(6)-C(1)-Ir(1)	122.3(3)
P(1)-Ir(1)-H(1A)	106.3(5)	C(2)-C(1)-Ir(1)	122.0(3)
Cl(1)-Ir(1)-H(1A)	86.3(8)	C(3)-C(2)-C(1)	121.4(4)
C(1)-Ir(1)-H(1B)	107.3(13)	C(3)-C(2)-C(8)	119.7(4)
P(2)-Ir(1)-H(1B)	94.7(5)	C(1)-C(2)-C(8)	118.9(4)
P(1)-Ir(1)-H(1B)	93.8(4)	C(4)-C(3)-C(2)	121.9(4)
Cl(1)-Ir(1)-H(1B)	76.3(12)	C(4)-C(3)-H(3)	119.0
H(1A)-Ir(1)-H(1B)	155.0(10)	C(2)-C(3)-H(3)	119.0
C(8)-P(1)-C(13)	104.1(2)	C(3)-C(4)-C(5)	117.5(4)
C(8)-P(1)-C(9)	104.9(2)	C(3)-C(4)-C(7)	120.9(4)
C(13)-P(1)-C(9)	112.1(2)	C(5)-C(4)-C(7)	121.6(4)
C(8)-P(1)-Ir(1)	102.75(15)	C(4)-C(5)-C(6)	121.2(4)
C(13)-P(1)-Ir(1)	122.47(15)	C(4)-C(5)-H(5)	119.4
C(9)-P(1)-Ir(1)	108.52(15)	C(6)-C(5)-H(5)	119.4
C(17B)-P(2)-C(17A)	26.1(4)	C(5)-C(6)-C(1)	122.1(4)
C(17B)-P(2)-C(18A)	78.9(5)	C(5)-C(6)-C(17B)	116.9(5)
C(17A)-P(2)-C(18A)	103.6(4)	C(1)-C(6)-C(17B)	118.1(5)
C(17B)-P(2)-C(22B)	106.7(5)	C(5)-C(6)-C(17A)	119.9(5)
C(17A)-P(2)-C(22B)	84.5(5)	C(1)-C(6)-C(17A)	116.5(4)
C(18A)-P(2)-C(22B)	129.3(4)	C(17B)-C(6)-C(17A)	30.7(5)
C(17B)-P(2)-C(22A)	122.2(4)	C(4)-C(7)-H(7A)	109.5
C(17A)-P(2)-C(22A)	104.2(4)	C(4)-C(7)-H(7B)	109.5
C(18A)-P(2)-C(22A)	112.6(4)	H(7A)-C(7)-H(7B)	109.5
C(22B)-P(2)-C(22A)	22.5(3)	C(4)-C(7)-H(7C)	109.5
C(17B)-P(2)-C(18B)	101.9(5)	H(7A)-C(7)-H(7C)	109.5
C(17A)-P(2)-C(18B)	123.6(4)	H(7B)-C(7)-H(7C)	109.5
C(18A)-P(2)-C(18B)	25.8(3)	C(2)-C(8)-P(1)	110.2(3)
C(22B)-P(2)-C(18B)	110.7(5)	C(2)-C(8)-H(8A)	109.6
C(22A)-P(2)-C(18B)	90.4(5)	P(1)-C(8)-H(8A)	109.6

C(2)-C(8)-H(8B)	109.6	C(13)-C(14)-H(14C)	109.5
P(1)-C(8)-H(8B)	109.6	H(14A)-C(14)-H(14C)	109.5
H(8A)-C(8)-H(8B)	108.1	H(14B)-C(14)-H(14C)	109.5
C(11)-C(9)-C(10)	110.3(5)	C(13)-C(15)-H(15A)	109.5
C(11)-C(9)-C(12)	109.3(5)	C(13)-C(15)-H(15B)	109.5
C(10)-C(9)-C(12)	107.0(4)	H(15A)-C(15)-H(15B)	109.5
C(11)-C(9)-P(1)	115.3(4)	C(13)-C(15)-H(15C)	109.5
C(10)-C(9)-P(1)	110.9(3)	H(15A)-C(15)-H(15C)	109.5
C(12)-C(9)-P(1)	103.5(3)	H(15B)-C(15)-H(15C)	109.5
C(9)-C(10)-H(10A)	109.5	C(13)-C(16)-H(16A)	109.5
C(9)-C(10)-H(10B)	109.5	C(13)-C(16)-H(16B)	109.5
H(10A)-C(10)-H(10B)	109.5	H(16A)-C(16)-H(16B)	109.5
C(9)-C(10)-H(10C)	109.5	C(13)-C(16)-H(16C)	109.5
H(10A)-C(10)-H(10C)	109.5	H(16A)-C(16)-H(16C)	109.5
H(10B)-C(10)-H(10C)	109.5	H(16B)-C(16)-H(16C)	109.5
C(9)-C(11)-H(11A)	109.5	C(6)-C(17A)-P(2)	106.6(4)
C(9)-C(11)-H(11B)	109.5	C(6)-C(17A)-H(17A)	110.4
H(11A)-C(11)-H(11B)	109.5	P(2)-C(17A)-H(17A)	110.4
C(9)-C(11)-H(11C)	109.5	C(6)-C(17A)-H(17B)	110.4
H(11A)-C(11)-H(11C)	109.5	P(2)-C(17A)-H(17B)	110.4
H(11B)-C(11)-H(11C)	109.5	H(17A)-C(17A)-H(17B)	108.6
C(9)-C(12)-H(12A)	109.5	C(21A)-C(18A)-C(20A)	106.0(8)
C(9)-C(12)-H(12B)	109.5	C(21A)-C(18A)-C(19A)	109.8(7)
H(12A)-C(12)-H(12B)	109.5	C(20A)-C(18A)-C(19A)	107.7(9)
C(9)-C(12)-H(12C)	109.5	C(21A)-C(18A)-P(2)	109.4(6)
H(12A)-C(12)-H(12C)	109.5	C(20A)-C(18A)-P(2)	115.8(9)
H(12B)-C(12)-H(12C)	109.5	C(19A)-C(18A)-P(2)	108.0(6)
C(14)-C(13)-C(16)	107.9(4)	C(23A)-C(22A)-C(25A)	110.0(9)
C(14)-C(13)-C(15)	109.3(4)	C(23A)-C(22A)-C(24A)	108.5(7)
C(16)-C(13)-C(15)	109.2(5)	C(25A)-C(22A)-C(24A)	107.6(10)
C(14)-C(13)-P(1)	111.9(3)	C(23A)-C(22A)-P(2)	111.3(6)
C(16)-C(13)-P(1)	106.2(3)	C(25A)-C(22A)-P(2)	114.1(10)
C(15)-C(13)-P(1)	112.2(3)	C(24A)-C(22A)-P(2)	105.0(5)
C(13)-C(14)-H(14A)	109.5	C(6)-C(17B)-P(2)	108.5(6)
C(13)-C(14)-H(14B)	109.5	C(6)-C(17B)-H(17C)	110.0
H(14A)-C(14)-H(14B)	109.5	P(2)-C(17B)-H(17C)	110.0

C(6)-C(17B)-H(17D)	110.0	H(21E)-C(21B)-H(21F)	109.5
P(2)-C(17B)-H(17D)	110.0	C(23B)-C(22B)-C(25B)	113.1(13)
H(17C)-C(17B)-H(17D)	108.4	C(23B)-C(22B)-C(24B)	105.8(10)
C(21B)-C(18B)-C(20B)	113.4(11)	C(25B)-C(22B)-C(24B)	104.9(11)
C(21B)-C(18B)-C(19B)	107.0(11)	C(23B)-C(22B)-P(2)	113.1(9)
C(20B)-C(18B)-C(19B)	106.7(10)	C(25B)-C(22B)-P(2)	114.3(12)
C(21B)-C(18B)-P(2)	106.2(9)	C(24B)-C(22B)-P(2)	104.5(8)
C(20B)-C(18B)-P(2)	114.2(10)	C(22B)-C(23B)-H(23D)	109.5
C(19B)-C(18B)-P(2)	109.0(8)	C(22B)-C(23B)-H(23E)	109.5
C(18B)-C(19B)-H(19D)	109.5	H(23D)-C(23B)-H(23E)	109.5
C(18B)-C(19B)-H(19E)	109.5	C(22B)-C(23B)-H(23F)	109.5
H(19D)-C(19B)-H(19E)	109.5	H(23D)-C(23B)-H(23F)	109.5
C(18B)-C(19B)-H(19F)	109.5	H(23E)-C(23B)-H(23F)	109.5
H(19D)-C(19B)-H(19F)	109.5	C(22B)-C(24B)-H(24D)	109.5
H(19E)-C(19B)-H(19F)	109.5	C(22B)-C(24B)-H(24E)	109.5
C(18B)-C(20B)-H(20D)	109.5	H(24D)-C(24B)-H(24E)	109.5
C(18B)-C(20B)-H(20E)	109.5	C(22B)-C(24B)-H(24F)	109.5
H(20D)-C(20B)-H(20E)	109.5	H(24D)-C(24B)-H(24F)	109.5
C(18B)-C(20B)-H(20F)	109.5	H(24E)-C(24B)-H(24F)	109.5
H(20D)-C(20B)-H(20F)	109.5	C(22B)-C(25B)-H(25D)	109.5
H(20E)-C(20B)-H(20F)	109.5	C(22B)-C(25B)-H(25E)	109.5
C(18B)-C(21B)-H(21D)	109.5	H(25D)-C(25B)-H(25E)	109.5
C(18B)-C(21B)-H(21E)	109.5	C(22B)-C(25B)-H(25F)	109.5
H(21D)-C(21B)-H(21E)	109.5	H(25D)-C(25B)-H(25F)	109.5
C(18B)-C(21B)-H(21F)	109.5	H(25E)-C(25B)-H(25F)	109.5
H(21D)-C(21B)-H(21F)	109.5		

Table 2.4 Anisotropic Displacement Parameters ($Å^2 x\ 10^3$) for (Me-PCP)IrHCl, **2-9**. The anisotropic displacement factor exponent takes the form: $-2\pi^2[\ h^2\ a^{*2}U^{11} + ...\ + 2\ h\ k\ a^*\ b^*\ U^{12}\ ]$

	U^{11}	U^{22}	U^{33}	U^{23}	U^{13}	U^{12}
Ir(1)	17(1)	12(1)	15(1)	1(1)	5(1)	-1(1)
P(1)	17(1)	11(1)	20(1)	2(1)	4(1)	0(1)
P(2)	16(1)	12(1)	20(1)	0(1)	5(1)	0(1)
Cl(1)	44(1)	23(1)	36(1)	12(1)	26(1)	9(1)
C(1)	21(2)	9(2)	17(2)	-1(1)	1(1)	-1(1)
C(2)	18(2)	10(2)	21(2)	-1(1)	4(1)	-1(1)
C(3)	20(2)	15(2)	18(2)	-1(1)	6(1)	-2(1)
C(4)	25(2)	16(2)	20(2)	2(1)	5(2)	2(2)
C(5)	51(3)	17(2)	35(3)	10(2)	23(2)	9(2)
C(6)	58(3)	17(2)	29(2)	9(2)	28(2)	12(2)
C(7)	37(3)	22(2)	25(2)	6(2)	14(2)	1(2)
C(8)	29(2)	15(2)	33(2)	3(2)	14(2)	-1(2)
C(9)	22(2)	20(2)	27(2)	0(2)	-2(2)	-2(2)
C(10)	35(3)	40(3)	49(3)	-4(2)	5(2)	-21(2)
C(11)	50(4)	52(4)	51(4)	-24(3)	3(3)	-8(3)
C(12)	34(3)	42(4)	63(4)	12(3)	-16(3)	0(3)
C(13)	20(2)	19(2)	30(2)	3(2)	1(2)	-1(2)
C(14)	34(2)	34(3)	29(2)	11(2)	3(2)	8(2)
C(15)	44(3)	38(3)	48(3)	9(2)	13(3)	23(3)
C(16)	41(3)	42(4)	67(4)	15(3)	-28(3)	-13(3)
C(17A)	13(3)	6(3)	19(3)	-3(2)	7(2)	-4(3)
C(18A)	12(3)	19(3)	26(3)	-1(3)	4(3)	0(3)
C(19A)	13(3)	24(4)	38(4)	-2(3)	5(3)	-5(3)
C(20A)	27(5)	29(4)	37(6)	0(4)	4(5)	10(4)
C(21A)	21(4)	26(4)	24(3)	1(3)	-8(3)	5(3)
C(22A)	21(3)	12(3)	16(3)	-3(2)	9(3)	0(3)
C(23A)	32(4)	22(4)	22(4)	-2(3)	17(3)	2(3)
C(24A)	31(4)	26(4)	21(4)	-8(3)	0(3)	4(3)
C(25A)	34(5)	17(4)	31(5)	-6(4)	16(4)	4(4)
C(17B)	43(5)	21(4)	33(4)	1(3)	14(4)	4(4)
C(18B)	23(4)	32(4)	53(4)	4(4)	5(4)	4(3)

C(19B)	45(6)	61(7)	72(6)	21(5)	25(5)	10(5)
C(20B)	25(5)	37(5)	48(7)	13(4)	6(5)	11(4)
C(21B)	43(5)	51(5)	77(6)	-2(5)	-6(5)	-5(5)
C(22B)	41(4)	27(4)	35(4)	-7(3)	-5(4)	6(4)
C(23B)	65(6)	45(5)	42(5)	-7(4)	-3(5)	-3(5)
C(24B)	43(5)	48(6)	60(6)	-5(5)	1(4)	0(4)
C(25B)	48(7)	30(5)	40(7)	-11(5)	4(5)	1(5)

Table 2.5 Hydrogen Coordinates (x 10^4) and Isotropic Displacement Parameters ($Å^2$x 10^3) for (Me-PCP)IrHCl, **2-9**.

	x	y	z	U(eq)
H(3)	4549	1739	10560	21
H(5)	6573	284	9957	39
H(7A)	5547	909	11869	41
H(7B)	5157	336	11321	41
H(7C)	3692	793	11278	41
H(8A)	5310	2567	9640	30
H(8B)	3877	2336	8810	30
H(10A)	8393	3654	7980	62
H(10B)	9205	3107	7608	62
H(10C)	10198	3434	8508	62
H(11A)	8723	3517	9985	77
H(11B)	7195	3105	10109	77
H(11C)	6862	3615	9388	77
H(12A)	10309	2692	9751	73
H(12B)	9956	2363	8759	73
H(12C)	8807	2247	9579	73
H(14A)	6129	3001	6218	48
H(14B)	6486	3558	6820	48
H(14C)	4723	3479	6111	48
H(15A)	3163	3688	7545	64
H(15B)	5014	3765	8166	64
H(15C)	3680	3343	8511	64
H(16A)	2697	2541	7439	81
H(16B)	3783	2353	6626	81
H(16C)	2559	2878	6455	81
H(1A)	9321(15)	1731(7)	8125(13)	20
H(17A)	6183	357	7770	14
H(17B)	7928	178	8436	14
H(19A)	11463	1642	7705	37
H(19B)	11709	1214	6875	37
H(19C)	13038	1222	7850	37

H(20A)	12654	267	8343	47
H(20B)	11654	203	7275	47
H(20C)	10796	-7	8166	47
H(21A)	11993	979	9377	37
H(21B)	10243	649	9372	37
H(21C)	10206	1296	9165	37
H(23A)	10481	601	5806	36
H(23B)	9423	1160	5595	36
H(23C)	8974	637	4913	36
H(24A)	6286	1144	5598	39
H(24B)	5469	679	6192	39
H(24C)	5924	543	5149	39
H(25A)	7900	-210	5602	40
H(25B)	7191	-182	6605	40
H(25C)	9207	-186	6585	40
H(1B)	5930(30)	1737(8)	6696(15)	20
H(17C)	7758	180	8356	38
H(17D)	9250	543	8951	38
H(19D)	10591	1299	6148	86
H(19E)	11193	680	6007	86
H(19F)	12535	1125	6500	86
H(20D)	12808	290	7870	54
H(20E)	11316	40	7098	54
H(20F)	11028	114	8189	54
H(21D)	11174	1239	8721	88
H(21E)	11438	1631	7844	88
H(21F)	12900	1204	8262	88
H(23D)	8296	784	5238	78
H(23E)	6833	1175	5532	78
H(23F)	6332	607	4987	78
H(24D)	4988	842	6710	77
H(24E)	5400	255	7202	77
H(24F)	4685	294	6080	77
H(25D)	7092	-286	5867	59
H(25E)	7889	-258	6979	59
H(25F)	9033	-97	6178	59

Table 2.6 Torsion Angles [°] for (Me-PCP)IrHCl, **2-9**

C(1)-Ir(1)-P(1)-C(8)	-10.73(19)	Ir(1)-C(1)-C(2)-C(3)	-175.7(3)
P(2)-Ir(1)-P(1)-C(8)	-29.8(2)	C(6)-C(1)-C(2)-C(8)	-172.2(4)
Cl(1)-Ir(1)-P(1)-C(8)	172.89(16)	Ir(1)-C(1)-C(2)-C(8)	7.7(5)
C(1)-Ir(1)-P(1)-C(13)	-126.9(2)	C(1)-C(2)-C(3)-C(4)	-1.3(6)
P(2)-Ir(1)-P(1)-C(13)	-145.9(2)	C(8)-C(2)-C(3)-C(4)	175.2(4)
Cl(1)-Ir(1)-P(1)-C(13)	56.75(18)	C(2)-C(3)-C(4)-C(5)	-1.0(6)
C(1)-Ir(1)-P(1)-C(9)	100.03(19)	C(2)-C(3)-C(4)-C(7)	-179.6(4)
P(2)-Ir(1)-P(1)-C(9)	81.0(2)	C(3)-C(4)-C(5)-C(6)	0.0(8)
Cl(1)-Ir(1)-P(1)-C(9)	-76.35(16)	C(7)-C(4)-C(5)-C(6)	178.7(5)
C(1)-Ir(1)-P(2)-C(17B)	-10.0(4)	C(4)-C(5)-C(6)-C(1)	3.3(9)
P(1)-Ir(1)-P(2)-C(17B)	9.1(4)	C(4)-C(5)-C(6)-C(17B)	163.3(7)
Cl(1)-Ir(1)-P(2)-C(17B)	166.5(4)	C(4)-C(5)-C(6)-C(17A)	-161.9(6)
C(1)-Ir(1)-P(2)-C(17A)	16.7(3)	C(2)-C(1)-C(6)-C(5)	-5.3(8)
P(1)-Ir(1)-P(2)-C(17A)	35.8(3)	Ir(1)-C(1)-C(6)-C(5)	174.7(4)
Cl(1)-Ir(1)-P(2)-C(17A)	-166.8(3)	C(2)-C(1)-C(6)-C(17B)	-165.1(6)
C(1)-Ir(1)-P(2)-C(18A)	-93.4(3)	Ir(1)-C(1)-C(6)-C(17B)	15.0(8)
P(1)-Ir(1)-P(2)-C(18A)	-74.3(3)	C(2)-C(1)-C(6)-C(17A)	160.3(5)
Cl(1)-Ir(1)-P(2)-C(18A)	83.0(3)	Ir(1)-C(1)-C(6)-C(17A)	-19.6(7)
C(1)-Ir(1)-P(2)-C(22B)	106.3(5)	C(3)-C(2)-C(8)-P(1)	166.3(3)
P(1)-Ir(1)-P(2)-C(22B)	125.4(5)	C(1)-C(2)-C(8)-P(1)	-17.1(5)
Cl(1)-Ir(1)-P(2)-C(22B)	-77.2(4)	C(13)-P(1)-C(8)-C(2)	145.8(3)
C(1)-Ir(1)-P(2)-C(22A)	131.1(3)	C(9)-P(1)-C(8)-C(2)	-96.3(3)
P(1)-Ir(1)-P(2)-C(22A)	150.2(3)	Ir(1)-P(1)-C(8)-C(2)	17.1(3)
Cl(1)-Ir(1)-P(2)-C(22A)	-52.4(3)	C(8)-P(1)-C(9)-C(11)	-41.1(5)
C(1)-Ir(1)-P(2)-C(18B)	-121.2(4)	C(13)-P(1)-C(9)-C(11)	71.3(5)
P(1)-Ir(1)-P(2)-C(18B)	-102.2(4)	Ir(1)-P(1)-C(9)-C(11)	-150.4(4)
Cl(1)-Ir(1)-P(2)-C(18B)	55.2(4)	C(8)-P(1)-C(9)-C(10)	-167.4(4)
P(2)-Ir(1)-C(1)-C(6)	-1.1(4)	C(13)-P(1)-C(9)-C(10)	-55.0(4)
P(1)-Ir(1)-C(1)-C(6)	-176.5(4)	Ir(1)-P(1)-C(9)-C(10)	83.4(4)
Cl(1)-Ir(1)-C(1)-C(6)	-77.8(18)	C(8)-P(1)-C(9)-C(12)	78.3(4)
P(2)-Ir(1)-C(1)-C(2)	178.9(3)	C(13)-P(1)-C(9)-C(12)	-169.4(4)
P(1)-Ir(1)-C(1)-C(2)	3.6(3)	Ir(1)-P(1)-C(9)-C(12)	-31.0(4)
Cl(1)-Ir(1)-C(1)-C(2)	102.2(18)	C(8)-P(1)-C(13)-C(14)	-179.6(3)
C(6)-C(1)-C(2)-C(3)	4.4(6)	C(9)-P(1)-C(13)-C(14)	67.5(4)

Ir(1)-P(1)-C(13)-C(14)	-64.1(4)	C(18A)-P(2)-C(22A)-C(23A)	-53.8(7)
C(8)-P(1)-C(13)-C(16)	-62.1(4)	C(22B)-P(2)-C(22A)-C(23A)	164.3(14)
C(9)-P(1)-C(13)-C(16)	-175.0(4)	C(18B)-P(2)-C(22A)-C(23A)	-40.4(7)
Ir(1)-P(1)-C(13)-C(16)	53.4(4)	Ir(1)-P(2)-C(22A)-C(23A)	81.3(6)
C(8)-P(1)-C(13)-C(15)	57.1(4)	C(17B)-P(2)-C(22A)-C(25A)	-19.5(11)
C(9)-P(1)-C(13)-C(15)	-55.8(4)	C(17A)-P(2)-C(22A)-C(25A)	-40.1(10)
Ir(1)-P(1)-C(13)-C(15)	172.6(3)	C(18A)-P(2)-C(22A)-C(25A)	71.5(10)
C(5)-C(6)-C(17A)-P(2)	-161.5(5)	C(22B)-P(2)-C(22A)-C(25A)	-70.4(13)
C(1)-C(6)-C(17A)-P(2)	32.5(7)	C(18B)-P(2)-C(22A)-C(25A)	84.8(10)
C(17B)-C(6)-C(17A)-P(2)	-68.5(9)	Ir(1)-P(2)-C(22A)-C(25A)	-153.4(9)
C(17B)-P(2)-C(17A)-C(6)	67.8(9)	C(17B)-P(2)-C(22A)-C(24A)	98.1(7)
C(18A)-P(2)-C(17A)-C(6)	87.2(5)	C(17A)-P(2)-C(22A)-C(24A)	77.5(6)
C(22B)-P(2)-C(17A)-C(6)	-143.6(6)	C(18A)-P(2)-C(22A)-C(24A)	-171.0(6)
C(22A)-P(2)-C(17A)-C(6)	-154.9(5)	C(22B)-P(2)-C(22A)-C(24A)	47.1(11)
C(18B)-P(2)-C(17A)-C(6)	105.0(6)	C(18B)-P(2)-C(22A)-C(24A)	-157.6(6)
Ir(1)-P(2)-C(17A)-C(6)	-29.2(5)	Ir(1)-P(2)-C(22A)-C(24A)	-35.9(7)
C(17B)-P(2)-C(18A)-C(21A)	-40.6(6)	C(5)-C(6)-C(17B)-P(2)	176.8(5)
C(17A)-P(2)-C(18A)-C(21A)	-49.2(7)	C(1)-C(6)-C(17B)-P(2)	-22.4(9)
C(22B)-P(2)-C(18A)-C(21A)	-143.3(7)	C(17A)-C(6)-C(17B)-P(2)	72.8(9)
C(22A)-P(2)-C(18A)-C(21A)	-161.1(6)	C(17A)-P(2)-C(17B)-C(6)	-70.3(9)
C(18B)-P(2)-C(18A)-C(21A)	166.9(12)	C(18A)-P(2)-C(17B)-C(6)	128.8(7)
Ir(1)-P(2)-C(18A)-C(21A)	60.0(6)	C(22B)-P(2)-C(17B)-C(6)	-103.2(7)
C(17B)-P(2)-C(18A)-C(20A)	79.0(9)	C(22A)-P(2)-C(17B)-C(6)	-121.3(6)
C(17A)-P(2)-C(18A)-C(20A)	70.5(9)	C(18B)-P(2)-C(17B)-C(6)	140.7(7)
C(22B)-P(2)-C(18A)-C(20A)	-23.6(11)	Ir(1)-P(2)-C(17B)-C(6)	18.8(7)
C(22A)-P(2)-C(18A)-C(20A)	-41.4(9)	C(17B)-P(2)-C(18B)-C(21B)	-78.6(9)
C(18B)-P(2)-C(18A)-C(20A)	-73.5(11)	C(17A)-P(2)-C(18B)-C(21B)	-94.3(9)
Ir(1)-P(2)-C(18A)-C(20A)	179.7(8)	C(18A)-P(2)-C(18B)-C(21B)	-51.0(11)
C(17B)-P(2)-C(18A)-C(19A)	-160.1(7)	C(22B)-P(2)-C(18B)-C(21B)	168.3(9)
C(17A)-P(2)-C(18A)-C(19A)	-168.6(6)	C(22A)-P(2)-C(18B)-C(21B)	158.4(9)
C(22B)-P(2)-C(18A)-C(19A)	97.3(8)	Ir(1)-P(2)-C(18B)-C(21B)	33.9(10)
C(22A)-P(2)-C(18A)-C(19A)	79.5(6)	C(17B)-P(2)-C(18B)-C(20B)	47.2(10)
C(18B)-P(2)-C(18A)-C(19A)	47.4(9)	C(17A)-P(2)-C(18B)-C(20B)	31.5(11)
Ir(1)-P(2)-C(18A)-C(19A)	-59.5(6)	C(18A)-P(2)-C(18B)-C(20B)	74.8(12)
C(17B)-P(2)-C(22A)-C(23A)	-144.7(7)	C(22B)-P(2)-C(18B)-C(20B)	-66.0(11)
C(17A)-P(2)-C(22A)-C(23A)	-165.3(6)	C(22A)-P(2)-C(18B)-C(20B)	-75.9(10)

Ir(1)-P(2)-C(18B)-C(20B)	159.6(8)	C(17B)-P(2)-C(22B)-C(25B)	-58.8(12)
C(17B)-P(2)-C(18B)-C(19B)	166.5(8)	C(17A)-P(2)-C(22B)-C(25B)	-72.6(12)
C(17A)-P(2)-C(18B)-C(19B)	150.8(7)	C(18A)-P(2)-C(22B)-C(25B)	30.5(14)
C(18A)-P(2)-C(18B)-C(19B)	-165.9(14)	C(22A)-P(2)-C(22B)-C(25B)	77.9(14)
C(22B)-P(2)-C(18B)-C(19B)	53.3(9)	C(18B)-P(2)-C(22B)-C(25B)	51.3(13)
C(22A)-P(2)-C(18B)-C(19B)	43.4(8)	Ir(1)-P(2)-C(22B)-C(25B)	-173.4(10)
Ir(1)-P(2)-C(18B)-C(19B)	-81.1(8)	C(17B)-P(2)-C(22B)-C(24B)	55.3(8)
C(17B)-P(2)-C(22B)-C(23B)	169.8(9)	C(17A)-P(2)-C(22B)-C(24B)	41.4(7)
C(17A)-P(2)-C(22B)-C(23B)	156.0(10)	C(18A)-P(2)-C(22B)-C(24B)	144.5(7)
C(18A)-P(2)-C(22B)-C(23B)	-100.9(9)	C(22A)-P(2)-C(22B)-C(24B)	-168.0(15)
C(22A)-P(2)-C(22B)-C(23B)	-53.5(12)	C(18B)-P(2)-C(22B)-C(24B)	165.4(7)
C(18B)-P(2)-C(22B)-C(23B)	-80.1(10)	Ir(1)-P(2)-C(22B)-C(24B)	-59.4(8)
Ir(1)-P(2)-C(22B)-C(23B)	55.2(10)		

References

(1) Moulton, C. J.; Shaw, B. L. *J. Chem. Soc., Dalton Trans.* **1976**, 1020.
(2) Albrecht, M.; Morales-Morales, D. *Iridium Complexes in Organic Synthesis* **2009**, 299.
(3) Azerraf, C.; Gelman, D. *Organometallics* **2009**, *28*, 6578.
(4) Nawara-Hultzsch, A. J.; Hackenberg, J.; Punji, B.; Supplee, C.; Emge, T.; Bailey, B.; Schrock, R. R.; Brookhart, M.; Goldman, A. S. *ACS Catal.* **2013**, *3*, 2505.
(5) Chianese, A. R.; Mo, A.; Lampland, N. L.; Swartz, R. L.; Bremer, P. T. *Organometallics* **2010**, *29*, 3019.
(6) *The Chemistry of Pincer Compounds*; Morales-Morales, D.; Jensen, C., Eds.; Elsevier: Amsterdam, 2007.
(7) Albrecht, M.; van Koten, G. *Angew. Chem., Intl. Ed.* **2001**, *40*, 3750.
(8) Choi, J.; MacArthur, A. H. R.; Brookhart, M.; Goldman, A. S. *Chem. Rev.* **2011**, *111*, 1761.
(9) Punji, B.; Emge, T. J.; Goldman, A. S. *Abstracts of Papers, 236th ACS National Meeting, Philadelphia, PA, United States, August 17-21, 2008* **2008**, INOR-268.
(10) Punji, B.; Emge, T. J.; Goldman, A. S. *Organometallics* **2010**, *29*, 2702.
(11) Adams, J. J.; Lau, A.; Arulsamy, N.; Roddick, D. M. *Organometallics* **2011**, *30*, 689.
(12) Göttker-Schnetmann, I.; White, P. S.; Brookhart, M. *Organometallics* **2004**, *23*, 1766.
(13) Flores, J. A.; Haibach, M. C.; Goldman, A. S.; American Chemical Society: 2012, p INOR-8.
(14) Ozerov, O. V.; Pelton, E.; Gerber, L.; Weng, W.; Parkin, S. R.; Foxman, B. M. *Abstracts of Papers, 234th ACS National Meeting, Boston, MA, United States, August 19-23, 2007* **2007**, INOR-218.
(15) Zhu, K.; Goldman, A. S., manuscript in preparation.
(16) van der Boom, M. E.; Milstein, D. *Chem. Rev.* **2003**, *103*, 1759.
(17) Kuznetsov, V. F.; Lough, A. J.; Gusev, D. G. *Inorg. Chim. Acta* **2006**, *359*, 2806.
(18) Bonnet, S.; Li, J.; Siegler, M. A.; von Chrzanowski, L. S.; Spek, A. L.; van Koten, G.; Klein Gebbink, R. J. M. *Chem.-Eur. J.* **2009**, *15*, 3340.
(19) Kossoy, E.; Rybtchinski, B.; Diskin-Posner, Y.; Shimon, L. J. W.; Leitus, G.; Milstein, D. *Organometallics* **2009**, *28*, 523.
(20) Boro, B. J.; Duesler, E. N.; Goldberg, K. I.; Kemp, R. A. *Inorg. Chem.* **2009**, *48*, 5081.
(21) Frech, C. M.; Shimon, L. J. W.; Milstein, D. *Organometallics* **2009**, *28*, 1900.
(22) Adams, J. J.; Lau, A.; Arulsamy, N.; Roddick, D. M. *Inorg. Chem.* **2007**, *46*, 11328.
(23) MacInnis, M. C.; MacLean, D. F.; Lundgren, R. J.; McDonald, R.; Turculet, L. *Organometallics* **2007**, *26*, 6522.
(24) Morales-Morales, D.; Lee, D. W.; Wang, Z.; Jensen, C. M. *Organometallics* **2001**, *20*, 1144.
(25) Lee, D. W.; Jensen, C. M.; Morales-Morales, D. *Organometallics* **2003**, *22*, 4744.
(26) Ghosh, R.; Kanzelberger, M.; Emge, T. J.; Hall, G. S.; Goldman, A. S. *Organometallics* **2006**, *25*, 5668.
(27) Laviska, D. A.; Field, K. D.; Wang, D. Y.; Krogh-Jespersen, K.; Goldman, A. S.; American Chemical Society: 2012, INOR-791.
(28) Kanzelberger, M.; Singh, B.; Czerw, M.; Krogh-Jespersen, K.; Goldman, A. S. *J. Am. Chem. Soc.* **2000**, *122*, 11017.
(29) Nemeh, S.; Jensen, C.; Binamira-Soriaga, E.; Kaska, W. C. *Organometallics* **1983**, *2*, 1442.
(30) Doherty, M. D.; Grills, D. C.; Huang, K.-W.; Muckerman, J. T.; Polyansky, D. E.; Eldik, R. v.; Fujita, E. *Inorg. Chem.* **2013**, *52*, 4160.
(31) Crabtree, R. H.; Mihelcic, J. M.; Quirk, J. M. *J. Am. Chem. Soc.* **1979**, *101*, 7738.
(32) Laviska, D. A., Rutgers, The State University of New Jersey, 2013.
(33) Lee, D. W.; Kaska, W. C.; Jensen, C. M. *Organometallics* **1998**, *17*, 1.
(34) Gusev, D. G.; Madott, M.; Dolgushin, F. M.; Lyssenko, K. A.; Antipin, M. Y. *Organometallics* **2000**, *19*, 1734.
(35) Kennedy, A. R.; Cross, R. J.; Muir, K. W. *Inorg. Chim. Acta* **1995**, *231*, 195.

(36) Gupta, M.; Hagen, C.; Flesher, R. J.; Kaska, W. C.; Jensen, C. M. *Chem. Commun.* **1996**, 2083.
(37) Kundu, S., Rutgers, The State University of New Jersey, 2010.
(38) Gupta, M.; Hagen, C.; Kaska, W. C.; Cramer, R. E.; Jensen, C. M. *J. Am. Chem. Soc.* **1997**, *119*, 840.

Chapter 3

Synthesis of Cyclometalated (PCP)Ir Complexes

Abstract

Pincer complexes have been well documented as excellent C-H activation catalysts. The structure of the active catalytic species has evaded elucidation but has been proposed as a 14e$^-$, agostic, solvated, or dimeric species via C-H activation of a subsequent PCP ligand backbone. Rather than isolation or observation of any of these proposed species, it has been found that the cyclometalation or C-H activation of the ^{t}butyl group attached to one of the phosphorous atoms occurs readily. Characterization of cyclometalated complexes is described along with an interesting cyclometalated insertion product which occurs upon reaction of a cyclometalated product with carbon monoxide. Two different mechanisms are proposed and discussed in relation previously cited pathways for the formation of cyclometalated complexes and synthesis of the cyclometalated insertion product.

3.1 Introduction

Initial synthesis of the pincer complex requires cyclometalation of the pincer ligand. As mentioned in chapter 2, the preferred method for synthesis of PCP systems is direct metalation of the pincer ligand via intermolecular C-H or C-C bond activation (Scheme 3.1). Whereas C-H activation of **A-H** and C-C activation of **A-CH$_3$** leads to the formation of the tridentate (PCP)M system, **B**, C-H bond activation of **A-CH$_3$** leads to the formation of **C**, in which a carbon bond has been inserted into the metal-backbone linkage.

Scheme 3.1 C-C and C-H Activation of Pincer Ligands

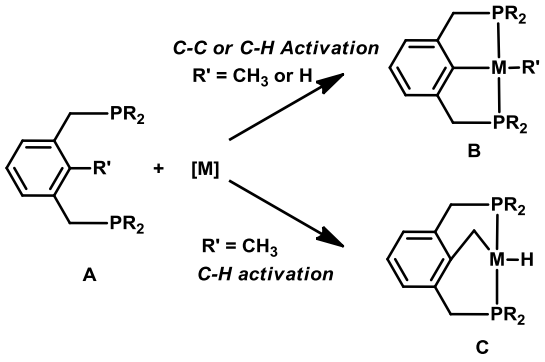

Milstein and coworkers have studied the formation of these C-H activation products extensively and have reported many pincer complexes with various metal centers (Figure 3.1).[1-7] These products exhibit a unique splitting pattern for the inequivalent splitting of the methylene protons (Ar*CH$_2$*P), as well as a signal for Ar*CH$_2$*M protons in the ^{1}H NMR spectra, whereas the splitting pattern of two inequivalent phosphorous atoms in the ^{31}P NMR spectra is distinct and the P-P coupling is observable and quite large.

Figure 3.1 Milstein Examples of C-H Activation Products

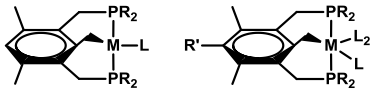

R = Ph, ^{i}Pr
M = Rh, Pt, Ni
L = PPh_3, Cl, I

R = ^{t}Bu, Ph, ^{i}Pr
R' = H, OMe
M = Rh, Ir, Ru
L = PPh_3, H, Aryl
L_2 = Cl, I

Various intermediates have been proposed to explain the appearance of both the inserted C-H activation products as well as the C-C activation products (Scheme 3.2). In all cases, intermediate **D,** in

which both phosphorous atoms are chelated to the metal center, is critical in the formation of both the C-H activation and C-C bond activation products. When the metal center is iridium or rhodium (M = Ir or Rh), the C-H and C-C pathways are parallel processes; direct insertion of the metal into the Ar-CH_3 bond yields a (PCP)M motif and direct C-H activation of Ar-CH_3 yields the inserted product.[3] The C-C bond activation process is slightly more favorable than the C-H activation process, with respect to kinetics and thermodynamics, hence the (PCP)M motif is the more easily isolated species. If the metal center is ruthenium or platinum (M = Ru or Pt), then C-H activation yields the expected activation product which subsequently leads to the C-C bond activation product through either intermediate **E** or **F**.[5] Intermediate **E** is a three centered transition state in which little to no interaction from the aryl π system is required. Intermediate **F** is a σ-arenium species in which the electron density has been removed from the aryl ring and transferred to the metal center. In this scenario, C-C bond activation is only thermodynamically favored whereas C-H activation is kinetically preferred. More work must be completed to harness these selectivity differences between different metal centers and pincer ligands.

Scheme 3.2 Formation of Proposed Intermediates in the C-H and C-C Bond Activation Pathways

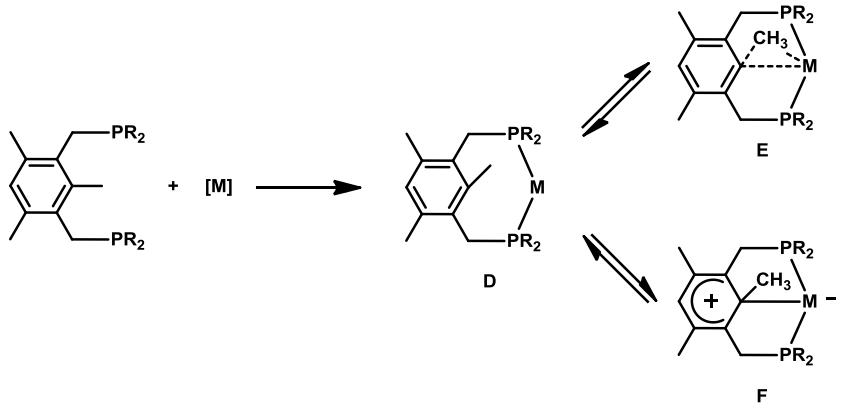

Goldman and coworkers report a similar series of inserted products with acetate type ligands (Figure 3.2).[8] These products exhibit the same splitting pattern for inequivalent methylene protons, a signal for Ar*CH*$_2$M protons in the ^{1}H NMR spectra, and the splitting pattern for two inequivalent phosphorous atoms in the ^{31}P NMR spectrum with a large P-P coupling as was observed for the C-H activation products published by Milstein. However, the synthesis of these inserted acetate products occurs via methylidene insertion into the aryl Ir-C(ipso) bond rather than direct C-H activation of a phosphinated xylene ligand, **A-**

CH_3 (Scheme 3.1). Intermediate **D** is cited as quite accessible via computational methods for the C-H reductive elimination of these (PCP)Ir(acetate) complexes and most likely the intermediate for the methylidene migration.

Figure 3.2 Inserted (PCP)Ir(acetate) Products

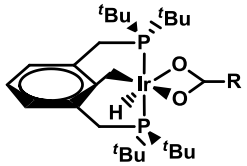

R = Ph, CH_3, CF_3

Interestingly, the C-H bond activation discussed above occurs in an intermolecular fashion. As proposed in the previous chapter, the intramolecular C-H activation at an aryl backbone of a second molecule of a pincer complex to form a dimer or oligomer, however, this type of scenario has not been supported by experimental evidence. Although the rigidity of the backbone inhibits C-H activation, it does not eliminate the possibility that the pincer complex can undergo a different intramolecular C-H activation at the phosphorous linked substituent (R) instead of aryl C-H bonds. This intramolecular C-H activation leads to a cyclometalated complex in which the C-H bond of one ^{t}butyl arm oxidatively adds to the iridium center to create an additional four membered ring (Figure 3.3).

In 1983, Kaska reported the reaction of (PCP)RhHCl with $NaN(SiMe_3)_2$ to yield the (PCP)Rh solvated complex, the C-H addition product of the solvent, and observation of C-H activation at the ^{t}butyl substituent of one of the (PCP)Rh arms.[9] This was the first report in which intramolecular C-H activation of the ^{t}butyl groups competes with intermolecular C-H activation of other ligands in the system. The first isolated iridium example was a crystallized sample of cyclometalated (MeO-PCP)IrCl showing the cyclometalation of the ^{t}butyl arm.[10] An equilibrium exists between (MeO-PCP)IrHCl and the cyclometalated complex upon loss of H_2 from the system. The additional four membered ring leads to loss of symmetry within the molecule, therefore the ^{31}P NMR spectra of these species are reported as two doublets with relatively large P-P coupling. The (MeO-PCP)IrHCl cyclometalated complex has reported ^{31}P NMR shifts of 50.8 and 9.8 with J_{PP} = 351.1 Hz for the trans positioning of the inequivalent phosphorous atoms. There is no indication of a hydride or a weakly bound hydrogen ligand. Other

examples, replacing the para methoxy substituent of the (PCP)Ir aryl backbone with a hydroxyl or nitro group, have also been cited. Cundari and Gunnoe reported a ruthenium example in which (PCP)Ru(NH_2)(CO) can eliminate NH_3 to form a cyclometalated CO complex.[11] The ^{31}P NMR spectrum for this species shows a doublet of doublets at 82.7 and 46.3 ppm with J_{PP} = 245 Hz. A few (POCOP)Ir examples were published in which both five and six coordinate cyclometalated species are formed in which the ligand is CO, Cl, or acetonitrile.[12] The ^{31}P NMR spectra for these species are shifted much farther downfield (154 and 87 ppm) and J_{PP} = 333 Hz, consistent with the general downfield shift of POCOP complexes versus PCP complexes.[13] Periana and Goddard report a (PNP)IrI_2 cyclometalated complex synthesized from reaction of the PNP ligand and $IrCl_3$•nH_2O[14] and the Goldman group has prepared and characterized a (PCP)Ir(acetate) cyclometalated complex.[8]

Figure 3.3 Examples of Cyclometalated Pincer Complexes

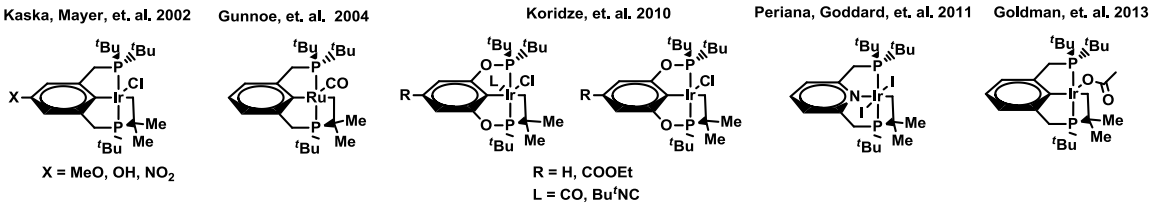

The electronics of the ligand backbone may have a significant effect on the isolation of these cyclometalated complexes. A series of resonance structures have been proposed for the (PCP)Ir complexes, in which the iridium metal center can be negative, neutral or positive in charge (Scheme 3.3). Modifications of the para-substituent can help achieve or influence the major resonance structure of the complex. A σ-donating methoxy or hydroxyl substituent leads to stabilization of electron density on the iridium center, facilitating intramolecular oxidative addition of the ^{t}butyl C-H bond within a short time frame. Conversely, the electron withdrawing nitro group facilitates conversion to the cylometalation complex in a few months and the cyclometalated parent (PCP)Ir complex, in which the para substituent is a hydrogen, was not isolated. Based on these resonance structures, π-donating or withdrawing characteristics of different substituents dominate the resonance structures and lead to synthesis of the cyclometalated complexes. Within the POCOP example isolated by Koridze the para position is occupied by a hydrogen instead of a significantly electron withdrawing or donating substituents. POCOP ligands generally allow

for a significant buildup of negative charge on the ipso carbon versus the parent PCP ligand which could lead to increased chance of cyclometalation.[15]

Scheme 3.3 Resonance Structures for (PCP)Ir Complexes

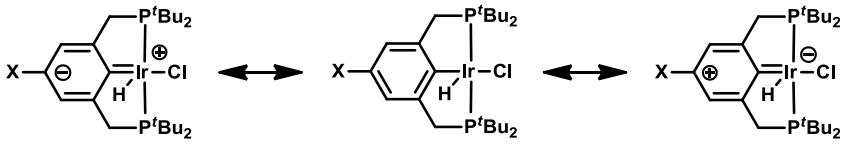

Alternatively, different computational and experimental studies have been conducted to elucidate some of the substituent effects on the addition of ligands to (PCP)Ir species.[16] It has been found that increased electron donation from the para substituent leads to increased C_{ipso}-Ir bond lengths due to repulsion between the filled d orbitals of the iridium metal center and the PCP p(π) orbitals in the 14e$^-$ species. Addition of H_2 mitigates this scenario and electron donating substituents on the PCP backbone leads to strengthening and shortening of C-Ir bonds. These results do not fully agree with the resonance structures proposed as shorter double bonds between the ipso carbon and iridium are depicted.

Kaska has proposed a mechanism for the formation of these cyclometalated species proceeding through two different pathways (Figure 3.4). The initial step is the formation of a 14e$^-$ species in which coordination of the two PH_3 groups occurs prior to C-H activation of the aryl ring. As discussed earlier in Chapter 2, 14e$^-$ species are not stable but have been reported for other metal complexes.[9,17] The precoordination of phosphines to the metal center prior to activation of the aryl ring has also been cited as an important intermediate by Milstein during his studies of the inserted products discussed in the beginning of this chapter.[3,5] After formation of the 14e$^-$ species, there are two possible pathways. In pathway A, the ^{t}butyl C-H bond oxidatively adds to the iridium followed by C-H activation of the aryl bond in the PCP backbone. In pathway B, C-H activation of the aryl ring is favored over C-H activation of ^{t}butyl, to give the (PCP)IrHCl complex. Then attack of the ^{t}butyl at a free coordination site opposite the hydride leads to a seven coordinate Ir(V) complex upon rearrangement. The equilibrium is favored for the formation of (PCP)IrHCl due to the strength of the aryl carbon-iridium bond, but loss of H_2 makes the reaction irreversible to give cyclometalated (PCP)IrCl.

Figure 3.4 Proposed Mechanism for the Formation of Cyclometalated Complexes

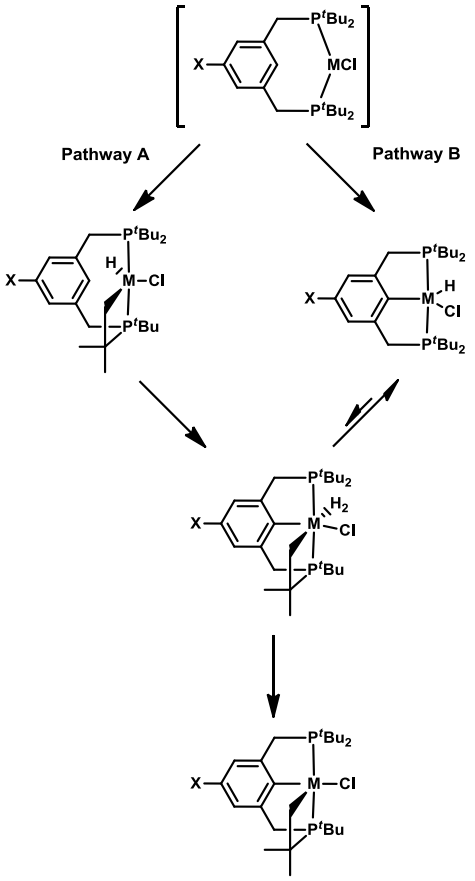

In this chapter, the synthesis and characterization (^{31}P, ^{19}F, ^{13}C, ^{1}H and 2D gCOSY NMR spectroscopy) of different cyclometalated species will be detailed. In one case the introduction of CO gas into the system leads to the insertion of the C-H activated ^{t}butyl group into the aryl-iridium bond of the backbone. The mechanistic pathways for the formation of the cyclometalated complexes and the inserted product will be discussed in relation to those proposed by Milstein and Kaska.

3.2 Results and Discussion

3.2.1 Formation of Cyclometalated (PCP)IrNBE Complexes

Norbornene is a strained cyclic molecule that acts as a hydrogen acceptor for (R-PCP)IrH_n (R = H or Me) to give access to the 14e$^-$ (R-PCP)Ir species via exchange with the π-bound species as discussed in Chapter 2. When the norbornene complex is heated at 100 °C for 12 hours, cyclometalated complexes **3-1** and **3-2** are formed in which intramolecular C-H activation of a ^{t}butyl group has occurred (Scheme 3.4).

Scheme 3.4 Synthesis of Cyclometalated Norbornene Complexes, **3-1** and **3-2**

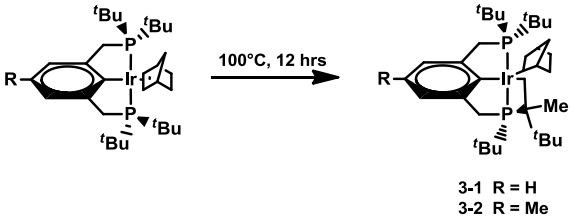

The ^{31}P NMR spectra of both complexes show a doublet of doublets, centered at approximately 86 and -20 ppm with a J_{PP} coupling of 230 MHz. The ^{1}H NMR spectra of both complexes clearly indicate the unsymmetrical nature of the complex. The methylene protons attached to the backbone exhibit splitting of the methylene signal into four multiplets ranging from 2.5 to 3.5 ppm, and the ^{t}butyl groups are split into three doublets at 1.5, 1.3 and 1.0 ppm. The methyl group signals of the newly created cyclometalated arm are also observed as doublets at approximately 2 and 1 ppm. The ^{1}H and ^{31}P NMR support a cyclometalated complex rather than an inserted product, as there is no observed shift for Ar*CH*$_2$M protons. Norbornene is presumably the stabilizing ligand, however any attempts to crystallize this complex have proven ineffective and the observance of the NBE proton signals was not successful. 2D gCOSY NMR spectroscopy of **3-2** did not provide any further information as only correlations between the methylene protons were definitively observed.

3.2.2 Reaction of Cyclometalated (Me-PCP)IrNBE Complex with CO

Due to π-backbonding ability, CO is known to stabilize four and five coordinate (PCP)Ir species to give the five or six coordinate CO adducts.[18] Upon addition of 1 atm CO gas to **3-2**, a 3:2 mixture of 4-coordinate (Me-PCP)Ir-CO and the cyclometalated inserted product, **3-3**, was formed (Scheme 3.5).

Scheme 3.5 Addition of CO to Cyclometalated Complex **3-2**

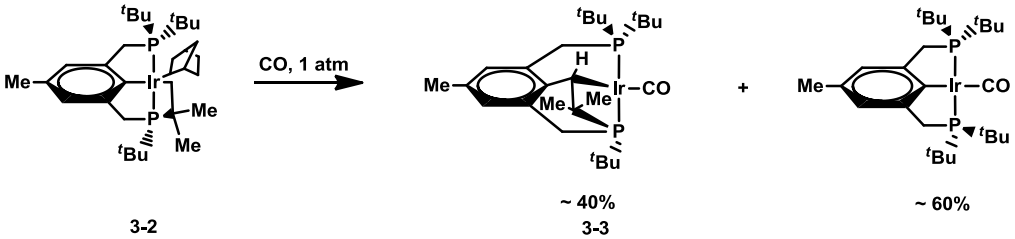

In complex **3-2**, the ^{t}butyl group which had initially undergone C-H activation has now inserted into the ipso C-Ir bond to form the cyclometalated inserted (Me-PCP)Ir-CO adduct **3-3**. This is the first

example of a PCP catalyst that has undergone both insertion and cyclometalation. Previously, examples of phenyl ring insertion into the (PCP) aryl-metal bond via a C-C coupling reaction have been cited, though not for the ligands previously attached to the phosphine arms.[2]

The ^{31}P NMR spectrum of **3-3** shows two doublets at 89.8 and 5.3 ppm with J_{PP} = 272.8 Hz. A combination of the product crystal structure, recrystallized from a benzene/pentane mixture, and ^{1}H and 2D gCOSY NMR spectroscopy techniques were used to determine the exact structure (Figures 3.5-7, respectively). The crystal structure of **3-3** shows the Ir-CO is 1.84 Å, which is comparably shorter than the Ir-CO bond length in most (PCP)Ir-CO complexes (1.873 Å).[19] The gCOSY NMR indicates correlations between the two cyclometalated methyl groups (H21-H20), between methylene and the cyclometalated methyl protons (H10b-H21), and between the inserted proton and cyclometalated methyl (H1-H20). Interestingly, there is an interaction between the inserted proton and the para methyl protons attached to aryl backbone (H1-H8). These correlations have been indentified on the 2D gCOSY NMR spectrum along with other expected correlations between the ^{t}butyl, methylene and aryl protons within the complex. All crystal data and full characterization have been included at the end of the chapter.

Figure 3.5 Crystal Structure of **3-3**

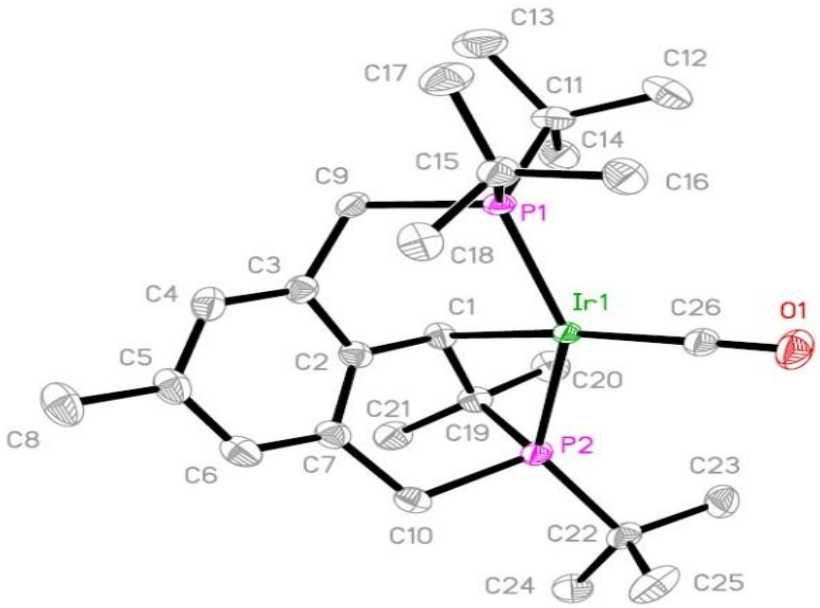

Figure 3.6 2D gCOSY NMR Spectrum of **3-3**

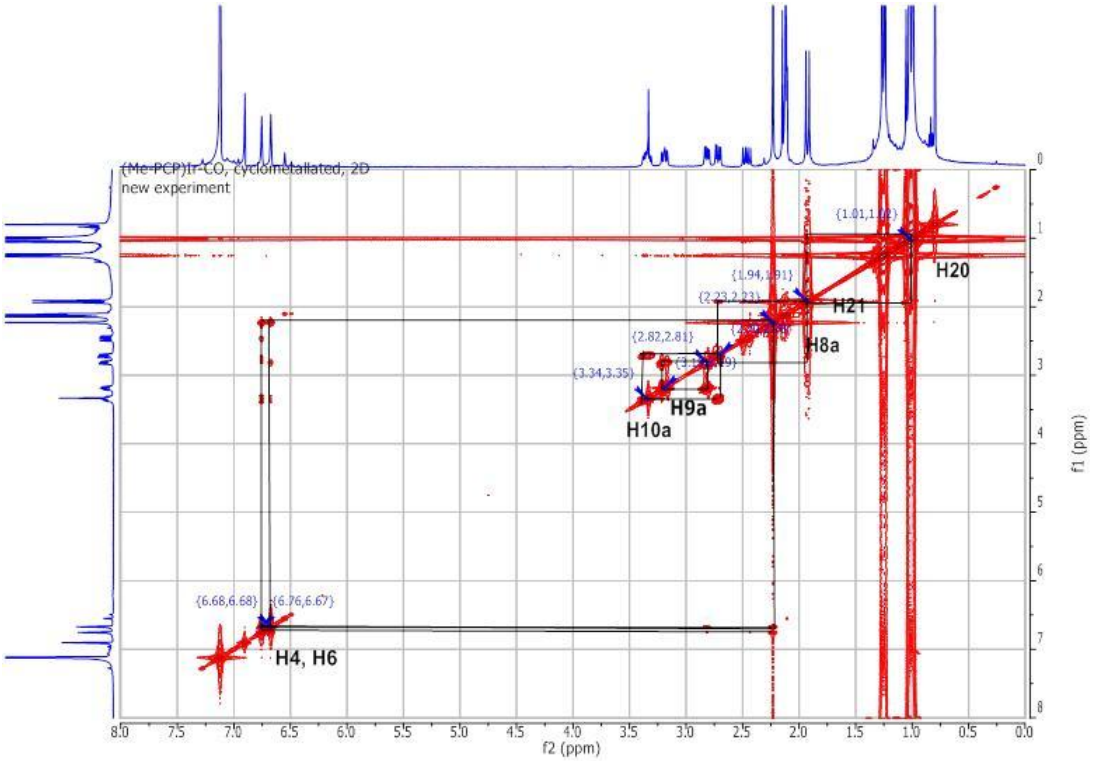

Figure 3.7 Expanded Region from 0.0 - 4.0 ppm of 2D gCOSY NMR Spectrum of **3-3**

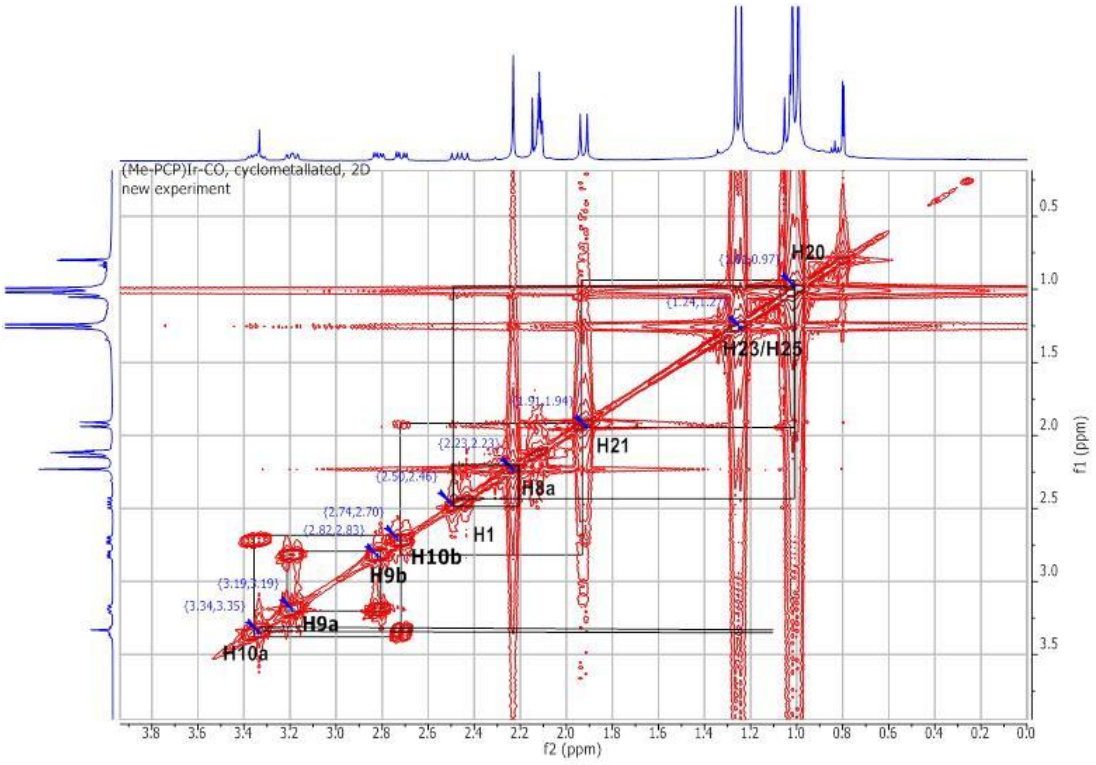

*3.2.3 Reactions of Cyclometalated Complex, **3-2**, with H_2 and Ethylene*

Reactions were conducted with H_2 and ethylene to give some insight into the reactivity of **3-2**. (Me-PCP)IrH_4 is formed when **3-2** is reacted with hydrogen (Scheme 3.6), which is supported by ^1H and ^{31}P NMR spectroscopy (see Chapter 2).

Scheme 3.6 Reaction of **3-2** with H_2

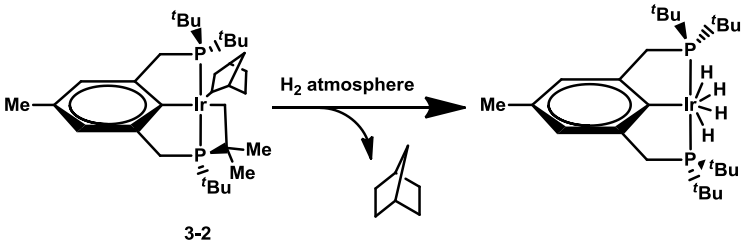

3-2

Norbornane should be observed in the proton spectrum as the byproduct of hydrogenation and ligand elimination, however singlets for the pincer ^{t}butyl groups (δ_H = ~ 1.20 ppm) overlap the signals for norbornane (δ_H = 1.0-1.6 ppm).[20] Therefore GC analysis was conducted to isolate and separate the organic products of this reaction. A standard solution of 20 mM norbornene and 40 mM norbornane in *p*-xylene give two signals at a retention time of 4.20 and 4.30 minutes respectively. A GC trace of the reaction mixture also gives similar signals at 4.26 and 4.33 minutes, which could possibly correlate to norbornane.

Table 3.1 Retention Times for the Reaction of **3-2** with H_2 to Release Norbornane

Retention time	Area %	Assignment
0.1	23.47	injection spike
3.43	76.213	C_6D_6
4.26	0.037	norbornane
4.33	0.034	norbornane
5.26	0.064	*p* -xylene
5.31	0.131	*p* -xylene

The addition of 1 atm of ethylene to **3-2** gives the ethylene complex as the main product as characterized by NMR spectroscopy (Scheme 3.7). Presumably, norbornene is released during this reaction, but was not confirmed by GC analysis.

Scheme 3.7 Reaction of **3-2** with Ethylene

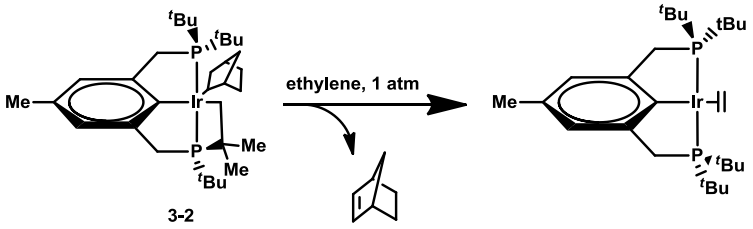

3.2.4 Proposed Mechanisms for the Formation of Cyclometalated Products

The proposed mechanism for the formation of the cyclometalated products **3-1** and **3-2** is detailed in Figure 3.8. The mechanism is most similar to pathway B proposed by Kaska (Figure 3.4) in which C-H activation of the aryl bond is favored versus C-H activation of ^{t}butyl followed by attack at the free coordination site.[10] Starting from the active 14e$^-$ species rather than bidentate species **D** proposed in Scheme 3.2, the ^{t}butyl arm undergoes C-H activation to form cyclometalated hydride intermediates **3-1a** or **3-2a**. This intermediate is akin to the seven coordinate Ir(V) complex proposed in Figure 3.4, however a hydride is located trans to the C-H activated ^{t}butyl arm instead of a dihydrogen ligand. Addition of norbornene leads to intermediates **3-1b** and **3-2b**. Finally, release of H_2 gas accompanied by addition of a norbornyl ligand makes the reaction irreversible and allows for isolation of **3-1** and **3-2**.

Figure 3.8 Proposed Mechanism for the Formation of **3-1** and **3-2**

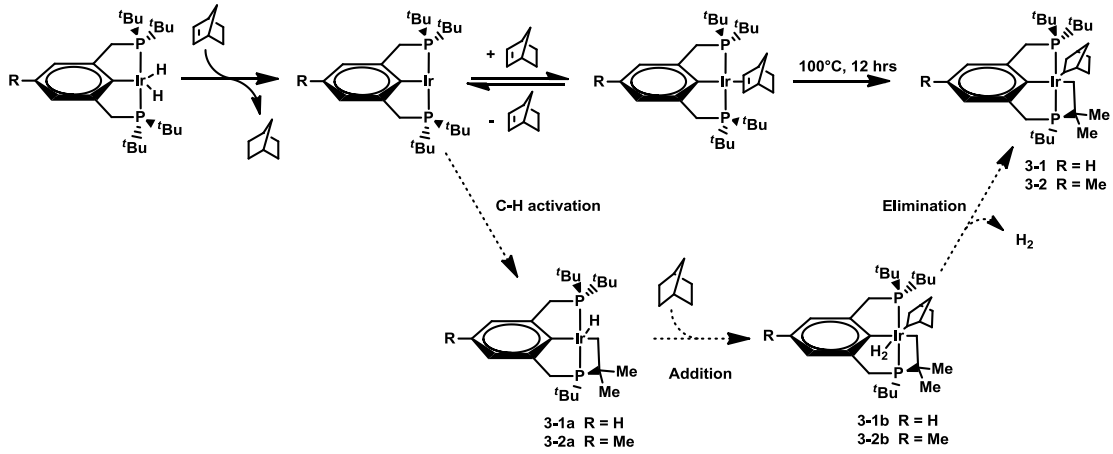

The addition of CO gas to the cyclometalated products leading to the 4-coordinate (Me-PCP)Ir-CO and cyclometalated inserted product, **3-3**, can be explained as follows. Beginning from **3-2**, addition of

CO gas leads to formation of the four coordinate CO species via loss of norbornene as has been shown previously.[18] There are two proposed pathways for the formation of the cyclometalated CO complex. Formation of the six coordinate intermediate species (**3-3a**) occurs through initial addition of CO followed by elimination of the norbornyl ligand leading to carbene intermediate **3-3b**; similar intermediates have been documented in the literature.[8,21,22] The carbene intermediate then undergoes insertion to form the cyclometalated insertion product. Secondarily, coupling of the ^{t}butyl arm to the ipso carbon of the aryl ring gives intermediate **3-3c**, similar to the reaction proposed by Milstein. After coupling, C-H activation of **3-3c** leads to **3-3d** and displacement of the NBE ligand with CO gives **3-3**.

Figure 3.9 Proposed Pathways for the Formation of the Cyclometalated Insertion CO product

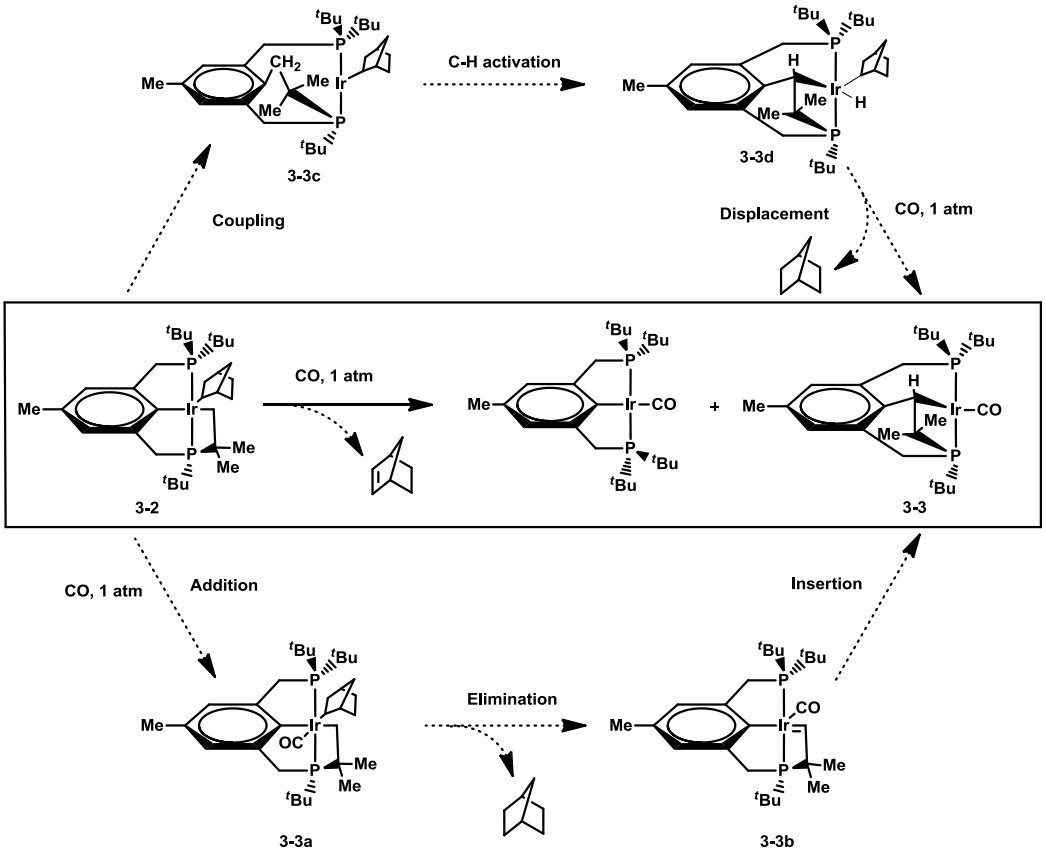

3.2.5 Synthesis of Cyclometalated (Me-PCP)IrCl, ***3-4***

Upon heating (Me-PCP)IrHCl in the presence of trifluoroacetic acid (CF_3COOH) in dichloromethane, a cyclometalated (Me-PCP)IrCl complex (**3-4**) is generated (Scheme 3.8). This species is analogous to the cyclometalated (POCOP)IrCl species isolated by Koridze et. al. using the same method.

Scheme 3.8 Synthesis of Cyclometalated (PCP)IrCl Complex, **3-4**

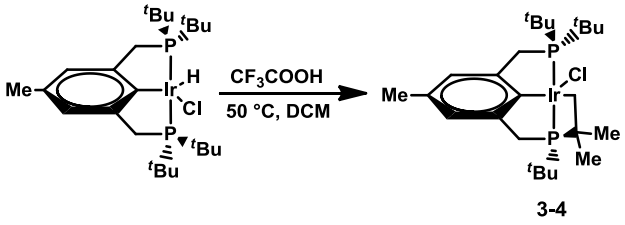

3-4

Synthesis of **3-4** and cyclometalated (POCOP)IrCl complexes presumably proceeds through a different pathway than those proposed for species **3-1** through **3-3.** As discussed in Chapter 2, the $14e^-$ species is commonly generated by reaction of the dihydride complex with a hydrogen acceptor.[23,24] Reaction of the (PCP)IrHCl with a base will also successfully generate the active $14e^-$ species.[13] Under acidic conditions, the $14e^-$ species will most likely not exist. The proposed mechanism for the formation of **3-4**, Figure 3.10, starts with protonation of (PCP)IrHCl to form intermediate **3.4a**. Elimination of H_2 and C-H activation of the ^{t}butyl arm allows for formation of **3-4b**. Finally, deprotonation regenerates CH_3COOH and **3-4** is isolated.

Figure 3.10 Potential Mechanism for the Formation of **3-4**

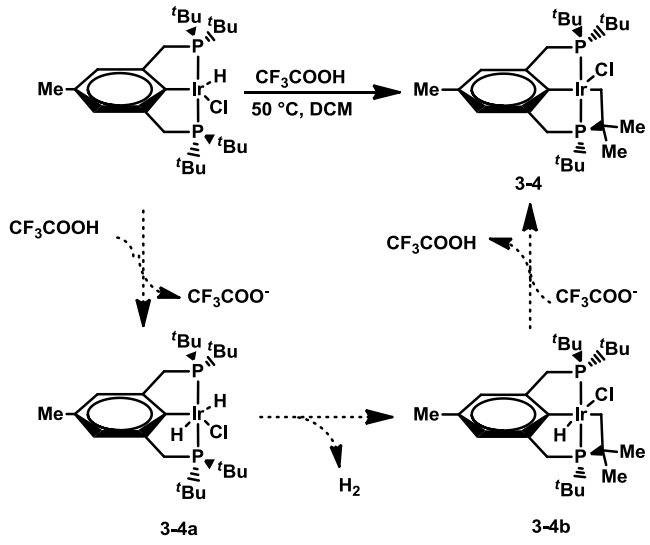

*3.2.6 Synthesis of Cyclometalated (PCP)IrFBF$_3$, **3-5***

When **3-4** is reacted with $AgBF_4$ in acetone, AgCl is formed as the precipitate and the BF_4 counterion is activated giving cyclometalated complex **3-5** (Scheme 3.9). This product was determined by ^1H, ^{31}P, and ^{19}F NMR spectroscopy. The observation of two signals in the ^{19}F NMR spectrum, a doublet at -185.9 ppm and a broad singlet at -186.5 ppm, for two different fluorine atoms indicates activation of the BF_4 counterion. Presumably

Scheme 3.9 Synthesis of Cyclometalated (PCP)IrFBF$_3$ Complex, **3-5**

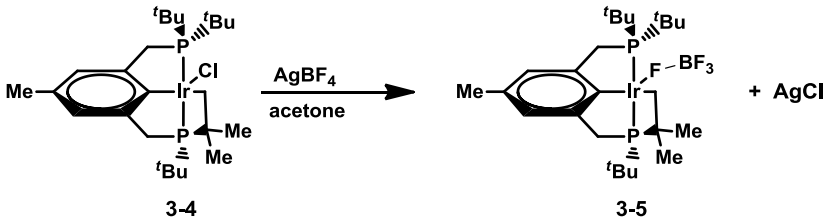

3-4 **3-5**

3.3 Conclusion

The synthesis and characterization of cyclometalated complexes **3-1**, **3-2**, **3-4**, and **3-5** have been reported. The cyclometalated inserted product **3-3** has also been isolated. These complexes represent interesting structural motifs of (PCP)Ir catalysts. The mechanistic pathway for the formation of **3-1** and **3-2** has been proposed and compared to previously cited mechanisms but the main difference is the starting 14e$^-$ species. The mechanism for the formation of **3-3** was postulated based on intermediates **3-3b** and **3-3c**, which have been documented in the literature. Finally, cyclometalated species **3-4** and **3-5** were isolated and characterized using an array of NMR techniques. The acid catalyzed mechanism for the formation of **3-4** was postulated. Overall, more research must be done to understand the synthesis and reactivity of these interesting complexes.

3.4 Experimental

General

All reactions were performed under an argon atmosphere using standard Schlenck techniques or in an argon-filled glove box. C_6H_6, C_6D_6, TBE, and *p*-xylene-d_{10} were dried over Na/K alloy and collected via vacuum transfer. Norbornene (NBE) was sublimed before use. (PCP)IrNBE and (PCP)IrHCl were synthesized according to literature procedures.[23,25,26] All other substrates were degassed before entry to

glovebox and used without further purification. ^{1}H, ^{13}C, ^{31}P, ^{19}F NMR spectra were obtained from either a 400 or 500 MHz Varian instrument. The residual peak of the deuterated solvent was used as a reference for all ^{1}H NMR spectra and an internal capillary standard of PMe_3 in *p*-xylene-d_{10} (-62.4 ppm) was used to reference ^{31}P NMR chemical shifts. ^{19}F NMR chemical shifts were referenced by an internal capillary standard of fluorobenzene in *p*-xylene-d_{10}.

(PCP)Ir cyclometalated product, 3-1

20 mg norbornene (0.21 mmol) was added to a *p*-xylene-d_{10} solution of 13.0 mg (PCP)IrH_2 (0.022 mmol) . The solution was heated in a 100 ˚C oil bath for 12 hours. The product was characterized *in situ*. **^{31}P NMR (*p*-xylene-d_{10}, 202.3 MHz):** δ 86.339 (d, J_{PP} = 230.7), -20.311 (d, J_{PP} = 230.7). **^{1}H NMR (*p*-xylene-d_{10}, 500 MHz):** δ 6.95 (d, 2H, Ar-*H*), 6.75 (t, 1H, Ar-*H*), 3.45-2.41 (m, 4H, CH_2P), 2.44 (d, J_{PH} = 8.8 Hz, 1H, C*H*), 2.41 (d, J_{PH} = 8.8 Hz, 1H, C*H*) 1.89 (d, 3H, Ar-CH_3), 1.36 (d, 9H, P^{t}Bu), 1.25 (d, 9H, P^{t}Bu), 1.03 (d, 3H, Me), 0.90 (d, 9H, P^{t}Bu).

(Me-PCP)Ir cyclometalated, 3-2

19.8 mg norbornene (0.21 mmol) was added to a *p*-xylene-d_{10} solution of 13.0 mg (Me-PCP)IrH_2 (0.022 mmol). The solution was heated in a 100 ˚C oil bath for 12 hours. The product was characterized *in situ*. **^{31}P NMR (*p*-xylene-d_{10}, 161.9 MHz):** δ 86.39 (d, J_{PP} =230.8), -20.37 (d, J_{PP} = 230.9). **^{1}H NMR (*p*-xylene-d_{10}, 400 MHz):** δ 6.78 (2H, Ar-*H*), 3.52-2.75 (m, 4H, CH_2P), 2.42 (s, 3H, Ar-CH_3), 1.98 (d, *J* = 14.5 Hz, 3H, Me), 1.50 (d, *J* = 11.4, 9H, P^{t}Bu), 1.38 (d, 9H, P^{t}Bu), 1.10 (d, *J* = 11.2, 3H, Me), 1.01 (d, *J* = 1.6, 9H, P^{t}Bu).

(Me-PCP)Ir–CO cyclometalated, 3-3

1 atm CO gas was added to a *p*-xylene-d_{10} solution of 13.0 mg **3-2** (0.022 mmol). Upon mixing, the solution immediately turned from red to yellow in color. The 4-coordinate (Me-PCP)Ir-CO and **3-3** were observed in a 3:1 ratio by ^{31}P NMR spectroscopy. Solvent was removed via vacuum, leaving behind a mixture of products as a powder. Dissolving the powder in pentane gave the 4-coordinate (Me-PCP)Ir-CO as a yellow liquid and **3-3** as a brown solid. The mixture was filtered and washed with pentane and product **3-3** was crystallized from a benzene/pentane mixture to obtain dark brown crystals. X-ray crystallography refinement and structure parameters are included in Tables 3.2 through 7. **^{31}P NMR (C_6D_6, 202.3 MHz):**

δ 89.78 (d, J_{PP} = 272.9 Hz), 5.33 (d, J_{PP} = 272.8 Hz). **^{1}H NMR (C_6D_6, 500 MHz):** δ 7.16 (s, C_6D_6), 6.79 (s, 1H, Ar-*H*), 6.71 (s, 1H, Ar-*H*), 3.38 (dd, 1H, H_3), 3.23 (m, 1H, H_1), 2.85 (dd, 1H, H_2), 2.75 (dd, 1H, H_4), 2.49 (dd, 1H, H), 2.27 (s, 3H, Ar-CH_3), 1.98 (d, 3H, Me), 1.29 (d, 9H, single P^{t}bu)*, 1.09 (d, 3H, Me), 1.06 (9H, P^{t}bu), 1.03 (9H, P^{t}bu). **^{13}C NMR (C_6D_6, 125.67 MHz):** δ 174 (CO), 138 (C3), 136 (C7), 131 (C2), 127.5 (C5), 123 (C4), 109 (C6), 52 (C9), 47.5 (C10), 37.05 (C15), 34.15 (C11), 29.5 (C8), 27.8 (C12-C14), 27.4 (C16-C18), 26.8 (C22), 26.1(dd), 24.7(C23-C25), 24.2, 18.6(s). *single ^{t}butyl is attached to cyclometalated phosphorous and numbered hydrogen and carbon atoms refer to the assignment within the crystal structure.

Reaction of 3-2 with H_2

A solution of 13.0 mg (Me-PCP)IrH_n (0.0216 mmol) and 26.2 mg NBE (0.28 mmol) in *p*-xylene-d_{10} was heated at 100 ˚C for 1.5 hours. Excess volatiles and solvent were removed *in vacuo*, leaving **3-2** as a brown waxy solid. The solid was dissolved in C_6D_6 and H_2 was bubbled through the solution. The solution changed color from dark brown to red within five minutes. (PCP)IrH_4 was confirmed as the major product via ^{31}P and ^{1}H NMR spectroscopy.[27] The hydrogenation of norbornane was confirmed via GC analysis, utilizing a Varian 430 GC.

Reaction of 3-2 with ethylene

A solution of 13.0 mg (Me-PCP)IrH_n (0.0216 mmol) and 19.8 mg NBE (0.21 mmol) in *p*-xylene-d_{10} was heated at 100 ˚C for 1.5 hours to synthesize **3-2** *in situ*. After degassing, 1 atm ethylene was added to the solution. The solution became yellow brown upon thawing and mixing. (PCP)Ir-ethylene was formed in quantitative yield as confirmed by ^{31}P and ^{1}H NMR spectroscopy.[28]

(Me-PCP)IrCl cyclometalated, 3-4

To a solution of 15.5 mg (Me-PCP)IrHCl (0.024 mmol) in benzene, 60 μL CF_3COOH (0.78 mmol) was added. The solution was heated in a 90 ˚C oil bath for 3 days under a constant flow of argon. The product was isolated in quantitative yield. **^{31}P NMR (C_6D_6, 161.9 MHz):** δ 48.77 (d, J_{PP} =345.2 Hz), 6.25 (d, J_{PP} = 344.9 Hz). **^{1}H NMR (C_6D_6, 400 MHz):** δ 6.95 (d, 2H, Ar-*H*), 3.418 (bs, 1H, C*H*), 3.14-3.02 (m, 4H, CH_2P), 2.39 (s, 3H, Ar-CH_3), 2.16 (m, 1H, C*H*), 1.44(d, *J* = 13.2 Hz, 3H, CH_3), 1.31 (d, *J* = 12.8

Hz, 3H, P^{t}Bu,), 1.16 (d, *J* =12.8 Hz, 9H, P^{t}Bu), 1.10 (d, *J* = 12.4 Hz, 9H, P ^{t}Bu,), 0.70 (d, *J* = 12.8 Hz, 3H, CH_3).

(Me-PCP)IrFBF$_3$ cyclometalated, 3-5

To a solution of 15.1 mg **3-4** (0.024 mmol) in acetone, 2.5 μL NH_4OH (0.063 mmol) was added. The solution was transferred to a vial containing 4.8 mg $AgBF_4$ (0.025 mmol). The solution turned from yellow to dark brown. AgCl precipitates as a dark grey powder within 5 minutes. The solution was washed with acetone to remove AgCl as a solid and volatiles were removed *in vacuo*, leaving behind the product as an orange powder. **^{31}P NMR (C_6D_6, 161.9 MHz):** δ 50.01 (d, J_{PP} =330.8 Hz), 4.13(d, J_{PP} = 330.8 Hz). **^{1}H NMR (C_6D_6, 400 MHz):** δ 6.95 (s, 1H, Ar-*H*), 6.88 (s, 1H, Ar-*H*), 3.00 (m, 2H, CH_2P), 2.28 (m, 2H, CH_2P), 1.51(s, 3H, Ar-CH_3), 1.19 (d, *J* =13.6 Hz, 9H, P^{t}Bu), 1.12 (d, *J* =14 Hz, 9H, P^{t}Bu), 0.99 (d, *J* =13.6 Hz, 9H, P^{t}Bu), 0.75 (d, *J* =16.8 Hz, 3H, CH_3), 0.65 (d, *J* =12.4 Hz, 3H, CH_3) 0.64 (d, *J* =12.8 Hz, IH, Ir-C*H*), 0.56 (d, *J* =13.2 Hz, IH, Ir-C*H*). **^{19}F NMR (C_6D_6):** δ -185.9 (d), -186.5 (bs).

Table 3.2 Crystal Data and Structure Refinement for (Me-PCP)Ir–CO Cyclometalated, **3-3**

Identification code	kf79a	
Empirical formula	C26 H43 Ir O P2	
Formula weight	625.74	
Temperature	100(2) K	
Wavelength	0.71073 Å	
Crystal system	Monoclinic	
Space group	P2(1)/n	
Unit cell dimensions	a = 11.4805(7) Å	α = 90°.
	b = 13.2153(8) Å	β = 93.162(1)°.
	c = 17.1667(10) Å	γ = 90°.
Volume	2600.5(3) $Å^3$	
Z	4	
Density (calculated)	1.598 Mg/m^3	
Absorption coefficient	5.273 mm^{-1}	
F(000)	1256	
Crystal size	0.36 x 0.30 x 0.06 mm^3	
Theta range for data collection	1.95 to 31.00°.	
Index ranges	-16<=h<=16, -19<=k<=18, -24<=l<=24	
Reflections collected	31263	
Independent reflections	8278 [R(int) = 0.0186]	
Completeness to theta = 31.00°	99.7 %	
Absorption correction	Semi-empirical from equivalents	
Max. and min. transmission	0.7427 and 0.2526	
Refinement method	Full-matrix least-squares on F^2	
Data / restraints / parameters	8278 / 0 / 283	
Goodness-of-fit on F^2	1.009	
Final R indices [I>2sigma(I)]	R1 = 0.0303, wR2 = 0.0785	
R indices (all data)	R1 = 0.0340, wR2 = 0.0813	
Largest diff. peak and hole	5.947 and -1.087	e.$Å^{-3}$

Table 3.3 Atomic Coordinates (x 10^4) and Equivalent Isotropic Displacement Parameters ($Å^2$x 10^3) for (Me-PCP)Ir–CO Cyclometalated, **3-3**. U(eq) is defined as one third of the trace of the orthogonalized U^{ij} tensor.

	x	y	z	U(eq)
Ir(1)	8918(1)	4930(1)	2528(1)	14(1)
P(1)	7567(1)	4788(1)	3478(1)	17(1)
P(2)	10820(1)	5199(1)	2231(1)	18(1)
C(1)	10208(2)	4631(2)	3457(2)	19(1)
C(2)	10150(2)	5664(2)	3783(2)	19(1)
C(3)	9308(2)	5872(2)	4334(2)	20(1)
C(4)	9289(3)	6816(2)	4693(2)	24(1)
C(5)	10032(3)	7594(2)	4489(2)	27(1)
C(6)	10732(3)	7428(2)	3860(2)	26(1)
C(7)	10778(3)	6487(2)	3494(2)	21(1)
C(8)	10001(3)	8609(3)	4892(2)	36(1)
C(9)	8356(3)	5088(2)	4434(2)	20(1)
C(10)	11341(3)	6380(2)	2724(2)	23(1)
C(11)	6998(3)	3463(2)	3662(2)	25(1)
C(12)	6096(3)	3161(3)	3021(2)	34(1)
C(13)	6493(4)	3321(3)	4471(2)	40(1)
C(14)	8047(3)	2752(2)	3628(2)	28(1)
C(15)	6341(3)	5727(2)	3398(2)	23(1)
C(16)	5677(3)	5644(3)	2598(2)	29(1)
C(17)	5471(3)	5638(3)	4038(2)	33(1)
C(18)	6910(3)	6772(2)	3455(2)	27(1)
C(19)	11302(2)	4330(2)	3017(2)	20(1)
C(20)	11186(3)	3229(3)	2767(2)	28(1)
C(21)	12481(3)	4485(3)	3465(2)	27(1)
C(22)	11542(3)	5157(3)	1293(2)	23(1)
C(23)	11168(3)	4187(3)	861(2)	35(1)
C(24)	12870(3)	5193(3)	1418(2)	31(1)
C(25)	11119(4)	6076(3)	817(2)	39(1)
C(26)	8036(3)	5001(2)	1600(2)	21(1)
O(1)	7547(3)	4957(2)	992(2)	34(1)

Table 3.4 Bond Lengths [Å] and Angles [°] for (Me-PCP)Ir–CO Cyclometalated, **3-3.**

Ir(1)-C(26)	1.843(3)	C(12)-H(12B)	0.9800
Ir(1)-C(1)	2.151(3)	C(12)-H(12C)	0.9800
Ir(1)-P(2)	2.2969(8)	C(13)-H(13A)	0.9800
Ir(1)-P(1)	2.3193(7)	C(13)-H(13B)	0.9800
P(1)-C(9)	1.874(3)	C(13)-H(13C)	0.9800
P(1)-C(15)	1.876(3)	C(14)-H(14A)	0.9800
P(1)-C(11)	1.901(3)	C(14)-H(14B)	0.9800
P(2)-C(19)	1.834(3)	C(14)-H(14C)	0.9800
P(2)-C(22)	1.851(3)	C(15)-C(18)	1.530(5)
P(2)-C(10)	1.859(3)	C(15)-C(17)	1.530(4)
C(1)-C(2)	1.478(4)	C(15)-C(16)	1.537(4)
C(1)-C(19)	1.553(4)	C(16)-H(16A)	0.9800
C(1)-H(1)	1.0000	C(16)-H(16B)	0.9800
C(2)-C(7)	1.411(4)	C(16)-H(16C)	0.9800
C(2)-C(3)	1.416(4)	C(17)-H(17A)	0.9800
C(3)-C(4)	1.392(4)	C(17)-H(17B)	0.9800
C(3)-C(9)	1.523(4)	C(17)-H(17C)	0.9800
C(4)-C(5)	1.392(5)	C(18)-H(18A)	0.9800
C(4)-H(4)	0.9500	C(18)-H(18B)	0.9800
C(5)-C(6)	1.399(5)	C(18)-H(18C)	0.9800
C(5)-C(8)	1.511(5)	C(19)-C(20)	1.521(4)
C(6)-C(7)	1.396(4)	C(19)-C(21)	1.533(4)
C(6)-H(6)	0.9500	C(20)-H(20A)	0.9800
C(7)-C(10)	1.509(4)	C(20)-H(20B)	0.9800
C(8)-H(8A)	0.9800	C(20)-H(20C)	0.9800
C(8)-H(8B)	0.9800	C(21)-H(21A)	0.9800
C(8)-H(8C)	0.9800	C(21)-H(21B)	0.9800
C(9)-H(9A)	0.9900	C(21)-H(21C)	0.9800
C(9)-H(9B)	0.9900	C(22)-C(25)	1.528(5)
C(10)-H(10A)	0.9900	C(22)-C(24)	1.529(5)
C(10)-H(10B)	0.9900	C(22)-C(23)	1.531(5)
C(11)-C(12)	1.521(5)	C(23)-H(23A)	0.9800
C(11)-C(14)	1.531(5)	C(23)-H(23B)	0.9800
C(11)-C(13)	1.547(5)	C(23)-H(23C)	0.9800
C(12)-H(12A)	0.9800	C(24)-H(24A)	0.9800

C(24)-H(24B)	0.9800	C(25)-H(25B)	0.9800
C(24)-H(24C)	0.9800	C(25)-H(25C)	0.9800
C(25)-H(25A)	0.9800	C(26)-O(1)	1.160(4)

C(26)-Ir(1)-C(1)	166.66(13)	C(4)-C(5)-C(6)	117.6(3)
C(26)-Ir(1)-P(2)	106.49(11)	C(4)-C(5)-C(8)	120.7(3)
C(1)-Ir(1)-P(2)	64.51(8)	C(6)-C(5)-C(8)	121.5(3)
C(26)-Ir(1)-P(1)	104.75(11)	C(7)-C(6)-C(5)	121.7(3)
C(1)-Ir(1)-P(1)	85.64(8)	C(7)-C(6)-H(6)	119.2
P(2)-Ir(1)-P(1)	148.18(3)	C(5)-C(6)-H(6)	119.2
C(9)-P(1)-C(15)	104.40(14)	C(6)-C(7)-C(2)	119.7(3)
C(9)-P(1)-C(11)	101.74(14)	C(6)-C(7)-C(10)	120.4(3)
C(15)-P(1)-C(11)	110.98(14)	C(2)-C(7)-C(10)	119.2(3)
C(9)-P(1)-Ir(1)	106.80(10)	C(5)-C(8)-H(8A)	109.5
C(15)-P(1)-Ir(1)	115.06(10)	C(5)-C(8)-H(8B)	109.5
C(11)-P(1)-Ir(1)	116.13(10)	H(8A)-C(8)-H(8B)	109.5
C(19)-P(2)-C(22)	119.34(14)	C(5)-C(8)-H(8C)	109.5
C(19)-P(2)-C(10)	96.54(14)	H(8A)-C(8)-H(8C)	109.5
C(22)-P(2)-C(10)	105.84(15)	H(8B)-C(8)-H(8C)	109.5
C(19)-P(2)-Ir(1)	89.51(9)	C(3)-C(9)-P(1)	111.1(2)
C(22)-P(2)-Ir(1)	131.68(11)	C(3)-C(9)-H(9A)	109.4
C(10)-P(2)-Ir(1)	108.33(10)	P(1)-C(9)-H(9A)	109.4
C(2)-C(1)-C(19)	118.4(2)	C(3)-C(9)-H(9B)	109.4
C(2)-C(1)-Ir(1)	93.87(18)	P(1)-C(9)-H(9B)	109.4
C(19)-C(1)-Ir(1)	103.24(18)	H(9A)-C(9)-H(9B)	108.0
C(2)-C(1)-H(1)	113.1	C(7)-C(10)-P(2)	109.6(2)
C(19)-C(1)-H(1)	113.1	C(7)-C(10)-H(10A)	109.8
Ir(1)-C(1)-H(1)	113.1	P(2)-C(10)-H(10A)	109.8
C(7)-C(2)-C(3)	117.8(3)	C(7)-C(10)-H(10B)	109.8
C(7)-C(2)-C(1)	123.0(3)	P(2)-C(10)-H(10B)	109.8
C(3)-C(2)-C(1)	118.6(3)	H(10A)-C(10)-H(10B)	108.2
C(4)-C(3)-C(2)	119.8(3)	C(12)-C(11)-C(14)	108.5(3)
C(4)-C(3)-C(9)	122.1(3)	C(12)-C(11)-C(13)	110.1(3)
C(2)-C(3)-C(9)	117.6(3)	C(14)-C(11)-C(13)	107.1(3)
C(5)-C(4)-C(3)	121.7(3)	C(12)-C(11)-P(1)	110.4(2)
C(5)-C(4)-H(4)	119.1	C(14)-C(11)-P(1)	106.3(2)
C(3)-C(4)-H(4)	119.1	C(13)-C(11)-P(1)	114.2(2)

C(11)-C(12)-H(12A)	109.5	C(15)-C(18)-H(18B)	109.5
C(11)-C(12)-H(12B)	109.5	H(18A)-C(18)-H(18B)	109.5
H(12A)-C(12)-H(12B)	109.5	C(15)-C(18)-H(18C)	109.5
C(11)-C(12)-H(12C)	109.5	H(18A)-C(18)-H(18C)	109.5
H(12A)-C(12)-H(12C)	109.5	H(18B)-C(18)-H(18C)	109.5
H(12B)-C(12)-H(12C)	109.5	C(20)-C(19)-C(21)	109.3(3)
C(11)-C(13)-H(13A)	109.5	C(20)-C(19)-C(1)	108.7(2)
C(11)-C(13)-H(13B)	109.5	C(21)-C(19)-C(1)	116.0(2)
H(13A)-C(13)-H(13B)	109.5	C(20)-C(19)-P(2)	111.9(2)
C(11)-C(13)-H(13C)	109.5	C(21)-C(19)-P(2)	120.5(2)
H(13A)-C(13)-H(13C)	109.5	C(1)-C(19)-P(2)	88.74(18)
H(13B)-C(13)-H(13C)	109.5	C(19)-C(20)-H(20A)	109.5
C(11)-C(14)-H(14A)	109.5	C(19)-C(20)-H(20B)	109.5
C(11)-C(14)-H(14B)	109.5	H(20A)-C(20)-H(20B)	109.5
H(14A)-C(14)-H(14B)	109.5	C(19)-C(20)-H(20C)	109.5
C(11)-C(14)-H(14C)	109.5	H(20A)-C(20)-H(20C)	109.5
H(14A)-C(14)-H(14C)	109.5	H(20B)-C(20)-H(20C)	109.5
H(14B)-C(14)-H(14C)	109.5	C(19)-C(21)-H(21A)	109.5
C(18)-C(15)-C(17)	108.5(3)	C(19)-C(21)-H(21B)	109.5
C(18)-C(15)-C(16)	108.0(3)	H(21A)-C(21)-H(21B)	109.5
C(17)-C(15)-C(16)	109.0(3)	C(19)-C(21)-H(21C)	109.5
C(18)-C(15)-P(1)	106.1(2)	H(21A)-C(21)-H(21C)	109.5
C(17)-C(15)-P(1)	114.4(2)	H(21B)-C(21)-H(21C)	109.5
C(16)-C(15)-P(1)	110.6(2)	C(25)-C(22)-C(24)	109.5(3)
C(15)-C(16)-H(16A)	109.5	C(25)-C(22)-C(23)	109.5(3)
C(15)-C(16)-H(16B)	109.5	C(24)-C(22)-C(23)	110.2(3)
H(16A)-C(16)-H(16B)	109.5	C(25)-C(22)-P(2)	107.3(2)
C(15)-C(16)-H(16C)	109.5	C(24)-C(22)-P(2)	111.6(2)
H(16A)-C(16)-H(16C)	109.5	C(23)-C(22)-P(2)	108.7(2)
H(16B)-C(16)-H(16C)	109.5	C(22)-C(23)-H(23A)	109.5
C(15)-C(17)-H(17A)	109.5	C(22)-C(23)-H(23B)	109.5
C(15)-C(17)-H(17B)	109.5	H(23A)-C(23)-H(23B)	109.5
H(17A)-C(17)-H(17B)	109.5	C(22)-C(23)-H(23C)	109.5
C(15)-C(17)-H(17C)	109.5	H(23A)-C(23)-H(23C)	109.5
H(17A)-C(17)-H(17C)	109.5	H(23B)-C(23)-H(23C)	109.5
H(17B)-C(17)-H(17C)	109.5	C(22)-C(24)-H(24A)	109.5
C(15)-C(18)-H(18A)	109.5	C(22)-C(24)-H(24B)	109.5

H(24A)-C(24)-H(24B)	109.5	H(25A)-C(25)-H(25B)	109.5
C(22)-C(24)-H(24C)	109.5	C(22)-C(25)-H(25C)	109.5
H(24A)-C(24)-H(24C)	109.5	H(25A)-C(25)-H(25C)	109.5
H(24B)-C(24)-H(24C)	109.5	H(25B)-C(25)-H(25C)	109.5
C(22)-C(25)-H(25A)	109.5	O(1)-C(26)-Ir(1)	172.7(3)
C(22)-C(25)-H(25B)	109.5		

Table 3.5 Anisotropic Displacement Parameters ($Å^2 x\ 10^3$) for (Me-PCP)Ir–CO Cyclometalated, **3-3**. The anisotropic displacement factor exponent takes the form: $-2\pi^2[\ h^2\ a^{*2}U^{11} + ...\ + 2\ h\ k\ a^*\ b^*\ U^{12}\ ]$.

	U^{11}	U^{22}	U^{33}	U^{23}	U^{13}	U^{12}
Ir(1)	10(1)	20(1)	13(1)	0(1)	1(1)	-1(1)
P(1)	12(1)	24(1)	15(1)	1(1)	2(1)	-1(1)
P(2)	12(1)	27(1)	15(1)	-2(1)	2(1)	0(1)
C(1)	15(1)	20(1)	21(1)	-4(1)	0(1)	1(1)
C(2)	15(1)	22(1)	20(1)	1(1)	-2(1)	0(1)
C(3)	18(1)	24(1)	17(1)	0(1)	-1(1)	2(1)
C(4)	23(1)	28(2)	22(1)	-7(1)	-1(1)	3(1)
C(5)	24(2)	24(1)	32(2)	-9(1)	0(1)	1(1)
C(6)	24(2)	22(1)	34(2)	-3(1)	2(1)	-3(1)
C(7)	18(1)	22(1)	24(1)	-2(1)	1(1)	0(1)
C(8)	38(2)	24(2)	44(2)	-13(1)	-1(2)	0(1)
C(9)	17(1)	29(1)	13(1)	0(1)	2(1)	1(1)
C(10)	18(1)	24(1)	25(1)	-1(1)	2(1)	-4(1)
C(11)	22(1)	24(1)	29(2)	2(1)	7(1)	-4(1)
C(12)	24(2)	27(2)	52(2)	-6(2)	2(2)	-6(1)
C(13)	45(2)	34(2)	42(2)	5(2)	17(2)	-8(2)
C(14)	30(2)	22(1)	33(2)	1(1)	1(1)	-2(1)
C(15)	17(1)	31(2)	22(1)	0(1)	2(1)	3(1)
C(16)	20(1)	36(2)	29(2)	1(1)	-4(1)	2(1)
C(17)	22(2)	48(2)	31(2)	3(2)	8(1)	7(1)
C(18)	26(2)	25(1)	31(2)	-2(1)	-2(1)	4(1)
C(19)	18(1)	21(1)	23(1)	-1(1)	2(1)	2(1)
C(20)	25(2)	26(2)	33(2)	-5(1)	3(1)	6(1)
C(21)	19(1)	35(2)	26(2)	2(1)	1(1)	4(1)
C(22)	17(1)	36(2)	18(1)	-1(1)	5(1)	1(1)
C(23)	32(2)	49(2)	25(2)	-15(2)	8(1)	-7(2)
C(24)	19(2)	46(2)	30(2)	-6(1)	9(1)	-4(1)
C(25)	42(2)	55(2)	21(2)	8(2)	8(1)	11(2)
C(26)	16(1)	28(2)	18(1)	-1(1)	2(1)	1(1)
O(1)	29(1)	52(2)	20(1)	-1(1)	-5(1)	3(1)

Table 3.6 Hydrogen Coordinates (x 10^4) and Isotropic Displacement Parameters ($Å^2$x 10 ^{3}) for (Me-PCP)Ir–CO Cyclometalated, **3-3**

	x	y	z	U(eq)
H(1)	9961	4096	3826	23
H(4)	8754	6933	5086	29
H(6)	11187	7970	3677	32
H(8A)	9558	9091	4558	53
H(8B)	10799	8859	4992	53
H(8C)	9625	8536	5388	53
H(9A)	7793	5350	4802	23
H(9B)	8708	4462	4659	23
H(10A)	12200	6358	2814	27
H(10B)	11140	6971	2389	27
H(12A)	6382	3341	2512	52
H(12B)	5363	3518	3097	52
H(12C)	5962	2429	3043	52
H(13A)	5801	3748	4508	59
H(13B)	7082	3514	4879	59
H(13C)	6278	2610	4540	59
H(14A)	7789	2051	3689	43
H(14B)	8625	2922	4049	43
H(14C)	8398	2828	3123	43
H(16A)	5352	4962	2533	43
H(16B)	6213	5778	2185	43
H(16C)	5042	6141	2566	43
H(17A)	5884	5711	4550	50
H(17B)	5090	4975	4004	50
H(17C)	4881	6172	3970	50
H(18A)	6326	7292	3314	41
H(18B)	7545	6808	3097	41
H(18C)	7223	6887	3990	41
H(20A)	11857	3039	2471	42
H(20B)	10467	3142	2439	42
H(20C)	11158	2798	3230	42
H(21A)	12550	4014	3906	40
H(21B)	12535	5182	3659	40

H(21C)	13113	4359	3116	40
H(23A)	11455	4200	333	52
H(23B)	10315	4140	828	52
H(23C)	11496	3599	1144	52
H(24A)	13141	4601	1719	47
H(24B)	13099	5811	1703	47
H(24C)	13223	5192	910	47
H(25A)	11415	6036	293	59
H(25B)	11408	6696	1074	59
H(25C)	10265	6085	777	59

Table 3.7 Torsion Angles [°] for (Me-PCP)Ir–CO Cyclometalated, **3-3**

C(26)-Ir(1)-P(1)-C(9)	-163.93(13)	C(3)-C(4)-C(5)-C(8)	-179.5(3)
C(1)-Ir(1)-P(1)-C(9)	24.56(13)	C(4)-C(5)-C(6)-C(7)	-6.3(5)
P(2)-Ir(1)-P(1)-C(9)	4.86(12)	C(8)-C(5)-C(6)-C(7)	179.0(3)
C(26)-Ir(1)-P(1)-C(15)	-48.60(15)	C(5)-C(6)-C(7)-C(2)	-3.0(5)
C(1)-Ir(1)-P(1)-C(15)	139.89(14)	C(5)-C(6)-C(7)-C(10)	167.7(3)
P(2)-Ir(1)-P(1)-C(15)	120.20(12)	C(3)-C(2)-C(7)-C(6)	12.7(4)
C(26)-Ir(1)-P(1)-C(11)	83.44(15)	C(1)-C(2)-C(7)-C(6)	-176.4(3)
C(1)-Ir(1)-P(1)-C(11)	-88.07(14)	C(3)-C(2)-C(7)-C(10)	-158.1(3)
P(2)-Ir(1)-P(1)-C(11)	-107.76(13)	C(1)-C(2)-C(7)-C(10)	12.8(4)
C(26)-Ir(1)-P(2)-C(19)	-146.53(13)	C(4)-C(3)-C(9)-P(1)	117.7(3)
C(1)-Ir(1)-P(2)-C(19)	22.91(13)	C(2)-C(3)-C(9)-P(1)	-54.5(3)
P(1)-Ir(1)-P(2)-C(19)	44.77(11)	C(15)-P(1)-C(9)-C(3)	-89.6(2)
C(26)-Ir(1)-P(2)-C(22)	-16.10(18)	C(11)-P(1)-C(9)-C(3)	154.9(2)
C(1)-Ir(1)-P(2)-C(22)	153.34(17)	Ir(1)-P(1)-C(9)-C(3)	32.7(2)
P(1)-Ir(1)-P(2)-C(22)	175.20(14)	C(6)-C(7)-C(10)-P(2)	-160.2(2)
C(26)-Ir(1)-P(2)-C(10)	116.74(14)	C(2)-C(7)-C(10)-P(2)	10.6(3)
C(1)-Ir(1)-P(2)-C(10)	-73.82(14)	C(19)-P(2)-C(10)-C(7)	-57.9(2)
P(1)-Ir(1)-P(2)-C(10)	-51.96(13)	C(22)-P(2)-C(10)-C(7)	179.1(2)
C(26)-Ir(1)-C(1)-C(2)	141.7(5)	Ir(1)-P(2)-C(10)-C(7)	33.8(2)
P(2)-Ir(1)-C(1)-C(2)	92.14(17)	C(9)-P(1)-C(11)-C(12)	167.2(2)
P(1)-Ir(1)-C(1)-C(2)	-76.51(16)	C(15)-P(1)-C(11)-C(12)	56.6(3)
C(26)-Ir(1)-C(1)-C(19)	21.4(6)	Ir(1)-P(1)-C(11)-C(12)	-77.3(2)
P(2)-Ir(1)-C(1)-C(19)	-28.20(15)	C(9)-P(1)-C(11)-C(14)	-75.4(2)
P(1)-Ir(1)-C(1)-C(19)	163.16(18)	C(15)-P(1)-C(11)-C(14)	174.0(2)
C(19)-C(1)-C(2)-C(7)	23.8(4)	Ir(1)-P(1)-C(11)-C(14)	40.1(3)
Ir(1)-C(1)-C(2)-C(7)	-83.5(3)	C(9)-P(1)-C(11)-C(13)	42.5(3)
C(19)-C(1)-C(2)-C(3)	-165.3(3)	C(15)-P(1)-C(11)-C(13)	-68.1(3)
Ir(1)-C(1)-C(2)-C(3)	87.4(3)	Ir(1)-P(1)-C(11)-C(13)	158.0(2)
C(7)-C(2)-C(3)-C(4)	-13.3(4)	C(9)-P(1)-C(15)-C(18)	57.5(2)
C(1)-C(2)-C(3)-C(4)	175.4(3)	C(11)-P(1)-C(15)-C(18)	166.4(2)
C(7)-C(2)-C(3)-C(9)	159.1(3)	Ir(1)-P(1)-C(15)-C(18)	-59.2(2)
C(1)-C(2)-C(3)-C(9)	-12.2(4)	C(9)-P(1)-C(15)-C(17)	-62.1(3)
C(2)-C(3)-C(4)-C(5)	4.1(5)	C(11)-P(1)-C(15)-C(17)	46.8(3)
C(9)-C(3)-C(4)-C(5)	-167.9(3)	Ir(1)-P(1)-C(15)-C(17)	-178.8(2)
C(3)-C(4)-C(5)-C(6)	5.7(5)	C(9)-P(1)-C(15)-C(16)	174.4(2)

C(11)-P(1)-C(15)-C(16)	-76.7(3)	C(10)-P(2)-C(19)-C(1)	79.25(18)
Ir(1)-P(1)-C(15)-C(16)	57.7(2)	Ir(1)-P(2)-C(19)-C(1)	-29.14(15)
C(2)-C(1)-C(19)-C(20)	177.7(3)	C(19)-P(2)-C(22)-C(25)	-169.9(2)
Ir(1)-C(1)-C(19)-C(20)	-80.4(3)	C(10)-P(2)-C(22)-C(25)	-62.8(3)
C(2)-C(1)-C(19)-C(21)	54.0(4)	Ir(1)-P(2)-C(22)-C(25)	70.9(3)
Ir(1)-C(1)-C(19)-C(21)	155.9(2)	C(19)-P(2)-C(22)-C(24)	-49.9(3)
C(2)-C(1)-C(19)-P(2)	-69.6(3)	C(10)-P(2)-C(22)-C(24)	57.2(3)
Ir(1)-C(1)-C(19)-P(2)	32.29(16)	Ir(1)-P(2)-C(22)-C(24)	-169.11(19)
C(22)-P(2)-C(19)-C(20)	-58.7(3)	C(19)-P(2)-C(22)-C(23)	71.7(3)
C(10)-P(2)-C(19)-C(20)	-171.0(2)	C(10)-P(2)-C(22)-C(23)	178.9(2)
Ir(1)-P(2)-C(19)-C(20)	80.6(2)	Ir(1)-P(2)-C(22)-C(23)	-47.4(3)
C(22)-P(2)-C(19)-C(21)	71.8(3)	C(1)-Ir(1)-C(26)-O(1)	17(3)
C(10)-P(2)-C(19)-C(21)	-40.5(3)	P(2)-Ir(1)-C(26)-O(1)	63(2)
Ir(1)-P(2)-C(19)-C(21)	-148.9(2)	P(1)-Ir(1)-C(26)-O(1)	-123(2)
C(22)-P(2)-C(19)-C(1)	-168.44(18)		

References

(1) van der Boom, M. E.; Kraatz, H.-B.; Ben-David, Y.; Milstein, D. *Chem. Commun.* **1996**, 2167.
(2) Cohen, R.; van der Boom, M. E.; Shimon, L. J. W.; Rozenberg, H.; Milstein, D. *J. Am. Chem. Soc.* **2000**, *122*, 7723.
(3) Rybtchinski, B.; Vigalok, A.; Ben-David, Y.; Milstein, D. *J. Am. Chem. Soc.* **1996**, *118*, 12406.
(4) Vigalok, A.; Rybtchinski, B.; Shimon, L. J. W.; Ben-David, Y.; Milstein, D. *Organometallics* **1999**, *18*, 895.
(5) Van der Boom, M. E.; Kraatz, H.-B.; Hassner, L.; Ben-David, Y.; Milstein, D. *Organometallics* **1999**, *18*, 3873.
(6) Gozin, M.; Weisman, A.; Bendavid, Y.; Milstein, D. *Nature* **1993**, *364*, 699.
(7) van der Boom, M. E.; Liou, S.-Y.; Shimon, L. J. W.; Ben-David, Y.; Milstein, D. *Inorg. Chim. Acta.* **2004**, *357*, 4015.
(8) Kundu, S.; Choi, J.; Wang, D. Y.; Choliy, Y.; Emge, T. J.; Krogh-Jespersen, K.; Goldman, A. S. *J. Am. Chem. Soc.* **2013**, *135*, 5127.
(9) Nemeh, S.; Jensen, C.; Binamira-Soriaga, E.; Kaska, W. C. *Organometallics* **1983**, *2*, 1442.
(10) Mohammad, H. A. Y.; Grimm, J. C.; Eichele, K.; Mack, H.-G.; Speiser, B.; Novak, F.; Quintanilla, M. G.; Kaska, W. C.; Mayer, H. A. *Organometallics* **2002**, *21*, 5775.
(11) Conner, D.; Jayaprakash, K. N.; Cundari, T. R.; Gunnoe, T. B. *Organometallics* **2004**, *23*, 2724.
(12) Koridze, A. A. *Russian Chemical Bulletin Int. Ed.* **2010**, *59*, 745.
(13) Göttker-Schnetmann, I.; White, P. S.; Brookhart, M. *Organometallics* **2004**, *23*, 1766.
(14) Lokare, K. S.; Nielsen, R. J.; Yousufuddin, M.; Goddard, W. A.; Periana, R. A. *Dalton Trans* **2011**, *40*, 9094.
(15) Zhu, K.; Achord, P. D.; Zhang, X.; Krogh-Jespersen, K.; Goldman, A. S. *J. Am. Chem. Soc.* **2004**, *126*, 13044.
(16) Krogh-Jespersen, K.; Czerw, M.; Zhu, K.; Singh, B.; Kanzelberger, M.; Darji, N.; Achord, P. D.; Renkema, K. B.; Goldman, A. S. *J. Am. Chem. Soc.* **2002**, *124*, 10797.
(17) Doherty, M. D.; Grills, D. C.; Huang, K.-W.; Muckerman, J. T.; Polyansky, D. E.; Eldik, R. v.; Fujita, E. *Inorg. Chem.* **2013**, *52*, 4160.
(18) Lee, D. W.; Jensen, C. M.; Morales-Morales, D. *Organometallics* **2003**, *22*, 4744.
(19) Morales-Morales, D.; Redon, R.; Wang, Z.; Lee, D. W.; Yung, C.; Magnuson, K.; Jensen, C. M. *Can. J. Chem.* **2001**, *79*, 823.
(20) Nguyen, B.; Brown, J. M. *Adv. Synth. Catal.* **2009**, *351*, 1333.
(21) Romero, P. E.; Whited, M. T.; Grubbs, R. H. *Organometallics* **2008**, *27*, 3422.
(22) Whited, M. T.; Grubbs, R. H. *J. Am. Chem. Soc.* **2008**, *130*, 5874.
(23) Kanzelberger, M.; Singh, B.; Czerw, M.; Krogh-Jespersen, K.; Goldman, A. S. *J. Am. Chem. Soc.* **2000**, *122*, 11017.
(24) Lee, D. W.; Kaska, W. C.; Jensen, C. M. *Organometallics* **1998**, *17*, 1.
(25) Laviska, D. A., Rutgers, The State University of New Jersey, 2013.
(26) Moulton, C. J.; Shaw, B. L. *J. Chem. Soc., Chem. Comm.* **1976**, 365.
(27) Gupta, M.; Hagen, C.; Flesher, R. J.; Kaska, W. C.; Jensen, C. M. *Chem. Commun.* **1996**, 2083.
(28) Kundu, S., Rutgers, The State University of New Jersey, 2010.

Chapter 4

Initial Studies on the Reactivity of (Me-PCP)Ir Towards Oxidants

Abstract

Transition metals have become easy targets for the selective oxidation of petroleum feedstocks, but the current understanding of these transformations is limited to oxygen activation and binding, the reactivity of oxidants and isolation of a few intermediates. The synthesis and characterization of two (Me-PCP)Ir oxygen species is detailed via direct reaction with oxygen. A discussion of (Me-PCP)Ir reactivity with different oxidants will follow. For example, reaction with dimethyldioxirane leads to ring opening of DMDO yielding an acetate ligand and reaction with hydrogen peroxide leads to a cyclometalated product. Finally, the efforts to react nitrous oxide with (Me-PCP)Ir are discussed.

4.1 Introduction

The selective oxidation of petroleum feedstocks to produce a variety of alcohols, esters, ethers, acids, etc. is one of the foremost challenges in the chemical world today.[1,2] Not only is the production of these useful chemicals important, but the development of more atom economical routes to these chemical products is also necessary, particularly through incorporation of carbon dioxide synthesized by use of hydrocarbons.[3] Transition metals have become easy targets for these goals, but the current understanding of these transformations stems from deficient knowledge of the reactivity of oxidants, including oxygen, towards transition metals and limited isolation of reactive intermediates to harness the selectivity of oxygen type complexes in catalytic cycles.[4]

Molecular oxygen has been shown to bind to all transition metals either in a monomeric fashion, through side-on (two oxygens bound to one metal center) or end-on (one oxygen bound to one metal center) binding modes, or in dimeric fashion (O_2 is shared between two metal centers).[5] One of the most important advances in the field of transition metal oxygen complexes was the discovery of reversible oxygen binding to the square planar iridium (I) complex synthesized by Vaska originally discussed in Chapter 1 (Scheme 4.1).[6] This was the first report of side-on binding of O_2 to a metal center. Since the synthesis of this complex and the study of its reversible nature, many analogous structures have been isolated.

Scheme 4.1 Reversible Binding of Oxygen to Vaska's Complex

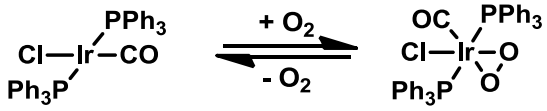

In reference to the work presented here, different pincer type complexes have been known to react with oxygen differently.[4] The insertion of O_2 into a Pd-H bond of (PCP)PdH yields a Pd(II) hydroperoxide complex as well as a hydroxide complex in small amounts.[4,7] This insertion is thought to proceed through direct attack of the oxygen at the Pd-H bond. Meanwhile, reaction of the 14e$^-$ (PCP)Ir fragment with O_2 leads to mono and bis di-oxygen complexes with no evidence of any oxygen insertion into the Ir-H bond.[4,8] Addition of oxygen to the 16e$^-$ (PCP)IrH_2 complex leads to observation of a dihydride dioxygen complex, suggesting O_2 coordinates to the open site then promotes reductive elimination of H_2 to form the mono bis-

oxygen complex. The addition of O_2 is found to be reversible as addition of hydrogen leads to elimination of water and formation of (PCP)IrH_4 (the oxidative addition of water to the active 14e$^-$ (PCP)Ir complex and formation of the hydrido hydroxyl species was previously discussed in Chapter 2).[9]

Even though O_2 is an attractive oxidant to utilize in terms of cost and accessibility, the formation of these bis di-oxygen complexes are generally very stable and oftentimes characterized as decomposition of the catalyst as no further transformations are observed. Conversely, O-O bond breakage, leading to a highly reactive metal-oxo complex in which a single oxygen is bound to a metal center, is quite difficult due to the high energy barrier and very rare. Generation of these metal-oxo complexes must proceed through alternative methods. Metal oxo complexes can lead to functionalization of many substrates and have been proposed as the active species in many systems.[2] Terminal oxo complexes for early transition metals are quite common and very stable.[10] However, for late transition metals, terminal oxo complexes are much rarer though the possibility of alkane functionalization seems more probable in the cases of late transition metal complexes due to their strong abilities for C-H activation. In fact, there exists an "oxo wall" in which late transition metal (d^4 and above) oxo complexes cannot exist in an octahedral environment. Terminal oxo ligands are excellent π donors as well as hard Lewis acids and require empty π orbitals for bonding, therefore the hard early transition metals with low oxidations states and low *d*-electron counts are preferred in order to satisfy the needs of a stable oxo complex. Oftentimes, in attempts to stabilize the oxo ligand, bridging will occur allowing for multiple metal centers to fulfill the electron orbital needs of the oxygen.

Various attempts have been used to synthesize these oxo complexes, including an array of oxidants (e.g. nitrous oxides (and derivatives), water, peroxides, etc.). The first reported example of a late transition metal oxo complex in the platinum group was a trimesityl iridium complex in which the oxo ligand is stabilized by a tetrahedral environment, minimizing the interactions between the iridium *d*-electrons and the oxo ligand.[11] This was accomplished via a quantitative reaction with $Ir(mes)_3$ and trimethylamine *N*-oxide (Me_3NO, TMAO) in diethylether. In relation to pincer type complexes, a dinuclear μ-oxo $PC_{sp2}P$ iridium complex, in which one oxygen bridges two iridium centers was synthesized starting from the hydroxide derivative.[12] A terminal cationic Pt(IV) oxo complex was synthesized via reaction of a

cationic (PCN)Pt(acetone) complex with dimethyldioxirane (DMDO, Scheme 4.2).[13-15] DMDO is a cyclic peroxide prepared in acetone and is the most common oxidant to rapidly oxidize alkenes.[16-18]

Scheme 4.2 Reaction of Cationic (PCN)Pt Pincer Complex with DMDO

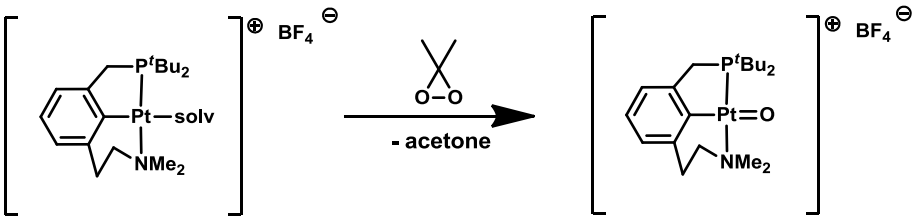

Little is known of the reactivity of nitrous oxide as an oxidant. N_2O is a poor ligand for transition metals because of its weak σ-donating and π-accepting abilities.[19] The molecule has a number of binding motifs as it can bind end-on through η^1-oxygen or nitrogen, though it also has η^2 and η^3 modes as well. Generally, reactions with N_2O and transition metals can be summarized into three categories: as an oxo transfer in which N_2 gas is released, an oxo or N_2O insertion into a metal-alkyl or hydride bond, and N-N bond scission. Recently, Caulton and coworkers reported a (PNP)Rh species (PNP =(^{t}Bu$_2$PCH$_2$SiMe$_2$)$_2$N) that undergoes oxidation by N_2O to yield the (PNP)RhN_2 species and a proposed terminal oxo species as an intermediate decomposing to a hydroxide species at room temperature.[20,21] The synthesis of the terminal oxo species is supported by DFT calculations and various spectroscopic techniques.

One of the advantages of using H_2O_2 as an oxidant is the mild byproducts created upon decomposition (either H_2O or H_2). De Bruin published the first example of the oxidation of rhodium and iridium olefin complexes utilizing hydrogen peroxide.[22] A series of hydroxo and oxo species were proposed as intermediates in the DFT calculated mechanism.[23] Hydrogen peroxide can also be thought of as an intermediate in the water oxidation cycle. Milstein et. al. proposed an approach to a catalytic cycle in which a (PNN)Ru complex activates water to form a dihydroxo complex and hydrogen, irradiation releases hydrogen peroxide, which decomposes to dioxygen and water, and addition of water regenerates the active catalyst to restart the cycle.[24]

This chapter will focus on introductory experiments conducted between (Me-PCP)Ir and different oxidants. Similar to the parent (PCP)Ir complex, the synthesis of mono and bis di-oxygen (Me-PCP)Ir complexes are detailed. A reaction with DMDO leads to ring opening of DMDO to form a (Me-

PCP)Ir(acetate) complex. Next, reaction with hydrogen peroxide leads to the mono oxygen complex as well as a cyclometalated product, similar to those described in Chapter 3. The characterization of this cyclometalated oxygen complex along with a six coordinate cyclometalated CO adduct is discussed. Finally, efforts to react nitrous oxide with (Me-PCP)Ir close this chapter.

4.2 Results and Discussion

4.2.1 Isolation of the (Me-PCP)Ir Dioxygen Complexes

When oxygen is bubbled through a solution of (Me-PCP)IrH_n in C_6D_6, **4-1** and **4-2** are isolated in approximately 3:2 ratio (Scheme 4.3).[25] Both of these complexes have similar NMR spectral characteristics to each other as well as to the parent bis oxygen complexes. Two peaks at 46.8 and 28.7 ppm are observed in the ^{31}P NMR spectrum for the mono and bis di-oxygen complexes, respectively. The only difference in the ^{1}H NMR spectra between the (Me-PCP)Ir and parent (PCP)Ir bis di-oxygen complexes is the inclusion of the para methyl shift observed as a singlet at 3.5 and 3.3 ppm for **4-1** and **4-2**, respectively.

Scheme 4.3 Reaction Between the (Me-PCP)IrH_n and O_2

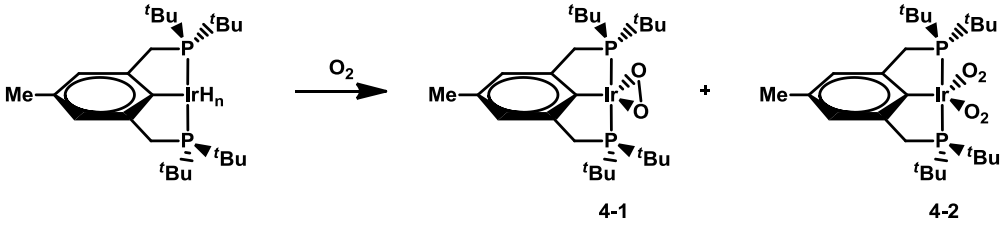

4.2.2 Reaction with DMDO, TMAO, Acetone, and H_2O_2

When (Me-PCP)IrH_n is reacted with DMDO in acetone and *p*-xylene-d_{10}, the major product for the reaction is the (Me-PCP)Ir(H)($OCOCH_3$) complex (**4-3**) and ethane, as determined by ^{31}P and ^{1}H NMR spectroscopy (Scheme 4.4). To achieve mass balance, for every 1 mol of iridium, 0.5 mol of ethane is produced, presumably formed through an iridium assisted CH_3 recombination. The overall mechanism is unknown but may proceed through ring opening of DMDO through a Baeyer-Villager type rearrangement occurs to give an acetate ligand. The parent (PCP)Ir(H)($OCOCH_3$) was previously synthesized by reacting (PCP)Ir-TBE complex with ethyl acetate to produce (PCP)Ir(H)($OCOCH_3$) and ethane.[26,27]

Scheme 4.4 Reaction of (Me-PCP)IrH_4 with DMDO

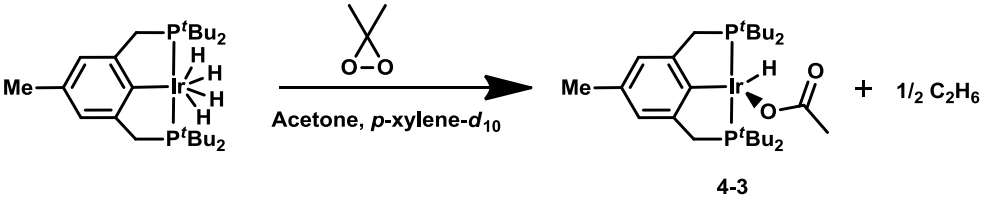

4-3

If the (Me-PCP)Ir fragment is reacted with acetone alone an unstable complex (PCP)Ir(acetone) complex (**4-4**) is formed (Scheme 4.5). The ^{31}P NMR spectrum shows a broad signal at approximately 68 ppm for species **4-4**, as well as a signal for the vinyl hydride (discussed in Chapter 2). The ^{1}H NMR spectrum shows a very broad signal at approximately -37 ppm for the Ir-H of this complex, unfortunately, no other ^{1}H NMR signals were distinguishable. Complex **4-4** is similar in nature to an intermediate proposed by Milstein in which acetone undergoes initial O-coordination to (PNP)IrCOE (COE = cyclooctene) followed by C-H activation and proton migration to the PNP backbone to form a (PNP)Ir(acetone) complex.[28] Over time, the broad peak observed at 69 ppm in the ^{31}P NMR spectrum fades into the noise and impurities become the major signals observed. It can be concluded that acetone is very labile and does not bind tightly to (Me-PCP)Ir, similar to other labile ligands (see Chapters 2 and 5).

Scheme 4.5 Addition of Acetone to (PCP)IrTBE Complex

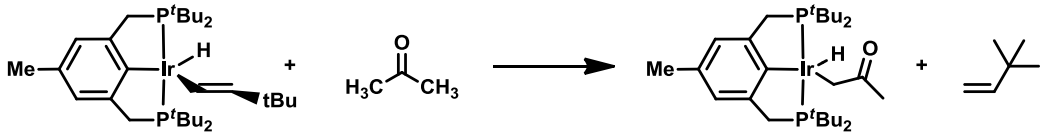

4-4

As in the case of the trimesityliridium oxo species reported by Wilkinson, the (Me-PCP)Ir fragment was reacted with TMAO in *p*-xylene-d_{10}. This reaction was not clean and no major species were detectable by ^{31}P NMR spectroscopy. Presumably, low solubility of TMAO in *p*-xylene leads to a slow and/or incomplete reaction.

Upon addition of hydrogen peroxide to the 14e$^-$ (Me-PCP)Ir species, the monomeric dioxygen species **4-1** is observed as the major product, supported by ^{1}H and ^{31}P NMR spectroscopy (Scheme 4.6). It would seem hydrogen is generated via dehydrogenation of H_2O_2, but as no free hydrogen gas is observed

by NMR, hydrogenation of norbornene to form norbornane most likely occurs. It is also noted that low solubility of H_2 in different solvents could contribute to the lack of free H_2 observed by NMR.

Scheme 4.6 Reaction of H_2O_2 with (Me-PCP)IrNBE Complex

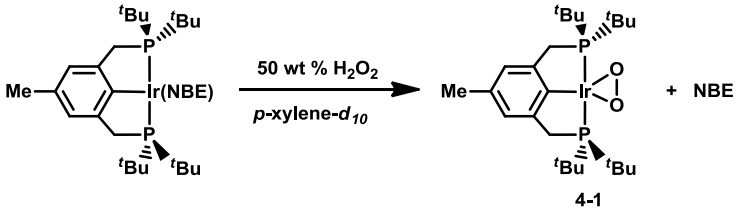

4-1

4.2.3 Cyclometalation in the Presence of Oxidants

Leaving the reaction mixture of Scheme 4.6 at room temperature for 24 hours or more, complex **4-5** is synthesized *in situ* (Scheme 4.7). Complex **4-5** exhibits spectroscopic data similar to the cyclometalated complexes discussed in Chapter 3. Two sets of doublets are observed at 44.6 and 3.5 ppm in the ^{31}P NMR spectrum with J_{PP} = 349 Hz. The methylene protons attached to the backbone exhibit splitting of the methylene signal into four multiplets ranging from 3.07 to 3.15 ppm. Meanwhile, the ^{t}butyl groups are distinctively split into three doublets at 1.36, 1.19 and 1.13 ppm which each integrate to 9 protons. The methyl group signals of the newly created cyclometalated arm are also observed as doublets at 1.5 and 0.73 ppm. Most likely, a hydroxide ligand stabilizes this five coordinate species as no hydride is observed in the hydride region of the ^1H NMR spectrum. Caulton also proposed a cyclometalated hydroxide product upon deoxygenation of (PNP)Rh with N_2O.[20] The hydroxide proton in Caulton's complex was observed as a signal at δ = -3.0 ppm. Unfortunately, no hydroxide shift was observed for **4-5**. As hydroxide ^1H NMR signals are often weak and or broad, the lack of observed hydroxide signal does not negate its presence.[29] Complex **4-5** can also be generated via **4-1** by reaction of (Me-PCP)IrNBE with gaseous O_2 rather than reaction with H_2O_2.

Scheme 4.7 Conversion of (Me-PCP)IrO_2 into Cyclometalated Hydroxide Product **4-5**

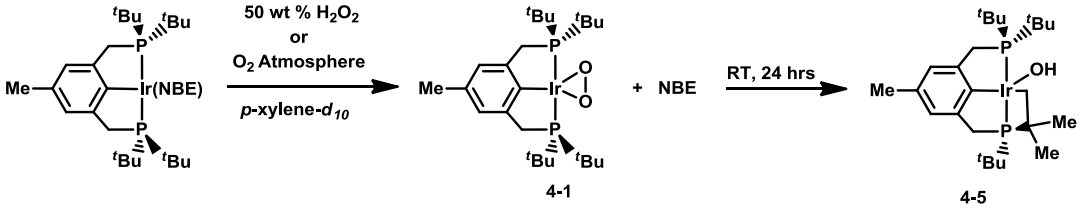

While data in Chapter 3 demonstrated that addition of CO led to an interesting cyclometalated insertion product, in this case addition of CO leads to six coordinate species **4-6** (Scheme 4.8). A doublet of doublets centered at 46 and -19 ppm are observed in the ^{31}P NMR spectrum in which J_{PP} = 315 Hz. Again, the ^{t}butyl groups are distinctively split into three doublets at 1.27, 1.18, and 1.08 ppm which each integrate to 9 protons and the methyl group signals of the cyclometalated arm are observed as doublets at 1.55 and 0.95 ppm. Unfortunately no hydroxide shift was observed for **4-6** either.

Scheme 4.8 Addition of CO to Cyclometalated Hydroxyl Species

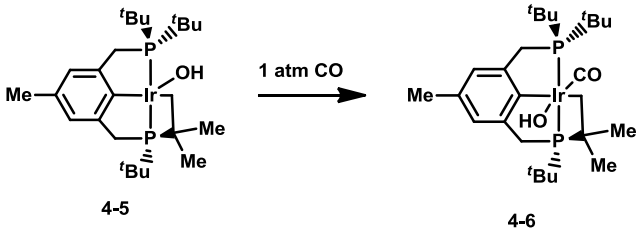

4.2.4 Reaction with N_2O

When the 14e$^-$ (Me-PCP)Ir fragment is reacted with 0.5 atm N_2O, the N_2 monomer species is formed in quantitative yield as confirmed by ^{31}P and ^{1}H NMR spectroscopy (Scheme 4.9).

Scheme 4.9 Reaction of (Me-PCP)Ir with N_2O

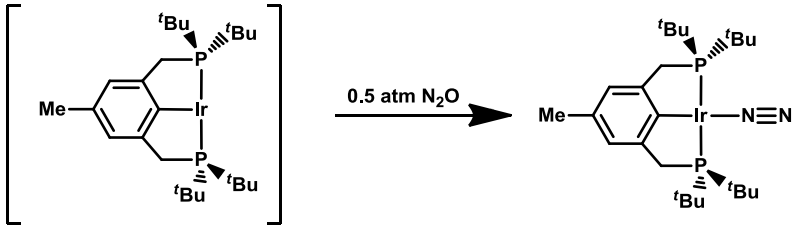

The major question has been the fate of the oxygen atom and multiple studies were undertaken to ascertain its outcome. Due to the absence of other phosphorous signals in ^{31}P NMR spectra and the

quantitative formation of (Me-PCP)IrN_2, it can be concluded that formation of a paramagnetic terminal oxo species or a phosphine oxide did not occur. If O_2 gas was formed via N-O bond scission the formation of **4-1** would be observed by ^{31}P NMR spectroscopy, but this is not the case. Independent experiments determined (Me-PCP)IrN_2 in the presence of either air or O_2 gas leads to displacement of the N_2 ligand generating **4-1** quantitatively. If oxidation of TBE occurred, an alcohol, epoxide, or ketone would be observed. Alternatively, hydride abstraction and subsequent dimerization of *p*-xylene would form 1,2-di-*p*-tolylethane and water. However, both ^{1}H NMR spectroscopy and GC analysis of the reaction mixture show no formation of new products (Tables 6.1 and 6.2).

Table 4.1 GC Data of Reaction Before Addition of N_2O

Peak	***Retention Time***	***Area %***
1	2.34	2.472
2	2.38	0.372
3	2.44	0.095
4	2.61	0.020
5	3.17	0.087
6	3.28	0.031
7	3.43	0.033
8	3.88	96.845
9	3.98	0.045

Table 4.2 GC Data for the Reaction After Addition of N_2O

Peak	***Retention Time***	***Area %***
1	2.35	2.186
2	2.39	0.363
3	2.45	0.103
4	3.18	0.084
5	3.29	0.030
6	3.44	0.032
7	3.88	97.149
8	3.99	0.052

Finally, mass spectrometry analysis was conducted to assess the purity of the N_2O. N_2O when ionized will generate N^+, O^+, NO^+, N_2^+, O_2^+ and N_2O^+ ions, whereas N_2 will generate N^+ and N_2^+ ions. At room temperature, the mass spectrum shows peaks for all six ions for N_2O; however the peak area ratios for N_2^+ at 28 m/z versus NO^+ at 30 m/z do not match the 1:3 ratio reported in the literature (Figure 4.1).[30] The

observed ratio of N_2^+: NO^+ is approximately 4:3, more consistent with a spectrum of N_2O plus N_2. Based on these results, it can be concluded that (PCP)Ir is much more reactive towards N_2 then N_2O and, hence, addition of N_2 is observed rather than any transformation with N_2O.

Figure 4.1 Room Temperature Mass Spectrum of N_2O

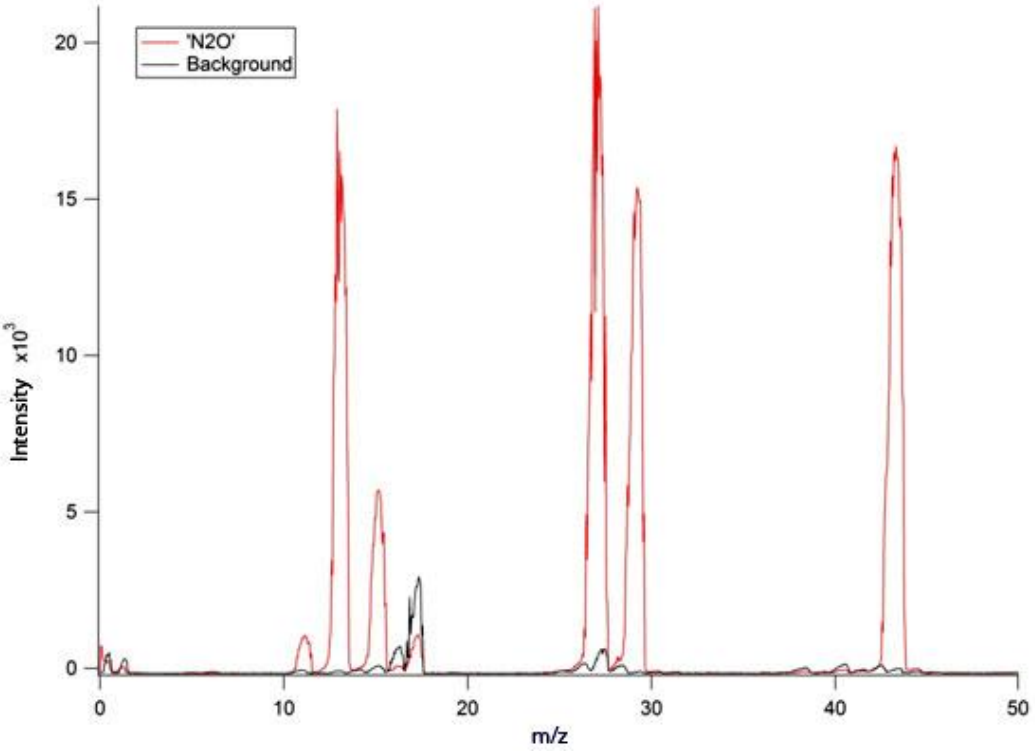

4.3 Summary

As expected addition of O_2 to (Me-PCP)Ir leads to mono and bis di-oxygen complexes **4-1** and **4-2**, which are similar to the parent bis oxygen complexes. Reaction with DMDO leads to the previously synthesized (Me-PCP)Ir(H)($OCOCH_3$) complex (**4-3**) and ethane, however the overall mechanism for this transformation is unknown. Addition of hydrogen peroxide yields species **4-1** via dehydrogenation of H_2O_2 and further reaction of **4-1** leads to an unexpected cyclometalation generating **4-5**. Finally, when the $14e^-$ (Me-PCP)Ir fragment is reacted with N_2O, the N_2 monomer species is formed quantitatively. However, it was discovered via mass spectrometry that the purity of the N_2O reactant was compromised by N_2 leading to the conclusion that that (PCP)Ir is much more reactive towards N_2 than N_2O. The reactions discussed

here lead to some initial studies with different oxidants, but more work is needed to understand the reactivity of pincer complexes in this interesting field.

4.4 Experimental

General

All reactions were performed under an argon atmosphere using standard Schlenck techniques or in an argon-filled glove box. C_6H_6, C_6D_6, TBE, and *p*-xylene-d_{10} were dried over Na/K alloy and collected via vacuum transfer. Norbornene (NBE) was sublimed before use. DMDO was synthesized as an acetone solution according the literature procedure, dried over molecular sieves and degassed prior to use (provided by the Lawrence Williams research group).[31] The concentration of DMDO solutions was determined via titration with PPh_3 as 0.202 M. H_2O_2 was purchased as 50 wt% solution from Sigma-Aldrich. N_2O was purchased as 98% purity grade gas from Aldrich. The mass spectrometry experiments were done with the assistance from the Jane Hinch Group. All other substrates were degassed before entry to glovebox and used without further purification. ^{1}H and ^{31}P NMR spectra were obtained from either a 400 or 500 MHz Varian instrument. The residual peak of the deuterated solvent was used as a reference for all ^{1}H NMR spectra and an internal capillary standard of PMe_3 in *p*-xylene-d_{10} (-62.4 ppm) was used to reference ^{31}P NMR chemical shifts.

(Me-PCP)IrO$_2$ and (Me-PCP)Ir(O$_2$)$_2$, 4-1 and 4-2

Oxygen was bubbled through a solution of 10.3 mg (Me-PCP)IrH_2 (17.1 μmol) in C_6D_6. Solution immediately changed from a deep red to green. Complexes were characterized *in situ*. **(Me-PCP)IrO$_2$, 4-1: ^{31}P NMR (C_6D_6, 161.9MHz):** δ 46.8 (s, (Me-PCP)IrO_2). **^{1}H NMR (C_6D_6, 400 MHz):** δ 6.87 (s, 2H, Ar-*H*), 3.49 (vt, *J* = 4 Hz, 4H, CH_2P), 2.36 (s, 3H, Ar-CH_3), 1.35 (t, *J* = 6 Hz, 36H, P^{t}bu). **(Me-PCP)Ir(O$_2$)$_2$, 4-2**: **^{31}P NMR (C_6D_6, 161.9MHz):** δ 28.7 (s, (Me-PCP)Ir$(O_2)_2$). **^{1}H NMR (C_6D_6, 400 MHz):** δ 6.79 (s, 2H, Ar-*H*), 3.29 (vt, *J* = 4 Hz, 4H, CH_2P), 2.31 (s, 3H, Ar-CH_3), 1.21 (t, *J* = 8 Hz, 36H, P^{t}bu).

(Me-PCP)Ir(acetone), 4-3

To a solution of 13.0 mg (Me-PCP)IrH_n (21.6 μmol) in *p*-xylene-d_{10}, 25 μL TBE (194 μmol) was added to generate the vinyl hydride complex *in situ*. Addition of 20 μL acetone (272 μmol) yielded

complex **4-3**, characterized *in situ*. **^{31}P NMR (*p*-xylene-d_{10}, 161.9 MHz):** δ 68.4 (bs). **^{1}H NMR (*p*-xylene-d_{10}, 400 MHz):** δ -37.10 (t, 1H, Ir-*H*).

(Me-PCP)Ir(H)(OCOCH$_3$), 4-4

To a solution of 9.5 mg (Me-PCP)IrHn (15.8 μmol) in *p*-xylene-d_{10}, 0.5 mL DMDO solution (101 μmol) was added. The solution instantly turned from dark red to red. The excess volatiles and solvent are removed *in vacuo* to leave behind a red powder. The powder was washed with hexanes. Hexanes were removed *in vacuo* and CD_2Cl_2 was added. **^{31}P NMR (C_6D_6, 161.9MHz)**: δ 59.9 (bs). **^{31}P NMR (*p*-xylene-d_{10}, 161.9MHz):** δ 60.23 (d, J = 10.4 Hz). **^{31}P NMR (CD_2Cl_2, 161.9MHz):** δ 59.7(d, J = 12 Hz). **^{1}H NMR (*p*-xylene-d_{10}, 400 MHz):** δ 6.52 (s, 2H, Ar-*H*), 3.07 (d of vt, J_{PH} = 3.3 Hz, J_{HH} = 17.2 Hz, 2H, CH_2P), 2.82 (d of vt, J_{PH} = 4.2 Hz, J_{HH} =16.8 Hz, 2H, CH_2P), *methyl not visible,* 1.95 (s, 3H, acetate), 1.23 (t, J_{HH} = 6.2 Hz, 18H, P^{t}bu), 1.16 (t, J_{HH} = 6.4 Hz, 18H, P^{t}bu), -30.7 (t, J_{HH} = 13.2 Hz, 1H, Ir-*H*). **^{1}H NMR (C_6D_6, 400 MHz):** δ 6.61 (bs, 2H, Ar-*H*), 3.10 (d of vt, J_{PH} = 3.3 Hz, J_{HH} = 16.8 Hz, 2H, CH_2P), 2.84 (d of vt, J_{PH} =4.0 Hz, J_{HH} = 17.2 Hz, 2H, CH_2P), 2.28 (s, 3H, Ar-CH_3), 1.81 (s, 3H, acetate), 1.27 (t, J_{HH} = 6.4 Hz, 18H, P^{t}bu), 1.18 (t, J_{HH} = 6.4 Hz, 18H, P^{t}bu), -30.07 (t, J_{HH} = 13.2 Hz, 1H, Ir-*H*). **^{1}H NMR (CD_2Cl_2, 400 MHz):** δ 6.65 (bs, 2H, Ar-*H*), 3.20 (d of vt, J_{PH} = 3.6 Hz, J_{HH} =17.2 Hz, 2H, CH_2P), 2.90 (d of vt, J_{PH} = 4 Hz, J_{HH} =17.2 Hz, 2H, CH_2P), 2.12 (s, 3H, Ar-CH_3), 1.80 (s, 3H, acetate), 1.35 (t, J_{HH} = 6.4 Hz, 18H, P^{t}bu), 1.28 (t, J_{HH} = 6.4, 18H, P^{t}bu), -30.4 (t, J_{PH} = 13.2 Hz, 1H, Ir-*H*).

Reaction of (Me-PCP)Ir with H_2O_2

To a solution of 12.4 mg (Me-PCP)IrH$_n$ (20.6 μmol) in *p*-xylene-d_{10}, excess NBE was added to generate the norbornene complex *in situ*. Upon addition of 2.4 μL H_2O_2 solution (42 μmol), the mixture released hydrogen gas and solution turned a brown green color. Complex **4-1** was observed as the major product by ^{31}P and ^{1}H NMR spectroscopy.

(Me-PCP)Ir cyclometalated O_2 product, 4-5

Method 1: To a solution of 12.4 mg (Me-PCP)IrH$_n$ (20.6 μmol) in *p*-xylene-d_{10}, excess NBE and 2.4 μL H_2O_2 solution (42 μmol) were added to generate complex **4-1**. *Method 2*: Oxygen was bubbled through a solution of 11.8 mg (Me-PCP)IrH$_n$ (19.6 μmol) with 20 μL NBE (106 μmol) stock solution in C_6D_6 and complex **4-1** was generated. The synthesis of **4-1** was confirmed via NMR spectroscopy and

after 24 hours at room temperature complex **4-5** was the major species in solution, characterized *in situ*. **^{31}P NMR (C_6D_6, 161.9 MHz):** δ 44.6 (d, J_{PP} = 349.7 Hz), 3.53 (d, J_{PP} = 349.3 Hz). **^{1}H NMR (C_6D_6, 400 MHz):** δ 6.99 (d, *J* = 18.4 Hz, 2H, Ar-*H*), 3.55 (m, 1H, C*H*), 3.15-3.07 (m, 4H, CH_2P), 2.40 (s, 3H, Ar-CH_3), 2.18 (m, 1H, C*H*), 1.51 (d, *J* = 13.6 Hz, 3H, Me), 1.36 (d, *J* = 13.6 Hz, 9H, P^{t}Bu), 1.19 (d, *J* = 12.8 Hz, 9H, P^{t}Bu), 1.13 (d, *J* = 12.8 Hz, 9H, P^{t}Bu), 0.73 (d, *J* = 12.8 Hz, 3H, CH_3).

(Me-PCP)Ir-CO cyclometalated O_2 product, 4-6

Complex **4-5** was prepared, degassed and 1 atm CO was added to J. Young NMR tube. Upon mixing the solution changes color to golden yellow. The excess volatiles and solvent were removed under vacuum, the sample was washed with pentane giving a yellow solid and the product as a yellow solution. The solvent was removed under vacuum, and sample was dissolved in C_6D_6 for characterization. **^{31}P NMR (C_6D_6, 161.9 MHz):** δ 46.59 (d, J_{PP} = 314.98 Hz), -18.90 (d, J_{PP} = 314.98 Hz). **^{1}H NMR (C_6D_6, 400 MHz):** δ 6.812 (s, 1H, Ar-*H*), 6.717 (s, 1H, Ar-*H*), 3.257 (d, 1H, C*H*), 2.875 (m, 4H, CH_2P), 2.334 (m, 1H, C*H*), 2.287 (s, 3H, Ar-CH_3), 1.545 (d, 3H, Me), 1.273 (d, 9H, P^{t}Bu), 1.179 (d, 9H, P^{t}Bu), 1.077 (d, 9H, P^{t}Bu), 0.945 (d, 3H, Me).

Reaction of (Me-PCP)Ir with N_2O

To a solution of 10 mg of (Me-PCP)IrH_2 (16.5 μmol) mixed with 20 μL TBE (155 μmol) in *p*-xylene-d_{10}, 0.5 atm N_2O gas was added to the sample. (Me-PCP)IrN_2 was confirmed as the quantitative product as determined by ^{31}P and ^{1}H NMR spectroscopy. Characterization for (Me-PCP)IrN_2 can be found in Chapter 2.

GC Experiments

10 mg of (Me-PCP)IrH_2 (16.5 μmol) was mixed with 20 μL TBE (155 μmol) to generate the 14e$^-$ species *in situ*. A GC analysis of the solution was collected via Varian 430 GC. 0.5 atm N_2O gas was added to the sample and secondary GC analysis of the solution was collected.

Mass Spectrometry of N_2O

Figure 4.2 General Schematic for the Detection of Ions from N_2O

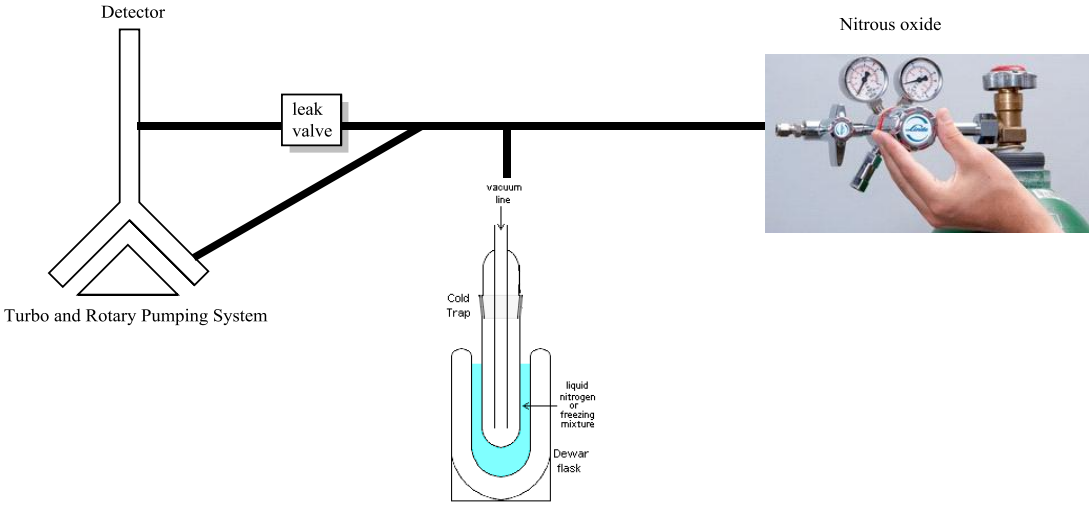

References

(1) Stahl, S. S. *Angew. Chem. Int. Ed.* **2004**, *43*, 3400.
(2) Gunay, A.; Theopold, K. H. *Chem. Rev.* **2010**, *110*, 1060.
(3) Piers, W. E. *Organometallics* **2011**, *30*, 13.
(4) Boisvert, L.; Goldberg, K. I. *Acc. Chem. Res.* **2012**, *45*, 899.
(5) Vaska, L. *Acc. Chem. Res.* **1976**, *9*, 175.
(6) Vaska, L. *Science* **1963**, *140*, 809.
(7) Denney, M. C.; Smythe, N. A.; Cetto, K. L.; Kemp, R. A.; Goldberg, K. I. *J. Am. Chem. Soc.* **2006**, *128*, 2508.
(8) Williams, D. B.; Kaminsky, W.; Mayer, J. M.; Goldberg, K. I. *Chem. Commun.* **2008**, 4195.
(9) Morales-Morales, D.; Lee, D. W.; Wang, Z.; Jensen, C. M. *Organometallics* **2001**, *20*, 1144.
(10) Winkler, J. R.; Gray, H. B. In *Molecular Electronic Structures of Transition Metal Complexes I*; Mingos, D. M. P., Day, P., Dahl, J. P., Eds.; Springer Berlin Heidelberg: 2012, p 17.
(11) Hay-Motherwell, R. S.; Wilkinson, G. *Polyhedron* **1993**, *12*, 2009.
(12) Burford, R. J.; Piers, W. E.; Ess, D. H.; Parvez, M. *J Am Chem Soc* **2014**, *Just Accepted Manuscript*.
(13) Limberg, C. *Angew. Chem. Int. Ed.* **2009**, *48*, 2270.
(14) Poverenov, E.; Efremenko, I.; Frenkel, A. I.; Ben-David, Y.; Shimon, L. J. W.; Leitus, G.; Konstantinovski, L.; Martin, J. M. L.; Milstein, D. *Nature* **2008**, *455*, 1093.
(15) Efremenko, I.; Poverenov, E.; Martin, J. M. L.; Milstein, D. *J. Am. Chem. Soc.* **2010**, *132*, 14886.
(16) Adam, W.; Curci, R.; Edwards, J. O. *Acc. Chem. Res.* **1989**, *22*.
(17) Adam, W.; Saha-Moller, C. R.; Zhao, C.-G. In *Organic Reactions*; John Wiley and Sons, Inc.: 2004.
(18) Murray, R. W. *Chem. Rev.* **1989**, *89*, 1187.
(19) Tolman, W. B. *Angew. Chem. Int. Ed.* **2010**, *49*, 1018.
(20) Verat, A. Y.; Fan, H.; Pink, M.; Chen, Y. S.; Caulton, K. G. *Chem.-Eur. J.* **2008**, *14*, 7680.
(21) Andino, J. G.; Caulton, K. G. *J. Am. Chem. Soc.* **2011**, *133*, 12576.
(22) Bruin, B. d.; Boerakker, M. J.; Donners, J. J. J. M.; Christiaans, B. E. C.; Schlebos, P. P. J.; Gelder, R. d.; Smits, J. M. M.; Spek, A. L.; Gal, A. W. *Angew. Chem. Int. Ed. Engl.* **1997**, *36*, 2064.
(23) Budzelaar, P. H. M.; Blok, A. N. J. *Eur. J. Inorg. Chem.* **2004**, 2385.
(24) Kohl, S. W.; Weiner, L.; Schwartsburd, L.; Konstantinovski, L.; Shimon, L. J. W.; Ben-David, Y.; Iron, M. A.; Milstein, D. *Science* **2009**, *324*, 74.
(25) Williams, D. B.; Mayer, J.; Goldberg, K. I. *Abstracts of Papers, 232nd ACS National Meeting, San Francisco, CA, United States, Sept. 10-14, 2006* **2006**, INOR.
(26) Kundu, S., Rutgers, The State University of New Jersey, 2010.
(27) Kundu, S.; Choi, J.; Wang, D. Y.; Choliy, Y.; Emge, T. J.; Krogh-Jespersen, K.; Goldman, A. S. *J. Am. Chem. Soc.* **2013**, *135*, 5127.
(28) Schwartsburd, L.; Iron, M. A.; Konstantinovski, L.; Diskin-Posner, Y.; Leitus, G.; Shimon, L. J. W.; Milstein, D. *Organometallics* **2010**, *29*, 3817.
(29) Sharp, P. R. *J. Chem. Soc. Dalton. Trans.* **2000**, 2647.
(30) NIST Mass Spec Data Center, S. E. S., director In *NIST Chemistry WebBook, NIST Standard Reference Database Number 69*; Mallard, P. J. L. a. W. G., Ed.; National Institute of Standards and Technology: Gaithersburg MD, 20899.
(31) Gibert, M.; Ferrer, M.; Sanchez-Baeza, F.; Messeguer, A. *Tetrahedron* **1997**, *53*, 8643.

Chapter 5

Determination of Metal-Ligand Bond Energies for (PCP)Ir Complexes

Abstract

The determination of bond energies for organic molecules can be easily determined via group increment theory or computational methods. However, the determination of bond energies of transition metal complexes is less reliable as there are no specific trends and computational methods for calculating such large molecules are still developing. The ability to accurately determine bond energies for metal complexes is important for developing new catalysts, determining catalytic intermediates and gaining insight into mechanisms for various transformations. This chapter reports the thermodynamic parameters for the addition of a range of ligands to (PCP)Ir, (PCP)IrH_2 and (PCP)IrHCl complexes. The experimentally determined values are compared to values derived from DFT calculations utilizing a variety of functionals with good agreement.

5.1 Introduction

A fundamental understanding of bond energies is critical to understanding modern chemistry. When organic molecules are considered, chemists can easily determine the specific energy of a molecule or reaction via group increment theory[1,2] or computational methods. For example, the energy of 2-methylpentane can be determined by the addition of energies for 3 methyl, 2 methylene, and 1 methine groups (Figure 5.1). Whereas, the energy for the hydrogenation of 2-methylpropene can be determined by subtraction of the enthalpy of products, -37.43 kcal/mol, from the reactants, -8.36 kcal/mol, gives the overall enthalpy for the transformation, -29.07 kcal/mol (Scheme 5.1).

Figure 5.1 Determination of Enthalpy for 2-methylpentane via Group Increment Theory

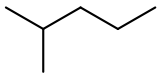

$\Delta H°_f = 3CH_3 + 2CH_2 + 1CH$
$\Delta H°_f = 3(-10.08) + 2(-4.95) + 1(-1.90)$
$= -42.04$ kcal/mol

Scheme 5.1 Hydrogenation of 2-methylpropene

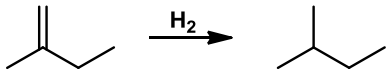

$\Delta H°_{rxn} = -29.07$ kcal/mol

$\Delta H°_f = -8.36$ kcal/mol $\Delta H°_f = -37.43$ kcal/mol

The determination of bond energies in transition metal complexes has been an area of equal importance, yet there is a lack of experimental and accurate computational data available.[3-17] The challenges with determining the thermodynamics of organometallic compounds can be attributed to the complexity, stability and reactivity of the complexes. Different functionals are limited when dealing the larger size of these systems in both accuracy and time, whereas the stability of these complexes in solution , thermally or over time changes as the reaction conditions change leading to the use of a variety of different methods for experimental determination each with its own set of accuracy considerations. Overall, a better understanding of the bond energies of transition metals will enable chemists to design new catalysts, gain insights into mechanisms, and determine intermediates within a catalytic cycle.

This chapter will outline the determination of enthalpy (ΔH°), entropy (ΔS°), and free energy (ΔG°), for the addition of various ligands (L) to (PCP)IrHCl (**5-1**, Scheme 5.2), (PCP)IrH_2 (**5-2),** (PCP)Ir

(**5-3**). The ligands studied undergo C, H, O, N, S, and P heteroatom additions to the metal center. Secondly, to assess the quality of various computational methods for the determination of metal-ligand binding energies for our catalyst systems, the experimental results are compared to computational values calculated using density functional theory (DFT)[18] and a range of functionals described below.

Scheme 5.2 Iridium (I) and (III) Pincer complexes

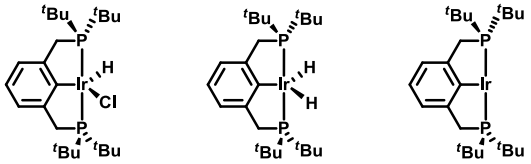

5-1 5-2 5-3

5.2 Results and Discussion

*5.2.1 Equilibrium Studies of (PCP)IrHCl, **5-1***

Initial addition of ligands (L = acetonitrile, isoquinoline, pyridine (N-type ligands) and PR_3 type ligands, R_3 = Et_3, Ph_2Me, Ph_2OMe, Me_2Ph, Me_3, OEt_3, $Ph(OEt)_2$, and $Me(OEt)_2$) to **5-1** leads to kinetic product **5-1a** in which L coordinates trans to chloride (Scheme 5.3a). This product then undergoes isomerization to give thermodynamic product **5-1b**, in which L is trans to the aryl ring of the PCP backbone (Scheme 5.3b). The isomerization is due to the steric demand of L when compared to chloride as the preferred orientation of the bulkiest ligand is trans to the phenyl ring of the PCP backbone.

Scheme 5.3 Addition of Ligands (L = PEt_3, acetonitrile (CH_3CN), PPh_2Me, isoquinoline, pyridine, PPh_2OMe, PMe_2Ph, PMe_3, $PPh(OEt)_2$, $P(OEt)_3$, $PMe(OEt)_2$) to **5-1** (a) Initial Formation of Kinetic Product, **5-1a** (b) Isomerization of **5-1a** to **5-1b**

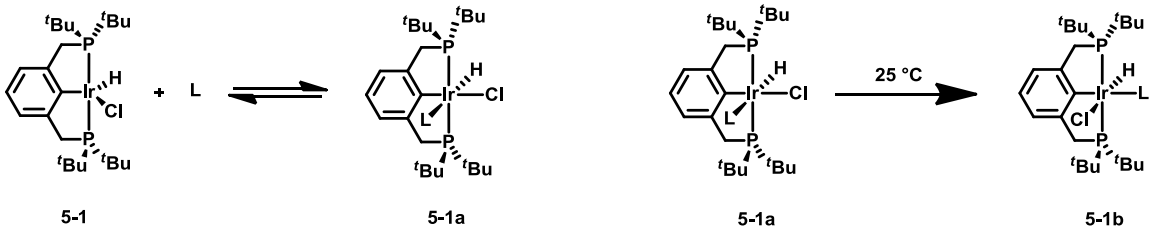

5-1 5-1a 5-1a 5-1b

(a) (b)

The characterization of **5-4** through **14,** where L = PEt_3, **5-4**, acetonitrile, **5-5**, PPh_2Me, **5-6,** isoquinoline, **5-7**, pyridine, **5-8**, PPh_2OMe, **5-9**, $PPhMe_2$, **5-10**, PMe_3, **5-11**, $PPh(OEt)_2$, **5-12**, $P(OEt)_3$, **5-13**, and $PMe(OEt)_2$, **5-14**, and have been included in the experimental section. The X-ray crystal structure of **5-11** has been previously reported.[19] Isomer **5-1a** has very broad shifts in the ^{31}P NMR spectrum and the hydride shift in the ^{1}H NMR spectrum is shifted upfield to ca. -10 ppm. The ^{31}P NMR shifts for **5-1b** are distinctively split into a doublet for the two phosphorous nuclei in the PCP backbone and a triplet for the PR_3 ligand. The hydride shifts for **5-1b** have been shifted upfield to ca. -22 ppm. The P-H coupling for the hydride shift of **5-1a** is very large (J_{PH} = 196 to 234 Hz) whereas the coupling in **5-1b** is much less (J_{PH} = 14.5 Hz). In the case where L = PPh_2Me, PPh_2OMe, $PPhMe_2$, PEt_3, or PMe_3, only one isomer has been characterized, all NMR spectra are indicative of isomer **5-1b** rather than isomer **5-1a** as they lack the characteristic hydride shift or coupling constant of **5-1a**. Similarly, both **5-1a** and **5-1b** are observed for $P(OEt)_3$, $PMe(OEt)_2$, $PPh(OEt)_2$ ligands due to rapid isomerization. The ligands PPh_2Me, PPh_2OMe, $PPhMe_2$, PEt_3, or PMe_3 are smaller PR_3 ligands and therefore isomerize much more quickly, whereas isomerization of the more sterically hindering $P(OEt)_3$, $PMe(OEt)_2$, $PPh(OEt)_2$ ligands can be observed on an NMR time scale.

The trans orientation of L to the phenyl ring of the PCP backbone is the more thermodynamically favored isomer and allows for easy elimination of L from the 'pocket' of **5-1**. This easy elimination allows for the equilibrium between **5-1** and **5-1b** to be monitored. Since no intermediates are formed during this process, the binding energy can be directly correlated to the energy of addition for each ligand. For example, upon addition of PPh_2Me to **1** an immediate color change is observed from dark red to pale yellow. At room temperature**,** in the ^{31}P NMR spectrum, **5-6** is the major product and only a small presence of the **5-1** is observed. As the temperature is raised from 45 to 105 ˚C, then the equilibrium shifts towards the reactant side, loss of PPh_2Me leads to five coordinate **5-1** becoming the major species in solution. Each species is observable by NMR spectroscopy and so concentration can be determined by integration. The concentrations of each species are then used to determine the equilibrium constant. All equilibrium constants have been included in the experimental section.

If L = pyridine, acetonitrile (CH_3CN), or isoquinoline, isomerization from **5-1a** to **5-1b** occurs on a much more rapid timescale and only one a broad peak is observed in the NMR spectrum after addition of

L to solution. DFT calculations have been completed for the two isomers of pyridine which conclude that **5-1a** is 1-3 kcal/mol (depending on the functional) more stable then **5-1b**. As temperature is increased, this peak will shift downfield according to the percentage of **5-1** and **5-1b** in solution. For example, at room temperature, mostly **5-8** is observed in the ^{31}P NMR spectrum, δ_{HClPy} = 46 ppm. As the temperature is increased, equilibrium shifts towards **5-1**, δ_{HCl} = 67 ppm. The concentration of each species at each temperature is determined by Equation 1 below, where the fraction of each species (f_{HCl} and f_{HClL}) in solution is related to the observed chemical shift (Δ_{obs}) and the chemical shift of the pure species (δ_{HCl} and δ_{HClL}). The fractions can then be converted to concentrations, allowing for determination of the K_{eq}.

$$\Delta_{obs} = \delta_{HCl} * f_{HCl} + \delta_{HClL} * f_{HClL} \qquad (1)$$

The change in the free energy, ΔG, of the overall equilibrium, the ΔG of the products minus the ΔG of the reactants, will determine the magnitude of the equilibrium constant, K_{eq}. So if the equilibrium constant can be determined via the ratio of the products to the reactants, then the value of ΔG° can be determined at each temperature, using Equation 2, where R is the gas constant (kcal/mol*K) and T is temperature (K).[20]

$$\Delta G^{\circ} = -RT \ln (K_{eq}) \qquad (2)$$

A graph of ΔG° versus temperature (Figure 5.2) will give the ΔH as the y-intercept and ΔS as the slope of a linear regression (Table 5.1).

Figure 5.2 Graph of ΔG˚ (kcal/mol) versus Temperature (K) for the Addition of L = PEt_3 (purple), CH_3CN (green), PPh_2Me (red), isoquinoline (orange), and pyridine (blue) to **5-1**

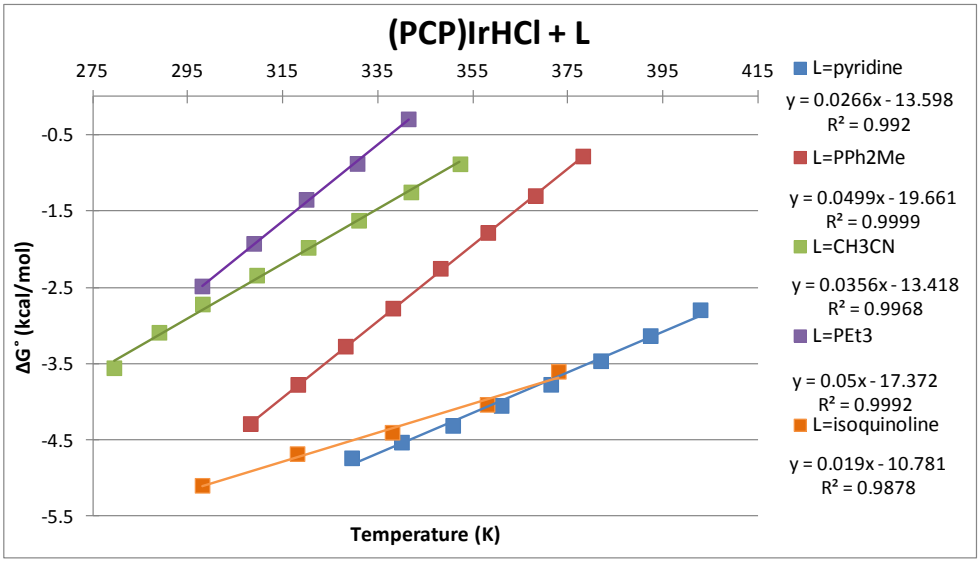

Table 5.1 Thermodynamic Parameters for the Addition of L = PEt_3, CH_3CN, PPh_2Me, isoquinoline and pyridine to **5-1**[21]

	Δ G vs. T Plot		
"L"	**ΔH˚ (kcal/mol)**	**ΔS˚ (cal/mol*K)**	**ΔG˚ (kcal/mol)**
PEt_3	-17.4 (0.3)	-50.0 (0.8)	-2.5 (0.3)
CH_3CN	-13.5 (0.3)	-35.9 (0.8)	-2.8 (0.3)
PPh_2Me	-19.7 (0.1)	-50.0 (0.2)	-4.8 (0.1)
Isoquinoline	-10.7 (0.4)	-18.9 (1.2)	-5.1 (0.4)
Pyridine	-13.5 (0.4)	-26.3 (1.0)	-5.7 (0.4)

This plot is modified from the usual Van 't Hoff plot ($\ln K_{eq}$ versus 1/T) which tends to be used for these types of experiments. The slope of a Van 't Hoff plot will be equal to –ΔH/RT whereas the y-intercept is ΔS/R and so one must multiply the slope or y-intercept by the gas constant (Van 't Hoff Equation shown as Equation 3) to get values for ΔH˚ or ΔS˚. The ΔG˚ versus T plot (Figure 5.2) lends itself to much easier mathematics in order to obtain the desired values. If the data is plotted in the traditional fashion, then values for the fit and resulting values for ΔH˚, ΔS˚, and ΔG˚ are within experimental error to those reported using the ΔG˚ versus T plot.

$$\ln (K_{eq}) = - \Delta H/RT + \Delta S/R \qquad (3)$$

The thermodynamic values for the addition of L to **5-1** range, where the most strongly binding ligand is pyridine at ΔG° = -6.0 (0.4) kcal/mol whereas the least strongly binding is PEt_3 at ΔG° = -2.6 (0.3) kcal/mol. Surprisingly, PEt_3 is less sterically hindered (Tolman[22] cone angle = 132 $^\circ$) in comparison to PPh_2Me (136 $^\circ$) yet binds much less strongly. The more electronic donating ligand PEt_3 (TEP = 2061.7 cm^{-1}) binds less strongly then PPh_2Me (2067.0 cm^{-1}). Overall, no trend can be reliably determined between the Tolman parameters and the binding energies of the PR_3 ligands. The ΔS° values for the PR_3 ligands are ca. -33 kcal/mol, whereas the ΔS° values are much more negative at ca. -50 kcal/mol for the N-type ligands. Since the N-type ligands undergo rapid isomerization from **5-1a** to **5-1b** (Scheme 5.3b) this may account for the more positive values of entropy that have been determined. The size of the N-type ligands may also be a reason for the observed entropy, as N-type ligands are much less bulky then the PR_3 ligands.

The experimentally determined thermodynamic parameters, were compared to a series of computational methods including wB97XD,[23] B97D,[24] M06-L, M06, M06-2X,[25] TPSSh, TPSS,[26] PBE,[27] and B3LYP[28] (Table 5.2). The right hand columns, PBE and B3LYP represent the oldest (before 2000) derived functionals, excluding the M06-L functionals (2008), the rest of the functionals were developed between 2000 and 2008. Overall, any functional that accounts for the long range interactions or Van der Waals forces between atoms, i.e. dispersion (B97D, wB97XD, M06-L, M06-2X, and M06), shows much better agreement with the experimental results, shown in red. This is not surprising as ^{t}butyl groups surrounding the metal center make **5-1** very sterically hindered. With the exception of L = pyridine all the functionals predict ΔS° fairly well (within ca. 10 e.u). However, the traditional functionals used in chemistry, PBE and B3LYP, grossly overestimate ΔH° and ΔG° for the addition of L to **5-1**. The more recently developed functionals M06-L and M06, shown in blue, have much better agreement with the experimentally determined values.[29] For example, PBE and B3LYP estimate ΔG° for the addition of PEt_3 as 12.5 and 22.6 kcal/mol, 14 and 24 units above the experimental value (-2.6 kcal/mol), whereas M06-L predicts ΔG° as -1.4 kcal/mol, only 1 unit above the experimental. PBE can only reliably predict the binding energy for **5-5**, most likely because $NCCH_3$ is a small ligand and the Van der Waals interactions are minimized.

Table 5.2 Comparison of Experimental Thermodynamic Parameters (red) to Computational Thermodynamic Values using Various DFT functionals.[30]

ΔH°	**EXP**	**wB97XD**	**B97D**	**M06-L**	**M06**	**M06-2X**	**TPSSh**	**TPSS**	**PBE**	**B3LYP**
PEt_3	-17.4	-20.3	-17.1	-17.4	-15.0	-11.1	-2.4	-1.8	-3.4	7.1
CH_3CN	-13.5	-12.0	-10.1	-13.2	-11.2	-8.5	-10.0	-10.4	-8.4	-4.0
PPh_2Me	-19.7	-26.2	-21.9	-22.3	-21.1	-16.0	-5.6	-5.0	-6.6	4.4
Pyridine	-13.5	-22.1	-20.1	-19.9	-19.0	-18.2	-12.7	-12.6	-10.8	-6.1
ΔS°	**EXP**	**wB97XD**	**B97D**	**M06-L**	**M06**	**M06-2X**	**TPSSh**	**TPSS**	**PBE**	**B3LYP**
PEt_3	-50	-57	-56	-54	-55	-56	-61	-53	-53	-52
CH_3CN	-36	-40	-34	-38	-30	-33	-34	-32	-32	-32
PPh_2Me	-50	-55	-57	-55	-55	-54	-55	-55	-55	-54
Pyridine	-26	-42	-43	-43	-42	-43	-44	-44	-43	-43
ΔG°	**EXP**	**wB97XD**	**B97D**	**M06-L**	**M06**	**M06-2X**	**TPSSh**	**TPSS**	**PBE**	**B3LYP**
PEt_3	-2.5	-3.1	-0.5	-1.4	1.4	5.5	13.4	15.9	12.5	22.6
CH_3CN	-2.8	0.1	0.0	-1.8	-2.2	1.3	0.3	1.0	1.2	5.6
PPh_2Me	-4.8	-9.8	-4.7	-5.7	-4.9	0.1	10.7	13.2	9.7	20.5
Pyridine	-5.6	-9.5	-7.1	-7.2	-6.7	-5.5	0.3	2.3	2.2	6.6

Interestingly, there is relatively good agreement of the experimentally determined entropy values to the computational entropy values. Oftentimes, calculated entropy values overestimate the experimental values by 50% and so a trend has been established to multiply the calculated entropies by a factor of 0.5 leading to better agreement.[31] Any corrections made are an attempt to account for the lack of computer simulations to accurately account for solvation effects.[32-35] It is important to note that none of these corrections have been applied in this study.

The thermodynamics for the addition of more strongly binding ligands can be determined via exchange equilibria with known ligands (Scheme 5.4). The ΔG° values, ranging from -2.6 to -13.3 kcal/mol, for the binding energies of **5-1** measured via exchange are reported in Table 5.3, and the equilibrium constants for all equilibria are included in the experimental information. The experimental ΔG° values were compared to computational values determined using the M06-L and PBE functionals. The M06-L functional was chosen because it agrees best with the experimentally determined thermodynamic values for the addition of L = PEt_3, CH_3CN, PPh_2Me, isoquinoline and pyridine to **5-1**, whereas the PBE functional was chosen as it is the better of the two functionals which agree least with experimental values (Table 5.2).

Scheme 5.4 Exchange Equilibrium for **5-1**

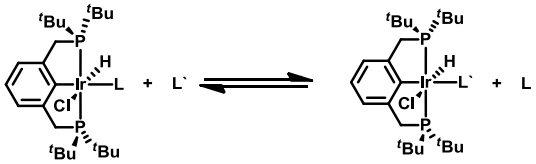

Table 5.3 Experimental ΔG˚ Values (kcal/mol) for the Addition of a Series of Ligands to **5-1** Compared to Computational ΔG˚ Values (kcal/mol) Determined using M06-L and PBE Functionals

Ligands	**Exp ΔG˚ (kcal/mol)**	**M06-L ΔG˚**	**PBE ΔG˚**
PEt_3	-2.5	-1.4	11.9
CH_3CN	-2.8	-1.8	-0.4
PPh_2Me	-4.8	-5.7	10.0
Isoquinoline	-5.1	-9.1	-0.7
Pyridine	-5.7	-8.6	0.1
PPh_2OMe	-5.8	-12.3	4.5
PMe_2Ph	-6.3	-7.7	6.0
PMe_3	-8.1	-7.8	2.0
$PPh(OEt)_2$	-10.9	-18.0	-1.6
$P(OEt)_3$	-11.9	-20	-8.3
$PMe(OEt)_2$	-12.9	-16.3	-3.4

The comparison of the experimental values and the computational results are better represented in a graph of the experimental values versus the computational values (Figure 5.3). The experimental values shown as a black line, in which the slope is equal to 1 with a y-intercept of 0. If the computational values predicted the experimental values exactly, then the slope of these regressions would also be equal to 1 and the y-intercept would also be equal to 0. The regression line for the PBE functional values, in red, overestimated the experimental by a factor of 9.9 units, whereas the regression line for M06-L values, in blue, is only 1.3 units over the experimental values. The root mean square is the average of the differences between the errors. It can be evaluated as the average difference from the computational value to the experimental. The root mean square for values determined via M06-L is 4.3 kcal/mol while the root mean square for PBE is 9.7 kcal/mol.

Figure 5.3 Graph of Experimental ΔG˚ Values versus Computational ΔG˚ Values for the Addition of Ligands to **5-1,** [Experimental (black), PBE (red), and M06-L (blue), ΔG˚ (kcal/mol)].

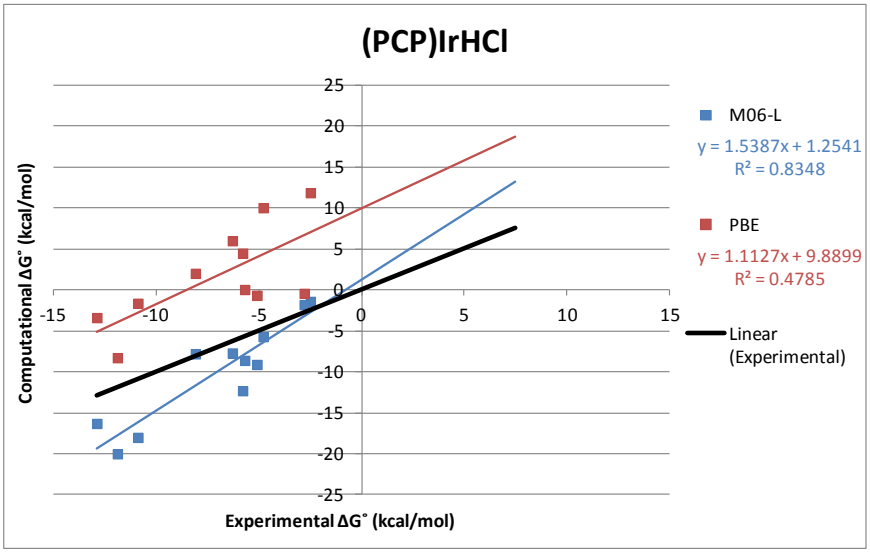

5.2.2 Equilibrium Studies of (PCP)IrH$_2$, **5-*2***

In the case of **5-1**, **5-1a** and **5-1b** can be identified and characterized easily when PR_3 ligands are studied but rapid isomerization is observed when L is an N-type ligand. A similar scenario is observed in the case of **5-2**, in which the kinetic products are isolated for the more sterically bulky ligands, PPh_2OMe, $P(OEt_3)$, $PMe(OEt)_2$, $PPh(OEt)_2$, and the thermodynamic product is isolated for all ligands (Scheme 5.5).

Scheme 5.5 Equilibrium between **5-2** and L

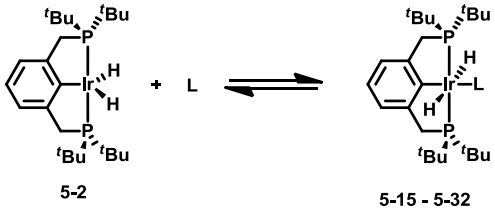

The NMR characterization for **5-15 – 5-32**, in which L = 2-picoline, **5-15**, NH_3, **5-16**, thiophene, **5-17**, PPh_3, **5-18**, dibenzothiophene (DBT), **5-19**, H_2, **5-20**, CH_3CN, **5-21**, PPh_2Et, **5-22**, pyridine, **5-23**, isoquinoline, **5-24**, PEt_3, **5-25**, PPh_2Me, **5-26**, PMe_2Ph, **5-27**, and PMe_3, **5-29**, and both **5-2a** and **5-2b** for L = PPh_2OMe, **5-28**, $PMe(OEt)_2$, **5-30**, $P(OEt_3)$, **5-31**, $PPh(OEt)_2$, **5-32**, have been included in the experimental section. Interestingly, all **5-2a** complexes exhibit nonequivalent ^{t}butyl groups, whereas all **5-**

2b complexes have equivalent ^{t}butyl groups. This is similar to the NMR spectra observed for **5-8**, **5-7**, and **5-5,** in which nonequivalent ^{t}butyl groups were indicative of formation of **5-1a** and equivalent ^{t}butyl groups for **5-1b**. Additionally, the trans hydrides shifts for **5-2b,** when L = PR_3, are observed as quartets, indicating coupling by three phosphorous nuclei. In the case of L = N-type or S-type ligands, then the hydrides are observed as a triplet, indicative of coupling to only two phosphorous nuclei. The crystal structure of **5-23**, previously reported, clearly shows the trans orientation of pyridine to the aryl ring of the (PCP) backbone (Figure 5.4) consistent with the NMR characterization.[19] The crystal structures of **5-21** and **5-32b**, which also show the trans orientation of $NCCH_3$ and $PPhOEt_2$ to the back bone of the PCP aryl backbone, are given in the same report.

Figure 5.4 Crystal Structure of **5-23**

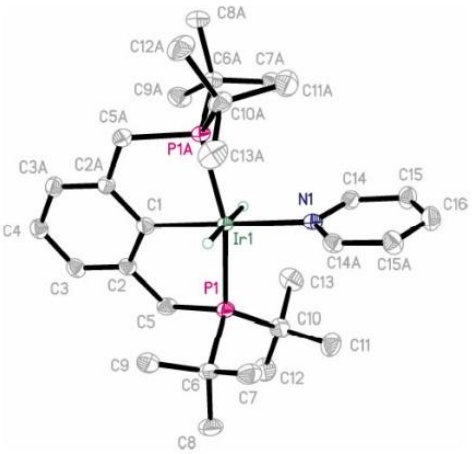

For **5-2a**, the cis hydrides are observed as having two distinct shifts in the ^{1}H NMR spectrum. The hydride trans to the PCP backbone is observed as a doublet of quartets, coupled by three phosphorous nuclei as well as the other hydride. The hydride trans to PR_3 is observed as a doublet of triplets of doublets; the hydride is coupled by the other hydride, two equivalent phosphorous nuclei and the trans PR_3 group, giving a large trans P-H coupling constant.

The additions of NH_3, PPh_3, and PPh_2Et to **5-2** were studied via direct equilibrium, as described for the addition of PR_3 type ligands to **5-1**. The addition of H_2 was studied via dehydrogenation of isopropanol to acetone.[36,37] This equilibrium was not measured by direct addition of H_2 gas to (PCP)IrH_2 because the exact concentration of H_2 gas in solution would need to be determined, rendering it less

feasible then the dehydrogenation reaction. The ΔH˚, ΔS˚, and ΔG˚ for this equilibrium were measured as 3 kcal/mol, 9 cal/mol*K, and 0.3 kcal/mol respectively. Subtraction of the values for the hydrogenation of acetone,[38] can give the overall thermodynamic values for the direct addition of H_2 to **5-2** to form **5-20**[39] (Table 5.4) in which ΔH˚, ΔS˚, and ΔG˚ are -13.4 kcal/mol, -27 cal/mol*K, and -5.4 kcal/mol respectively.

Table 5.4 Determination of the Thermodynamic Values for the Addition of H_2 to **5-2** via Dehydrogenation of Acetone

Reaction	ΔH˚ (kcal/mol)	ΔS˚ (cal/mol*K)	ΔG˚ (kcal/mol) at 298 K
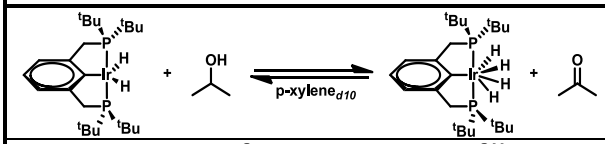	3.0	9	0.3
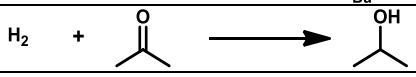	-16.4	-36	-5.7
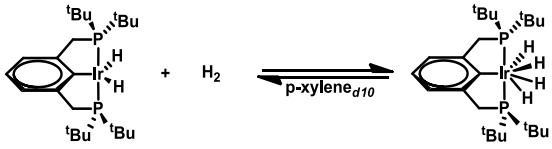	-13.4	-27	-5.4

Again, a graph of ΔG˚ versus temperature (Figure 5.5) for the addition of L = NH_3, PPh_3, H_2, and PPh_2Et to **5-2** gives ΔH˚ as the y-intercept and ΔS˚ as the slope of a linear regression (Table 5.5).

Figure 5.5 Graph of ΔG˚ (kcal/mol) versus Temperature (K) for the Addition of L = NH_3 (purple), PPh_2Et (green), PPh_3 (red), and H_2 (blue) to **5-2**

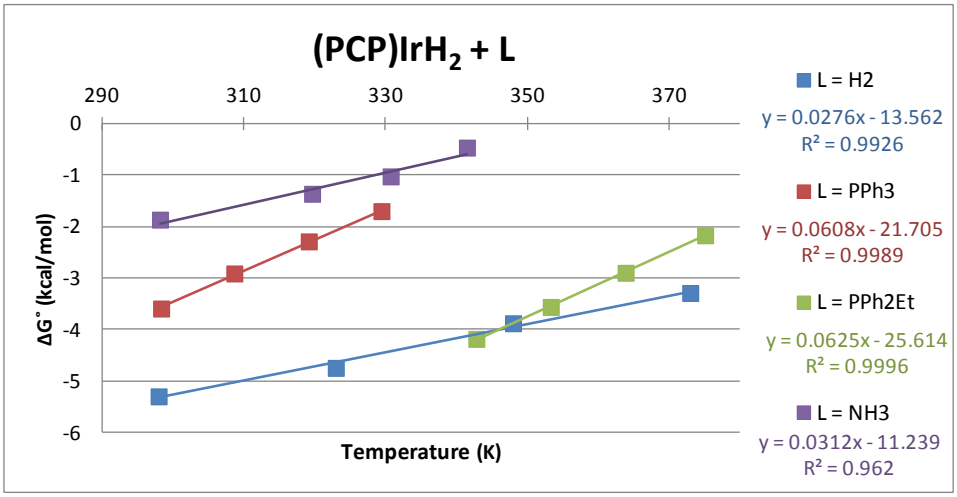

Table 5.5 Thermodynamic Parameters for the Addition of L = NH_3, PPh_3, H_2 and PPh_2Et to **5-2**

"L"	ΔH (kcal/mol)	ΔS (cal/mol*K)	ΔG (kcal/mol)
NH_3	-11.2 (0.4)	-31.2 (1.4)	-1.9 (0.4)
PPh_3	-21.7 (0.4)	-60.8 (1.4)	-3.5 (0.4)
H_2	-13.6 (0.6)	-27.6 (1.7)	-5.4 (0.6)
PPh_2Et	-25.6 (0.3)	-62.5 (0.9)	-7.0 (0.3)

The most weakly binding ligand in this series is NH_3, ΔG° = -1.9 (0.4) kcal/mol, and the most strongly binding ligand measured directly is PPh_2Et, ΔG° = -7.0 (0.3) kcal/mol. In this case, the more sterically hindered PPh_3 (145 °) does bind less strongly then PPh_2Et (140 °). Still, a distinct trend cannot be established between the binding energies for **5-2** and the Tolman parameters. The experimentally determined values for the addition of PPh_3 and H_2 to **5-2,** were compared to computational values derived from the same functionals as were used for **5-1** (Table 5.6).

Table 5.6 Comparison of Experimental Thermodynamic Parameters (red) to Computational Thermodynamic Values using Various DFT functionals.[40]

ΔH°	EXP	wB97XD	B97D	M06-L	M06	M06-2X	TPSSh	TPSS	PBE	B3LYP
PPh_3	-21.7	-30.3	**-26.1**	**-23.5**	-19.0	**-19.6**	-6.3	-5.2	-6.0	6.3
H_2	-13.6	-20.0	**-14.4**	**-15.9**	-11.0	**-14.5**	-18.0	-17.1	-18.7	-12.2
ΔS°	**EXP**	**wB97XD**	**B97D**	**M06-L**	**M06**	**M06-2X**	**TPSSh**	**TPSS**	**PBE**	**B3LYP**
PPh_3	-61	-64	**-65**	**-65**	-62	**-66**	-62	-62	-61	-61
H_2	-28	-29	**-31**	**-33**	-36	**-32**	-30	-30	-32	-32
ΔG°	**EXP**	**wB97XD**	**B97D**	**M06-L**	**M06**	**M06-2X**	**TPSSh**	**TPSS**	**PBE**	**B3LYP**
PPh_3	-3.5	-11.4	**-6.6**	**-4.2**	-0.4	**0.0**	12.1	13.0	12.2	24.2
H_2	-5.4	-11.5	**-5.3**	**-6.1**	-0.4	**-5.0**	-9.1	-8.2	-9.2	-2.5

For the addition of H_2 and PPh_3 to **5-2**, M06-L, B97D and M06-2X most closely correlate to the experimental values. Not surprisingly, all functionals predict the energy for addition of H_2 much more accurately then for PPh_3. PPh_3 is much more sterically demanding then H_2 and interacts with the ^{t}butyl groups of **5-2**, therefore Van der Waals forces and the correction for dispersion play a bigger role in the accuracy of the Minnesota functionals. TPSSh, TPSS, PBE overestimate both ΔH° and ΔG° for the

addition of PPh_3 to **5-2** but are the values are very close together. B3LYP overestimates ΔH° and ΔG° the greatest of all the functionals that were examined.

The thermodynamics for the addition of more strongly binding ligands can again be determined via exchange equilibria as was done for **5-1**. The ΔG° values range from -1.0 to -20.4 kcal/mol, and account for the addition of a wider range of ligands, including N-type, S-type, and PR_3 (Table 5.7). The experimentally determined values were again compared to values obtained from the M06-L and PBE functionals. The equilibrium constants for all equilibria are included in the experimental section. The same trend is observed with **5-2** as with **5-1**, PBE is much less successful at accurately predicting the experimental values. The only complexes that PBE predicts fairly accurately are **5-16**, **5-20** and **5-21**, which is not surprising because, as was seen for **5-5**, NH_3, H_2 and $NCCH_3$ are small organic ligands and are not affected by the Van der Waals forces as much as with the PR_3 ligands.

Table 5.7 Experimental ΔG° Values (kcal/mol) for the Addition of a Series of Ligands to **5-2** Compared to Computational Values (kcal/mol) Determined using M06-L and PBE functionals

Ligands	**Exp ΔG° (kcal/mol)**	**M06-L ΔG°**	**PBE ΔG°**
2-picoline	-1.0	-3.5	7.7
NH_3	-1.9	-4.5	-2.2
Thiophene	-3.0	-0.5	4.8
PPh_3	-3.5	-4.2	12.2
Dibenzothiophene	-4.5	-4.2	5.3
H_2	-5.4	-6.1	-9.2
CH_3CN	-5.5	-6.2	-4.6
PPh_2Et	-7.0	-6.2	7.8
Pyridine	-8.5	-7.8	-0.9
Isoquinoline	-8.8	-8.3	-1.0
PEt_3	-11.0	-8.5	5.0
PPh_2Me	-11.5	-9.1	5.5
PMe_2Ph	-13.2	-12.1	-0.4
PPh_2OMe	-14.3	-14.4	-0.1
PMe_3	-16.2	-10.8	-2.2
$PMe(OEt)_2$	-19.8	-21.1	-8.5
$P(OEt)_3$	-19.9	-24.7	-14.3
$PPh(OEt)_2$	-20.4	-23.0	-7.5

A comparison of the experimental values and the computational results are better represented in a graph of the experimental values versus the computational values (Figure 5.6). The linear regression for values predicted by the PBE functional, in red, is higher than the experimental regression by a factor of 6.2 units, whereas the regression lines for the values predicted by M06-L, in blue, is only 0.2 units higher than the experimental values, shown by black line. In fact, the regression for M06-L lies directly on the experimental regression.

Figure 5.6 Graph of Experimental ΔG˚ Values versus Computational ΔG˚ Values for the Addition of Ligands to **5-2,** [Experimental (black), PBE (red), and M06-L (blue), ΔG (kcal/mol)].

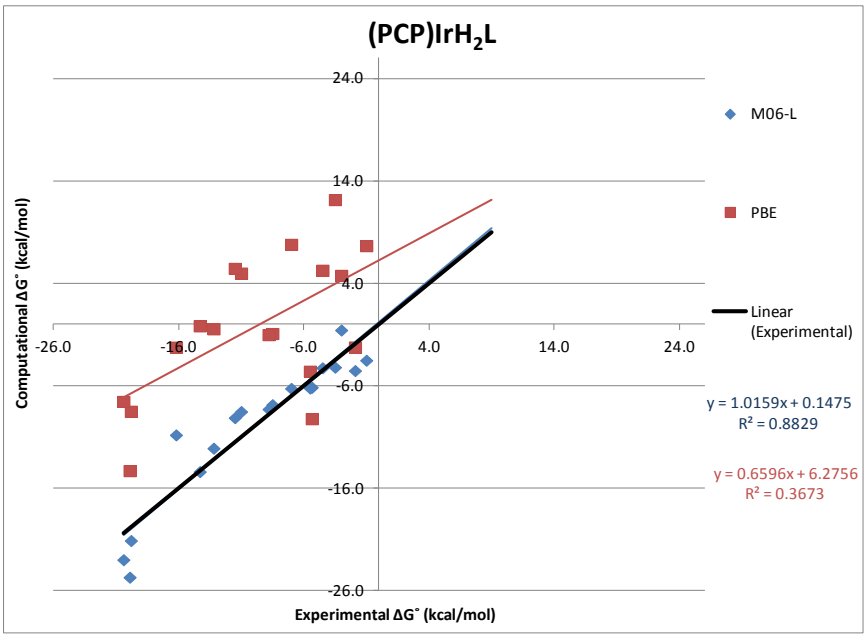

These two functionals show much better agreement for the addition of L to **5-2** then was observed for addition of L to **5-1**. This may be due to the difference in the steric hindrance of a chloride versus a hydride ligand. Essentially, the chloride should pose a greater challenge for the functionals to calculate as it may interact with ligands more than a hydride ligand, hence PBE does a better job of predicting energies for **5-2** then **5-1**. Also, the rapid isomerization of **5-1a** to **5-1b** for the N-type ligands may also lead to decreased accuracy for **5-1** versus **5-2**. The root mean square for the addition of ligands to **5-2** determined using the M06-L functional is 2.3 kcal/mol, meanwhile it is 11.2 kcal/mol for the values determined by the PBE functional.

5.2.3 Equilibrium Studies of (PCP)Ir, ***5-3***

Addition of L to 3-coordinate $14e^-$ species **5-3** leads to synthesis of the four coordinate species. All complexes **5-33 - 5-59,** in which L = norbornene, **5-33**, cyclooctene, **5-34**, trans-2-hexene, **5-35**, benzene, **5-36**, aniline, **5-37**, 2-picoline, **5-38**, 1-hexene, **5-39**, furan, **5-40**, DBT, **5-41**, propylene, 5-42, PPh_2Et, **5-43,** PPh_3, **5-44**, thiophene, **5-45**, N_2, **5-46**, pyridine, **5-47,** isoquinoline, **5-48,** PEt_3, **5-49**, CH_3CN, **5-50**, PPh_2Me, **5-51**, phenol, **5-52**, ethylene, **5-53**, PMe_2Ph, **5-54**, PMe_3, **5-55**, PPh_2OMe, **5-56**, $PPh(OEt)_2$, **5-57**, $PMe(OEt)_2$, **5-58**, and $P(OEt_3)$, **5-59**, have been characterized by ^{31}P and ^1H NMR spectroscopy, which have been included in the experimental section whereas the crystal structure of **5-50, 5-54**, and **5-59** has been included following the experimental section.

As discussed in Chapter 2, species **5-3** has never been isolated and all attempts to do so have proven unsuccessful. It is now understood, that the equilibrium between **5-3** and L lies too far to the right to be directly measured (Scheme 5.6). Therefore, the binding energies of L to **5-3** must be determined relatively using exchange equilibria, vide infra.

Scheme 5.6 Equilibrium Exchange between **5-3** and L

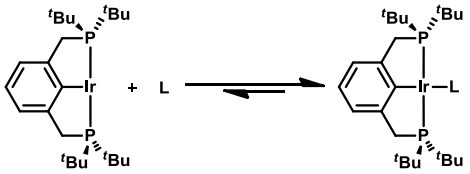

5-3 **5-33 - 5-59**

An anchor point is needed to calibrate the relative thermodynamics of **5-3**. The displacement of pyridine by CH_3CN was studied with varying concentrations of both pyridine and CH_3CN by Sabuj Kundu.[19] Displacement of pyridine can either follow a dissociative (Scheme 5.7) or associative pathway.

Scheme 5.7 Dissociative Pathway for the Displacement Pathway of Pyridine by Acetonitrile

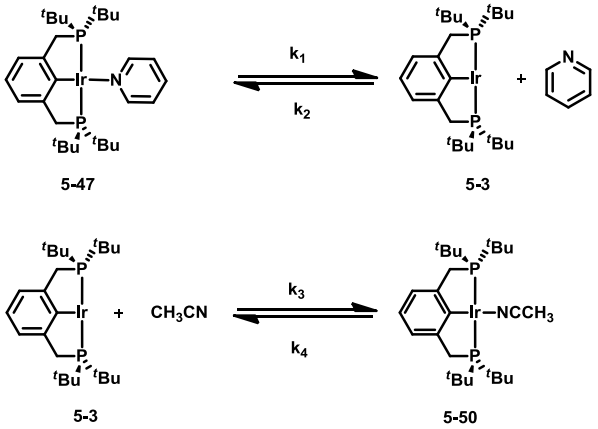

The results from these kinetics experiments are shown in Figure 5.7. The dots correspond to experimental data, whereas the lines correspond to fitted data using the Gepasi Software program[41] Varying the concentration of CH_3CN shows no change in the rate, whereas, an increase in pyridine concentration shows a decrease in reaction rate. The rate of reaction is only dependent upon loss of pyridine from the iridium center, as shown by the fit of the data, therefore this reaction follows a dissociative pathway.

Figure 5.7 Experimental and Gepasi Fit Data for the Dissociation of Pyridine from **5-3**

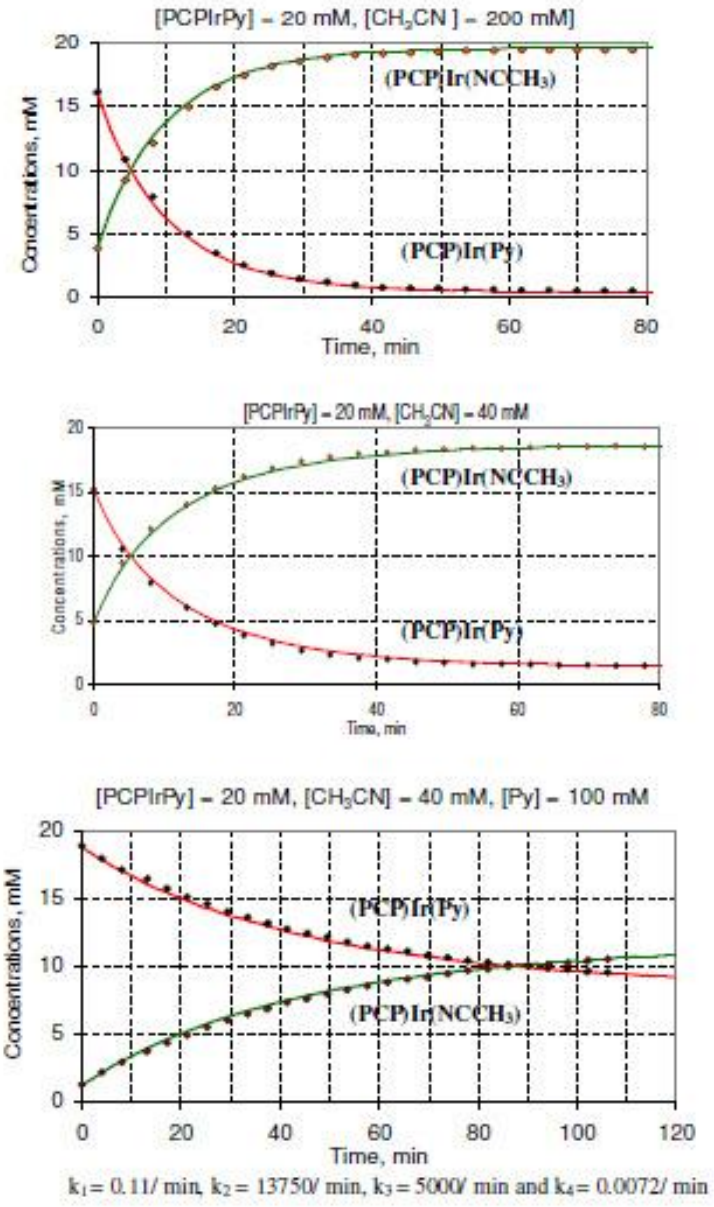

An Eyring plot of ln(k/T) versus 1/T of this data (Figure 5.8) gives $\Delta H^{\ddagger}$ = 24.9 (1) kcal/mol and $\Delta S^{\ddagger}$ = 12.1 (4) cal/mol*K.

Figure 5.8 Eyring Plot for the Dissociation of Pyridine

[(PCP)Ir-Py] = 20 mM, [Py] = 80 mM, [CH_3CN] = 200 mM

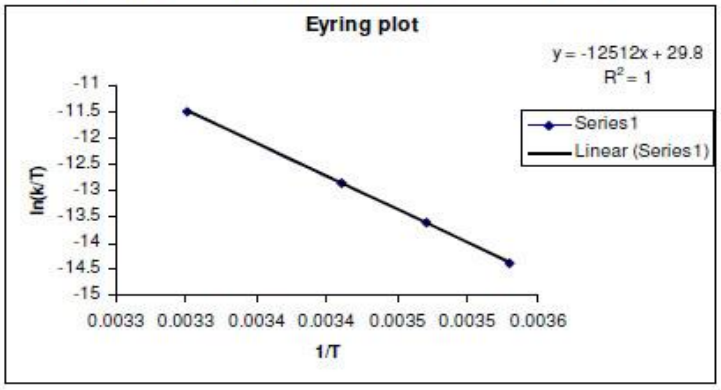

T (K)	k_1 (M^{-1} s^{-1})
303	0.00308203
293	0.00076552
288	0.0003519
283	0.0001619

$\Delta H^{\ddagger}$ = 24.9 (1) kcal/mol, $\Delta S^{\ddagger}$ = 12.1 (4) cal/mol*K

The $\Delta H^{\ddagger}$ = 24.9 kcal/mol is considered to be the upper limit for the ΔH of **5-3** binding. The barrier to addition is assumed to be very small and therefore only slightly above the actual value of ΔH. All ΔH values for other L are determined relative to pyridine via equilibrium exchange experiments. We can assume that ΔΔS will be negligible and so the ΔG for addition of pyridine can be set to 0.0 kcal/mol. For example, the exchange equilibrium between pyridine and PEt_3 was measured from 25 to 65 ˚C. The ΔG˚ versus temperature graph is shown in Figure 5.9 and the ΔH˚, ΔS˚ and ΔG˚ are shown below the graph. Therefore, ΔG_{rel} for the addition of PEt_3 is -1.5 kcal/mol.

Figure 5.9 Graph of ΔG° (kcal/mol) versus Temperature (K) for the Equilibrium Exchange between Pyridine and PEt_3

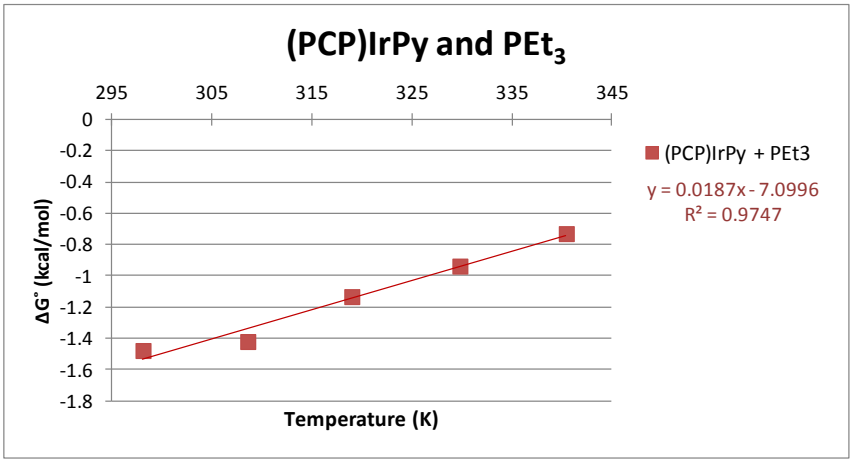

ΔH° (kcal/mol)	ΔS° (cal/mol*K)	ΔG° at 298 K (kcal/mol)
-7.1(0.4)	-18 (1.3)	-1.5 (0.1)

The ΔG_{rel} values for addition of L relative to addition of pyridine to **5-3** are listed in Table 5.8. The equilibrium constants for all equilibria have also been included in the experimental section. The most strongly binding ligand is $P(OEt)_3$, ΔG_{rel} = -10.9 kcal/mol, and the most weakly binding ligand is norbornene, ΔG_{rel} = -9.9 kcal/mol. The experimental ΔG_{rel} values were compared to computational values determined using the M06-L and PBE functionals, just as was done for **5-1** and **5-2**.

Table 5.8 Relative Experimental ΔG Values (kcal/mol) for the Addition of Ligands to **5-3** Compared to Computational Values (kcal/mol) Determined using M06-L and PBE Functionals

Ligand	**ΔG_{rel} (kcal/mol)**	**M06-L ΔG_{rel}**	**PBE ΔG_{rel}**
Norbornene	9.9	11.2	16.4
Cyclooctene	9.6	10.6	14.8
trans-2-hexene	8.8	10.1	13.1
Benzene	8.9	14.4	11.3
Aniline	6.2	6.1	5.5
2-picoline	4.6	4.3	6.6
1-hexene	4.3	4.8	5.0
Furan	3.7	13.0	16.6
Dibenzothiophene	3.3	5.1	7.7
Propylene	1.2	2.9	3.9
PPh_2Et	1.0	0.7	10.3
PPh_3	0.8	0.2	12.4
Thiophene	0.7	6.8	4.9
N_2	0.5	-6.9	3.0
Pyridine	0.0	0.0	0.0
Isoquinoline	-0.2	-0.5	0.1
PEt_3	-1.5	0.3	9.3
CH_3CN	-2.1	-2.1	-9.0
PPh_2Me	-3.3	-2.7	6.4
Phenol	-3.8	-2.5	-6.6
Ethylene	-3.8	-2.3	-2.9
$PPhMe_2$	-3.9	-3.5	2.6
PMe_3	-5.1	-2.8	1.4
PPh_2OMe	-7.4	-8.0	2.1
$PPh(OEt)_2$	-8.3	-15.8	-5.8
$PMe(OEt)_2$	-9.8	-13.2	-6.0
$P(OEt)_3$	-10.9	-18.1	-12.6

Interestingly, mixed results are obtained. M06-L does very well at predicting the energies for addition of the phosphines, but this functional cannot predict the addition of the phosphites well. PBE does a better job at predicting the values of **5-59**, **5-58**, and **5-57**, but does not predict the values of the phosphines, i.e., **5-44**, **5-49**, or **5-56**, accurately. Neither PBE or M06-L does a very good job at predicting **5-40** or **5-45**, underestimating the binding energies by more than 4 kcal/mol. Oddly, M06-L overestimates the binding of **5-46** by more than 7 kcal/mol. Overall, M06-L predicts the binding energies much more accurately then PBE and this much easier to observe as a pictorial representation, a graph of the

experimental values versus the computational values for the addition of L to **5-3** is shown below in Figure 5.10.

Figure 5.10 Graph of Experimental ΔG Values versus Computational ΔG Values for the Addition of Ligands to **5-3,** [Experimental (black), PBE (red), and M06-L (blue), ΔG (kcal/mol)].

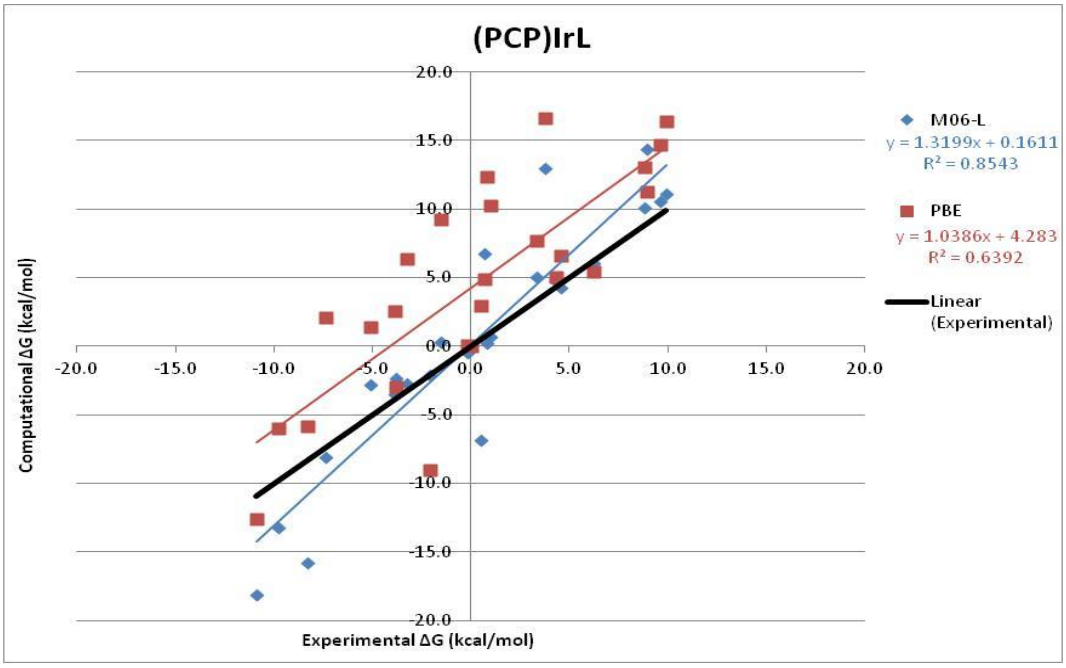

The values predicted by the PBE functional, in red, are much overestimated by a factor of 4.3 units, whereas the values predicted by M06-L, in blue, are only 0.2 units over the experimental values. The root mean square for values determined via M06-L is 3.6 kcal/mol while the root mean square for PBE is 6.1 kcal/mol. In comparison, PBE did best in predicting the energies for **5-3** rather than **5-1** or **5-2**.

5.3 Conclusions

The binding energies for a range of C, H, O, N, S-type and PR_3 ligands were determined for addition to **5-1**, **5-2**, and **5-3**. In the case of **5-1**, an isomerization between **5-1a** and **5-1b** isomers is observed when PR_3 ligands are studied but isomerization is not observed when L is an N-type ligand. The isomerization is due to bulkiness of PR_3 in comparison to the chloride, so, the N-type ligands experience exchange and have much more positive entropy values in comparison to the PR_3 ligands. In the case of **5-2**, isomerization is observed for all ligands including the N-type ligands. The equilibrium between **5-3** and L lies too far to the right in order for direct measurement. Therefore, the barrier to addition ($\Delta H^{\ddagger}$ = 24.9

kcal/mol) of acetonitrile and displacement of pyridine is considered to be the anchor point and all other ΔH and ΔG values for the addition of L are determined relative to pyridine via equilibrium exchange experiments. Overall, the M06-L and M06 functionals have much better agreement with the experimentally determined values for the addition of ligands to all three catalyst systems most likely due to the inclusion of dispersion.

5.4 Experimental

5.4.1 General Methods

All reactions were performed under an argon atmosphere using standard Schlenck techniques or in an argon-filled glove box. Phosphines, phosphonites, phosphinites, dibenzothiophene and pyridine were purchased from Aldrich or VWR. Cyclooctene, 1-hexene, trans-2-hexene, C_6H_6, C_6D_6, and *p*-xylene-d_{10} were dried over Na/K alloy and collected via vacuum transfer. Norbornene (NBE) was sublimed before use. All other substrates were degassed before entry to glovebox and used without further purification. **5-1** and **5-2** were synthesized according to literature.[42] ^{1}H, ^{13}C, and ^{31}P NMR spectra were obtained from either a 400 or 500 MHz Varian instrument. The residual peak of the deuterated solvent was used as a reference for all ^{1}H NMR spectra and an internal capillary standard of PMe_3 in *p*-xylene-d_{10} (-62.4 ppm) was used to reference ^{31}P NMR chemical shifts.

5.4.2 Chemical Equilibria

To a 0.5 mL *p*-xylene-d_{10} solution, 5 mg **5-1** (8.04 μmol), 5 mg **5-2** (8.5 μmol) or a combination of 5 mg **5-2** (8.5 μmol) and 2.4 mg NBE (25.5 μmol) in an NMR tube, ligand was added (stock solutions in *p*-xylene-d_{10} of each ligand were utilized and amounts have been listed in the Tables 5.9 through 5.11). The solution was sealed in an NMR tube under an argon atmosphere. The solution was monitored by ^{1}H and ^{31}P NMR spectroscopy at varying temperatures, ranging from -10 to 105 °C. The temperature of the NMR was calibrated by ethylene glycol.[43] All products were characterized by ^{31}P and ^{1}H NMR spectroscopy. The characterization has been included in the experimental section, whereas crystal structures and data of select products have been included following the experimental section. The concentration of each species was determined by integration of each species, by both integration of each ^{31}P NMR shift or integration of the hydride shift for (PCP)IrHCl and (PCP)IrH_2 or by the methylene protons in (PCP)Ir. The concentration

was also determined by correlation of the NMR shift of the ^{31}P or ^{1}H hydride shifts to the percentage of each species in solution for the addition of N-type ligands. The concentration was determined by correlation to the known concentration of added species or to the known concentration of an internal standard.

5.4.3 Exchange Equilibria

In typical equilibrium measurements, to a 0.5 mL *p*-xylene-d_{10} solutions of 5 mg **5-1** (8.04 μmol), 5 mg **5-2** (8.5 μmol) or a combination of 5 mg **5-2** (8.5 μmol) and 2.4 mg NBE (25.5 μmol) in an NMR tube, two ligands were added. The ratio of ligands has been included in Tables 5.9 – 5.11 below along with reported K values. The NMR tube was sealed under an argon atmosphere. The solution was monitored by ^{31}P and ^{1}H NMR spectroscopy.

Table 5.9 Substrate Ratio, Equilibrium Constants, and ΔG Values for the Equilibria of **5-1**

Ligand	Substrate Ratio	K[a]	Equilibrium ΔG (kcal/mole)
PEt_3	26.7 μmol	80.9 M^{-1}	-2.6
CH_3CN	26.8 μmol	113.5 M^{-1}	-2.8
PPh_2Me	26. 9 μmol	3944 M^{-1}	-4.9
Isoquinoline	26.7 μmol	5530 M^{-1}	-5.1
Pyridine	26.7 μmol	25304 M^{-1}	-6.0
$PMe(OEt)_2/P(OEt)_3$	8.9 μmol/8.9 μmol	4.0	-0.8
$PMe(OEt)_2/PPh(OEt)_2$	8.9 μmol/8.9 μmol	21	-2.0
PPh_2OMe/PEt_3	8.9 μmol/8.9 μmol	246	-3.3
$P(OEt)_3/PPh(OEt)_2$	8.9 μmol/8.9 μmol	5.3	-1.0
$PPh(OEt)_2/PMe_3$	8.9 μmol/8.9 μmol	108	-2.8
PPh_2OMe/Py	8.9 μmol/8.9 μmol	1.7	-0.3
PMe_3/PMe_2Ph	8.9 μmol/8.9 μmol	20.6	-1.8
PMe_2Ph/PPh_2OMe	8.9 μmol/8.9 μmol	2.4	-0.5
PPh_2OMe/PPh_2Me	17.8 μmol/8.9 μmol	14.9	-1.6

[a] Unless otherwise noted, K is unitless

Table 5.10 Substrate Ratio, Equilibrium Constants, and ΔG Values for the Equilibria of **5-2**

Ligand	Substrate Ratio	K[a]	Equilibrium ΔG (kcal/mole)
NH_3	90 µmol	20 M^{-1}	2.1
PPh_3	8.3 µmol	370.3 M^{-1}	-3.5
H_2	n/a	8437 M^{-1}	-5.4
PPh_2Et	26.9 µmol	97786 M^{-1}	-6.7
CH_3CN/PPh_3	8.3 µmol/8.3 µmol	27.9	-2.0
$PPh(OEt)_2/PMe(OEt)_2$	8.3 µmol/8.3 µmol	2.5	-0.6
$P(OEt)_3/PMe(OEt)_2$	8.3 µmol/8.3 µmol	1.0	-0.03
PMe_3/PPh_2OMe	8.3 µmol/8.3 µmol	4.3	-0.9
$PPh(OEt)_2/PPh_2OMe$	8.3 µmol/8.3 µmol	4137	-5.0
PEt_3/Py	8.3 µmol/8.3 µmol	69.4	-2.5
Py/DBT	8.3 µmol/8.3 µmol	726	-4.0
DBT/PPh_3	8.8 µmol/ 43.7 µmol	5.4	-1.0
PPh_2OMe/PMe_2Ph	8.3 µmol/8.3 µmol	6.5	-1.1
$PMe(OEt)_2/PMe_3$	8.3 µmol/8.3 µmol	409	-3.6
PMe_3/PMe_2Ph	8.3 µmol/8.3 µmol	24.8	-1.9
PMe_2Ph/PEt_3	8.3 µmol/8.3 µmol	43.3	-2.2
PPh_2Me/PEt_3	90.27 µmol/ 35.99 µmol	2.2	-0.5
Isoquinoline/Py	17.9 µmol/ 44.5 µmol	1.6	-0.3
PPh_3/Thiophene	12.6 µmol/ 9.0 µmol	2.3	-0.5
PPh_3/2-picoline	11.4 µmol/ 8.91 µmol	67	-2.5

[a] Unless otherwise noted, K is unitless

Table 5.11 Substrate Ratio, Equilibrium Constants, and ΔG Values for the Equilibria of **5-3**

Ligand	Substrate Ratio	K[a]	Equilibrium ΔG (kcal/mole)
1-hexene/NBE	4.2 μmol/ 500 μmol	11828	-5.6
1-hexene/COE	4.2 μmol/ 417 μmol	7454	-5.3
1-hexene/t-2-hexene	8.3 μmol/ 318 μmol	1949	-4.5
Py/1-hexene	8.3 μmol/8.3 μmol	1534	-4.3
Py/DBT	18 μmol/ 44.5 μmol	254	-3.3
PPh_3/DBT	8.9 μmol/8.9 μmol	65	-2.5
Aniline/Benzene	8.3 μmol/8.3 μmol	98	-2.7
DBT/Aniline	8.3 μmol/8.3 μmol	134	-2.9
PEt_3/Py	17.8 μmol/44.1 μmol	13	-1.5
Py/PPh_2Et	44.1 μmol/ 26.9 μmol	5	-1.0
CH_3CN/Py	17.8 μmol/44.5 μmol	35	-2.1
PPh_2Me/PEt_3	17.7 μmol/49.2 μmol	38	-2.2
Ethylene/CH_3CN	1 atm/8.3 μmol	18	-1.7
PMe_3/PEt_3	8.3 μmol/8.3 μmol	438	-3.6
PPh_2OMe/PMe_3	8.3 μmol/8.3 μmol	49	-2.3
$PPh(OEt)_2$/PPh_2OMe	8.9 μmol/ 8.9 μmol	5	-0.9
$PMe(OEt)_2$/$PPh(OEt)_2$	8.3 μmol/8.3 μmol	13	-1.5
$P(OEt)_3$/$PMe(OEt)_2$	8.3 μmol/8.3 μmol	7	-1.1
$P(OEt)_3$/$PPh(OEt)_2$	17.8 μmol/42.6 μmol	81	-2.6
Isoquinoline/Py	45.1 μmol/18 μmol	1.3	-0.2
PMe_3/$PPhMe_2$	18 μmol/ 44.3 μmol	7.8	-1.2
Thiophene/PPh_3	9.0 μmol/12.6 μmol	1.1	-0.1
PPh_3/Furan	8.9 μmol/ 17.6 μmol	143	-2.9
PPh_3/2-picoline	8.9 μmol/44.5 μmol	598	-3.8
PEt_3/N_2	19.5 μmol/ 1 atm	30	-2.0
phenol/PPh_2Me	9.6 μmol/ 8.06 μmol	2.3	-0.5
propylene/DBT	1 atm/ 10.6 μmol	3.5	-2.1

[a] Unless otherwise noted, K is unitless

5.4.4 Dehydrogenation of Isopropanol

To a 0.5 mL *p*-xylene-d_{10} solution of 8.93 μL **5-2** (8.93 μmol) in a J. Young NMR tube, 45 μL 2-propanol (42.48 μmol) was added. The solution was heated for ten days at 100 ˚C and equilibrium was reached. The concentrations of **5-2** and **5-2H$_2$** were monitored by ^{31}P and ^{1}H NMR spectroscopy, whereas the concentrations of acetone and 2-propanol were monitored by ^{1}H NMR spectroscopy only.

5.4.5 Synthesis of (PCP)IrHCl(L), **5-*4* – *5-14***

To a 0.5 ml *p*-xylene-d_{10} solution of 5 mg **5-1** (8.3 μmol) in a J. Young NMR tube, 8.9 μmol substrate was added and **5-4** through **5-14** were synthesized.

(*PCP*)IrHCl(PPh$_2$Me), 5-6

^{31}P NMR (*p*-xylene-d_{10}, 161.9 MHz): δ 44.07 (d, J_{PP} = 14.1 Hz, (*PCP*)IrHCl(PPh$_2$Me), -27.48 (t, J_{PP} = 14.2 Hz, (PCP)IrHCl(*P*Ph$_2$Me). **^{1}H NMR (*p*-xylene-d_{10}, 400 MHz):** δ 7.73 (t, 4H, Ar-*H*), 7.37 (d, 2H, Ar-*H*), 7.331 (d, 2H Ar-*H*), 7.16 (d, 1H, Ar-*H*), 7.10 (2H, Ar-*H*), 7.06 (2H, Ar-*H*), 4.20 (d of vt, J_{PH} = 14.0 Hz, J_{PH} = 3.6, 2H, C*H*$_2$P), 3.12 (d of vt, J_{PH} = 14.4 Hz, J_{PH} = 3.6, 2H, C*H*$_2$P), 2.71 (d, J_{PH} = 7.6 Hz, 3H, PPh$_2$*Me*), 1.25 (t, J_{PH} = 5.8 Hz, 18H, P^{t}Bu), 0.82 (t, J_{PH} = 5.8 Hz, 18H, P^{t}Bu), -22.42 (dt, J_{PH} = 10.4 Hz, J_{PH} = 15.2 Hz, 1H, Ir-*H*).

(PCP)IrHCl(isoquinoline), 5-7

^{31}P NMR (*p*-xylene-d_{10}, 161.9 MHz): δ 46.84 (s, (PCP)IrHCl(isoquinoline)). **^{1}H NMR (*p*-xylene-d_{10}, 400 MHz):** δ 9.1 (s, 1H, isoquinoline), 8.5 (s, 1H, isoquinoline), 7.47 (d, J_{HH} = 7.6 Hz, 2H, isoquinoline), 7.37 (d, J_{HH} = 7.6 Hz, 1H, isoquinoline), 7.28 (t, J_{HH} = 7.6 Hz, 1H, isoquinoline), 7.19 (m, 2H, isoquinoline), 7.10 (d, J_{HH} = 7.2 Hz, 2H, PCP), 7.05 (t, J_{HH} = 6 Hz, 1H, Ar-*H*), 2.99 (vt, 4H, C*H*$_2$P). 1.42 (t, J_{HH} = 6 Hz, 18H, P^{t}Bu$_2$), 0.97 (t, J_{HH} = 6 Hz, 18H, P^{t}Bu$_2$), -21.18 (t, J_{PH} =16 Hz, 1H, Ir-*H*).

(PCP)IrHClPy, 5-8

Complex was crystallized via slow evaporation from toluene. A crystal structure is included in Figure 5.11 and X-ray crystallography refinement and structure parameters are included in Tables 5.12 through 5.15.

(PCP)IrHClPPh$_2$OMe, 5-9[19]

^{31}P NMR (*p*-xylene-d_{10}, 161.8 MHz): δ 98.4 (t, J_{PP} = 14.6 Hz, (*PCP*)IrHClPPh$_2$OMe), 51.3 (broad, (PCP)IrHCl*P*Ph$_2$OMe). **^{1}H NMR (*p*-xylene-d_{10}, 400 MHz):** δ 8.05 (t, J_{HH} = 8.0 Hz, 4H, Ar-*H*), 7.19 (d, J_{HH} = 6.5 Hz, 2H, Ar-*H*), 7.17 (t, J_{HH} = 6.1 Hz, 1H, Ar-*H*), 7.10 (m, 4H, Ar-*H*), 7.04 (t, J_{HH} = 7.0 Hz, 2H, Ar-*H*), 4.16 (d of vt, J_{PH} = 3.2 Hz, J_{HH} = 15.2 Hz, 2H, C*H*$_2$P), 3.14 (d of vt, J_{PH} = 3.2 Hz, J_{HH} = 15.2 Hz, 2H, C*H*$_2$P), 3.06 (d, J_{PH} = 10.4 Hz, 3H, PO*Me*), 1.23 (t, J_{PH} = 6.2

Hz, 18H, P^{t}Bu), 1.04 (t, J_{PH} = 6.0 Hz, 18H, P^{t}Bu), -23.28 (dt, J_{PH} = 15.4 Hz, J_{PH} = 13.2 Hz, 1H, Ir-*H*).

The synthesis and characterization of the following complexes have been described elsewhere: (^{tbu4}PCP)IrHClPEt$_3$, **5-4**, (PCP)IrHClNCCH$_3$, **5-5**, (PCP)IrHClPPhMe$_2$, **5-10**, (PCP)IrHClPMe$_3$, **5-11**, (PCP)IrHClPPh(OEt)$_2$, **5-12a, 5-12b**, (PCP)IrHClP(OEt)$_3$, **5-13a**, **5-13b**, (PCP)IrHClPMe(OEt)$_2$, **5-14a**, **5-14b**[19]

5.4.6 Synthesis of (PCP)IrH$_2$L, **5-*15* – *5-32***

To a 0.5 mL *p*-xylene-d$_{10}$ solution of 5 mg **5-2** (8.3 μmol) in a J. Young NMR tube, 8.3 μmol substrate was added and **5-15** through **5-32** were synthesized.

(PCP)IrH$_2$(2-picoline), 5-15

^{31}P NMR (*p*-xylene-*d*$_{10}$, 161.9 MHz): δ 63.93 (s, (PCP)IrH$_2$(2-picoline)). **^{1}H NMR (*p*-xylene-*d*$_{10}$, 400 MHz):** δ 10.3 (d, 1H, 2-picoline), 6.98 (bs, 1H, 2-picoline), 6.77 (bs, 1H, 2-picoline), 6.46 (d, J_{HH} = 7.6 Hz, 1H, Ar-*H*), 6.43 (t, 2H, Ar-*H*), 6.13 (t, 1H, 2-picoline), 3.14 (bs, 3H, 2-picoline CH$_3$), 3.05 (d of vt, J_{HH} = 3.6 Hz, 4H, C*H*$_2$P), 1.12 (t, J_{HH} = 5.6 Hz, 36H, P^{t}Bu), -7.33 (dt, 1H, Ir-*H*), -8.55 (dt, 1H, Ir-*H*).

(PCP)IrH$_2$(NH$_3$), 5-16

^{31}P NMR (*p*-xylene-*d*$_{10}$, 161.9 MHz): δ 67.2 (s, (*PCP*)IrH$_2$(NH$_3$)). **^{1}H NMR (*p*-xylene-*d*$_{10}$, 400 MHz):** δ 6.79 (d, J_{HH} = 7.5 Hz, 2H, Ar-*H*), 6.67 (t, J_{HH} = 7.3 Hz, 1H, Ar-*H*), 3.10 (t, J_{HH} = 3.5 Hz, 4H, *CH*$_2$P), 1.35 (t, J_{PH} = 5.8 Hz, 36H, P^{t}Bu$_2$), -8.75 (t, J_{PH} = 14.8 Hz, 2H, Ir-*H*$_2$).

(PCP)IrH$_2$(thiophene), 5-17

^{31}P NMR (*p*-xylene-*d*$_{10}$, 161.9 MHz): δ 62.816 (s, (PCP)IrH$_2$thiophene). **^{1}H NMR (*p*-xylene-*d*$_{10}$, 400 MHz):** δ 7.048(s, 2H, Ar-*H*), 6.91 (bs, 4H, thiophene), 6.89 (bs, 1H, Ar-*H*), 3.13 (vt, 4H, C*H*$_2$P), 1.26 (t, J_{PH} = 6.4 Hz, 36H, P^{t}Bu$_2$), -9.16 (t, J_{HH} = 9.6 Hz, 2H, Ir*H*$_2$).

(PCP)IrH$_2$PPh$_3$, 5-18

^{31}P NMR (*p*-xylene-d_{10}, 202 MHz): δ 51.1 (d, J_{PP} = 17.5 Hz, (*PCP*)IrH$_2$PPh$_3$), 7.40 (t, J_{PP} = 17.5 Hz, (PCP)IrH$_2$*PPh*$_3$). **^{1}H NMR (*p*-xylene-d_{10}, 500 MHz):** δ 3.48 (vt, 4H, J_{PH} = 4.3 Hz), 0.96 (vt, 36H, J_{PH} = 7.5 Hz, P^{t}Bu), -10.24 (q, 2H, J_{PH} = 17.8 Hz, Ir-*H*$_2$).

(PCP)IrH$_2$NCCH$_3$, 5-21

Upon addition of NCCH$_3$ to solution, a 1:1 mixture of **2b-NCCH$_3$** and **3-NCCH$_3$** is formed. **^{31}P NMR (*p*-xylene-d_{10}, 202 MHz):** δ 69.1 (s, (PCP)IrH$_2$NCCH$_3$). **^{1}H NMR (*p*-xylene-d_{10}, 500 MHz):** δ 6.93 (d, J_{HH} = 7.5 Hz, 2H, Ar-*H*), 6.88 (t, J_{HH} = 6.5 Hz, 1H, Ar-*H*), 3.14 (vt, J_{PH} = 4.8 Hz, 4H, C*H*$_2$P), 1.43 (t, J_{PH} = 7.5 Hz, 36H, P^{t}Bu), 1.120 (s, 3H, Ir(NCCH$_3$)), -9.02 (t, J_{PH} = 18 Hz, 2H, Ir-*H*$_2$).

(PCP)IrH$_2$PPh$_2$Et, 5-22

^{31}P NMR (*p*-xylene-d_{10}, 161.9 MHz): δ 54.6 (d, J_{PP} = 14.9 Hz, (*PCP*)IrH$_2$PPh$_2$Et), -4.7 (t, J_{PP} = 14.9 Hz, (PCP)IrH$_2$*P*Ph$_2$Et). **^{1}H NMR (*p*-xylene-d_{10}, 400 MHz):** δ 8.08 (t, 3H, Ar-*H*), 7.2 - 6.99 (Ar-*H)*, 3.49 (t, J_{HH} = 3.2 Hz, 4H, C*H*$_2$P), 2.63 (m, 3H, PPh$_2$CH$_2$*CH*$_3$), 1.10 (t, J_{PH} = 5.6 Hz, 36H, P^{t}Bu), -10.70 (q, 2H, J_{HH} = 14.4 Hz, Ir-*H*$_2$). *unable to observe some shifts due to overlap with free PPh$_2$Et.

(PCP)IrH$_2$isoquinoline, 5-24

^{31}P NMR (*p*-xylene-d_{10}, 161.9 MHz): δ 64.62 (s). **^{1}H NMR (*p*-xylene-d_{10}, 400 MHz):** δ 10.41 (s, 1H, H$_A$), 9.47 (d, J_{HH} = 6.4 Hz, 1H, H$_B$), 7.46 (d, J_{HH} = 7.6 Hz, 1H, H$_C$), 7.24 (d, J_{HH} = 8 Hz, 1H, H$_D$), 7.09 (m, 2H, H$_F$ and H$_G$), 6.95 (t, 2H, Ar-*H*)*, 6.83 (d, J_{HH} = 6.4 Hz, 1H, Ar-*H*), 3.29 (t, J_{HH} = 3.6 Hz, 4H, C*H*$_2$P), 1.29 (t, J_{HH} = 5.6 Hz, 36H, P^{t}Bu), -7.69 (dt, 1H, Ir-*H*), -7.80 (dt, 1H, Ir-*H*). *Aryl PCP shifts overlap with solvent, therefore unable to calculate coupling constants.

(PCP)IrH$_2$PPh$_2$Me, 5-26

^{31}P NMR (*p*-xylene-d_{10}, 161.9 MHz): δ 55.30 (d, J_{PP} = 15.5 Hz (*PCP*)IrH$_2$PPh$_2$Me), -31.44 (t, J_{PP} = 15.54 Hz, (PCP)IrH$_2$*P*Ph$_2$Me). **^{1}H NMR (*p*-xylene-d_{10}, 400 MHz):** δ 7.84 (t, 4H, Ar-*H*), 7.206 (s, 1H, Ar-*H*), 7.024 (m, 4H, Ar-*H*), 6.93 (s, 2H, Ar-*H*), 3.44 (t, 4H, J_{HH} = 3.2 Hz, C*H*$_2$P), 2.56 (d, 3H, J_{PH} = 6.8 Hz, PPh$_2$*Me*), 1.08 (t, 36H, J_{PH} = 6 Hz, P^{t}Bu), -10.75 (q, 2H, J_{HH} = 14.8 Hz, Ir-*H*$_2$). *some shifts overlap with free PPh$_2$Me.

The synthesis and characterization of the following complexes have been described elsewhere: (PCP)IrH$_4$, **5-20**[42], (PCP)IrH$_2$DBT, **5-19**, (PCP)IrH$_2$Py, **5-23**[19], (PCP)IrH$_2$PEt$_3$, **5-25**, (PCP)IrH$_2$PPhMe$_2$, **5-27a, 5-27b**, (PCP)IrH$_2$PPh$_2$OMe, **5-28a, 5-28b**, (PCP)IrH$_2$PMe$_3$, **5-29a, 5-29b,** (PCP)IrH$_2$PMe(OEt)$_2$, **5-30a**, **5-30b**, (PCP)IrH$_2$P(OEt)$_3$, **5-31a**, **5-31b**, (PCP)IrH$_2$PPh(OEt)$_2$, **5-32a**, **5-32b**[19]

5.4.7 Synthesis of (PCP)IrL, **5-33 – 5-59**

To a 0.5 mL *p*-xylene-d_{10} solution of 5 mg **5-2** (8.3 μmol) in a J. Young NMR tube, 2.4 mg NBE (25 μmol) was added. After 3 hours at room temperature, 8.3 μmol substrate was added and **5-33** through **5-59** were synthesized in $\geq$ 98% yield as measured by ^{31}P NMR spectroscopy.

(PCP)Ir(2-picoline), 5-38

^{31}P NMR (*p*-xylene-d_{10}, 161.9 MHz): δ 68.1 (s, (PCP)Ir(2-picoline)), 66.7 (d, (PCP)Ir(H)(2-picoline)), 66.3 (d, (PCP)Ir(H)(2-picoline)). **^{1}H NMR (*p*-xylene-d_{10}, 400 MHz):** δ 9.6 (d, J_{HH} = 5.6 Hz, 1H, 2-picoline), 9.1*(d, J_{HH} = 5.6 Hz, 1H, 2-picoline), 8.8*(d, J_{HH} = 5.6 Hz, 1H, 2-picoline), 7.6 (d, J_{HH} = 5.6 Hz, 1H, 2-picoline), 7.3 (d, J_{HH} = 5.6 Hz, 1H, 2-picoline),* 7.1 (d, J_{HH} = 7.2 Hz, 2H, Ar-*H*), 7.0 (d, J_{HH} = 7.2 Hz, 2H, Ar-*H*),* 6.8 (t, J_{HH} = 7.6, 1H, Ar-*H*), 6.4 (t, J_{HH} = 7.6, 1H, Ar-*H*),* 3.2 (s, 3H, 2-picoline CH_3), 3.1 (vt, J_{HH} = 2.8 Hz, 4H, CH_2P), 1.35*(t, J_{PH} = 6.0 Hz, 36H, P^{t}Bu), 1.28 (t, J_{PH} = 6.0 Hz, 36H, P^{t}Bu$_2$), 1.17*(t, J_{PH} = 6.0 Hz, 36H, P^{t}Bu$_2$), -45.4 (dt, 1H, Ir-*H*).* *signals for C-H activation product (PCP)Ir(H)(2-picoline).

(PCP)Irfuran, 5-40

^{31}P NMR (*p*-xylene-d_{10}, 161.9 MHz): δ 70.816 (s, (PCP)Ir(H)(furan)). **^{1}H NMR (*p*-xylene-d_{10}, 400 MHz):** δ 8.03 (d, *J* = 1 Hz, 1H, furan), 7.26 (d, *J* = 7 Hz, 1H, Ar-*H*), 7.09 (t, *J* = 7.5 Hz, 2H, Ar-*H*), 6.61 (dd, 1H, furan), 6.14 (d, 1H, furan), 3.46 (d of vt, 2H, CH_2P), 3.36 (d of vt, 2H, CH_2P), 1.11 (t, J_{PH} = 6.0 Hz, 36H, P^{t}Bu$_2$), -44.8 (t, J_{HH} = 13 Hz, 1H, Ir-*H*).

(PCP)IrDBT, 5-41

^{31}P NMR (*p*-xylene-d_{10}, 202 MHz): δ 66.2 (s, (PCP)IrDBT). **^{1}H NMR (*p*-xylene-d_{10}, 500 MHz):** δ 8.15 (d, J_{HH} = 8.0 Hz, 2H, Ar-*H*), 7.36 (m, 4H, Ar-*H*), 7.09 (t, *J*= 7.5 Hz, 2H, Ar-*H*), 3.18 (t, J_{PH} = 3.0 Hz, 4H, CH_2P), 1.20 (vt, J_{PH} = 6.0 Hz, 36H, P^{t}Bu$_2$).

(PCP)IrPPh$_2$Et, 5-43

^{31}P NMR (*p*-xylene-d_{10}, 161.9 MHz): δ 65.6 (d, J_{PP} = 12.1 Hz (*PCP*)IrPPh$_2$Et), 7.8 (t, J_{PP} = 12.1 Hz, (PCP)Ir*P*Ph$_2$Et). **^{1}H NMR (*p*-xylene-d_{10}, 400 MHz):** δ 8.19 (t, 4H, P*Ph*$_2$CH$_2$CH$_3$), 7.2-7.0 (Ar-*H*), 3.36 (t, J_{HH} = 3.2 Hz, 4H, C*H*$_2$P), 2.73 (m, 2H, PPh$_2$C*H*$_2$CH$_3$), 1.10 (t, J_{PH} = 6 Hz, 36H, P^{t}Bu$_2$), 0.96 (t, J_{HH} = 6.8 Hz, 3H, PPh$_2$CH$_2$*CH*$_3$). *unable to observe some shifts due to overlap with free PPh$_2$Et.

(PCP)IrPPh$_3$, 5-44

^{31}P NMR (*p*-xylene-d_{10}, 161.9 MHz): δ 64.65 (d, J_{PH} = 14.7Hz, (*PCP*)Ir), 14.24 (t, J_{PH} = 14.7Hz, Ir*P*Ph$_3$). **^{1}H NMR (*p*-xylene-d_{10}, 400MHz):** δ 8.26 (t, 6H, PPh$_3$ Ar-*H*), 7.36 (m, 6H, PPh$_3$ Ar-*H*), 7.20 - 7.10 (Ar-*H*), 7.07 (t, 3H, PPh$_3$ Ar-*H*), 3.35 (vt, 4H, *CH*$_2$P), 0.96 (t, J_{HH} = 5.6 Hz, 36H, P^{t}Bu$_2$). *unable to observe distinct shifts for the PCP aryl protons due to overlap with free PPh$_3$.

(PCP)Irthiophene, 5-45

^{31}P NMR (*p*-xylene-d_{10}, 161.9 MHz): δ 67.26 (d, (PCP)Ir(H)(thiophene)), 67.75 (s, (PCP)Irthiophene). **^{1}H NMR (*p*-xylene-d_{10}, 400 MHz):** δ 7.23 (d, 1H, Ar-*H*), 7.15(t, 1H, thiophene), 7.09 (t, 2H, Ar-*H*), 7.06 (t, 1H, thiophene), 3.38 (d of vt, 4H, C*H*$_2$P), 1.10 (t, J_{PH} = 6.0 Hz, 36H, P^{t}Bu), -44.17 (vt, 1H, Ir-*H*)*. ^{*1}H NMR characterization for (PCP)Ir(H)(Thiophene).

(PCP)Ir(isoquinoline), 5-48

^{31}P NMR (*p*-xylene-d_{10}, 161.9 MHz): δ 67.760 (s, (PCP)Ir(isoquinoline). **^{1}H NMR (*p*-xylene-d_{10}, 400 MHz):** δ 10.20 (s, 1H, H$_A$), 9.29 (d, J_{HH} = 6.5 Hz, 1H, H$_B$), 7.49 (d, J_{HH} = 8.5 Hz, 1H, H$_C$), 7.24 (d, J_{HH} = 8 Hz, 1H, H$_D$), 7.16 (m, 2H, H$_F$ and H$_G$), 7.04 (t, J_{HH} = 7 Hz 2H, Ar-*H*), 6.96 (d, J_{HH} = 6.5 Hz, 1H, Ar-*H*), 3.13 (t, J_{HH} = 3.0 Hz, 4H, C*H*$_2$P), 1.26 (t, J_{HH} = 5.5 Hz, 36H, P^{t}Bu).

(PCP)IrNCCH$_3$, 5-50

Complex was crystallized from a *p*-xylene/pentane mixture via slow evaporation. A crystal structure is included as Figure 5.12 and X-ray crystallography refinement and structure parameters are included in Tables 5.16 through 19. **^{31}P NMR (*C$_6$D$_6$*, 161.9 MHz):** δ 70.1 (s, (PCP)IrNCCH$_3$). **^{1}H NMR (*C$_6$D$_6$*, 400 MHz):** δ 7.25 (d, J_{HH} = 7.2 Hz, 2H, Ar-*H*), 7.13 (t, J_{HH} = 6.8 Hz, 1H, Ar-*H*), 3.16 (t, J_{PH} = 3.6 Hz, 4H, C*H*$_2$P), 1.40 (t, 36H, J_{PH} = 6.0 Hz, P^{t}Bu$_2$), 0.93 (s, 3H, Ir(NCCH$_3$)). **^{13}C NMR (*C$_6$D$_6$*, 125 MHz):** 167.2 (t, J_{CP} = 3.0 Hz, Ir(N*C*CH$_3$), 153.8 (d, J_{CP} = 11.6 Hz, Aryl), 122.3

(s, Aryl), 120.9 (s, Aryl), 120.2 (t, J_{CP} = 8.6 Hz, Aryl), 38.1 (vt, J_{CP} = 13.4 Hz, *C*H_2P), 36.3 (vt, J_{CP} = 9.1 Hz, P*C*$(CH_3)_3$), 30.2 (vt, J_{CP} = 3.1 Hz, PC(*C*$H_3)_3$).

(PCP)IrPPh$_2$Me, 5-51

^{31}P NMR (*p*-xylene-d_{10}, 161.9 MHz): δ 66.35 (d, J_{PP} = 15.4 Hz (*PCP*)IrHClPPh$_2$Me), -9.99 (t, J_{PP} = 15.4 Hz, (PCP)IrHCl*P*Ph$_2$Me). **^{1}H NMR (*p*-xylene-d_{10}, 400 MHz):** δ 8.09 (t, 4H, Ar-*H*), 7.21-7.12 (Ar-*H*), 3.35 (t, J_{HH} = 3.2 Hz, 4H, C*H*$_2$P), 2.33 (d, J_{PH} = 5.2 Hz, 3H, PPh$_2$*Me*), 1.09 (t, J_{PH} = 6 Hz, 36H, P^{t}Bu$_2$). *some shifts overlap with free PPh$_2$Me.

(PCP)IrPPhMe$_2$, 5-54

Complex was crystallized from a benzene/pentane mixture. A crystal structure is included as Figure 5.13 and X-ray crystallography refinement and structure parameters are included in Tables 5.20 through 5.23. **^{31}P NMR (*p*-xylene-d_{10}, 161.9 MHz):** δ 67.86 (d, J_{PP} = 16.2 Hz (*PCP*)IrPPhMe$_2$), -25.4 (t, J_{PP} = 16.2 Hz, (PCP)Ir*P*PhMe$_2$). **^{1}H NMR (*p*-xylene-d_{10}, 400 MHz):** δ 8.05 (t, J_{HH} = 8 Hz, 1H, Ar-*H*), 7.1-7.2 (Ar-*H*), 3.35 (t, J_{HH} = 2.8 Hz, 4H, C*H*$_2$P), 2.00 (d, J_{PH} = 5.6 Hz, 3H, PPh*Me*$_2$), 1.23 (t, J_{PH} = 6 Hz, 36H, P^{t}Bu$_2$).

(PCP)IrPPh$_2$OMe, 5-56

^{31}P NMR (*p*-xylene-d_{10}, 161.9 MHz): δ 103.1 (t, J_{PP} = 11 Hz, (*PCP*)IrPPh$_2$OMe), 66.1 (d, J_{PP} = 11 Hz, (*PCP*)IrPPh$_2$OMe). **^{1}H NMR (*p*-xylene-d_{10}, 400 MHz):** δ 8.26 (t, 4H, Ar-*H*), 7.55 (m, 1H, Ar-*H*), 7.31 (t, 4H, Ar-*H*), 7.21 (m, 2H, Ar-*H*), 3.38 (t, J_{HH} = 4.2 Hz, 4H, C*H*$_2$P), 3.00 (d, J_{HH} = 10.4 Hz, 3H, PO*Me*) 1.15 (t, J_{PH} = 6 Hz, 36H, P^{t}Bu$_2$).

(PCP)IrPPh(OEt)$_2$, 5-57

^{31}P NMR (*p*-xylene-d_{10}, 161.9 MHz): δ 147.6 (t, J_{PP} = 11 Hz, (*PCP*)IrPPh(OEt)$_2$), 72.6 (d, J_{PP} = 11 Hz, (*PCP*)IrPPh(OEt)$_2$). **^{1}H NMR (*p*-xylene-d_{10}, 400 MHz):** δ 8.24 (t, 2H, P*Ph*(OCH$_2$CH$_3)_2$), 7.67 (t, 1H, P*Ph*(OCH$_2$CH$_3)_2$), 7.3-7.1 (5H, Ar-*H*), 4.0 (m, 4H, PPh(O*C*H$_2$CH$_3)_2$), 3.43 (t, J_{HH} = 3.2 Hz, 4H, C*H*$_2$P), 1.27 (t, J_{PH} = 6 Hz, 36H, P^{t}Bu$_2$), 1.17 (t, J_{HH} = 7.2 Hz, 6H, PPh(OCH$_2$*C*H$_3)_2$).

(PCP)IrPMe(OEt)$_2$, 5-58

^{31}P NMR (*p*-xylene-d_{10}, 161.9 MHz): δ 160.77 (t, J_{PP} = 19.3 Hz, (PCP)Ir*PMe(OEt)$_2$*), 72.04 (d, J_{PP} = 19.1 Hz, (*PCP*)IrPMe(OEt)$_2$). **^{1}H NMR (*p*-xylene-d_{10}, 400 MHz):** δ 7.16 (d, J_{HH} = 6.8 Hz, 2H, Ar-*H*), 7.06 (t, J_{HH} = 7.6 Hz, 1H, Ar-*H*), 3.96 (m, 2H, PMe(OCH$_2$CH$_3)_2$), 3.72 (m,

$PMe(OCH_2CH_3)_2$), 3.33 (t, J_{PH} = 3.2 Hz, 4H, CH_2P), 1.26 (t, J_{PH} = 6 Hz, 36H, P^tBu_2), 1.18 (t, J_{HH} = 7.1 Hz, 6H, $PMe(OCH_2CH_3)_2$).

(PCP)IrP(OEt)$_3$, 5-59[19]

Complex was crystallized via slow evaporation of pentane. A crystal structure is included as Figure 5.14 and X-ray crystallography refinement and structure parameters are included in Tables 5.24 through 5.27.

The synthesis and characterization of the following complexes have been described elsewhere: (PCP)IrNBE, **5-33**[44], (PCP)IrCOE, **5-34**[19], (PCP)Ir(trans-2-hexene), **5-35**[19], (PCP)Ir(Ph)(H), **5-36**[44], (PCP)Ir(H)(NHPh), **5-37**[45], (PCP)Ir(1-hexene), **5-39**[19], (PCP)IrN_2, **5-46**[46], (PCP)IrPy, **5-47**[19], (PCP)Ir(PhO)(H), **5-52**[47], (PCP)IrEthylene, **5-53**[19], (PCP)$IrPMe_3$, **5-5**.[19]

5.4.8 Computational Details

DFT studies were completed by Dr. Karsten Krogh-Jespersen. All calculations used DFT methodology as implemented by Gaussian03[48] and 09[49] computer programs. The LANL08[50] basis set was utilized for Ir atom, and all other atoms were treated with the 6-311G (d,p) basis set.

Figure 5.11 Crystal Structure of (PCP)IrHClPy, **5-8**

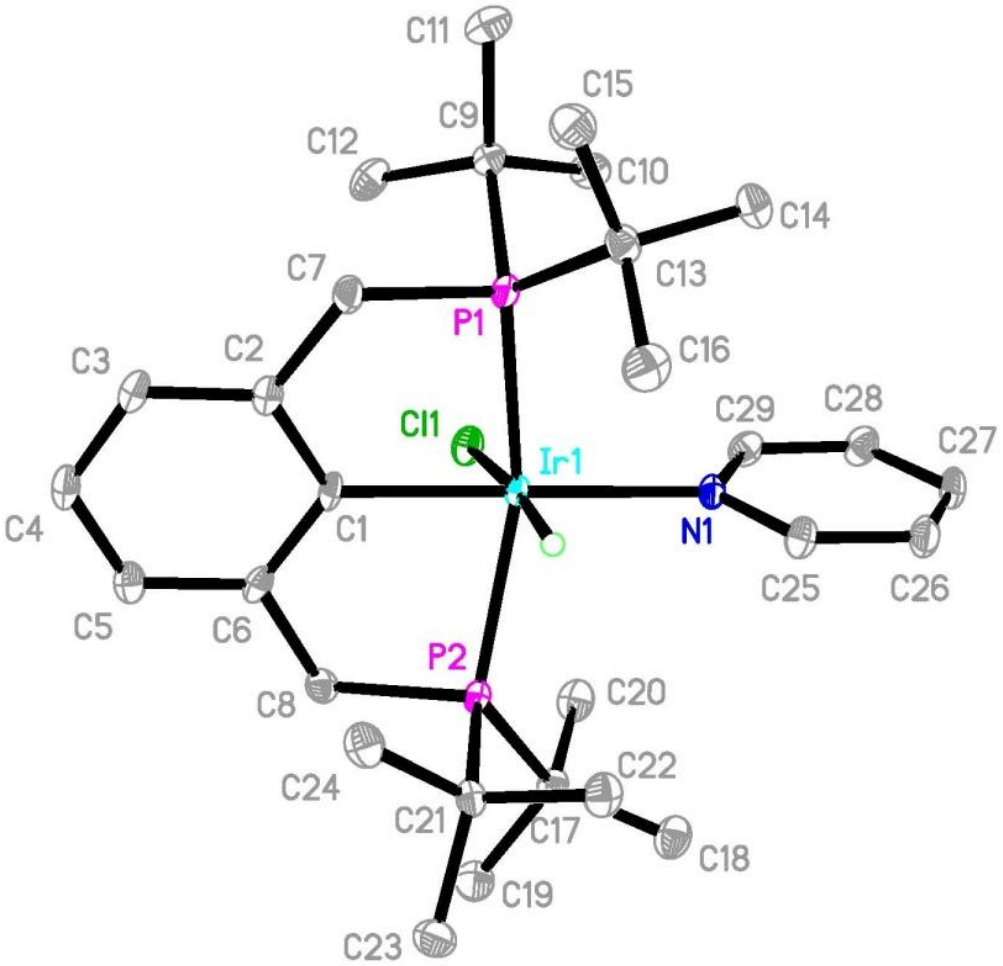

Table 5.12 Crystal Data and Structure Refinement for (PCP)IrHClPy, **5-8**

Identification code	irhclpy_p21n	
Empirical formula	C33 H54 Cl Ir N P2	
Formula weight	754.36	
Temperature	100(2) K	
Wavelength	0.71073 Å	
Crystal system	Monoclinic	
Space group	P2(1)/n	
Unit cell dimensions	a = 9.2545(7) Å	ά= 90°.
	b = 20.6253(15) Å	β= 92.305(1)°
	c = 17.0181(12) Å	γ = 90°.
Volume	3245.7(4) $Å^3$	
Z	4	
Density (calculated)	1.544 Mg/m^3	
Absorption coefficient	4.317 mm^{-1}	
F(000)	1532	
Crystal size	0.27 x 0.18 x 0.02 mm^3	
Theta range for data collection	1.55 to 30.03°.	
Index ranges	-13<=h<=13, -29<=k<=29, -23<=l<=23	
Reflections collected	36843	
Independent reflections	9474 [R(int) = 0.0565]	
Completeness to theta = 30.03°	99.9 %	
Absorption correction	Semi-empirical from equivalents	
Max. and min. transmission	0.7461 and 0.5645	
Refinement method	Full-matrix least-squares on F^2	
Data / restraints / parameters	9474 / 1 / 360	
Goodness-of-fit on F^2	1.001	
Final R indices [I >2sigma(I)]	R1 = 0.0376, wR2 = 0.0802	
R indices (all data)	R1 = 0.0528, wR2 = 0.0857	
Largest diff. peak and hole	3.892 and -1.359 $e.Å^{-3}$	

Table 5.13 Atomic Coordinates (x 10^4) and Equivalent Isotropic Displacement Parameters ($Å^2$x 10^3) for (PCP)IrHClPy, **5-8**. U(eq) is defined as one third of the trace of the orthogonalized U^{ij} tensor.

	x	y	z	U(eq)
Ir(1)	5285(1)	-2287(1)	2214(1)	10(1)
Cl(1)	3856(1)	-2674(1)	3358(1)	16(1)
P(1)	5013(1)	-3167(1)	1360(1)	12(1)
P(2)	5214(1)	-1215(1)	2627(1)	11(1)
C(1)	3350(4)	-2015(2)	1691(2)	12(1)
C(2)	2748(4)	-2341(2)	1029(2)	14(1)
C(3)	1387(4)	-2178(2)	710(2)	16(1)
C(4)	622(4)	-1668(2)	1022(2)	16(1)
C(5)	1224(4)	-1320(2)	1646(2)	16(1)
C(6)	2570(4)	-1490(2)	1981(2)	13(1)
C(7)	3654(4)	-2856(2)	641(2)	15(1)
C(8)	3250(4)	-1096(2)	2648(2)	14(1)
C(9)	4177(4)	-3945(2)	1721(2)	15(1)
C(10)	5016(4)	-4166(2)	2471(2)	18(1)
C(11)	4107(5)	-4513(2)	1136(2)	21(1)
C(12)	2619(4)	-3782(2)	1928(2)	21(1)
C(13)	6583(4)	-3358(2)	710(2)	15(1)
C(14)	7719(4)	-3773(2)	1162(3)	21(1)
C(15)	6124(4)	-3705(2)	-60(2)	21(1)
C(16)	7300(4)	-2720(2)	475(3)	21(1)
C(17)	5904(4)	-920(2)	3630(2)	14(1)
C(18)	7537(4)	-789(2)	3642(2)	20(1)
C(19)	5086(4)	-322(2)	3914(2)	20(1)
C(20)	5646(4)	-1469(2)	4216(2)	19(1)
C(21)	5859(4)	-632(2)	1858(2)	14(1)
C(22)	7432(4)	-779(2)	1672(2)	17(1)
C(23)	5732(4)	89(2)	2090(2)	19(1)
C(24)	4929(4)	-715(2)	1093(2)	18(1)
N(1)	7329(3)	-2584(2)	2821(2)	13(1)
C(25)	8614(4)	-2386(2)	2557(2)	16(1)
C(26)	9925(4)	-2574(2)	2902(2)	18(1)

C(27)	9942(4)	-2977(2)	3550(2)	20(1)
C(28)	8628(4)	-3173(2)	3833(2)	19(1)
C(29)	7350(4)	-2967(2)	3456(2)	15(1)
C(30)	1154(5)	371(2)	341(2)	20(1)
C(31)	-277(5)	573(2)	375(2)	20(1)
C(32)	-1408(5)	214(2)	44(2)	20(1)
C(33)	2356(5)	779(2)	677(3)	28(1)

Table 5.14 Bond Lengths [Å] and Angles [°] for (PCP)IrHClPy, **5-8**

Ir(1)-C(1)	2.046(3)	C(11)-H(11C)	0.9800
Ir(1)-N(1)	2.205(3)	C(12)-H(12A)	0.9800
Ir(1)-P(2)	2.3209(10)	C(12)-H(12B)	0.9800
Ir(1)-P(1)	2.3331(10)	C(12)-H(12C)	0.9800
Ir(1)-Cl(1)	2.5274(9)	C(13)-C(16)	1.535(5)
Ir(1)-H(1)	1.589(10)	C(13)-C(14)	1.536(5)
P(1)-C(7)	1.836(4)	C(13)-C(15)	1.539(5)
P(1)-C(9)	1.893(4)	C(14)-H(14A)	0.9800
P(1)-C(13)	1.903(4)	C(14)-H(14B)	0.9800
P(2)-C(8)	1.836(4)	C(14)-H(14C)	0.9800
P(2)-C(21)	1.892(4)	C(15)-H(15A)	0.9800
P(2)-C(17)	1.899(4)	C(15)-H(15B)	0.9800
C(1)-C(6)	1.403(5)	C(15)-H(15C)	0.9800
C(1)-C(2)	1.408(5)	C(16)-H(16A)	0.9800
C(2)-C(3)	1.393(5)	C(16)-H(16B)	0.9800
C(2)-C(7)	1.520(5)	C(16)-H(16C)	0.9800
C(3)-C(4)	1.386(5)	C(17)-C(20)	1.533(5)
C(3)-H(3)	0.9500	C(17)-C(18)	1.535(5)
C(4)-C(5)	1.380(5)	C(17)-C(19)	1.536(5)
C(4)-H(4)	0.9500	C(18)-H(18A)	0.9800
C(5)-C(6)	1.393(5)	C(18)-H(18B)	0.9800
C(5)-H(5)	0.9500	C(18)-H(18C)	0.9800
C(6)-C(8)	1.511(5)	C(19)-H(19A)	0.9800
C(7)-H(7A)	0.9900	C(19)-H(19B)	0.9800
C(7)-H(7B)	0.9900	C(19)-H(19C)	0.9800
C(8)-H(8A)	0.9900	C(20)-H(20A)	0.9800
C(8)-H(8B)	0.9900	C(20)-H(20B)	0.9800
C(9)-C(12)	1.535(5)	C(20)-H(20C)	0.9800
C(9)-C(10)	1.536(5)	C(21)-C(22)	1.532(5)
C(9)-C(11)	1.537(5)	C(21)-C(24)	1.542(5)
C(10)-H(10A)	0.9800	C(21)-C(23)	1.545(5)
C(10)-H(10B)	0.9800	C(22)-H(22A)	0.9800
C(10)-H(10C)	0.9800	C(22)-H(22B)	0.9800
C(11)-H(11A)	0.9800	C(22)-H(22C)	0.9800
C(11)-H(11B)	0.9800	C(23)-H(23A)	0.9800

C(23)-H(23B)	0.9800	C(28)-C(29)	1.389(5)
C(23)-H(23C)	0.9800	C(28)-H(28)	0.9500
C(24)-H(24A)	0.9800	C(29)-H(29)	0.9500
C(24)-H(24B)	0.9800	C(30)-C(31)	1.392(6)
C(24)-H(24C)	0.9800	C(30)-C(32)#1	1.396(6)
N(1)-C(29)	1.339(5)	C(30)-C(33)	1.490(6)
N(1)-C(25)	1.351(5)	C(31)-C(32)	1.383(6)
C(25)-C(26)	1.381(5)	C(31)-H(31)	0.9500
C(25)-H(25)	0.9500	C(32)-C(30)#1	1.396(6)
C(26)-C(27)	1.381(6)	C(32)-H(32)	0.9500
C(26)-H(26)	0.9500	C(33)-H(33A)	0.9800
C(27)-C(28)	1.387(5)	C(33)-H(33B)	0.9800
C(27)-H(27)	0.9500	C(33)-H(33C)	0.9800

C(1)-Ir(1)-N(1)	177.82(13)	C(21)-P(2)-C(17)	108.31(17)
C(1)-Ir(1)-P(2)	80.56(11)	C(8)-P(2)-Ir(1)	99.98(12)
N(1)-Ir(1)-P(2)	99.03(9)	C(21)-P(2)-Ir(1)	112.52(12)
C(1)-Ir(1)-P(1)	82.60(11)	C(17)-P(2)-Ir(1)	124.36(12)
N(1)-Ir(1)-P(1)	98.32(9)	C(6)-C(1)-C(2)	117.2(3)
P(2)-Ir(1)-P(1)	157.83(3)	C(6)-C(1)-Ir(1)	120.8(3)
C(1)-Ir(1)-Cl(1)	86.90(10)	C(2)-C(1)-Ir(1)	122.0(3)
N(1)-Ir(1)-Cl(1)	90.98(8)	C(3)-C(2)-C(1)	121.3(3)
P(2)-Ir(1)-Cl(1)	92.63(3)	C(3)-C(2)-C(7)	120.4(3)
P(1)-Ir(1)-Cl(1)	100.77(3)	C(1)-C(2)-C(7)	118.3(3)
C(1)-Ir(1)-H(1)	93.5(16)	C(4)-C(3)-C(2)	120.1(4)
N(1)-Ir(1)-H(1)	88.5(16)	C(4)-C(3)-H(3)	119.9
P(2)-Ir(1)-H(1)	79.5(17)	C(2)-C(3)-H(3)	119.9
P(1)-Ir(1)-H(1)	87.2(17)	C(5)-C(4)-C(3)	119.5(4)
Cl(1)-Ir(1)-H(1)	172.0(17)	C(5)-C(4)-H(4)	120.2
C(7)-P(1)-C(9)	103.56(18)	C(3)-C(4)-H(4)	120.2
C(7)-P(1)-C(13)	101.74(17)	C(4)-C(5)-C(6)	120.7(4)
C(9)-P(1)-C(13)	110.16(17)	C(4)-C(5)-H(5)	119.6
C(7)-P(1)-Ir(1)	101.36(12)	C(6)-C(5)-H(5)	119.6
C(9)-P(1)-Ir(1)	119.53(12)	C(5)-C(6)-C(1)	121.0(3)
C(13)-P(1)-Ir(1)	117.21(12)	C(5)-C(6)-C(8)	120.7(3)
C(8)-P(2)-C(21)	105.59(17)	C(1)-C(6)-C(8)	118.3(3)
C(8)-P(2)-C(17)	103.72(17)	C(2)-C(7)-P(1)	109.3(3)

C(2)-C(7)-H(7A)	109.8	C(14)-C(13)-C(15)	109.2(3)
P(1)-C(7)-H(7A)	109.8	C(16)-C(13)-P(1)	108.8(3)
C(2)-C(7)-H(7B)	109.8	C(14)-C(13)-P(1)	110.3(3)
P(1)-C(7)-H(7B)	109.8	C(15)-C(13)-P(1)	113.6(3)
H(7A)-C(7)-H(7B)	108.3	C(13)-C(14)-H(14A)	109.5
C(6)-C(8)-P(2)	107.2(2)	C(13)-C(14)-H(14B)	109.5
C(6)-C(8)-H(8A)	110.3	H(14A)-C(14)-H(14B)	109.5
P(2)-C(8)-H(8A)	110.3	C(13)-C(14)-H(14C)	109.5
C(6)-C(8)-H(8B)	110.3	H(14A)-C(14)-H(14C)	109.5
P(2)-C(8)-H(8B)	110.3	H(14B)-C(14)-H(14C)	109.5
H(8A)-C(8)-H(8B)	108.5	C(13)-C(15)-H(15A)	109.5
C(12)-C(9)-C(10)	108.8(3)	C(13)-C(15)-H(15B)	109.5
C(12)-C(9)-C(11)	107.5(3)	H(15A)-C(15)-H(15B)	109.5
C(10)-C(9)-C(11)	108.6(3)	C(13)-C(15)-H(15C)	109.5
C(12)-C(9)-P(1)	106.8(3)	H(15A)-C(15)-H(15C)	109.5
C(10)-C(9)-P(1)	108.7(3)	H(15B)-C(15)-H(15C)	109.5
C(11)-C(9)-P(1)	116.2(3)	C(13)-C(16)-H(16A)	109.5
C(9)-C(10)-H(10A)	109.5	C(13)-C(16)-H(16B)	109.5
C(9)-C(10)-H(10B)	109.5	H(16A)-C(16)-H(16B)	109.5
H(10A)-C(10)-H(10B)	109.5	C(13)-C(16)-H(16C)	109.5
C(9)-C(10)-H(10C)	109.5	H(16A)-C(16)-H(16C)	109.5
H(10A)-C(10)-H(10C)	109.5	H(16B)-C(16)-H(16C)	109.5
H(10B)-C(10)-H(10C)	109.5	C(20)-C(17)-C(18)	107.5(3)
C(9)-C(11)-H(11A)	109.5	C(20)-C(17)-C(19)	107.3(3)
C(9)-C(11)-H(11B)	109.5	C(18)-C(17)-C(19)	110.6(3)
H(11A)-C(11)-H(11B)	109.5	C(20)-C(17)-P(2)	107.0(3)
C(9)-C(11)-H(11C)	109.5	C(18)-C(17)-P(2)	111.4(3)
H(11A)-C(11)-H(11C)	109.5	C(19)-C(17)-P(2)	112.8(3)
H(11B)-C(11)-H(11C)	109.5	C(17)-C(18)-H(18A)	109.5
C(9)-C(12)-H(12A)	109.5	C(17)-C(18)-H(18B)	109.5
C(9)-C(12)-H(12B)	109.5	H(18A)-C(18)-H(18B)	109.5
H(12A)-C(12)-H(12B)	109.5	C(17)-C(18)-H(18C)	109.5
C(9)-C(12)-H(12C)	109.5	H(18A)-C(18)-H(18C)	109.5
H(12A)-C(12)-H(12C)	109.5	H(18B)-C(18)-H(18C)	109.5
H(12B)-C(12)-H(12C)	109.5	C(17)-C(19)-H(19A)	109.5
C(16)-C(13)-C(14)	108.3(3)	C(17)-C(19)-H(19B)	109.5
C(16)-C(13)-C(15)	106.5(3)	H(19A)-C(19)-H(19B)	109.5

C(17)-C(19)-H(19C)	109.5	C(29)-N(1)-C(25)	117.5(3)
H(19A)-C(19)-H(19C)	109.5	C(29)-N(1)-Ir(1)	121.8(2)
H(19B)-C(19)-H(19C)	109.5	C(25)-N(1)-Ir(1)	120.7(3)
C(17)-C(20)-H(20A)	109.5	N(1)-C(25)-C(26)	122.9(4)
C(17)-C(20)-H(20B)	109.5	N(1)-C(25)-H(25)	118.5
H(20A)-C(20)-H(20B)	109.5	C(26)-C(25)-H(25)	118.5
C(17)-C(20)-H(20C)	109.5	C(25)-C(26)-C(27)	119.3(4)
H(20A)-C(20)-H(20C)	109.5	C(25)-C(26)-H(26)	120.3
H(20B)-C(20)-H(20C)	109.5	C(27)-C(26)-H(26)	120.3
C(22)-C(21)-C(24)	107.8(3)	C(26)-C(27)-C(28)	118.1(4)
C(22)-C(21)-C(23)	109.1(3)	C(26)-C(27)-H(27)	121.0
C(24)-C(21)-C(23)	106.1(3)	C(28)-C(27)-H(27)	121.0
C(22)-C(21)-P(2)	110.2(3)	C(27)-C(28)-C(29)	119.5(4)
C(24)-C(21)-P(2)	109.4(3)	C(27)-C(28)-H(28)	120.2
C(23)-C(21)-P(2)	113.9(3)	C(29)-C(28)-H(28)	120.2
C(21)-C(22)-H(22A)	109.5	N(1)-C(29)-C(28)	122.6(3)
C(21)-C(22)-H(22B)	109.5	N(1)-C(29)-H(29)	118.7
H(22A)-C(22)-H(22B)	109.5	C(28)-C(29)-H(29)	118.7
C(21)-C(22)-H(22C)	109.5	C(31)-C(30)-C(32)#1	117.2(4)
H(22A)-C(22)-H(22C)	109.5	C(31)-C(30)-C(33)	120.8(4)
H(22B)-C(22)-H(22C)	109.5	C(32)#1-C(30)-C(33)	122.0(4)
C(21)-C(23)-H(23A)	109.5	C(32)-C(31)-C(30)	121.8(4)
C(21)-C(23)-H(23B)	109.5	C(32)-C(31)-H(31)	119.1
H(23A)-C(23)-H(23B)	109.5	C(30)-C(31)-H(31)	119.1
C(21)-C(23)-H(23C)	109.5	C(31)-C(32)-C(30)#1	121.0(4)
H(23A)-C(23)-H(23C)	109.5	C(31)-C(32)-H(32)	119.5
H(23B)-C(23)-H(23C)	109.5	C(30)#1-C(32)-H(32)	119.5
C(21)-C(24)-H(24A)	109.5	C(30)-C(33)-H(33A)	109.5
C(21)-C(24)-H(24B)	109.5	C(30)-C(33)-H(33B)	109.5
H(24A)-C(24)-H(24B)	109.5	H(33A)-C(33)-H(33B)	109.5
C(21)-C(24)-H(24C)	109.5	C(30)-C(33)-H(33C)	109.5
H(24A)-C(24)-H(24C)	109.5	H(33A)-C(33)-H(33C)	109.5
H(24B)-C(24)-H(24C)	109.5	H(33B)-C(33)-H(33C)	109.5

Symmetry transformations used to generate equivalent atoms: #1 -x,-y,-z

Table 5.15 Torsion Angles [°] for (PCP)IrHClPy, **5-8**

C(1)-Ir(1)-P(1)-C(7)	17.93(17)	C(6)-C(1)-C(2)-C(7)	172.5(3)
N(1)-Ir(1)-P(1)-C(7)	-164.07(15)	Ir(1)-C(1)-C(2)-C(7)	-7.3(5)
P(2)-Ir(1)-P(1)-C(7)	-22.88(17)	C(1)-C(2)-C(3)-C(4)	2.8(6)
Cl(1)-Ir(1)-P(1)-C(7)	103.33(13)	C(7)-C(2)-C(3)-C(4)	-174.1(4)
C(1)-Ir(1)-P(1)-C(9)	-94.95(17)	C(2)-C(3)-C(4)-C(5)	0.5(6)
N(1)-Ir(1)-P(1)-C(9)	83.06(16)	C(3)-C(4)-C(5)-C(6)	-2.1(6)
P(2)-Ir(1)-P(1)-C(9)	-135.75(15)	C(4)-C(5)-C(6)-C(1)	0.4(6)
Cl(1)-Ir(1)-P(1)-C(9)	-9.55(14)	C(4)-C(5)-C(6)-C(8)	178.1(3)
C(1)-Ir(1)-P(1)-C(13)	127.60(17)	C(2)-C(1)-C(6)-C(5)	2.8(5)
N(1)-Ir(1)-P(1)-C(13)	-54.39(16)	Ir(1)-C(1)-C(6)-C(5)	-177.4(3)
P(2)-Ir(1)-P(1)-C(13)	86.80(16)	C(2)-C(1)-C(6)-C(8)	-174.9(3)
Cl(1)-Ir(1)-P(1)-C(13)	-146.99(14)	Ir(1)-C(1)-C(6)-C(8)	4.9(5)
C(1)-Ir(1)-P(2)-C(8)	29.02(16)	C(3)-C(2)-C(7)-P(1)	-159.4(3)
N(1)-Ir(1)-P(2)-C(8)	-148.81(15)	C(1)-C(2)-C(7)-P(1)	23.6(4)
P(1)-Ir(1)-P(2)-C(8)	70.09(15)	C(9)-P(1)-C(7)-C(2)	98.4(3)
Cl(1)-Ir(1)-P(2)-C(8)	-57.40(13)	C(13)-P(1)-C(7)-C(2)	-147.3(3)
C(1)-Ir(1)-P(2)-C(21)	-82.59(16)	Ir(1)-P(1)-C(7)-C(2)	-26.0(3)
N(1)-Ir(1)-P(2)-C(21)	99.58(15)	C(5)-C(6)-C(8)-P(2)	-154.9(3)
P(1)-Ir(1)-P(2)-C(21)	-41.53(16)	C(1)-C(6)-C(8)-P(2)	22.9(4)
Cl(1)-Ir(1)-P(2)-C(21)	-169.01(13)	C(21)-P(2)-C(8)-C(6)	82.3(3)
C(1)-Ir(1)-P(2)-C(17)	143.35(18)	C(17)-P(2)-C(8)-C(6)	-163.9(3)
N(1)-Ir(1)-P(2)-C(17)	-34.48(17)	Ir(1)-P(2)-C(8)-C(6)	-34.6(3)
P(1)-Ir(1)-P(2)-C(17)	-175.59(15)	C(7)-P(1)-C(9)-C(12)	-48.6(3)
Cl(1)-Ir(1)-P(2)-C(17)	56.93(15)	C(13)-P(1)-C(9)-C(12)	-156.7(3)
N(1)-Ir(1)-C(1)-C(6)	56(4)	Ir(1)-P(1)-C(9)-C(12)	63.1(3)
P(2)-Ir(1)-C(1)-C(6)	-23.1(3)	C(7)-P(1)-C(9)-C(10)	-165.8(3)
P(1)-Ir(1)-C(1)-C(6)	171.4(3)	C(13)-P(1)-C(9)-C(10)	86.0(3)
Cl(1)-Ir(1)-C(1)-C(6)	70.1(3)	Ir(1)-P(1)-C(9)-C(10)	-54.1(3)
N(1)-Ir(1)-C(1)-C(2)	-124(3)	C(7)-P(1)-C(9)-C(11)	71.3(3)
P(2)-Ir(1)-C(1)-C(2)	156.7(3)	C(13)-P(1)-C(9)-C(11)	-36.8(3)
P(1)-Ir(1)-C(1)-C(2)	-8.9(3)	Ir(1)-P(1)-C(9)-C(11)	-177.0(2)
Cl(1)-Ir(1)-C(1)-C(2)	-110.1(3)	C(7)-P(1)-C(13)-C(16)	74.5(3)
C(6)-C(1)-C(2)-C(3)	-4.4(5)	C(9)-P(1)-C(13)-C(16)	-176.2(3)
Ir(1)-C(1)-C(2)-C(3)	175.8(3)	Ir(1)-P(1)-C(13)-C(16)	-35.0(3)

C(7)-P(1)-C(13)-C(14)	-166.9(3)	C(17)-P(2)-C(21)-C(23)	-42.5(3)
C(9)-P(1)-C(13)-C(14)	-57.5(3)	Ir(1)-P(2)-C(21)-C(23)	176.2(2)
Ir(1)-P(1)-C(13)-C(14)	83.6(3)	C(1)-Ir(1)-N(1)-C(29)	27(4)
C(7)-P(1)-C(13)-C(15)	-44.0(3)	P(2)-Ir(1)-N(1)-C(29)	106.3(3)
C(9)-P(1)-C(13)-C(15)	65.4(3)	P(1)-Ir(1)-N(1)-C(29)	-87.6(3)
Ir(1)-P(1)-C(13)-C(15)	-153.4(2)	Cl(1)-Ir(1)-N(1)-C(29)	13.4(3)
C(8)-P(2)-C(17)-C(20)	79.8(3)	C(1)-Ir(1)-N(1)-C(25)	-153(3)
C(21)-P(2)-C(17)-C(20)	-168.3(2)	P(2)-Ir(1)-N(1)-C(25)	-74.2(3)
Ir(1)-P(2)-C(17)-C(20)	-32.7(3)	P(1)-Ir(1)-N(1)-C(25)	91.9(3)
C(8)-P(2)-C(17)-C(18)	-162.9(3)	Cl(1)-Ir(1)-N(1)-C(25)	-167.1(3)
C(21)-P(2)-C(17)-C(18)	-51.1(3)	C(29)-N(1)-C(25)-C(26)	1.4(6)
Ir(1)-P(2)-C(17)-C(18)	84.5(3)	Ir(1)-N(1)-C(25)-C(26)	-178.1(3)
C(8)-P(2)-C(17)-C(19)	-37.9(3)	N(1)-C(25)-C(26)-C(27)	-0.5(6)
C(21)-P(2)-C(17)-C(19)	73.9(3)	C(25)-C(26)-C(27)-C(28)	-0.7(6)
Ir(1)-P(2)-C(17)-C(19)	-150.4(2)	C(26)-C(27)-C(28)-C(29)	0.8(6)
C(8)-P(2)-C(21)-C(22)	-168.9(3)	C(25)-N(1)-C(29)-C(28)	-1.3(6)
C(17)-P(2)-C(21)-C(22)	80.5(3)	Ir(1)-N(1)-C(29)-C(28)	178.2(3)
Ir(1)-P(2)-C(21)-C(22)	-60.8(3)	C(27)-C(28)-C(29)-N(1)	0.2(6)
C(8)-P(2)-C(21)-C(24)	-50.5(3)	C(32)#1-C(30)-C(31)-C(32)	0.1(6)
C(17)-P(2)-C(21)-C(24)	-161.1(3)	C(33)-C(30)-C(31)-C(32)	177.8(4)
Ir(1)-P(2)-C(21)-C(24)	57.6(3)	C(30)-C(31)-C(32)-C(30)#1	-0.1(7)
C(8)-P(2)-C(21)-C(23)	68.1(3)		

Symmetry transformations used to generate equivalent atoms: #1 -x,-y,-z

Figure 5.12 Crystal Structure of (PCP)IrNCCH$_3$, **5-50**

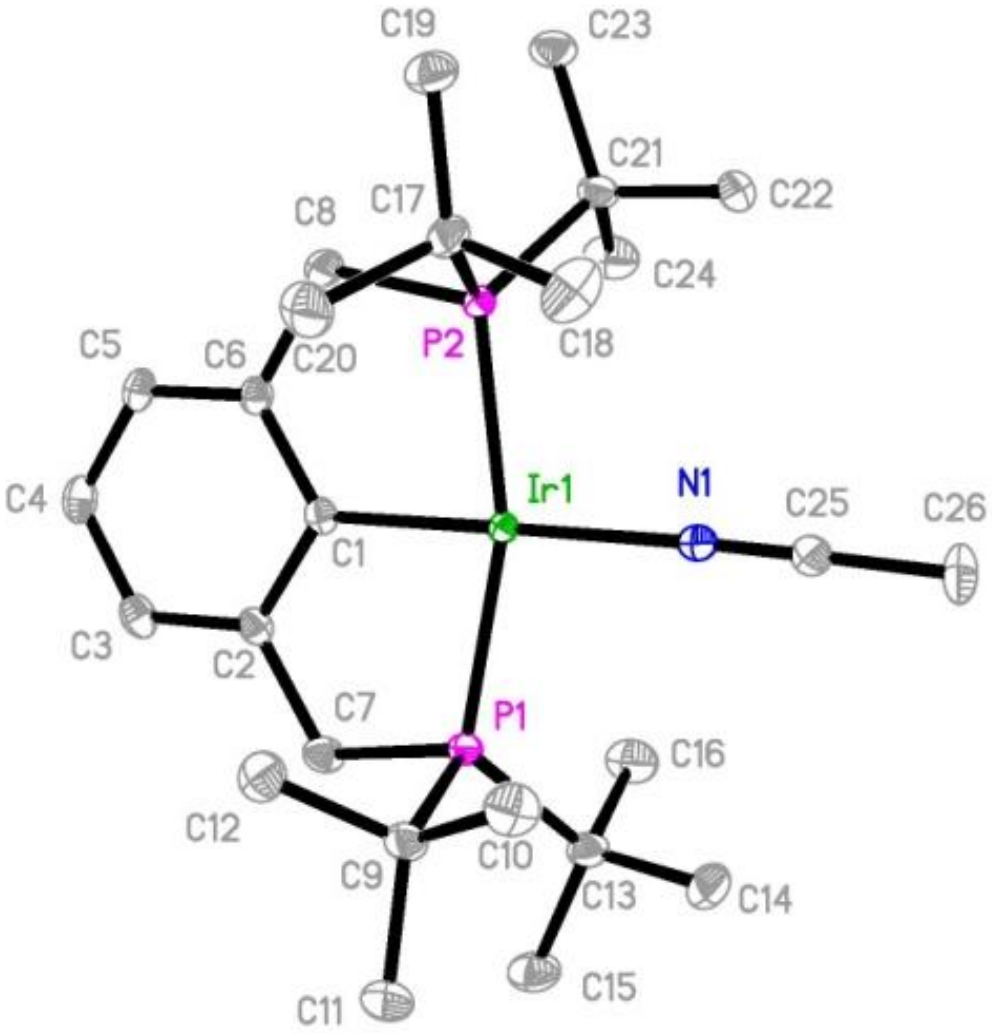

Table 5.16 Crystal Data and Structure Refinement for (PCP)IrNCCH$_3$, **5-50**

Identification code	irch3cn	
Empirical formula	C26 H46 Ir N P2	
Formula weight	626.78	
Temperature	100(2) K	
Wavelength	0.71073 Å	
Crystal system	Monoclinic	
Space group	P2(1)/c	
Unit cell dimensions	a = 12.0844(5) Å	ά= 90°.
	b = 15.6225(7) Å	β= 104.710(1)°.
	c = 14.9898(7) Å	γ = 90°.
Volume	2737.1(2) Å^3	
Z	4	
Density (calculated)	1.521 Mg/m^3	
Absorption coefficient	5.008 mm^{-1}	
F(000)	1264	
Crystal size	0.42 x 0.14 x 0.12 mm^3	
Theta range for data collection	1.74 to 31.51°.	
Index ranges	-17<=h<=17, -22<=k<=22, -22<=l<=22	
Reflections collected	34042	
Independent reflections	9093 [R(int) = 0.0279]	
Completeness to theta = 31.51°	99.9 %	
Absorption correction	Semi-empirical from equivalents	
Max. and min. transmission	0.5848 and 0.2275	
Refinement method	Full-matrix least-squares on F^2	
Data / restraints / parameters	9093 / 0 / 292	
Goodness-of-fit on F^2	1.001	
Final R indices [I>2sigma(I)]	R1 = 0.0230, wR2 = 0.0549	
R indices (all data)	R1 = 0.0267, wR2 = 0.0564	
Largest diff. peak and hole	2.128 and -0.707 e.Å^{-3}	

Table 5.17 Atomic Coordinates (x 10^4) and Equivalent Isotropic Displacement Parameters ($Å^2$x 10^3) for (PCP)IrNCCH$_3$, **5-50**. U(eq) is defined as one third of the trace of the orthogonalized U^{ij} tensor.

	x	y	z	U(eq)
Ir(1)	2341(1)	3528(1)	7766(1)	11(1)
P(1)	895(1)	4474(1)	7674(1)	12(1)
P(2)	4040(1)	2910(1)	7758(1)	12(1)
C(1)	2694(2)	4287(1)	6780(1)	12(1)
C(2)	1949(2)	4960(1)	6351(1)	14(1)
C(3)	2195(2)	5478(1)	5670(2)	18(1)
C(4)	3174(2)	5344(2)	5363(2)	19(1)
C(5)	3901(2)	4678(1)	5741(1)	16(1)
C(6)	3676(2)	4164(1)	6432(1)	14(1)
C(7)	824(2)	5070(1)	6606(2)	17(1)
C(8)	4463(2)	3415(2)	6785(2)	19(1)
C(9)	1245(2)	5316(1)	8608(2)	17(1)
C(10)	1657(2)	4867(2)	9546(2)	23(1)
C(11)	274(2)	5938(2)	8629(2)	23(1)
C(12)	2258(2)	5833(2)	8444(2)	22(1)
C(13)	-606(2)	4065(2)	7524(2)	18(1)
C(14)	-772(2)	3733(2)	8441(2)	26(1)
C(15)	-1552(2)	4716(2)	7111(2)	25(1)
C(16)	-719(2)	3302(2)	6855(2)	27(1)
C(17)	5210(2)	3209(2)	8802(2)	16(1)
C(18)	4830(2)	2992(2)	9675(2)	28(1)
C(19)	6376(2)	2807(2)	8848(2)	22(1)
C(20)	5325(2)	4192(2)	8767(2)	27(1)
C(21)	4101(2)	1735(1)	7497(2)	16(1)
C(22)	3922(2)	1204(2)	8307(2)	22(1)
C(23)	5202(2)	1437(1)	7254(2)	20(1)
C(24)	3076(2)	1571(2)	6668(2)	26(1)
C(25)	1654(2)	2308(2)	9234(2)	17(1)
N(1)	1925(2)	2743(1)	8712(1)	16(1)
C(26)	1282(2)	1751(2)	9883(2)	24(1)

Table 5.18 Bond Lengths [Å] and Angles [°] for (PCP)IrNCCH$_3$, **5-50**

Ir(1)-C(1)	2.023(2)	C(12)-H(12A)	0.9800
Ir(1)-N(1)	2.0333(18)	C(12)-H(12B)	0.9800
Ir(1)-P(1)	2.2662(5)	C(12)-H(12C)	0.9800
Ir(1)-P(2)	2.2721(5)	C(13)-C(14)	1.529(3)
P(1)-C(7)	1.835(2)	C(13)-C(15)	1.537(3)
P(1)-C(13)	1.882(2)	C(13)-C(16)	1.541(3)
P(1)-C(9)	1.889(2)	C(14)-H(14A)	0.9800
P(2)-C(8)	1.841(2)	C(14)-H(14B)	0.9800
P(2)-C(21)	1.882(2)	C(14)-H(14C)	0.9800
P(2)-C(17)	1.882(2)	C(15)-H(15A)	0.9800
C(1)-C(6)	1.425(3)	C(15)-H(15B)	0.9800
C(1)-C(2)	1.427(3)	C(15)-H(15C)	0.9800
C(2)-C(3)	1.393(3)	C(16)-H(16A)	0.9800
C(2)-C(7)	1.512(3)	C(16)-H(16B)	0.9800
C(3)-C(4)	1.390(3)	C(16)-H(16C)	0.9800
C(3)-H(3)	0.9500	C(17)-C(19)	1.528(3)
C(4)-C(5)	1.387(3)	C(17)-C(18)	1.531(3)
C(4)-H(4)	0.9500	C(17)-C(20)	1.544(3)
C(5)-C(6)	1.392(3)	C(18)-H(18A)	0.9800
C(5)-H(5)	0.9500	C(18)-H(18B)	0.9800
C(6)-C(8)	1.516(3)	C(18)-H(18C)	0.9800
C(7)-H(7A)	0.9900	C(19)-H(19A)	0.9800
C(7)-H(7B)	0.9900	C(19)-H(19B)	0.9800
C(8)-H(8A)	0.9900	C(19)-H(19C)	0.9800
C(8)-H(8B)	0.9900	C(20)-H(20A)	0.9800
C(9)-C(11)	1.530(3)	C(20)-H(20B)	0.9800
C(9)-C(10)	1.536(3)	C(20)-H(20C)	0.9800
C(9)-C(12)	1.538(3)	C(21)-C(22)	1.531(3)
C(10)-H(10A)	0.9800	C(21)-C(23)	1.537(3)
C(10)-H(10B)	0.9800	C(21)-C(24)	1.537(3)
C(10)-H(10C)	0.9800	C(22)-H(22A)	0.9800
C(11)-H(11A)	0.9800	C(22)-H(22B)	0.9800
C(11)-H(11B)	0.9800	C(22)-H(22C)	0.9800
C(11)-H(11C)	0.9800	C(23)-H(23A)	0.9800

C(23)-H(23B)	0.9800	C(25)-N(1)	1.145(3)
C(23)-H(23C)	0.9800	C(25)-C(26)	1.459(3)
C(24)-H(24A)	0.9800	C(26)-H(26A)	0.94(4)
C(24)-H(24B)	0.9800	C(26)-H(26B)	0.93(4)
C(24)-H(24C)	0.9800	C(26)-H(26C)	0.98(3)

C(1)-Ir(1)-N(1)	177.36(8)	C(4)-C(5)-C(6)	120.9(2)
C(1)-Ir(1)-P(1)	82.86(6)	C(4)-C(5)-H(5)	119.5
N(1)-Ir(1)-P(1)	96.44(5)	C(6)-C(5)-H(5)	119.5
C(1)-Ir(1)-P(2)	83.51(6)	C(5)-C(6)-C(1)	122.19(19)
N(1)-Ir(1)-P(2)	97.54(5)	C(5)-C(6)-C(8)	118.76(19)
P(1)-Ir(1)-P(2)	163.98(2)	C(1)-C(6)-C(8)	118.94(18)
C(7)-P(1)-C(13)	103.78(10)	C(2)-C(7)-P(1)	108.45(14)
C(7)-P(1)-C(9)	104.24(10)	C(2)-C(7)-H(7A)	110.0
C(13)-P(1)-C(9)	110.65(10)	P(1)-C(7)-H(7A)	110.0
C(7)-P(1)-Ir(1)	104.38(7)	C(2)-C(7)-H(7B)	110.0
C(13)-P(1)-Ir(1)	119.40(7)	P(1)-C(7)-H(7B)	110.0
C(9)-P(1)-Ir(1)	112.61(7)	H(7A)-C(7)-H(7B)	108.4
C(8)-P(2)-C(21)	102.70(10)	C(6)-C(8)-P(2)	109.35(15)
C(8)-P(2)-C(17)	104.54(11)	C(6)-C(8)-H(8A)	109.8
C(21)-P(2)-C(17)	110.78(10)	P(2)-C(8)-H(8A)	109.8
C(8)-P(2)-Ir(1)	104.75(7)	C(6)-C(8)-H(8B)	109.8
C(21)-P(2)-Ir(1)	119.94(7)	P(2)-C(8)-H(8B)	109.8
C(17)-P(2)-Ir(1)	112.26(7)	H(8A)-C(8)-H(8B)	108.3
C(6)-C(1)-C(2)	115.07(18)	C(11)-C(9)-C(10)	110.10(19)
C(6)-C(1)-Ir(1)	122.53(15)	C(11)-C(9)-C(12)	108.38(19)
C(2)-C(1)-Ir(1)	122.34(15)	C(10)-C(9)-C(12)	107.43(19)
C(3)-C(2)-C(1)	122.06(19)	C(11)-C(9)-P(1)	115.39(16)
C(3)-C(2)-C(7)	119.42(19)	C(10)-C(9)-P(1)	108.70(16)
C(1)-C(2)-C(7)	118.39(18)	C(12)-C(9)-P(1)	106.51(15)
C(2)-C(3)-C(4)	120.9(2)	C(9)-C(10)-H(10A)	109.5
C(2)-C(3)-H(3)	119.6	C(9)-C(10)-H(10B)	109.5
C(4)-C(3)-H(3)	119.6	H(10A)-C(10)-H(10B)	109.5
C(5)-C(4)-C(3)	118.8(2)	C(9)-C(10)-H(10C)	109.5
C(5)-C(4)-H(4)	120.6	H(10A)-C(10)-H(10C)	109.5
C(3)-C(4)-H(4)	120.6	H(10B)-C(10)-H(10C)	109.5

C(9)-C(11)-H(11A)	109.5	C(19)-C(17)-C(18)	110.1(2)
C(9)-C(11)-H(11B)	109.5	C(19)-C(17)-C(20)	108.74(19)
H(11A)-C(11)-H(11B)	109.5	C(18)-C(17)-C(20)	107.3(2)
C(9)-C(11)-H(11C)	109.5	C(19)-C(17)-P(2)	115.12(16)
H(11A)-C(11)-H(11C)	109.5	C(18)-C(17)-P(2)	109.32(15)
H(11B)-C(11)-H(11C)	109.5	C(20)-C(17)-P(2)	105.88(16)
C(9)-C(12)-H(12A)	109.5	C(17)-C(18)-H(18A)	109.5
C(9)-C(12)-H(12B)	109.5	C(17)-C(18)-H(18B)	109.5
H(12A)-C(12)-H(12B)	109.5	H(18A)-C(18)-H(18B)	109.5
C(9)-C(12)-H(12C)	109.5	C(17)-C(18)-H(18C)	109.5
H(12A)-C(12)-H(12C)	109.5	H(18A)-C(18)-H(18C)	109.5
H(12B)-C(12)-H(12C)	109.5	H(18B)-C(18)-H(18C)	109.5
C(14)-C(13)-C(15)	109.43(19)	C(17)-C(19)-H(19A)	109.5
C(14)-C(13)-C(16)	108.2(2)	C(17)-C(19)-H(19B)	109.5
C(15)-C(13)-C(16)	108.4(2)	H(19A)-C(19)-H(19B)	109.5
C(14)-C(13)-P(1)	110.51(16)	C(17)-C(19)-H(19C)	109.5
C(15)-C(13)-P(1)	114.76(17)	H(19A)-C(19)-H(19C)	109.5
C(16)-C(13)-P(1)	105.28(15)	H(19B)-C(19)-H(19C)	109.5
C(13)-C(14)-H(14A)	109.5	C(17)-C(20)-H(20A)	109.5
C(13)-C(14)-H(14B)	109.5	C(17)-C(20)-H(20B)	109.5
H(14A)-C(14)-H(14B)	109.5	H(20A)-C(20)-H(20B)	109.5
C(13)-C(14)-H(14C)	109.5	C(17)-C(20)-H(20C)	109.5
H(14A)-C(14)-H(14C)	109.5	H(20A)-C(20)-H(20C)	109.5
H(14B)-C(14)-H(14C)	109.5	H(20B)-C(20)-H(20C)	109.5
C(13)-C(15)-H(15A)	109.5	C(22)-C(21)-C(23)	109.19(18)
C(13)-C(15)-H(15B)	109.5	C(22)-C(21)-C(24)	107.7(2)
H(15A)-C(15)-H(15B)	109.5	C(23)-C(21)-C(24)	109.07(19)
C(13)-C(15)-H(15C)	109.5	C(22)-C(21)-P(2)	110.01(15)
H(15A)-C(15)-H(15C)	109.5	C(23)-C(21)-P(2)	115.23(16)
H(15B)-C(15)-H(15C)	109.5	C(24)-C(21)-P(2)	105.32(15)
C(13)-C(16)-H(16A)	109.5	C(21)-C(22)-H(22A)	109.5
C(13)-C(16)-H(16B)	109.5	C(21)-C(22)-H(22B)	109.5
H(16A)-C(16)-H(16B)	109.5	H(22A)-C(22)-H(22B)	109.5
C(13)-C(16)-H(16C)	109.5	C(21)-C(22)-H(22C)	109.5
H(16A)-C(16)-H(16C)	109.5	H(22A)-C(22)-H(22C)	109.5
H(16B)-C(16)-H(16C)	109.5	H(22B)-C(22)-H(22C)	109.5

C(21)-C(23)-H(23A)	109.5
C(21)-C(23)-H(23B)	109.5
H(23A)-C(23)-H(23B)	109.5
C(21)-C(23)-H(23C)	109.5
H(23A)-C(23)-H(23C)	109.5
H(23B)-C(23)-H(23C)	109.5
C(21)-C(24)-H(24A)	109.5
C(21)-C(24)-H(24B)	109.5
H(24A)-C(24)-H(24B)	109.5
C(21)-C(24)-H(24C)	109.5
H(24A)-C(24)-H(24C)	109.5
H(24B)-C(24)-H(24C)	109.5
N(1)-C(25)-C(26)	178.7(3)
C(25)-N(1)-Ir(1)	177.78(18)
C(25)-C(26)-H(26A)	112(2)
C(25)-C(26)-H(26B)	108(2)
H(26A)-C(26)-H(26B)	109(3)
C(25)-C(26)-H(26C)	111(2)
H(26A)-C(26)-H(26C)	112(3)
H(26B)-C(26)-H(26C)	105(3)

Table 5.19 Torsion Angles (˚) for (PCP)IrNCCH$_3$, **5-50**

C(1)-Ir(1)-P(1)-C(7)	14.13(10)	C(2)-C(1)-C(6)-C(5)	1.5(3)
N(1)-Ir(1)-P(1)-C(7)	-163.31(9)	Ir(1)-C(1)-C(6)-C(5)	178.67(16)
P(2)-Ir(1)-P(1)-C(7)	46.05(11)	C(2)-C(1)-C(6)-C(8)	-174.65(19)
C(1)-Ir(1)-P(1)-C(13)	129.38(10)	Ir(1)-C(1)-C(6)-C(8)	2.5(3)
N(1)-Ir(1)-P(1)-C(13)	-48.06(10)	C(3)-C(2)-C(7)-P(1)	-167.78(17)
P(2)-Ir(1)-P(1)-C(13)	161.30(10)	C(1)-C(2)-C(7)-P(1)	16.2(2)
C(1)-Ir(1)-P(1)-C(9)	-98.32(10)	C(13)-P(1)-C(7)-C(2)	-145.24(15)
N(1)-Ir(1)-P(1)-C(9)	84.25(9)	C(9)-P(1)-C(7)-C(2)	98.87(16)
P(2)-Ir(1)-P(1)-C(9)	-66.40(11)	Ir(1)-P(1)-C(7)-C(2)	-19.46(16)
C(1)-Ir(1)-P(2)-C(8)	-6.99(10)	C(5)-C(6)-C(8)-P(2)	175.11(16)
N(1)-Ir(1)-P(2)-C(8)	170.57(10)	C(1)-C(6)-C(8)-P(2)	-8.6(3)
P(1)-Ir(1)-P(2)-C(8)	-38.86(12)	C(21)-P(2)-C(8)-C(6)	135.94(16)
C(1)-Ir(1)-P(2)-C(21)	-121.46(10)	C(17)-P(2)-C(8)-C(6)	-108.33(17)
N(1)-Ir(1)-P(2)-C(21)	56.10(10)	Ir(1)-P(2)-C(8)-C(6)	9.90(17)
P(1)-Ir(1)-P(2)-C(21)	-153.33(10)	C(7)-P(1)-C(9)-C(11)	71.61(19)
C(1)-Ir(1)-P(2)-C(17)	105.85(10)	C(13)-P(1)-C(9)-C(11)	-39.4(2)
N(1)-Ir(1)-P(2)-C(17)	-76.58(9)	Ir(1)-P(1)-C(9)-C(11)	-175.86(15)
P(1)-Ir(1)-P(2)-C(17)	73.98(11)	C(7)-P(1)-C(9)-C(10)	-164.18(16)
N(1)-Ir(1)-C(1)-C(6)	-110.0(16)	C(13)-P(1)-C(9)-C(10)	84.84(17)
P(1)-Ir(1)-C(1)-C(6)	175.16(17)	Ir(1)-P(1)-C(9)-C(10)	-51.65(17)
P(2)-Ir(1)-C(1)-C(6)	3.60(16)	C(7)-P(1)-C(9)-C(12)	-48.70(17)
N(1)-Ir(1)-C(1)-C(2)	66.9(17)	C(13)-P(1)-C(9)-C(12)	-159.69(15)
P(1)-Ir(1)-C(1)-C(2)	-7.90(16)	Ir(1)-P(1)-C(9)-C(12)	63.83(16)
P(2)-Ir(1)-C(1)-C(2)	-179.46(17)	C(7)-P(1)-C(13)-C(14)	-166.67(17)
C(6)-C(1)-C(2)-C(3)	-2.6(3)	C(9)-P(1)-C(13)-C(14)	-55.39(19)
Ir(1)-C(1)-C(2)-C(3)	-179.74(16)	Ir(1)-P(1)-C(13)-C(14)	77.76(17)
C(6)-C(1)-C(2)-C(7)	173.35(18)	C(7)-P(1)-C(13)-C(15)	-42.36(19)
Ir(1)-C(1)-C(2)-C(7)	-3.8(3)	C(9)-P(1)-C(13)-C(15)	68.93(19)
C(1)-C(2)-C(3)-C(4)	1.6(3)	Ir(1)-P(1)-C(13)-C(15)	-157.92(14)
C(7)-C(2)-C(3)-C(4)	-174.3(2)	C(7)-P(1)-C(13)-C(16)	76.74(18)
C(2)-C(3)-C(4)-C(5)	0.6(3)	C(9)-P(1)-C(13)-C(16)	-171.98(16)
C(3)-C(4)-C(5)-C(6)	-1.7(3)	Ir(1)-P(1)-C(13)-C(16)	-38.83(19)
C(4)-C(5)-C(6)-C(1)	0.6(3)	C(8)-P(2)-C(17)-C(19)	-67.71(19)
C(4)-C(5)-C(6)-C(8)	176.8(2)	C(21)-P(2)-C(17)-C(19)	42.2(2)

Ir(1)-P(2)-C(17)-C(19)	179.31(15)
C(8)-P(2)-C(17)-C(18)	167.79(17)
C(21)-P(2)-C(17)-C(18)	-82.24(19)
Ir(1)-P(2)-C(17)-C(18)	54.82(18)
C(8)-P(2)-C(17)-C(20)	52.44(18)
C(21)-P(2)-C(17)-C(20)	162.40(15)
Ir(1)-P(2)-C(17)-C(20)	-60.54(16)
C(8)-P(2)-C(21)-C(22)	172.69(16)
C(17)-P(2)-C(21)-C(22)	61.54(17)
Ir(1)-P(2)-C(21)-C(22)	-71.77(16)
C(8)-P(2)-C(21)-C(23)	48.74(19)
C(17)-P(2)-C(21)-C(23)	-62.40(19)
Ir(1)-P(2)-C(21)-C(23)	164.28(14)
C(8)-P(2)-C(21)-C(24)	-71.49(18)
C(17)-P(2)-C(21)-C(24)	177.36(16)
Ir(1)-P(2)-C(21)-C(24)	44.05(18)
C(26)-C(25)-N(1)-Ir(1)	24(15)
C(1)-Ir(1)-N(1)-C(25)	-43(6)
P(1)-Ir(1)-N(1)-C(25)	31(5)
P(2)-Ir(1)-N(1)-C(25)	-157(5)

Figure 5.13 Crystal Structure of (PCP)IrPMe$_2$Ph, **5-54**

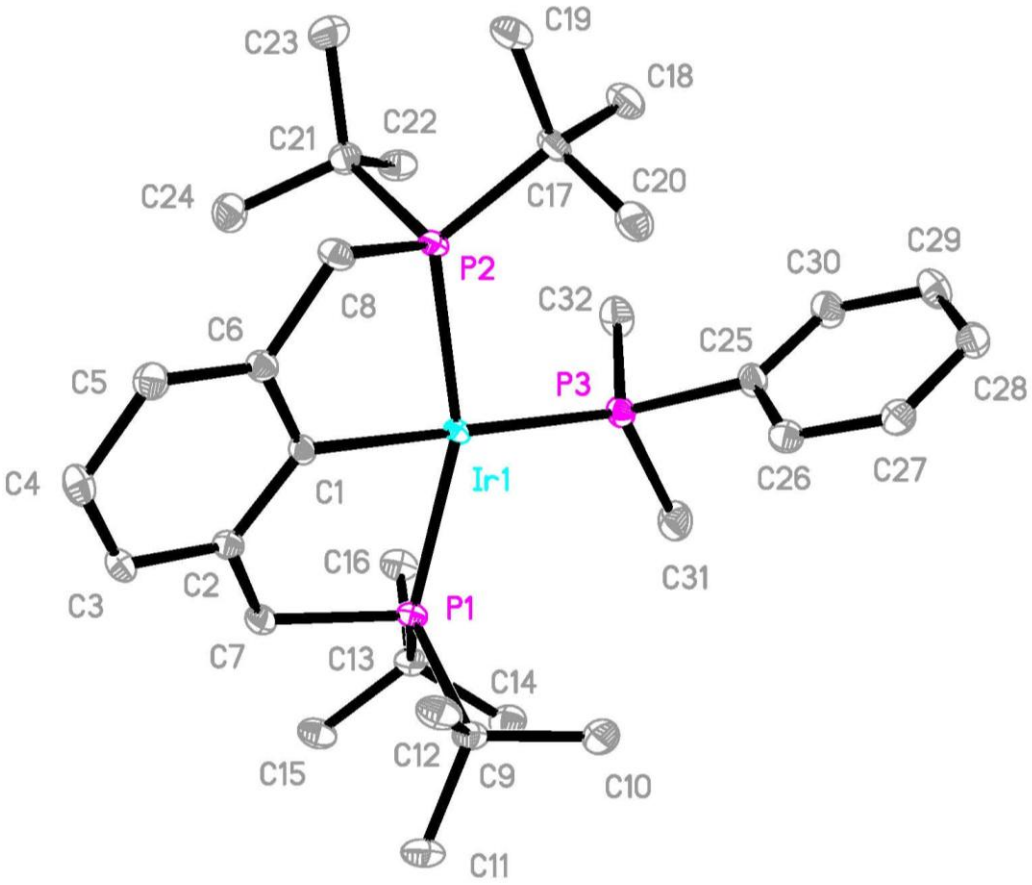

Table 5.20 Crystal Data and Structure Refinement for(PCP)IrPMe$_2$Ph, **5-54**

Identification code	mepirh2	
Empirical formula	C32 H54 Ir P3	
Formula weight	723.86	
Temperature	100(2) K	
Wavelength	0.71073 Å	
Crystal system	Triclinic	
Space group	P-1	
Unit cell dimensions	a = 10.5794(9) Å	α= 106.947(2)°.
	b = 10.9039(10) Å	β= 99.442(2)°.
	c = 15.5416(14) Å	γ = 105.492(2)°.
Volume	1594.7(2) Å^3	
Z	2	
Density (calculated)	1.507 Mg/m^3	
Absorption coefficient	4.356 mm^{-1}	
F(000)	736	
Crystal size	0.20 x 0.18 x 0.02 mm^3	
Theta range for data collection	2.06 to 30.03°.	
Index ranges	-14<=h<=14, -15<=k<=15, -21<=l<=21	
Reflections collected	18172	
Independent reflections	9158 [R(int) = 0.0248]	
Completeness to theta = 30.03°	98.2 %	
Absorption correction	Semi-empirical from equivalents	
Max. and min. transmission	0.7461 and 0.5487	
Refinement method	Full-matrix least-squares on F^2	
Data / restraints / parameters	9158 / 0 / 339	
Goodness-of-fit on F^2	1.002	
Final R indices [I>2sigma(I)]	R1 = 0.0241, wR2 = 0.0576	
R indices (all data)	R1 = 0.0265, wR2 = 0.0588	
Largest diff. peak and hole	1.988 and -1.561 e.Å^{-3}	

Table 5.21 Atomic Coordinates (x 10^4) and Equivalent Isotropic Displacement Parameters ($Å^2$x 10^3) for (PCP)IrPMe$_2$Ph, **5-54.** U(eq) is defined as one third of the trace of the orthogonalized U^{ij} tensor.

	x	y	z	U(eq)
Ir(1)	8725(1)	6784(1)	7409(1)	9(1)
P(1)	6864(1)	5104(1)	7486(1)	11(1)
P(2)	9923(1)	8498(1)	6938(1)	11(1)
P(3)	10532(1)	6339(1)	8183(1)	13(1)
C(1)	7113(2)	7279(2)	6759(2)	11(1)
C(2)	5755(2)	6406(2)	6480(2)	13(1)
C(3)	4670(2)	6759(3)	6104(2)	16(1)
C(4)	4907(3)	7996(3)	5974(2)	17(1)
C(5)	6240(3)	8859(3)	6204(2)	16(1)
C(6)	7319(2)	8508(2)	6587(2)	13(1)
C(7)	5504(2)	5031(2)	6553(2)	15(1)
C(8)	8750(2)	9447(2)	6819(2)	14(1)
C(9)	6219(3)	5584(3)	8564(2)	15(1)
C(10)	7304(3)	5797(3)	9431(2)	20(1)
C(11)	4873(3)	4565(3)	8522(2)	20(1)
C(12)	5996(3)	6947(3)	8672(2)	19(1)
C(13)	6647(3)	3202(2)	7112(2)	15(1)
C(14)	7033(3)	2712(3)	7917(2)	20(1)
C(15)	5169(3)	2298(3)	6579(2)	19(1)
C(16)	7533(3)	2941(3)	6436(2)	18(1)
C(17)	11514(2)	9983(3)	7701(2)	16(1)
C(18)	12780(3)	9549(3)	7734(2)	22(1)
C(19)	11782(3)	11245(3)	7404(2)	21(1)
C(20)	11308(3)	10447(3)	8684(2)	20(1)
C(21)	10142(3)	7855(3)	5712(2)	16(1)
C(22)	10857(3)	6792(3)	5629(2)	19(1)
C(23)	10941(3)	8964(3)	5400(2)	22(1)
C(24)	8709(3)	7159(3)	5035(2)	21(1)
C(25)	11717(2)	7660(3)	9260(2)	15(1)
C(26)	11212(3)	8411(3)	9929(2)	17(1)
C(27)	12086(3)	9367(3)	10770(2)	18(1)

C(28)	13474(3)	9587(3)	10956(2)	18(1)
C(29)	13980(3)	8840(3)	10305(2)	21(1)
C(30)	13110(3)	7877(3)	9463(2)	19(1)
C(31)	10272(3)	4977(3)	8678(2)	22(1)
C(32)	11667(3)	5794(3)	7497(2)	21(1)

Table 5.22 Bond Lengths [Å] and Angles [°] for (PCP)IrPMe$_2$Ph, **5-54**.

Ir(1)-C(1)	2.112(2)	C(11)-H(11A)	0.9600
Ir(1)-P(3)	2.3289(6)	C(11)-H(11B)	0.9600
Ir(1)-P(2)	2.3395(6)	C(11)-H(11C)	0.9600
Ir(1)-P(1)	2.3503(6)	C(12)-H(12A)	0.9600
P(1)-C(7)	1.835(3)	C(12)-H(12B)	0.9600
P(1)-C(9)	1.898(2)	C(12)-H(12C)	0.9600
P(1)-C(13)	1.921(3)	C(13)-C(14)	1.534(4)
P(2)-C(8)	1.835(2)	C(13)-C(16)	1.535(3)
P(2)-C(21)	1.904(2)	C(13)-C(15)	1.542(4)
P(2)-C(17)	1.905(2)	C(14)-H(14A)	0.9600
P(3)-C(32)	1.835(3)	C(14)-H(14B)	0.9600
P(3)-C(31)	1.841(3)	C(14)-H(14C)	0.9600
P(3)-C(25)	1.841(3)	C(15)-H(15A)	0.9600
C(1)-C(2)	1.408(3)	C(15)-H(15B)	0.9600
C(1)-C(6)	1.409(3)	C(15)-H(15C)	0.9600
C(2)-C(3)	1.398(3)	C(16)-H(16A)	0.9600
C(2)-C(7)	1.492(3)	C(16)-H(16B)	0.9600
C(3)-C(4)	1.385(4)	C(16)-H(16C)	0.9600
C(3)-H(3)	0.9300	C(17)-C(18)	1.532(4)
C(4)-C(5)	1.390(4)	C(17)-C(20)	1.535(4)
C(4)-H(4)	0.9300	C(17)-C(19)	1.547(4)
C(5)-C(6)	1.395(3)	C(18)-H(18A)	0.9600
C(5)-H(5)	0.9300	C(18)-H(18B)	0.9600
C(6)-C(8)	1.500(3)	C(18)-H(18C)	0.9600
C(7)-H(7A)	0.9700	C(19)-H(19A)	0.9600
C(7)-H(7B)	0.9700	C(19)-H(19B)	0.9600
C(8)-H(8A)	0.9700	C(19)-H(19C)	0.9600
C(8)-H(8B)	0.9700	C(20)-H(20A)	0.9600
C(9)-C(12)	1.532(4)	C(20)-H(20B)	0.9600
C(9)-C(11)	1.532(4)	C(20)-H(20C)	0.9600
C(9)-C(10)	1.534(4)	C(21)-C(23)	1.531(4)
C(10)-H(10A)	0.9600	C(21)-C(22)	1.532(4)
C(10)-H(10B)	0.9600	C(21)-C(24)	1.542(4)
C(10)-H(10C)	0.9600	C(22)-H(22A)	0.9600

C(22)-H(22B)	0.9600	C(27)-H(27)	0.9300
C(22)-H(22C)	0.9600	C(28)-C(29)	1.380(4)
C(23)-H(23A)	0.9600	C(28)-H(28)	0.9300
C(23)-H(23B)	0.9600	C(29)-C(30)	1.396(4)
C(23)-H(23C)	0.9600	C(29)-H(29)	0.9300
C(24)-H(24A)	0.9600	C(30)-H(30)	0.9300
C(24)-H(24B)	0.9600	C(31)-H(31A)	0.9600
C(24)-H(24C)	0.9600	C(31)-H(31B)	0.9600
C(25)-C(30)	1.394(3)	C(31)-H(31C)	0.9600
C(25)-C(26)	1.399(3)	C(32)-H(32A)	0.9600
C(26)-C(27)	1.394(3)	C(32)-H(32B)	0.9600
C(26)-H(26)	0.9300	C(32)-H(32C)	0.9600
C(27)-C(28)	1.389(4)		

C(1)-Ir(1)-P(3)	177.22(6)	C(31)-P(3)-Ir(1)	122.24(9)
C(1)-Ir(1)-P(2)	79.23(7)	C(25)-P(3)-Ir(1)	119.30(8)
P(3)-Ir(1)-P(2)	99.87(2)	C(2)-C(1)-C(6)	115.5(2)
C(1)-Ir(1)-P(1)	80.20(7)	C(2)-C(1)-Ir(1)	121.98(17)
P(3)-Ir(1)-P(1)	100.93(2)	C(6)-C(1)-Ir(1)	122.46(17)
P(2)-Ir(1)-P(1)	158.69(2)	C(3)-C(2)-C(1)	122.5(2)
C(7)-P(1)-C(9)	103.43(11)	C(3)-C(2)-C(7)	120.0(2)
C(7)-P(1)-C(13)	98.93(11)	C(1)-C(2)-C(7)	117.4(2)
C(9)-P(1)-C(13)	108.33(11)	C(4)-C(3)-C(2)	120.3(2)
C(7)-P(1)-Ir(1)	101.33(8)	C(4)-C(3)-H(3)	119.9
C(9)-P(1)-Ir(1)	116.02(8)	C(2)-C(3)-H(3)	119.9
C(13)-P(1)-Ir(1)	124.54(8)	C(3)-C(4)-C(5)	118.7(2)
C(8)-P(2)-C(21)	103.26(11)	C(3)-C(4)-H(4)	120.6
C(8)-P(2)-C(17)	98.88(11)	C(5)-C(4)-H(4)	120.6
C(21)-P(2)-C(17)	108.79(11)	C(4)-C(5)-C(6)	120.8(2)
C(8)-P(2)-Ir(1)	103.13(8)	C(4)-C(5)-H(5)	119.6
C(21)-P(2)-Ir(1)	113.97(8)	C(6)-C(5)-H(5)	119.6
C(17)-P(2)-Ir(1)	125.02(8)	C(5)-C(6)-C(1)	122.0(2)
C(32)-P(3)-C(31)	96.17(13)	C(5)-C(6)-C(8)	119.8(2)
C(32)-P(3)-C(25)	103.20(12)	C(1)-C(6)-C(8)	118.1(2)
C(31)-P(3)-C(25)	94.69(12)	C(2)-C(7)-P(1)	109.45(16)
C(32)-P(3)-Ir(1)	116.62(9)	C(2)-C(7)-H(7A)	109.8

P(1)-C(7)-H(7A)	109.8	C(16)-C(13)-C(15)	107.2(2)
C(2)-C(7)-H(7B)	109.8	C(14)-C(13)-P(1)	114.73(17)
P(1)-C(7)-H(7B)	109.8	C(16)-C(13)-P(1)	106.78(16)
H(7A)-C(7)-H(7B)	108.2	C(15)-C(13)-P(1)	112.03(17)
C(6)-C(8)-P(2)	109.08(16)	C(13)-C(14)-H(14A)	109.5
C(6)-C(8)-H(8A)	109.9	C(13)-C(14)-H(14B)	109.5
P(2)-C(8)-H(8A)	109.9	H(14A)-C(14)-H(14B)	109.5
C(6)-C(8)-H(8B)	109.9	C(13)-C(14)-H(14C)	109.5
P(2)-C(8)-H(8B)	109.9	H(14A)-C(14)-H(14C)	109.5
H(8A)-C(8)-H(8B)	108.3	H(14B)-C(14)-H(14C)	109.5
C(12)-C(9)-C(11)	107.6(2)	C(13)-C(15)-H(15A)	109.5
C(12)-C(9)-C(10)	107.7(2)	C(13)-C(15)-H(15B)	109.5
C(11)-C(9)-C(10)	109.5(2)	H(15A)-C(15)-H(15B)	109.5
C(12)-C(9)-P(1)	107.11(17)	C(13)-C(15)-H(15C)	109.5
C(11)-C(9)-P(1)	114.62(17)	H(15A)-C(15)-H(15C)	109.5
C(10)-C(9)-P(1)	109.97(17)	H(15B)-C(15)-H(15C)	109.5
C(9)-C(10)-H(10A)	109.5	C(13)-C(16)-H(16A)	109.5
C(9)-C(10)-H(10B)	109.5	C(13)-C(16)-H(16B)	109.5
H(10A)-C(10)-H(10B)	109.5	H(16A)-C(16)-H(16B)	109.5
C(9)-C(10)-H(10C)	109.5	C(13)-C(16)-H(16C)	109.5
H(10A)-C(10)-H(10C)	109.5	H(16A)-C(16)-H(16C)	109.5
H(10B)-C(10)-H(10C)	109.5	H(16B)-C(16)-H(16C)	109.5
C(9)-C(11)-H(11A)	109.5	C(18)-C(17)-C(20)	109.7(2)
C(9)-C(11)-H(11B)	109.5	C(18)-C(17)-C(19)	108.1(2)
H(11A)-C(11)-H(11B)	109.5	C(20)-C(17)-C(19)	106.2(2)
C(9)-C(11)-H(11C)	109.5	C(18)-C(17)-P(2)	111.01(18)
H(11A)-C(11)-H(11C)	109.5	C(20)-C(17)-P(2)	107.02(17)
H(11B)-C(11)-H(11C)	109.5	C(19)-C(17)-P(2)	114.67(18)
C(9)-C(12)-H(12A)	109.5	C(17)-C(18)-H(18A)	109.5
C(9)-C(12)-H(12B)	109.5	C(17)-C(18)-H(18B)	109.5
H(12A)-C(12)-H(12B)	109.5	H(18A)-C(18)-H(18B)	109.5
C(9)-C(12)-H(12C)	109.5	C(17)-C(18)-H(18C)	109.5
H(12A)-C(12)-H(12C)	109.5	H(18A)-C(18)-H(18C)	109.5
H(12B)-C(12)-H(12C)	109.5	H(18B)-C(18)-H(18C)	109.5
C(14)-C(13)-C(16)	109.8(2)	C(17)-C(19)-H(19A)	109.5
C(14)-C(13)-C(15)	106.2(2)	C(17)-C(19)-H(19B)	109.5

H(19A)-C(19)-H(19B)	109.5	C(26)-C(25)-P(3)	119.73(19)
C(17)-C(19)-H(19C)	109.5	C(27)-C(26)-C(25)	120.6(2)
H(19A)-C(19)-H(19C)	109.5	C(27)-C(26)-H(26)	119.7
H(19B)-C(19)-H(19C)	109.5	C(25)-C(26)-H(26)	119.7
C(17)-C(20)-H(20A)	109.5	C(28)-C(27)-C(26)	120.4(2)
C(17)-C(20)-H(20B)	109.5	C(28)-C(27)-H(27)	119.8
H(20A)-C(20)-H(20B)	109.5	C(26)-C(27)-H(27)	119.8
C(17)-C(20)-H(20C)	109.5	C(29)-C(28)-C(27)	119.4(2)
H(20A)-C(20)-H(20C)	109.5	C(29)-C(28)-H(28)	120.3
H(20B)-C(20)-H(20C)	109.5	C(27)-C(28)-H(28)	120.3
C(23)-C(21)-C(22)	107.9(2)	C(28)-C(29)-C(30)	120.5(2)
C(23)-C(21)-C(24)	108.2(2)	C(28)-C(29)-H(29)	119.7
C(22)-C(21)-C(24)	108.1(2)	C(30)-C(29)-H(29)	119.7
C(23)-C(21)-P(2)	114.52(18)	C(25)-C(30)-C(29)	120.8(2)
C(22)-C(21)-P(2)	110.49(17)	C(25)-C(30)-H(30)	119.6
C(24)-C(21)-P(2)	107.46(17)	C(29)-C(30)-H(30)	119.6
C(21)-C(22)-H(22A)	109.5	P(3)-C(31)-H(31A)	109.5
C(21)-C(22)-H(22B)	109.5	P(3)-C(31)-H(31B)	109.5
H(22A)-C(22)-H(22B)	109.5	H(31A)-C(31)-H(31B)	109.5
C(21)-C(22)-H(22C)	109.5	P(3)-C(31)-H(31C)	109.5
H(22A)-C(22)-H(22C)	109.5	H(31A)-C(31)-H(31C)	109.5
H(22B)-C(22)-H(22C)	109.5	H(31B)-C(31)-H(31C)	109.5
C(21)-C(23)-H(23A)	109.5	P(3)-C(32)-H(32A)	109.5
C(21)-C(23)-H(23B)	109.5	P(3)-C(32)-H(32B)	109.5
H(23A)-C(23)-H(23B)	109.5	H(32A)-C(32)-H(32B)	109.5
C(21)-C(23)-H(23C)	109.5	P(3)-C(32)-H(32C)	109.5
H(23A)-C(23)-H(23C)	109.5	H(32A)-C(32)-H(32C)	109.5
H(23B)-C(23)-H(23C)	109.5	H(32B)-C(32)-H(32C)	109.5
C(21)-C(24)-H(24A)	109.5		
C(21)-C(24)-H(24B)	109.5		
H(24A)-C(24)-H(24B)	109.5		
C(21)-C(24)-H(24C)	109.5		
H(24A)-C(24)-H(24C)	109.5		
H(24B)-C(24)-H(24C)	109.5		
C(30)-C(25)-C(26)	118.3(2)		
C(30)-C(25)-P(3)	121.82(19)		

Table 5.23 Torsion Angles [°] for (PCP)IrPMe$_2$Ph, **5-54**

C(1)-Ir(1)-P(1)-C(7)	21.80(10)	C(6)-C(1)-C(2)-C(3)	-3.3(3)
P(3)-Ir(1)-P(1)-C(7)	-160.79(8)	Ir(1)-C(1)-C(2)-C(3)	175.88(18)
P(2)-Ir(1)-P(1)-C(7)	6.52(11)	C(6)-C(1)-C(2)-C(7)	173.5(2)
C(1)-Ir(1)-P(1)-C(9)	-89.38(11)	Ir(1)-C(1)-C(2)-C(7)	-7.3(3)
P(3)-Ir(1)-P(1)-C(9)	88.04(9)	C(1)-C(2)-C(3)-C(4)	1.3(4)
P(2)-Ir(1)-P(1)-C(9)	-104.66(10)	C(7)-C(2)-C(3)-C(4)	-175.5(2)
C(1)-Ir(1)-P(1)-C(13)	131.07(11)	C(2)-C(3)-C(4)-C(5)	1.6(4)
P(3)-Ir(1)-P(1)-C(13)	-51.51(10)	C(3)-C(4)-C(5)-C(6)	-2.2(4)
P(2)-Ir(1)-P(1)-C(13)	115.79(11)	C(4)-C(5)-C(6)-C(1)	-0.1(4)
C(1)-Ir(1)-P(2)-C(8)	22.61(10)	C(4)-C(5)-C(6)-C(8)	179.3(2)
P(3)-Ir(1)-P(2)-C(8)	-154.72(8)	C(2)-C(1)-C(6)-C(5)	2.7(3)
P(1)-Ir(1)-P(2)-C(8)	37.93(11)	Ir(1)-C(1)-C(6)-C(5)	-176.48(18)
C(1)-Ir(1)-P(2)-C(21)	-88.58(11)	C(2)-C(1)-C(6)-C(8)	-176.6(2)
P(3)-Ir(1)-P(2)-C(21)	94.10(9)	Ir(1)-C(1)-C(6)-C(8)	4.2(3)
P(1)-Ir(1)-P(2)-C(21)	-73.26(11)	C(3)-C(2)-C(7)-P(1)	-155.38(19)
C(1)-Ir(1)-P(2)-C(17)	133.53(12)	C(1)-C(2)-C(7)-P(1)	27.7(3)
P(3)-Ir(1)-P(2)-C(17)	-43.80(10)	C(9)-P(1)-C(7)-C(2)	88.49(18)
P(1)-Ir(1)-P(2)-C(17)	148.85(10)	C(13)-P(1)-C(7)-C(2)	-160.11(17)
C(1)-Ir(1)-P(3)-C(32)	-129.9(13)	Ir(1)-P(1)-C(7)-C(2)	-32.02(17)
P(2)-Ir(1)-P(3)-C(32)	-59.04(11)	C(5)-C(6)-C(8)-P(2)	-161.66(19)
P(1)-Ir(1)-P(3)-C(32)	116.31(11)	C(1)-C(6)-C(8)-P(2)	17.7(3)
C(1)-Ir(1)-P(3)-C(31)	112.8(13)	C(21)-P(2)-C(8)-C(6)	91.18(18)
P(2)-Ir(1)-P(3)-C(31)	-176.31(11)	C(17)-P(2)-C(8)-C(6)	-156.99(17)
P(1)-Ir(1)-P(3)-C(31)	-0.96(11)	Ir(1)-P(2)-C(8)-C(6)	-27.73(17)
C(1)-Ir(1)-P(3)-C(25)	-4.9(13)	C(7)-P(1)-C(9)-C(12)	-58.80(19)
P(2)-Ir(1)-P(3)-C(25)	66.00(10)	C(13)-P(1)-C(9)-C(12)	-163.11(17)
P(1)-Ir(1)-P(3)-C(25)	-118.65(10)	Ir(1)-P(1)-C(9)-C(12)	51.15(19)
P(3)-Ir(1)-C(1)-C(2)	-126.0(13)	C(7)-P(1)-C(9)-C(11)	60.5(2)
P(2)-Ir(1)-C(1)-C(2)	162.65(19)	C(13)-P(1)-C(9)-C(11)	-43.8(2)
P(1)-Ir(1)-C(1)-C(2)	-11.75(17)	Ir(1)-P(1)-C(9)-C(11)	170.48(16)
P(3)-Ir(1)-C(1)-C(6)	53.2(14)	C(7)-P(1)-C(9)-C(10)	-175.61(18)
P(2)-Ir(1)-C(1)-C(6)	-18.20(18)	C(13)-P(1)-C(9)-C(10)	80.08(19)
P(1)-Ir(1)-C(1)-C(6)	167.39(19)	Ir(1)-P(1)-C(9)-C(10)	-65.66(19)

C(7)-P(1)-C(13)-C(14)	-149.54(19)	C(17)-P(2)-C(21)-C(23)	-34.7(2)
C(9)-P(1)-C(13)-C(14)	-42.1(2)	Ir(1)-P(2)-C(21)-C(23)	-179.25(16)
Ir(1)-P(1)-C(13)-C(14)	100.00(18)	C(8)-P(2)-C(21)-C(22)	-168.24(18)
C(7)-P(1)-C(13)-C(16)	88.62(18)	C(17)-P(2)-C(21)-C(22)	87.4(2)
C(9)-P(1)-C(13)-C(16)	-163.95(17)	Ir(1)-P(2)-C(21)-C(22)	-57.13(19)
Ir(1)-P(1)-C(13)-C(16)	-21.8(2)	C(8)-P(2)-C(21)-C(24)	-50.6(2)
C(7)-P(1)-C(13)-C(15)	-28.42(19)	C(17)-P(2)-C(21)-C(24)	-154.90(18)
C(9)-P(1)-C(13)-C(15)	79.02(19)	Ir(1)-P(2)-C(21)-C(24)	60.55(19)
Ir(1)-P(1)-C(13)-C(15)	-138.88(15)	C(32)-P(3)-C(25)-C(30)	-10.4(3)
C(8)-P(2)-C(17)-C(18)	-166.44(19)	C(31)-P(3)-C(25)-C(30)	87.1(2)
C(21)-P(2)-C(17)-C(18)	-59.1(2)	Ir(1)-P(3)-C(25)-C(30)	-141.65(19)
Ir(1)-P(2)-C(17)-C(18)	80.59(19)	C(32)-P(3)-C(25)-C(26)	174.2(2)
C(8)-P(2)-C(17)-C(20)	73.87(19)	C(31)-P(3)-C(25)-C(26)	-88.3(2)
C(21)-P(2)-C(17)-C(20)	-178.77(17)	Ir(1)-P(3)-C(25)-C(26)	43.0(2)
Ir(1)-P(2)-C(17)-C(20)	-39.1(2)	C(30)-C(25)-C(26)-C(27)	1.2(4)
C(8)-P(2)-C(17)-C(19)	-43.6(2)	P(3)-C(25)-C(26)-C(27)	176.7(2)
C(21)-P(2)-C(17)-C(19)	63.8(2)	C(25)-C(26)-C(27)-C(28)	-0.2(4)
Ir(1)-P(2)-C(17)-C(19)	-156.55(15)	C(26)-C(27)-C(28)-C(29)	-0.6(4)
C(8)-P(2)-C(21)-C(23)	69.6(2)	C(27)-C(28)-C(29)-C(30)	0.4(4)

Figure 5.14 Crystal Structure of (PCP)IrPOEt$_3$, **5-59**

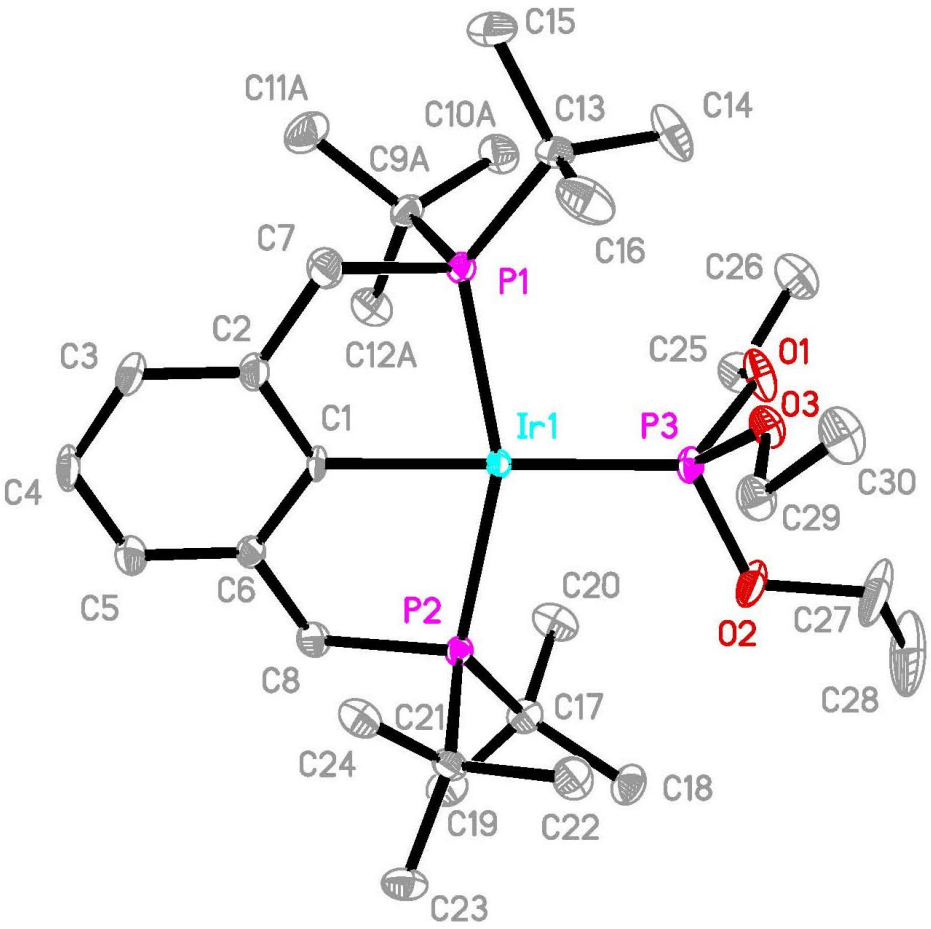

Table 5.24 Crystal Data and Structure Refinement for (PCP)IrPOEt$_3$, **5-59**

Identification code	irpoet_p21n	
Empirical formula	C30 H58 Ir O3 P3	
Formula weight	751.87	
Temperature	100(2) K	
Wavelength	0.71073 Å	
Crystal system	Monoclinic	
Space group	P2(1)/n	
Unit cell dimensions	a = 12.9320(7) Å	α= 90°.
	b = 17.2703(10) Å	β= 110.857(1)°.
	c = 15.8727(9) Å	γ = 90°.
Volume	3312.7(3) Å^3	
Z	4	
Density (calculated)	1.508 Mg/m^3	
Absorption coefficient	4.203 mm^{-1}	
F(000)	1536	
Crystal size	0.55 x 0.14 x 0.03 mm^3	
Theta range for data collection	1.75 to 30.03°.	
Index ranges	-18<=h<=17, -24<=k<=24, -22<=l<=22	
Reflections collected	36131	
Independent reflections	9540 [R(int) = 0.0503]	
Completeness to theta = 30.03°	98.4 %	
Absorption correction	Semi-empirical from equivalents	
Max. and min. transmission	0.8843 and 0.2058	
Refinement method	Full-matrix least-squares on F^2	
Data / restraints / parameters	9540 / 513 / 377	
Goodness-of-fit on F^2	1.006	
Final R indices [I>2sigma(I)]	R1 = 0.0350, wR2 = 0.0731	
R indices (all data)	R1 = 0.0483, wR2 = 0.0779	
Largest diff. peak and hole	2.318 and -1.812 e.Å^{-3}	

Table 5.25 Atomic Coordinates (x 10^4) and Equivalent Isotropic Displacement Parameters ($Å^2$x 10^3) for (PCP)IrPOEt$_3$, **5-59.** U(eq) is defined as one third of the trace of the orthogonalized U^{ij} tensor.

	x	y	z	U(eq)
Ir(1)	4157(1)	7655(1)	1375(1)	10(1)
P(1)	5914(1)	7862(1)	1337(1)	12(1)
P(2)	2424(1)	7985(1)	1382(1)	11(1)
P(3)	3984(1)	6386(1)	1136(1)	13(1)
O(1)	4286(2)	5977(2)	334(2)	21(1)
O(2)	2793(2)	6009(2)	999(2)	26(1)
O(3)	4805(2)	5796(1)	1877(2)	17(1)
C(1)	4438(3)	8822(2)	1783(2)	12(1)
C(2)	5520(3)	9123(2)	2178(2)	16(1)
C(3)	5708(3)	9877(2)	2495(3)	21(1)
C(4)	4831(3)	10369(2)	2423(3)	22(1)
C(5)	3754(3)	10097(2)	2011(3)	20(1)
C(6)	3564(3)	9339(2)	1690(2)	14(1)
C(7)	6457(3)	8591(2)	2239(3)	20(1)
C(8)	2410(3)	9041(2)	1228(3)	17(1)
C(9A)	5835(4)	8418(3)	285(4)	17(1)
C(10A)	5968(6)	7870(3)	-424(4)	24(1)
C(11A)	6695(4)	9068(3)	478(4)	27(1)
C(12A)	4689(4)	8797(3)	-139(3)	21(1)
C(9B)	5976(10)	8335(8)	232(11)	17(1)
C(10B)	5363(12)	7822(7)	-574(9)	17(3)
C(11B)	7128(9)	8529(8)	223(9)	18(3)
C(12B)	5341(11)	9105(6)	108(9)	17(3)
C(13)	7099(3)	7143(2)	1675(3)	18(1)
C(14)	6899(4)	6454(2)	1030(3)	31(1)
C(15)	8217(3)	7510(3)	1771(4)	40(1)
C(16)	7196(3)	6825(3)	2599(3)	30(1)
C(17)	1094(3)	7705(2)	437(2)	17(1)
C(18)	579(3)	6950(2)	622(3)	21(1)
C(19)	193(3)	8338(2)	224(3)	22(1)
C(20)	1405(3)	7590(2)	-400(3)	23(1)

C(21)	2234(3)	7872(2)	2505(2)	15(1)
C(22)	2334(3)	7018(2)	2765(3)	21(1)
C(23)	1149(3)	8209(2)	2530(3)	21(1)
C(24)	3193(3)	8300(2)	3220(2)	19(1)
C(25)	3740(3)	6213(2)	-583(2)	21(1)
C(26)	4327(3)	5831(2)	-1139(3)	27(1)
C(27)	2618(4)	5181(2)	864(4)	45(1)
C(28)	1555(5)	5006(3)	193(4)	56(2)
C(29)	4799(3)	5790(2)	2783(2)	20(1)
C(30)	5670(3)	5218(2)	3324(3)	25(1)

Table 5.26 Bond Lengths [Å] and Angles [°] for (PCP)IrPOEt$_3$, **5-59**

Ir(1)-C(1)	2.108(3)	C(9A)-C(12A)	1.538(7)
Ir(1)-P(3)	2.2235(9)	C(10A)-H(10A)	0.9800
Ir(1)-P(2)	2.3163(8)	C(10A)-H(10B)	0.9800
Ir(1)-P(1)	2.3214(9)	C(10A)-H(10C)	0.9800
P(1)-C(7)	1.847(4)	C(11A)-H(11A)	0.9800
P(1)-C(13)	1.895(4)	C(11A)-H(11B)	0.9800
P(1)-C(9A)	1.897(6)	C(11A)-H(11C)	0.9800
P(1)-C(9B)	1.963(17)	C(12A)-H(12A)	0.9800
P(2)-C(8)	1.840(4)	C(12A)-H(12B)	0.9800
P(2)-C(21)	1.893(4)	C(12A)-H(12C)	0.9800
P(2)-C(17)	1.899(4)	C(9B)-C(10B)	1.526(10)
P(3)-O(2)	1.613(3)	C(9B)-C(11B)	1.532(10)
P(3)-O(1)	1.620(3)	C(9B)-C(12B)	1.538(10)
P(3)-O(3)	1.631(3)	C(10B)-H(10D)	0.9800
O(1)-C(25)	1.431(4)	C(10B)-H(10E)	0.9800
O(2)-C(27)	1.452(5)	C(10B)-H(10F)	0.9800
O(3)-C(29)	1.441(4)	C(11B)-H(11D)	0.9800
C(1)-C(6)	1.406(5)	C(11B)-H(11E)	0.9800
C(1)-C(2)	1.413(5)	C(11B)-H(11F)	0.9800
C(2)-C(3)	1.386(5)	C(12B)-H(12D)	0.9800
C(2)-C(7)	1.496(5)	C(12B)-H(12E)	0.9800
C(3)-C(4)	1.389(5)	C(12B)-H(12F)	0.9800
C(3)-H(3)	0.9500	C(13)-C(16)	1.529(5)
C(4)-C(5)	1.392(5)	C(13)-C(14)	1.531(5)
C(4)-H(4)	0.9500	C(13)-C(15)	1.535(5)
C(5)-C(6)	1.396(5)	C(14)-H(14A)	0.9800
C(5)-H(5)	0.9500	C(14)-H(14B)	0.9800
C(6)-C(8)	1.499(5)	C(14)-H(14C)	0.9800
C(7)-H(7A)	0.9900	C(15)-H(15A)	0.9800
C(7)-H(7B)	0.9900	C(15)-H(15B)	0.9800
C(8)-H(8A)	0.9900	C(15)-H(15C)	0.9800
C(8)-H(8B)	0.9900	C(16)-H(16A)	0.9800
C(9A)-C(10A)	1.527(7)	C(16)-H(16B)	0.9800
C(9A)-C(11A)	1.532(7)	C(16)-H(16C)	0.9800

C(17)-C(20)	1.532(5)	C(24)-H(24A)	0.9800
C(17)-C(18)	1.540(5)	C(24)-H(24B)	0.9800
C(17)-C(19)	1.545(5)	C(24)-H(24C)	0.9800
C(18)-H(18A)	0.9800	C(25)-C(26)	1.507(5)
C(18)-H(18B)	0.9800	C(25)-H(25A)	0.9900
C(18)-H(18C)	0.9800	C(25)-H(25B)	0.9900
C(19)-H(19A)	0.9800	C(26)-H(26A)	0.9800
C(19)-H(19B)	0.9800	C(26)-H(26B)	0.9800
C(19)-H(19C)	0.9800	C(26)-H(26C)	0.9800
C(20)-H(20A)	0.9800	C(27)-C(28)	1.439(6)
C(20)-H(20B)	0.9800	C(27)-H(27A)	0.9900
C(20)-H(20C)	0.9800	C(27)-H(27B)	0.9900
C(21)-C(22)	1.525(5)	C(28)-H(28A)	0.9800
C(21)-C(23)	1.532(5)	C(28)-H(28B)	0.9800
C(21)-C(24)	1.540(5)	C(28)-H(28C)	0.9800
C(22)-H(22A)	0.9800	C(29)-C(30)	1.515(5)
C(22)-H(22B)	0.9800	C(29)-H(29A)	0.9900
C(22)-H(22C)	0.9800	C(29)-H(29B)	0.9900
C(23)-H(23A)	0.9800	C(30)-H(30A)	0.9800
C(23)-H(23B)	0.9800	C(30)-H(30B)	0.9800
C(23)-H(23C)	0.9800	C(30)-H(30C)	0.9800

C(1)-Ir(1)-P(3)	172.38(10)	C(9A)-P(1)-Ir(1)	110.73(17)
C(1)-Ir(1)-P(2)	79.91(9)	C(9B)-P(1)-Ir(1)	116.0(3)
P(3)-Ir(1)-P(2)	101.79(3)	C(8)-P(2)-C(21)	103.20(16)
C(1)-Ir(1)-P(1)	78.34(9)	C(8)-P(2)-C(17)	100.64(16)
P(3)-Ir(1)-P(1)	100.79(3)	C(21)-P(2)-C(17)	109.45(16)
P(2)-Ir(1)-P(1)	156.91(3)	C(8)-P(2)-Ir(1)	101.92(11)
C(7)-P(1)-C(13)	100.44(17)	C(21)-P(2)-Ir(1)	115.44(11)
C(7)-P(1)-C(9A)	102.9(2)	C(17)-P(2)-Ir(1)	122.62(12)
C(13)-P(1)-C(9A)	111.4(2)	O(2)-P(3)-O(1)	101.81(15)
C(7)-P(1)-C(9B)	106.5(4)	O(2)-P(3)-O(3)	101.01(14)
C(13)-P(1)-C(9B)	103.8(4)	O(1)-P(3)-O(3)	90.99(13)
C(9A)-P(1)-C(9B)	7.7(4)	O(2)-P(3)-Ir(1)	116.99(11)
C(7)-P(1)-Ir(1)	100.98(12)	O(1)-P(3)-Ir(1)	121.73(10)
C(13)-P(1)-Ir(1)	126.33(12)	O(3)-P(3)-Ir(1)	119.49(10)

C(25)-O(1)-P(3)	120.3(2)	C(10A)-C(9A)-P(1)	110.5(4)
C(27)-O(2)-P(3)	120.5(3)	C(11A)-C(9A)-P(1)	112.8(4)
C(29)-O(3)-P(3)	119.4(2)	C(12A)-C(9A)-P(1)	110.0(4)
C(6)-C(1)-C(2)	116.4(3)	C(9A)-C(10A)-H(10A)	109.5
C(6)-C(1)-Ir(1)	122.0(2)	C(9A)-C(10A)-H(10B)	109.5
C(2)-C(1)-Ir(1)	121.5(2)	H(10A)-C(10A)-H(10B)	109.5
C(3)-C(2)-C(1)	121.7(3)	C(9A)-C(10A)-H(10C)	109.5
C(3)-C(2)-C(7)	121.3(3)	H(10A)-C(10A)-H(10C)	109.5
C(1)-C(2)-C(7)	117.0(3)	H(10B)-C(10A)-H(10C)	109.5
C(2)-C(3)-C(4)	120.8(3)	C(9A)-C(11A)-H(11A)	109.5
C(2)-C(3)-H(3)	119.6	C(9A)-C(11A)-H(11B)	109.5
C(4)-C(3)-H(3)	119.6	H(11A)-C(11A)-H(11B)	109.5
C(3)-C(4)-C(5)	118.9(3)	C(9A)-C(11A)-H(11C)	109.5
C(3)-C(4)-H(4)	120.5	H(11A)-C(11A)-H(11C)	109.5
C(5)-C(4)-H(4)	120.5	H(11B)-C(11A)-H(11C)	109.5
C(4)-C(5)-C(6)	120.3(3)	C(9A)-C(12A)-H(12A)	109.5
C(4)-C(5)-H(5)	119.8	C(9A)-C(12A)-H(12B)	109.5
C(6)-C(5)-H(5)	119.8	H(12A)-C(12A)-H(12B)	109.5
C(5)-C(6)-C(1)	121.8(3)	C(9A)-C(12A)-H(12C)	109.5
C(5)-C(6)-C(8)	121.0(3)	H(12A)-C(12A)-H(12C)	109.5
C(1)-C(6)-C(8)	117.2(3)	H(12B)-C(12A)-H(12C)	109.5
C(2)-C(7)-P(1)	107.0(2)	C(10B)-C(9B)-C(11B)	109.6(11)
C(2)-C(7)-H(7A)	110.3	C(10B)-C(9B)-C(12B)	107.5(10)
P(1)-C(7)-H(7A)	110.3	C(11B)-C(9B)-C(12B)	106.6(10)
C(2)-C(7)-H(7B)	110.3	C(10B)-C(9B)-P(1)	109.5(9)
P(1)-C(7)-H(7B)	110.3	C(11B)-C(9B)-P(1)	116.6(9)
H(7A)-C(7)-H(7B)	108.6	C(12B)-C(9B)-P(1)	106.5(9)
C(6)-C(8)-P(2)	108.3(2)	C(9B)-C(10B)-H(10D)	109.5
C(6)-C(8)-H(8A)	110.0	C(9B)-C(10B)-H(10E)	109.5
P(2)-C(8)-H(8A)	110.0	H(10D)-C(10B)-H(10E)	109.5
C(6)-C(8)-H(8B)	110.0	C(9B)-C(10B)-H(10F)	109.5
P(2)-C(8)-H(8B)	110.0	H(10D)-C(10B)-H(10F)	109.5
H(8A)-C(8)-H(8B)	108.4	H(10E)-C(10B)-H(10F)	109.5
C(10A)-C(9A)-C(11A)	109.7(5)	C(9B)-C(11B)-H(11D)	109.5
C(10A)-C(9A)-C(12A)	106.6(5)	C(9B)-C(11B)-H(11E)	109.5
C(11A)-C(9A)-C(12A)	107.1(4)	H(11D)-C(11B)-H(11E)	109.5

C(9B)-C(11B)-H(11F)	109.5	C(20)-C(17)-P(2)	106.0(2)
H(11D)-C(11B)-H(11F)	109.5	C(18)-C(17)-P(2)	113.4(2)
H(11E)-C(11B)-H(11F)	109.5	C(19)-C(17)-P(2)	113.1(3)
C(9B)-C(12B)-H(12D)	109.5	C(17)-C(18)-H(18A)	109.5
C(9B)-C(12B)-H(12E)	109.5	C(17)-C(18)-H(18B)	109.5
H(12D)-C(12B)-H(12E)	109.5	H(18A)-C(18)-H(18B)	109.5
C(9B)-C(12B)-H(12F)	109.5	C(17)-C(18)-H(18C)	109.5
H(12D)-C(12B)-H(12F)	109.5	H(18A)-C(18)-H(18C)	109.5
H(12E)-C(12B)-H(12F)	109.5	H(18B)-C(18)-H(18C)	109.5
C(16)-C(13)-C(14)	107.4(3)	C(17)-C(19)-H(19A)	109.5
C(16)-C(13)-C(15)	107.5(4)	C(17)-C(19)-H(19B)	109.5
C(14)-C(13)-C(15)	108.4(3)	H(19A)-C(19)-H(19B)	109.5
C(16)-C(13)-P(1)	106.8(2)	C(17)-C(19)-H(19C)	109.5
C(14)-C(13)-P(1)	113.1(3)	H(19A)-C(19)-H(19C)	109.5
C(15)-C(13)-P(1)	113.3(3)	H(19B)-C(19)-H(19C)	109.5
C(13)-C(14)-H(14A)	109.5	C(17)-C(20)-H(20A)	109.5
C(13)-C(14)-H(14B)	109.5	C(17)-C(20)-H(20B)	109.5
H(14A)-C(14)-H(14B)	109.5	H(20A)-C(20)-H(20B)	109.5
C(13)-C(14)-H(14C)	109.5	C(17)-C(20)-H(20C)	109.5
H(14A)-C(14)-H(14C)	109.5	H(20A)-C(20)-H(20C)	109.5
H(14B)-C(14)-H(14C)	109.5	H(20B)-C(20)-H(20C)	109.5
C(13)-C(15)-H(15A)	109.5	C(22)-C(21)-C(23)	110.5(3)
C(13)-C(15)-H(15B)	109.5	C(22)-C(21)-C(24)	107.2(3)
H(15A)-C(15)-H(15B)	109.5	C(23)-C(21)-C(24)	107.7(3)
C(13)-C(15)-H(15C)	109.5	C(22)-C(21)-P(2)	109.1(2)
H(15A)-C(15)-H(15C)	109.5	C(23)-C(21)-P(2)	114.4(2)
H(15B)-C(15)-H(15C)	109.5	C(24)-C(21)-P(2)	107.7(2)
C(13)-C(16)-H(16A)	109.5	C(21)-C(22)-H(22A)	109.5
C(13)-C(16)-H(16B)	109.5	C(21)-C(22)-H(22B)	109.5
H(16A)-C(16)-H(16B)	109.5	H(22A)-C(22)-H(22B)	109.5
C(13)-C(16)-H(16C)	109.5	C(21)-C(22)-H(22C)	109.5
H(16A)-C(16)-H(16C)	109.5	H(22A)-C(22)-H(22C)	109.5
H(16B)-C(16)-H(16C)	109.5	H(22B)-C(22)-H(22C)	109.5
C(20)-C(17)-C(18)	108.7(3)	C(21)-C(23)-H(23A)	109.5
C(20)-C(17)-C(19)	108.2(3)	C(21)-C(23)-H(23B)	109.5
C(18)-C(17)-C(19)	107.3(3)	H(23A)-C(23)-H(23B)	109.5

C(21)-C(23)-H(23C)	109.5	O(2)-C(27)-H(27A)	109.2
H(23A)-C(23)-H(23C)	109.5	C(28)-C(27)-H(27B)	109.2
H(23B)-C(23)-H(23C)	109.5	O(2)-C(27)-H(27B)	109.2
C(21)-C(24)-H(24A)	109.5	H(27A)-C(27)-H(27B)	107.9
C(21)-C(24)-H(24B)	109.5	C(27)-C(28)-H(28A)	109.5
H(24A)-C(24)-H(24B)	109.5	C(27)-C(28)-H(28B)	109.5
C(21)-C(24)-H(24C)	109.5	H(28A)-C(28)-H(28B)	109.5
H(24A)-C(24)-H(24C)	109.5	C(27)-C(28)-H(28C)	109.5
H(24B)-C(24)-H(24C)	109.5	H(28A)-C(28)-H(28C)	109.5
O(1)-C(25)-C(26)	107.6(3)	H(28B)-C(28)-H(28C)	109.5
O(1)-C(25)-H(25A)	110.2	O(3)-C(29)-C(30)	107.6(3)
C(26)-C(25)-H(25A)	110.2	O(3)-C(29)-H(29A)	110.2
O(1)-C(25)-H(25B)	110.2	C(30)-C(29)-H(29A)	110.2
C(26)-C(25)-H(25B)	110.2	O(3)-C(29)-H(29B)	110.2
H(25A)-C(25)-H(25B)	108.5	C(30)-C(29)-H(29B)	110.2
C(25)-C(26)-H(26A)	109.5	H(29A)-C(29)-H(29B)	108.5
C(25)-C(26)-H(26B)	109.5	C(29)-C(30)-H(30A)	109.5
H(26A)-C(26)-H(26B)	109.5	C(29)-C(30)-H(30B)	109.5
C(25)-C(26)-H(26C)	109.5	H(30A)-C(30)-H(30B)	109.5
H(26A)-C(26)-H(26C)	109.5	C(29)-C(30)-H(30C)	109.5
H(26B)-C(26)-H(26C)	109.5	H(30A)-C(30)-H(30C)	109.5
C(28)-C(27)-O(2)	111.9(4)	H(30B)-C(30)-H(30C)	109.5
C(28)-C(27)-H(27A)	109.2		

Table 5.27 Torsion Angles [°] for (PCP)IrPOEt$_3$, **5-59**

C(1)-Ir(1)-P(1)-C(7)	30.59(16)	O(3)-P(3)-O(2)-C(27)	-46.9(4)
P(3)-Ir(1)-P(1)-C(7)	-141.69(13)	Ir(1)-P(3)-O(2)-C(27)	-178.3(3)
P(2)-Ir(1)-P(1)-C(7)	50.50(16)	O(2)-P(3)-O(3)-C(29)	-69.0(3)
C(1)-Ir(1)-P(1)-C(13)	142.42(18)	O(1)-P(3)-O(3)-C(29)	-171.2(3)
P(3)-Ir(1)-P(1)-C(13)	-29.86(16)	Ir(1)-P(3)-O(3)-C(29)	60.9(3)
P(2)-Ir(1)-P(1)-C(13)	162.33(16)	P(3)-Ir(1)-C(1)-C(6)	-118.8(6)
C(1)-Ir(1)-P(1)-C(9A)	-77.8(2)	P(2)-Ir(1)-C(1)-C(6)	-15.1(3)
P(3)-Ir(1)-P(1)-C(9A)	109.88(18)	P(1)-Ir(1)-C(1)-C(6)	157.1(3)
P(2)-Ir(1)-P(1)-C(9A)	-57.9(2)	P(3)-Ir(1)-C(1)-C(2)	60.2(8)
C(1)-Ir(1)-P(1)-C(9B)	-84.0(4)	P(2)-Ir(1)-C(1)-C(2)	163.8(3)
P(3)-Ir(1)-P(1)-C(9B)	103.7(4)	P(1)-Ir(1)-C(1)-C(2)	-24.0(3)
P(2)-Ir(1)-P(1)-C(9B)	-64.1(4)	C(6)-C(1)-C(2)-C(3)	2.9(5)
C(1)-Ir(1)-P(2)-C(8)	24.22(16)	Ir(1)-C(1)-C(2)-C(3)	-176.2(3)
P(3)-Ir(1)-P(2)-C(8)	-163.34(13)	C(6)-C(1)-C(2)-C(7)	-177.0(3)
P(1)-Ir(1)-P(2)-C(8)	4.43(16)	Ir(1)-C(1)-C(2)-C(7)	3.9(4)
C(1)-Ir(1)-P(2)-C(21)	-86.80(16)	C(1)-C(2)-C(3)-C(4)	-0.8(6)
P(3)-Ir(1)-P(2)-C(21)	85.63(13)	C(7)-C(2)-C(3)-C(4)	179.1(4)
P(1)-Ir(1)-P(2)-C(21)	-106.60(14)	C(2)-C(3)-C(4)-C(5)	-1.2(6)
C(1)-Ir(1)-P(2)-C(17)	135.28(17)	C(3)-C(4)-C(5)-C(6)	1.1(6)
P(3)-Ir(1)-P(2)-C(17)	-52.28(14)	C(4)-C(5)-C(6)-C(1)	1.1(6)
P(1)-Ir(1)-P(2)-C(17)	115.48(15)	C(4)-C(5)-C(6)-C(8)	-178.8(3)
C(1)-Ir(1)-P(3)-O(2)	104.0(7)	C(2)-C(1)-C(6)-C(5)	-3.0(5)
P(2)-Ir(1)-P(3)-O(2)	1.80(14)	Ir(1)-C(1)-C(6)-C(5)	176.0(3)
P(1)-Ir(1)-P(3)-O(2)	-173.35(13)	C(2)-C(1)-C(6)-C(8)	176.9(3)
C(1)-Ir(1)-P(3)-O(1)	-130.2(7)	Ir(1)-C(1)-C(6)-C(8)	-4.1(4)
P(2)-Ir(1)-P(3)-O(1)	127.60(12)	C(3)-C(2)-C(7)-P(1)	-154.8(3)
P(1)-Ir(1)-P(3)-O(1)	-47.54(12)	C(1)-C(2)-C(7)-P(1)	25.1(4)
C(1)-Ir(1)-P(3)-O(3)	-18.3(7)	C(13)-P(1)-C(7)-C(2)	-168.7(3)
P(2)-Ir(1)-P(3)-O(3)	-120.49(11)	C(9A)-P(1)-C(7)-C(2)	76.3(3)
P(1)-Ir(1)-P(3)-O(3)	64.36(11)	C(9B)-P(1)-C(7)-C(2)	83.3(4)
O(2)-P(3)-O(1)-C(25)	74.4(3)	Ir(1)-P(1)-C(7)-C(2)	-38.2(3)
O(3)-P(3)-O(1)-C(25)	175.9(3)	C(5)-C(6)-C(8)-P(2)	-153.6(3)
Ir(1)-P(3)-O(1)-C(25)	-58.0(3)	C(1)-C(6)-C(8)-P(2)	26.5(4)
O(1)-P(3)-O(2)-C(27)	46.5(4)	C(21)-P(2)-C(8)-C(6)	86.5(3)

C(17)-P(2)-C(8)-C(6)	-160.4(2)	C(7)-P(1)-C(13)-C(14)	-179.2(3)
Ir(1)-P(2)-C(8)-C(6)	-33.5(3)	C(9A)-P(1)-C(13)-C(14)	-70.8(3)
C(7)-P(1)-C(9A)-C(10A)	151.7(4)	C(9B)-P(1)-C(13)-C(14)	-69.2(5)
C(13)-P(1)-C(9A)-C(10A)	44.9(5)	Ir(1)-P(1)-C(13)-C(14)	68.7(3)
C(9B)-P(1)-C(9A)-C(10A)	33(3)	C(7)-P(1)-C(13)-C(15)	-55.3(4)
Ir(1)-P(1)-C(9A)-C(10A)	-101.1(4)	C(9A)-P(1)-C(13)-C(15)	53.1(4)
C(7)-P(1)-C(9A)-C(11A)	28.6(4)	C(9B)-P(1)-C(13)-C(15)	54.7(5)
C(13)-P(1)-C(9A)-C(11A)	-78.2(4)	Ir(1)-P(1)-C(13)-C(15)	-167.4(3)
C(9B)-P(1)-C(9A)-C(11A)	-90(3)	C(8)-P(2)-C(17)-C(20)	87.3(3)
Ir(1)-P(1)-C(9A)-C(11A)	135.8(3)	C(21)-P(2)-C(17)-C(20)	-164.5(2)
C(7)-P(1)-C(9A)-C(12A)	-90.9(4)	Ir(1)-P(2)-C(17)-C(20)	-24.4(3)
C(13)-P(1)-C(9A)-C(12A)	162.3(3)	C(8)-P(2)-C(17)-C(18)	-153.5(3)
C(9B)-P(1)-C(9A)-C(12A)	151(4)	C(21)-P(2)-C(17)-C(18)	-45.3(3)
Ir(1)-P(1)-C(9A)-C(12A)	16.3(4)	Ir(1)-P(2)-C(17)-C(18)	94.8(3)
C(7)-P(1)-C(9B)-C(10B)	-170.5(8)	C(8)-P(2)-C(17)-C(19)	-31.1(3)
C(13)-P(1)-C(9B)-C(10B)	84.0(8)	C(21)-P(2)-C(17)-C(19)	77.2(3)
C(9A)-P(1)-C(9B)-C(10B)	-107(3)	Ir(1)-P(2)-C(17)-C(19)	-142.8(2)
Ir(1)-P(1)-C(9B)-C(10B)	-59.1(9)	C(8)-P(2)-C(21)-C(22)	-174.9(2)
C(7)-P(1)-C(9B)-C(11B)	64.3(9)	C(17)-P(2)-C(21)-C(22)	78.6(3)
C(13)-P(1)-C(9B)-C(11B)	-41.2(9)	Ir(1)-P(2)-C(21)-C(22)	-64.6(3)
C(9A)-P(1)-C(9B)-C(11B)	128(4)	C(8)-P(2)-C(21)-C(23)	60.8(3)
Ir(1)-P(1)-C(9B)-C(11B)	175.7(7)	C(17)-P(2)-C(21)-C(23)	-45.7(3)
C(7)-P(1)-C(9B)-C(12B)	-54.6(8)	Ir(1)-P(2)-C(21)-C(23)	171.1(2)
C(13)-P(1)-C(9B)-C(12B)	-160.1(7)	C(8)-P(2)-C(21)-C(24)	-58.8(3)
C(9A)-P(1)-C(9B)-C(12B)	9(3)	C(17)-P(2)-C(21)-C(24)	-165.3(2)
Ir(1)-P(1)-C(9B)-C(12B)	56.9(8)	Ir(1)-P(2)-C(21)-C(24)	51.5(3)
C(7)-P(1)-C(13)-C(16)	62.9(3)	P(3)-O(1)-C(25)-C(26)	170.6(3)
C(9A)-P(1)-C(13)-C(16)	171.3(3)	P(3)-O(2)-C(27)-C(28)	-139.6(4)
C(9B)-P(1)-C(13)-C(16)	172.9(4)	P(3)-O(3)-C(29)-C(30)	-177.6(2)
Ir(1)-P(1)-C(13)-C(16)	-49.2(3)		

References and Footnotes

(1) Benson, S. W.; Cruickshank, F. R.; Golden, D. M.; Haugen, G. R.; O'Neal, H. E.; Rodgers, A. S.; Shaw, R.; Walsh, R. *Chem. Rev.* **1969**, *69*, 279.
(2) Stull, D. R.; Westrum, E. F.; Sinke, G. C. *The Chemical Thermodynamics of Organic Compounds*; Robert E. Kreiger Publishing: Malabar, FL, 1987.
(3) Marks, T. J. In *Bonding Energetics in Organometallic Compounds*; American Chemical Society: Washington, DC, 1990, p 1.
(4) Ng, F. T. T.; Rempel, G. L.; Halpern, J. *J. Am. Chem. Soc.* **1982**, *104*, 621.
(5) Halpern, J. *Inorg. Chim. Acta.* **1985**, *100*, 41.
(6) Nappa, M. J.; Santi, R.; Diefenbach, S. P.; Halpern, J. *J. Am. Chem. Soc.* **1982**, *104*, 619.
(7) Clot, E.; Besora, M.; Maseras, F.; Megret, C.; Eisenstein, O.; Oelckers, B.; Perutz, R. N. *Chem. Commun.* **2003**, 490.
(8) Abu-Hasanayn, F.; Krogh-Jespersen, K.; Goldman, A. S. *Inorg. Chem.* **1993**, *32*, 495.
(9) Marks, T. J.; Gagne, M. R.; Nolan, S. P.; Schock, L. E.; Seyam, A. M.; Stern, D. *Pure Appl. Chem* **1989**, *61*, 1665.
(10) Koppen, P. A. M. v.; Bowers, M. T.; Beauchamp, J. L.; Dearden, D. V. In *Bonding Energetics in Organometallic Compounds*; Marks, T. J., Ed.; American Chemical Society: Washington, DC, 1990, p 34.
(11) *Bonding Energetics in Organometallic Compounds*; Marks, T. J., Ed.; American Chemical Society: Washington, DC, 1990.
(12) Hoff, C. D. *Prog. Inorg. Chem.* **1992**, *40*, 503.
(13) Martinho Simoes, J. A.; Beauchamp, J. L. *Chem. Rev.* **1990**, *90*, 629.
(14) Cox, J. D.; Pilcher, G. *Thermochemistry of Organic and Organometallic Compounds*; Academic Press: New York, 1970.
(15) Bryndza, H. E.; Fong, L. K.; Paciello, R. A.; Tam, W.; Bercaw, J. E. *J. Am. Chem. Soc.* **1987**, *109*, 1444.
(16) Halpern, J. *Acc. Chem. Res.* **1982**, *15*, 238.
(17) Huang, J.; Haar, C. M.; Nolan, S. P.; Marshall, W. J.; Moloy, K. G. *J Am Chem Soc* **1998**, *120*, 7806.
(18) Parr, R. G.; Yang, W. *Density-Functional Theory of Atoms and Molecules*; University Press: Oxford, 1989.
(19) Kundu, S., PhD Thesis, Rutgers, The State University of New Jersey, 2010.
(20) All temperatures cited in the main text are approximate, calibrated temperatures were used for all calculations and data points.
(21) The errors in enthalpy and entropy were calculated via standard deviation of repetitive samples, while the error in free energy was calculated using least square analysis of the regression line.
(22) Tolman, C. A. *Chem. Rev.* **1977**, *77*, 313.
(23) Chai, J. D.; Head-Gordon, M. *Phys. Chem. Chem. Phys.* **2008**, *10*, 6615.
(24) Grimme, S. *J Comp. Chem.* **2010**, *27*, 1787.
(25) Zhao, C. Y.; Truhlar, D. G. *Theo. Chem. Acc.* **2008**, *120*, 215.
(26) Tao, J. M.; Perdew, J. P.; Staroverov, V. N.; Scuseria, G. E. *Phys Rev. Lett.* **2003**, *91*.
(27) Perdew, J. P.; Burke, K.; Ernzerhof, M. *Phys Rev. Lett.* **1996**, *77*, 3865.
(28) Becke, A. D. *J. Chem. Phys.* **1993**, *98*, 5648.
(29) Gusev, D. G. *Organometallics* **2013**, *32*, 4239.
(30) Units for Delta H and Delta G are kcal/mol, Units for Delta S are cal/mol*K
(31) Yu, Z. X.; Houk, K. N. *J Am Chem Soc* **2003**, *125*, 13825.
(32) Amzel, L. M. *Proteins* **1997**, *28*, 144.
(33) Strajbl, M.; Sham, Y. Y.; Villa, J.; Chu, Z. T.; Warshel, A. *J. Phys. Chem.* **2000**, *104*, 4578.
(34) Chen, Y.; Ye, S.; Jiao, L.; Sinha-Mahaptra, D. K.; Herndon, J. W.; Yu, Z.-X. *J Am Chem Soc* **2007**, *129*, 10773.
(35) Hermans, J.; Wang, L. *J Am Chem Soc* **1997**, *119*, 2707.

(36) Morales-Morales, D.; Redon, R.; Wang, Z.; Lee, D. W.; Yung, C.; Magnuson, K.; Jensen, C. M. *Can. J. Chem.* **2001**, *79*, 823.
(37) Morales-Morales, D.; Redon, R.; Chen, W.; Yung, C.; Jensen, C. M. *Abstracts of Papers, 220th ACS National Meeting, Washington, DC, United States, August 20-24, 2000* **2000**, INOR-274.
(38) Wilberg, K. B.; Crocker, L. S.; Morgan, K. M. *J Am Chem Soc* **1991**, *113*, 3447.
(39) $(PCP)IrH_4$ is synthesized in correlation with $(PCP)IrH_2$, see reference for synthesis of $(PCP)IrH_2$ for characterization and synthesis details of $(PCP)IrH_4$.
(40) Units for Delta H and Delta G are kcal/mol, Units for Delta S are cal/mol*K
(41) Mendes, P. *Computer applications in the biosciences : CABIOS* **1993**, *9*, 563.
(42) (a) Gupta, M.; Hagen, C.; Flesher, R. J.; Kaska, W. C.; Jensen, C. M. *Chem. Commun.* **1996**, 2083-2084. (b) Gupta, M.; Hagen, C.; Kaska, W. C.; Cramer, R. E.; Jensen, C. M. *J. Am. Chem. Soc.* **1997**, 119, 840-841. (c) Gupta, M.; Kaska, W. C.; Jensen, C. M. *Chem. Commun.* **1997**, 461-462.
(43) Amman, C.; Meier, P.; Merbach, A. E. *Journal of Magnetic Resonance* **1982**, *46*, 319.
(44) Kanzelberger, M.; Singh, B.; Czerw, M.; Krogh-Jespersen, K.; Goldman, A. S. *J. Am. Chem. Soc.* **2000**, *122*, 11017.
(45) Kanzelberger, M.; Zhang, X.; Emge, T. J.; Goldman, A. S.; Zhao, J.; Incarvito, C.; Hartwig, J. F. *J. Am. Chem. Soc.* **2003**, *125*, 13644.
(46) Ghosh, R.; Kanzelberger, M.; Emge, T. J.; Hall, G. S.; Goldman, A. S. *Organometallics* **2006**, *25*, 5668.
(47) Zhang, X.; Wang, D. Y.; Emge, T. J.; Goldman, A. S. *Inorg. Chim. Acta* **2011**, *369*, 253.
(48) Gaussian 03, Revision B.03, Frisch, M. J.; Trucks, G. W.; Schlegel, H. B.; Scuseria, G. E.; Robb, M. A.; Cheeseman, J. R.; Montgomery, Jr., J. A.; Vreven, T.; Kudin, K. N.; Burant, J. C.; Millam, J. M.; Iyengar, S. S.; Tomasi, J.; Barone, V.; Mennucci, B.; Cossi, M.; Scalmani, G.; Rega, N.; Petersson, G. A.; Nakatsuji, H.; Hada, M.; Ehara, M.; Toyota, K.; Fukuda, R.; Hasegawa, J.; Ishida, M.; Nakajima, T.; Honda, Y.; Kitao, O.; Nakai, H.; Klene, M.; Li, X.; Knox, J. E.; Hratchian, H. P.; Cross, J. B.; Bakken, V.; Adamo, C.; Jaramillo, J.; Gomperts, R.; Stratmann, R. E.; Yazyev, O.; Austin, A. J.; Cammi, R.; Pomelli, C.; Ochterski, J. W.; Ayala, P. Y.; Morokuma, K.; Voth, G. A.; Salvador, P.; Dannenberg, J. J.; Zakrzewski, V. G.; Dapprich, S.; Daniels, A. D.; Strain, M. C.; Farkas, O.; Malick, D. K.; Rabuck, A. D.; Raghavachari, K.; Foresman, J. B.; Ortiz, J. V.; Cui, Q.; Baboul, A. G.; Clifford, S.; Cioslowski, J.; Stefanov, B. B.; Liu, G.; Liashenko, A.; Piskorz, P.; Komaromi, I.; Martin, R. L.; Fox, D. J.; Keith, T.; Al-Laham, M. A.; Peng, C. Y.; Nanayakkara, A.; Challacombe, M.; Gill, P. M. W.; Johnson, B.; Chen, W.; Wong, M. W.; Gonzalez, C.; and Pople, J. A.*; Gaussian, Inc., Pittsburgh, PA, 2003.*
(49) Frisch, M. J. T., G. W.; Schlegel, H. B.; Scuseria, G. E.; Robb, M. A.; Cheeseman, J. R.; Scalmani, G.; Barone, V.; Mennucci, B.; Petersson, G. A.; Nakatsuji, H.; Caricato, M.; Li, X.; Hratchian, H. P.; Izmaylov, A. F.; Bloino, J.; Zheng, G.; Sonnenberg, J. L.; Hada, M.; Ehara, M.; Toyota, K.; Fukuda, R.; Hasegawa, J.; Ishida, M.; Nakajima, T.; Honda, Y.; Kitao, O.; Nakai, H.; Vreven, T.; Montgomery, Jr., J. A.; Peralta, J. E.; Ogliaro, F.; Bearpark, M.; Heyd, J. J.; Brothers, E.; Kudin, K. N.; Staroverov, V. N.; Kobayashi, R.; Normand, J.; Raghavachari, K.; Rendell, A.; Burant, J. C.; Iyengar, S. S.; Tomasi, J.; Cossi, M.; Rega, N.; Millam, N. J.; Klene, M.; Knox, J. E.; Cross, J. B.; Bakken, V.; Adamo, C.; Jaramillo, J.; Gomperts, R.; Stratmann, R. E.; Yazyev, O.; Austin, A. J.; Cammi, R.; Pomelli, C.; Ochterski, J. W.; Martin, R. L.; Morokuma, K.; Zakrzewski, V. G.; Voth, G. A.; Salvador, P.; Dannenberg, J. J.; Dapprich, S.; Daniels, A. D.; Farkas, Ö.; Foresman, J. B.; Ortiz, J. V.; Cioslowski, J.; Fox, D. J.; Gaussian, Inc.: Wallingford, CT, 2009.
(50) Roy, L. E.; Hay, P. J.; Martin, R. L. *J. Chem. Theory Comput.* **2008**, *4*, 1029.

Chapter 6

Dual Reactivity of Pincer Iridium Complexes towards Hydrazine

Abstract

The synthesis of ammonia via the Haber-Bosch process is one of the most important industrial processes in the world today. Unfortunately, it is also one of the most energy intensive processes accounting for more than 1% of the world's energy. Hydrazine (N_2H_4) is a potential key intermediate in the conversion of N_2 and H_2 to ammonia. We report both the dehydrogenation of hydrazine by the parent (PCP)Ir catalyst to N_2 and H_2 as well as the hydrogenation of hydrazine to form ammonia. (PCP)Ir complexes with hydrazine derivatives are isolated and characterized. Additionally, a computationally calculated mechanism is proposed for both pathways. Finally, the reactivity of other pincer systems towards the synthesis of ammonia is also explored.

6.1 Introduction

Diatomic nitrogen (N_2) persists as one the world's most plentiful molecules accounting for 78% percentage of the world's atmosphere, yet it is also considered one of the most inert molecules in chemistry.[1,2] N_2 is a poor ligand as it has little σ-donating and weak π-accepting abilities. Therefore it is no surprise that activation of the nitrogen triple bond has proved challenging. The first transition metal dinitrogen complex ($[(H_3N)_5Ru(N_2)]^{+2}$) was isolated in 1965.[3,4] Since that time, the coordination chemistry of N_2 has greatly expanded and dinitrogen complexes of almost every transition metal exist, becoming a promising platform for the reduction of nitrogen.[1,5-7] Pincer dinitrogen species have been isolated for both the parent PCP and the more electron deficient POCOP systems as has been discussed in Chapter 2.[8-10]

The conversion of N_2 and H_2 to ammonia, NH_3, is an exothermic process, -92 kJ/mol (-22 kcal/mol), and believed to occur through three consecutive steps (Equation 1).[11]

$$N_2 \underset{}{\overset{H_2}{\rightleftharpoons}} N_2H_2 \overset{H_2}{\rightleftharpoons} N_2H_4 \overset{H_2}{\rightleftharpoons} 2NH_3 \qquad (1)$$

Nature has utilized an iron-molybdenum-sulfur enzyme to catalyze this reaction under ambient conditions on the order of 10^8 tons per year.[12,13] And although the enzymatic hydrogenation of N_2 has been of great interest, the ability to mimic and understand this process is extremely limited. There are different proposed mechanisms for the synthesis of ammonia, but the generally accepted pathways involve stepwise additions of protons and electrons to reduce N_2 (i.e Chatt or Schrock type mechanisms).[14-17]

Industrially, N_2 has become a feedstock for three different processes: the Birkeland-Eyde process which generates nitric acid via electric discharge into an oxygen-nitrogen gas mixture, the Frank-Caro cyanamide process which reacts N_2 with calcium carbide to produce $CaCN_2$, and the Haber-Bosch process which generates NH_3 from N_2 and H_2.[1,11] The Haber-Bosch process reaction utilizes an iron catalyst at high temperatures (350-550 ˚C) and high pressures of N_2 and H_2 (150-350 atm) and consumes 1.5% of the global energy.[18] This process relies on the use of H_2, in the form of syngas, rather than use of proton and electron sources.

The challenge with the conversion of dinitrogen and hydrogen to ammonia lies with the high stability and inertness of N_2.[2] The N_2 molecule has a very high bond energy, high ionization potential and

negative electron affinity. The first bond dissociation of the N_2 triple bond requires at least 410 kJ/mol (98 kcal/mol), whereas acetylene requires 222 kJ/mol (53 kcal/mol) for the analogous bond dissociation. The difference between the two molecules stems from the repulsion of the two electron pairs in the π-bond of diazene. Consequently, the 2-electron addition of H_2 to acetylene to give ethylene is permitted and highly exothermic, whereas the same reaction for N_2 to make N_2H_2 is forbidden and highly endothermic. Conversely, 4- and 6-electron reactions with N_2 are much more favorable. Therefore any reduction of N_2 should go through a hydrazine intermediate or directly to ammonia. Not only is hydrazine an intermediate in the formation of ammonia, the reverse process could potentially allow for the reduction of hydrazine to give hydrogen and nitrogen.[19,20] The decomposition of hydrazine can occur via the following reactions.

$$3\ N_2H_4 \rightarrow 4\ NH_3 + N_2 \quad (2)$$

$$N_2H_4 \rightarrow N_2 + 2\ H_2 \quad (3)$$

$$N_2H_4 \rightarrow NH_3 + ½\ N_2 + ½\ H_2 \quad (4)$$

Hydrazine as a hydrogen storage feedstock will generate 12.5% hydrogen by mass, in comparison to the reduction of ammonia which is the highest reported source (17.8%). Other feedstocks, including boranes and borohydrides tend to give between 5.6% and 13.6% hydrogen by mass. Advantageously, hydrazine can be reduced at room temperature or slightly above, rather than 600 ˚C as for the decomposition of ammonia.

C-H activation has been studied extensively using pincer complexes; therefore the examination of N-H activation by pincer iridium complexes is a natural progression given that N-H and C-H bonds have similar homolytic bond strengths (D°_{298} = 338 kJ/mol, 81 kcal/mol[21]).[22] Hydroamination using pincer iridium complexes has yet to be reported, but the oxidative addition of N-H bonds using the parent ($^{t\text{Bu4}}$PCP)Ir (Scheme 6.1), the more electron withdrawing (POCOP)Ir complex, and other pincer motifs have been previously reported.[23-28] Milstein and coworkers also reported the N-H activation of anilines using dearomatized pincer complexes.[29,30] The dehydrogenation of secondary amines to give imines, involving both C-H and N-H activation in which hydrogen elimination occurs across the C-N bond rather than the C-C bonds, has also been published.[31]

Scheme 6.1 N-H Activation of Ammonia and Aniline by ($^{t\text{Bu4}}$PCP)Ir

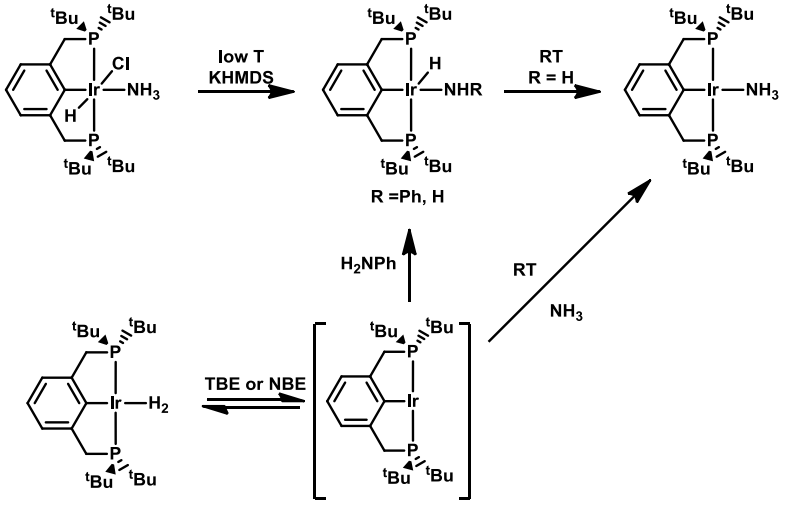

The conversion of nitrogen and hydrogen to ammonia, either directly or through potential intermediates, has been investigated with a few pincer type complexes. Similar to the conversion process observed in nature, Nishibayashi and coworkers describe the conversion of dinitrogen to ammonia in the presence of cobaltocene and lutidinium triflate as the electron and proton source, respectively, with a tridentate PNP pincer type molybdenum catalyst.[32] A (NNN)Fe complex has been reported for the cleavage of hydrazine utilizing proton-coupled electron transfer via transfer from the bis(pyrazole) backbone to the redox active iron center.[33] Arnold and Rozenel have explored bimetallic ruthenium pincer complexes that support a series of hydrogen, nitrogen, diazene and hydrazine complexes in hopes to gain insight into nitrogenase-like activity.[34]

Each of these systems requires the assistance of electron and proton sources, either through an external additive or via ligand assisted transformations. The ability to use H_2 directly as in the Haber Bosch Process is much more enticing as it is more atom-economical. There have been some previous studies with non pincer type complexes. For example, Chirik has investigated the hydrogenation of nitrogen extensively using early transition metals.[6,35-42] Fryzuk has also published the stoichiometric addition of H_2 to a side-on bound zirconium complex.[43] Nishibayshi published the protonation of tungsten dinitrogen complexes assisted via a hydrogenated ruthenium complex.[44] Only one report using a pincer complex has reported the direct use of H_2 via hydrogenolysis of a ruthenium nitride complex, using a PNP-type ligand, to produce ammonia.[45]

An extensive computational study was conducted by Leitner, et. al to discuss the applications of pincer complexes for the synthesis of ammonia from N_2 and H_2.[46] Ruthenium, iron, and osmium complexes with a variety of ligand backbones containing N, O and S donor atoms were investigated. The authors discovered a (POP)Ru catalyst is the most feasible for the catalytic conversion of N_2 and H_2 to ammonia. However, generation of a dihydride dinitrogen complex, in which the dinitrogen ligand is side-on bound rather than end-on, is necessary for the catalytic cycle which may impede experimental applications due to rarity. The Hartwig group has explored the oxidative addition of hydrazine derivatives to iridium(I) complexes.[47] Initial addition leads to N-H bond activation rather than C-H activation of the R groups (Scheme 6.2).

Scheme 6.2 Addition of Hydrazine Derivatives to (PCP)IrPhH

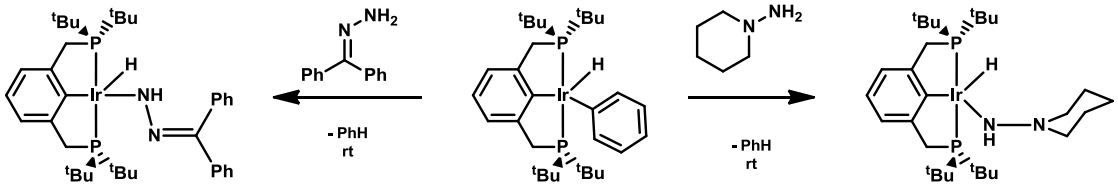

Specifically, reactions with methylphenylhydrazine ($MePhNNH_2$) and dimethylhydrazine, (Me_2NNH_2) proceed through both double N-H activation and/or α-methyl C-H activation followed by subsequent N-N bond cleavage (Scheme 6.3). Two mechanistic pathways are proposed for the formation of these products. Double N-H activations leads to the evolution of H_2 and a diazene adduct, whereas initial C-H activation followed N-N bond cleavage leads to formation of ammonia and the isocyanide complex. The N-N bond is weaker in hydrazine than within substituted hydrazines, therefore, it potentially has a higher reactivity for the formation of ammonia.

Scheme 6.3 Addition of $MePhNNH_2$ and Me_2NNH_2 to (PCP)Ir Fragment

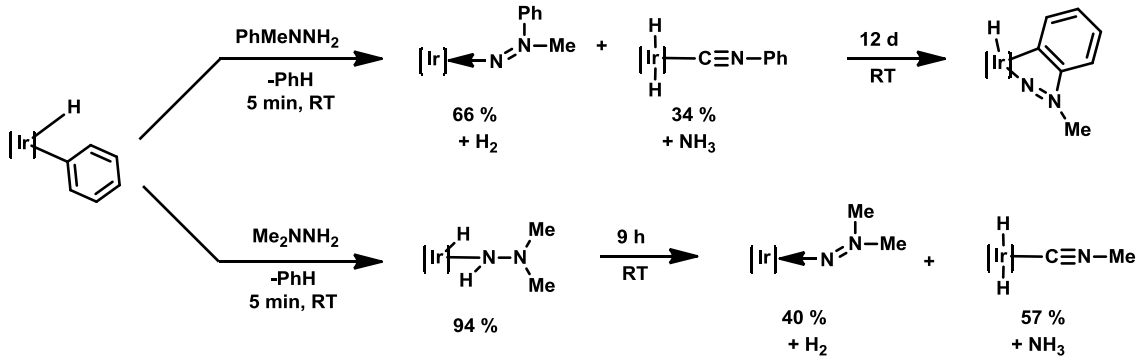

This chapter will report both the dehydrogenation of hydrazine by the parent (PCP)Ir catalyst to N_2 and H_2 as well as the hydrogenation of hydrazine to form ammonia. A series of (PCP)Ir hydrazine complexes are isolated and characterized. Thermodynamic and kinetics experiments were used to support a computationally calculated mechanism. Interestingly, hydrazine acts as both a hydrogen donor and acceptor, and no external proton source or reductant is needed to promote this reaction.

6.2 Results and Discussion

6.2.1 Synthesis of Hydrazine Complexes

At room temperature, hydrazine (1M in THF[48,49]) is reacted with (PCP)Ir(Ph)(H),[50] to initially generate (PCP)IrN_2H_4 (**6-1**, Scheme 6.4) which is qualitatively observable by a red to orange color change. The NMR spectra of **6-1** show a major peak at 68.9 ppm in the ^{31}P NMR spectrum and no observable hydride in the proton NMR. The hydrazine protons for the iridium bound nitrogen (β-N) protons appear as a broad singlet at 4.8 ppm and the protons attached to the nitrogen bound to the iridium center (α-N) triplet at 3.2 ppm in the proton spectrum. Presumably, the broad nature of the signal for β -N protons is due to the rotation around the N-N bond on the NMR timescale or due to the ^{14}N quadrapole moment. Complex **6-1** is not stable at room temperature and within a few minutes, the transformation from **6-1** to (PCP)Ir$H_2N_2H_4$ (**6-2a**) is observed by NMR spectroscopy. The ^{31}P NMR spectrum of **6-2a** shows a major peak at 66.4 ppm and a hydride signal appears at -8.8 ppm as a triplet in the ^{1}H NMR spectrum, indicative of a six-coordinate Ir(I) species (see Chapter 5 for other examples of six coordinate species). A coupled ^{31}P NMR spectrum of **6-2a** gives a triplet, indicating coupling to two hydrides. The signals for the protons bound β-N appear as a broad singlet at 3.8 ppm (also due to rotation around N-N bond on the NMR timescale or the ^{14}N

quadrapole moment), whereas the signals of the protons attached to the α-N appear as a triplet at 2.95 ppm. Reacting (PCP)IrH_2 with hydrazine at room temperature, instead of (PCP)Ir(Ph)(H), gives species **6-2a** immediately and **6-1** is not observed**.**

Scheme 6.4 Addition of Hydrazine and Phenylhydrazine to (PCP)Ir Complexes to Synthesize (PCP)Ir Hydrazine Complexes **6-1** through **6-2d**

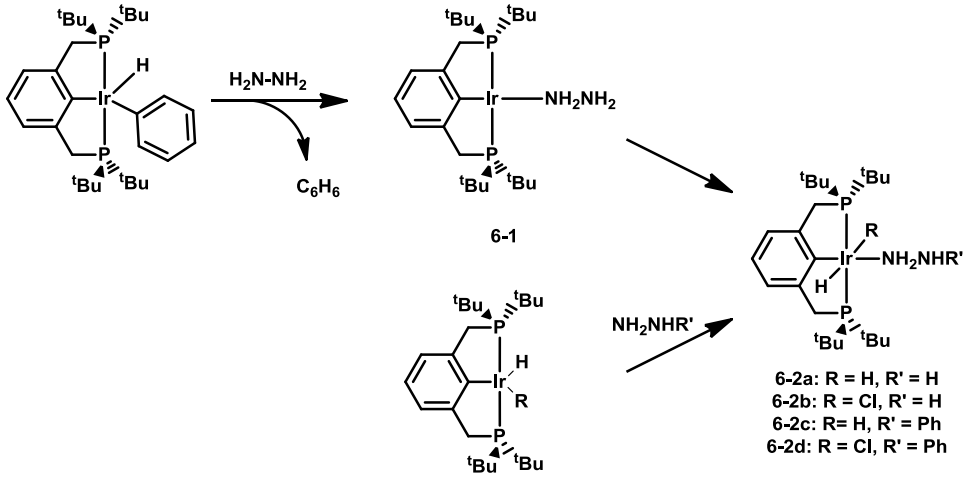

Complex **6-2a** was crystallized from a solution of pentane and excess hydrazine solution (1 M in THF). The crystal structure contains hydrazine bound in an end-on binding mode. The β-N in the hydrazine ligand shows slight disorder of 15% as the hydrazine ligand can swing either to the left or right (Hydrogen atoms for the PCP ligand have been omitted for clarity, Figure 6.1). Interestingly, the two isomers have different N-N bond lengths. The major isomer has a N-N bond length of 1.45 Å whereas the minor isomer has an N-N bond length of 1.50 Å, which is slightly elongated from the N-N bond length of free hydrazine (1.46 Å).[51] The N-N bond lengths for the (PCP)IrN_2 monomer and dimer, reported as 1.107 and 1.134-1.176 Å, respectively, have also been lengthened in comparison to the N-N bond length of free nitrogen (1.095 Å).[2,8,9]

Figure 6.1 Crystal Structure of (PCP)Ir$H_2N_2H_4$, **6-2a**

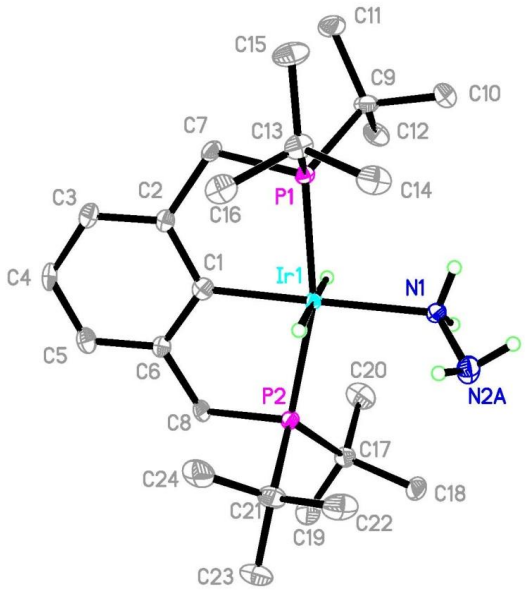

Low temperature NMR experiments were conducted in mesitylene-d_{12} to monitor the formation of **6-1** after the addition of hydrazine to (PCP)Ir(Ph)(H). At -30 ˚C, there is one major peak at 45.4 ppm in the ^{31}P NMR spectrum and a hydride signal appearing as a triplet at -21 ppm, integrating to one hydrogen in relation to the ^{t}butyl protons in the ^{1}H NMR spectrum, most likely corresponding to the hydrazine adduct of (PCP)Ir(Ph)(H) (**6-1b**). As the temperature is raised from -30 ˚C to 0 ˚C, the ^{31}P NMR shift for **6-1** emerges while the signals for **6-1b** decrease. Due to the transient nature of **6-1b,** further spectroscopic characterization was not achieved, but presumably loss of benzene from the reaction mixture leads to observance of **6-1**. Again, **6-1** is not stable at room temperature and **6-2a** is observed as the major species in solution upon warming from 0 ˚C to room temperature.

Scheme 6.5 Low Temperature Reactions for the Addition of Hydrazine to (PCP)Ir

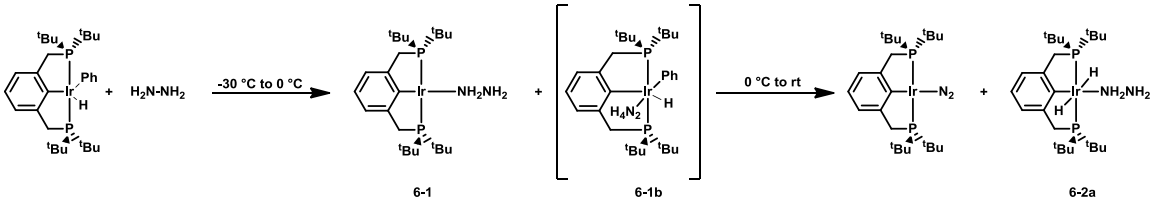

Other hydrazine complexes can be generated using similar methods. Upon reaction of (PCP)IrHCl with hydrazine at room temperature, a yellow partially soluble product is formed which was subsequently characterized as the hydrazine adduct (PCP)IrHClN_2H_4 (**6-2b**, Scheme 6.4). The NMR spectra of **6-2b** shows a major peak at 50.3 ppm in the ^{31}P NMR spectrum and a hydride at -21.2 ppm in the ^{1}H NMR spectrum. The hydrazine protons are observed as broad singlets at 4.2 ppm and 4.1 ppm in the proton spectrum. Presumably, the low solubility of the complex in arene solvents does not allow for complete resolution of any coupling as was observed for **6-1** or **6-2a**.[52] Addition of phenylhydrazine to (PCP)IrH_2 leads to six coordinate (PCP)IrH_2(NH_2NHPh) and reaction with (PCP)IrHCl leads to (PCP)IrHCl(NH_2NHPh) at room temperature (**6-2c** and **6-2d**, respectively). The NMR spectra show major peaks at 66.6 and 47.8 ppm in the ^{31}P NMR spectrum and hydrides at -8.5 and -22 ppm in the ^{1}H NMR, respectively. The hydrazine protons are observed at ~5.4 ppm for the β-nitrogen proton and ~5.0 ppm for the two α-nitrogen protons in the ^{1}H NMR spectrum. As in the reaction with (PCP)IrHCl and hydrazine, **6-2d** is only sparingly soluble in arene solvents.

6.2.2 Dehydrogenation of Hydrazine

Placing a solution of **6-2a** under extended vacuum and slightly elevated temperatures (50 ˚C) results in the observation of (PCP)IrN_2 and (PCP)IrH_2 in a 1 to 3 ratio as confirmed by NMR spectroscopy (Scheme 6.6).[8] Depending upon the concentrations of H_2 and N_2 in solution, (PCP)IrN_2 dimer and (PCP)IrH_4 have also been observed by NMR spectroscopy. Presumably, successive N-H activation of hydrazine generates free hydrogen and nitrogen which coordinate to the naked 14e$^-$ (PCP)Ir species in accordance with decomposition Equation 3. Alternatively, dehydrogenation to give diazene and H_2 followed by disproportionation to produce N_2 could also be a possibility.

Scheme 6.6 Formation of (PCP)IrN_2 and (PCP)IrH_2 from (PCP)Ir$H_2N_2H_4$

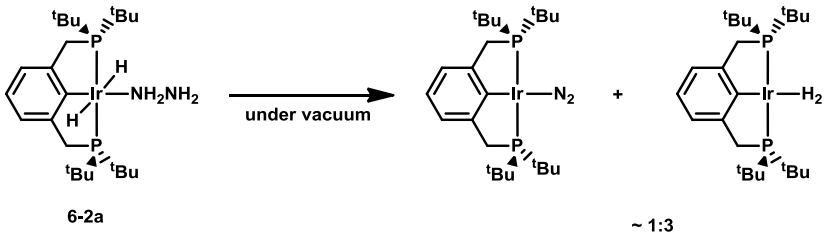

This is the first example of an unassisted dehydrogenation of hydrazine using a transition metal complex. The base-induced dehydrogenation of ruthenium hydrazine complexes has been previously reported.[53] The base initiates deprotonation followed by release of a pendant phosphine arm allowing for disproportionation and, finally, rearrangement of the diazene intermediate generates hydrogen and nitrogen. There is no indication of any transitional species or pendant phosphine arms in the above reaction. The dehydrogenation or more aptly phrased decomposition of hydrazine has been extensively studied as use as a hydrogen storage material but mostly with heterogeneous type catalysts.[19,20]

6.2.3 Synthesis of Ammonia

If (PCP)IrH_2 is heated to 100 ˚C for 1 hour in the presence of 5 equivalents hydrazine, the solution changes from yellow to dark green yielding (PCP)IrH_2NH_3 (**6-3**) either (PCP)IrH_4 or (PCP)IrH_2 and free ammonia which are observable by NMR spectroscopy (Scheme 6.7). Free nitrogen is not observable by NMR, but is presumably also formed as a product following decomposition Equation 6. The ^{31}P NMR spectrum of **6-3** shows a signal at 67.4 ppm and a hydride signal is present in the ^{1}H NMR spectrum for two protons at -8.7 ppm, observed as a triplet, which are indicative of a six-coordinate species. The amine protons are observed as a broad signal at approximately 2.2 ppm. (PCP)IrH_2 was reacted with 10 eq. ammonia, independently, successfully generating **6-3** as the sole iridium product. Free ammonia is observed in solution as a broad triplet at 0 ppm in the ^{1}H NMR spectrum. The observed splitting is due to ^{14}N-^{1}H coupling (J_{obs} = 41.2 Hz). Other literature sources have cited a triplet with a coupling constant ranging from 38.1 to 43.5 Hz.[45,54]

Scheme 6.7 Formation of Ammonia from (PCP)$IrH_2N_2H_4$

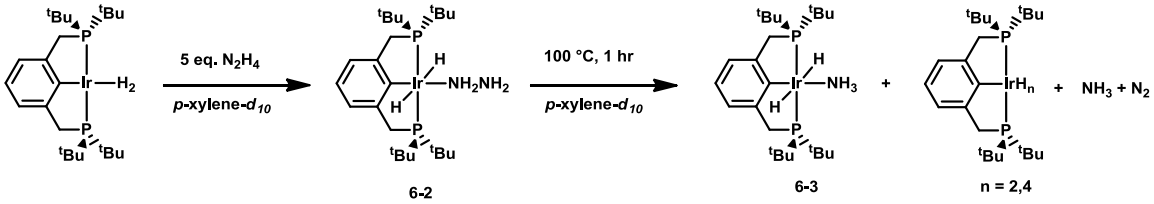

6.2.4 Preliminary Catalytic Screening

When 0.1 M hydrazine is heated in the presence of a 0.02 M (PCP)IrH_2 catalyst solution, no decomposition of catalyst was detected and, within 30 minutes the reaction reached 98% completion

generating ammonia *in situ* (Table 1). The concentration of NH_3 was determined by the comparison against a 14 mM PMe_3 capillary insert. When a hydrazine solution is heated in a 100 ˚C oil bath for 72 hours without the presence of any catalyst, less then ~5% conversion to ammonia was observed, supporting an iridium-catalyzed pathway rather than thermal decomposition. It is also important to note no external reductants or proton sources were added to the reaction solution. Previously, transition metal catalyzed transformations of hydrazine to ammonia using a necessary reductant and proton source have been reported.[55,56] Varying the concentration of the catalyst from 20 mM to 5 mM increases the reaction time from 30 minutes to 2 hours, and a similar yield is achieved. Increasing the concentration of hydrazine to 0.4 M takes longer for completion and 87% yield is achieved after 24 hours. When the reaction is conducted under a hydrogen atmosphere rather than an argon atmosphere, less than 60% completion is observed after 65 hours. Presumably, hydrogen inhibits the catalyst through formation of $(PCP)IrH_4$ at low concentrations of hydrazine or during the catalytic cycle.

It has been noted that replacing the *t*butyl groups attached to the phosphorous arms with isopropyl groups leads to less steric bulk surrounding the metal center, thus generating (^{iPr4}PCP)IrH_2.[57] Addition of hydrazine to (^{iPr4}PCP)IrH_2 yields (^{iPr4}PCP)$IrH_2(N_2H_4)$ (**6-4**, Scheme 6.8). The ^{31}P NMR spectrum of **6-4** shows a major peak at 53.8 ppm and a hydride signal appears at -9.3 ppm as a triplet in the ^{1}H NMR spectrum. The signals for the protons bound to the α-N appear as a broad singlet at 2.99 ppm, whereas the signals of the protons attached to the β-N appear as a triplet at 3.7 ppm. If **6-4** is heated to 100 ˚C under similar catalytic conditions only 34% ammonia yield is produced after 3.5 hours. This catalyst is much less effective than the parent (^{tBu4}PCP) catalyst and possible reactivity explanations will be discussed *vide infra*.

Scheme 6.8 Addition of Hydrazine to (^{iPr4}PCP)IrH_2 to yield (^{iPr4}PCP)$IrH_2(N_2H_4)$, **6-4**

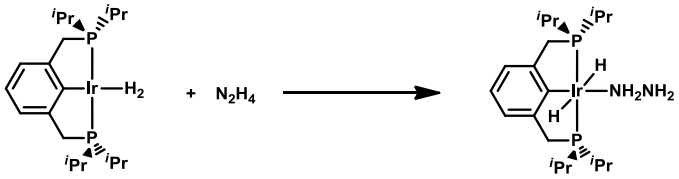

6-4

Replacing the methylene linkers in the ligand backbone with oxygen atoms generates the more electron deficient POCOP ligand.[58] Utilizing the $(POCOP)IrH_2$ catalyst for the decomposition of hydrazine yields similar results as the parent (^{tBu4}PCP) catalyst. When 0.1 M hydrazine is heated in the presence of a

0.02 M solution of (POCOP)IrH_2 catalyst, the reaction reaches 95% completion within 30 minutes. Most likely, the electronic difference between methylene and oxygen linkers does not impact this reaction. Unfortunately, no catalytic species were isolated for the (POCOP)Ir catalyzed reaction.

Table 6.1 Ammonia Production for the Catalytic Reduction of Hydrazine with Varied Catalytic Conditions

Catalyst	[Catalyst] M	[Hydrazine] M	Time	[NH_3] M	% yield	TON (final time)
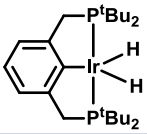	0.020	0.10	30 min	0.10	99	5 (30 min)
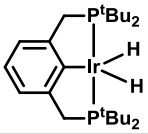	0.005	0.10	1 hr	0.03	~ 30	20 (2 hrs)
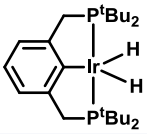	0.017	0.40	1 hr	0.16	40	24 (24 hrs)
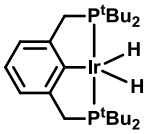 1 atm H_2	0.025	0.14	65 hours	0.06	58	4
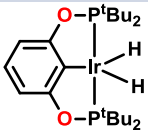	0.016	0.10	30 min	0.10	95	8 (30 min)
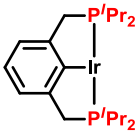	0.016	0.10	1 hr	0.03	32	2 (3.5 hrs)

6.2.5 Thermodynamic Studies

As described in Chapter 5, the equilibrium constant (K_{eq}) between (PCP)IrH_2 and **6-2a** or **6-3** can be measured by changing the temperature of the reaction mixture thereby shifting the equilibrium position. Since no intermediates are formed during this process, the binding energy can be directly correlated to the energy of addition for each ligand. The concentration of each species can be determined by integration of either the ^{31}P NMR signals of each species or by the hydride signals in the ^{1}H NMR spectrum. These concentrations are then used to determine the K_{eq}. Separate equilibrium studies were conducted allowing for the measurement of binding energy for hydrazine and ammonia to (PCP)IrH_2. The equilibrium between the five coordinate (PCP)IrH_2 with free ammonia and six coordinate **6-3** was monitored by NMR

spectroscopy from 25-65 ˚C (Scheme 6.9), giving an equilibrium constant for the addition as 20 M^{-1} (Table 6.2). The enthalpy (ΔH), entropy (ΔS), and free energy (ΔG) values were determined as -11.2 (0.4) kcal/mol, -44.9 (1.1) cal/mol*K, and 2.1 (0.3) kcal/mol respectively. Based on these values, NH_3 binds relatively weakly and can be easily eliminated from the (PCP)IrH_2 catalyst at room temperature and under reaction conditions the equilibrium will be even more favorable.

Scheme 6.9 Equilibrium Between (PCP)IrH_2 and NH_3

6-3

The direct measurement of the binding energy of hydrazine to (PCP)IrH_2 is inaccessible. Hence a competition experiment was conducted between hydrazine and PEt_3 using a similar method as the competition experiments detailed in Chapter 5. PEt_3 binds more strongly than hydrazine by 1.1 kcal/mol and since PEt_3 binds to (PCP)IrH_2 with a free energy of -11.0 kcal/mol, the addition of hydrazine has a free energy of -9.9 kcal/mol relative to NH_3. Hydrazine can be converted to ammonia and subsequently released, which is promoted by the weak binding energy at high concentrations of hydrazine. As discussed earlier, both free ammonia and hydrogen, in the form of (PCP)IrH_4, are observed by NMR spectroscopy as the reaction nears completion. Also, performing the reaction under a hydrogen atmosphere significantly impacts the reaction yield and time; 60% yield in 65 hours as compared to 98% in 30 minutes. These observations indicate there is competitive binding between hydrogen, to form (PCP)IrH_4, and ammonia, to form **6-3,** as the hydrazine becomes consumed. The formation of the tetrahydride complex is favorable by 5.4 kcal/mol in comparison to hydrazine and ammonia. As nitrogen is also synthesized during this reaction, experiments were conducted to determine the possibility of nitrogen binding to (PCP)IrH_2. Addition of a 1:1 nitrogen: hydrogen atmosphere to (PCP)IrH_2 leads to (PCP)IrH_4 and (PCP)Ir(N_2) monomer. Over time, the (PCP)Ir(N_2) monomer loses dinitrogen and (PCP)IrH_4 is the only observable species in solution. Previously, the addition of hydrogen to a three coordinate aliphatic pincer rhodium complex was calculated as 1.24 kcal/mol more favorable then addition of dinitrogen.[59] It can be presumed

that hydrogen addition to (PCP)IrH_2 is even more preferred due to the stabilizing nature of the four hydrogen ligands.

Table 6.2 Equilibrium Constants (K, M^{-1}) and Free Energy Values (ΔG, kcal/mol) for the Addition of NH_3, H_2, Hydrazine, and PEt_3 to (PCP)IrH_2 at 298 K

Ligands	K (M^{-1})	ΔG (kcal/mol)
NH_3	23 (4)	-1.9 (0.4)
H_2	8437	-5.4 (0.6)
Hydrazine	6.2	-9.9
PEt_3		-11.0

Overall, the thermodynamics for the addition of ligands to (PCP)IrH_2 support a catalytic mechanism in which hydrazine can be converted to ammonia and its subsequent release is promoted by the weak binding energy.

6.2.6 Reactivity of Other Pincer Catalysts

As the catalytic reactions of (^{iPr4}PCP)IrH_2 and (POCOP)IrH_2 have already been discussed, other pincer catalysts were tested to determine their feasibility. All reactions were conducted at 100 ˚C. The catalyst concentrations, concentrations of hydrazine and ammonia, reaction time, percent yield, and turnover numbers have been reported in Table 6.3. Again, the concentration of NH_3 was determined by the comparison against a 14 mM PMe_3 capillary insert. Hemilabile pincer complexes have interesting reactivity differences in comparison to the parent PCP complexes.[60,61] The recently synthesized (NCOP)IrHCl complex was reacted with hydrazine under basic conditions and, within 72 hours, 78% NH_3 yield was observed. Starting from the (NCOP)Ir(ethylene) complex does shorten the time frame from 72 hours to 24 hours and the yield improves to 97%. Previously, it has been shown that pyridine stabilizes the NCOP catalyst.[62] In the presence of pyridine, 17% yield of ammonia was observed after one hour. However, no catalytic species have been identified due to poor resolution of NMR signals. Asymmetrical catalysts have also been synthesized in which both a methylene and an oxygen linker have been used to give a PCOP type backbone.[63] When (^{iPr4}PCOP)Ir is reacted with hydrazine, 24 hours of heating is required to give ammonia in 52% yield.[64] The (^{iPr4}PCOP)Ir catalyst seems to have reactivity similar to (^{iPr4}PCP)Ir, presumably due to the steric environment created by the isopropyl groups and not the electronic differences

between the oxygen and methylene linkers. Overall, the parent (^{tbu4}PCP)IrH$_2$ catalyst is the most active and stable under these reaction conditions.

Table 6.3 Catalytic Conversion of Ammonia Using Various Pincer Complexes

Catalyst	[Hydrazine] M	Time	Temp (˚ C)	[NH_3] M	% yield
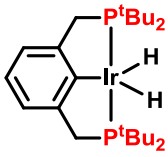 20 mM	0.10	30 min	100	0.10	99
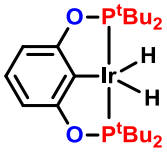 16 mM	0.10	30 min	100	0.10	95
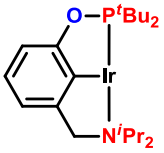 16 mM	0.09	72 hours	100	0.08	87
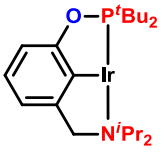 21 mM and 1eq. pyridine	0.11	6 hours	100	0.04	41
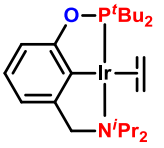 20 mM	0.10	24 hours	100	0.10	97
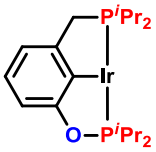	~0.1	24 hours	100	0.05	

6.2.7 Kinetic Results

The conversion of hydrazine to ammonia was studied using varying concentrations of (PCP)IrH$_2$ as the catalyst. The reaction was conducted at 85 ˚C for these studies to slow down the reaction and allow for easy monitoring over time. The production of ammonia and consumption of hydrazine was monitored by ^{1}H NMR spectroscopy. The concentration data for conversion of hydrazine at 85 °C in the presence of 20 mM and 10 mM (PCP)IrH$_2$ solutions are listed in Tables 6.4 and 6.5, respectively. The concentration of N_2 was calculated via product balance based on the observed concentrations of free NH_3 and N_2H_4 measured during the reaction.[65] The ratio of NH_3 produced versus the concentration of hydrazine consumed within

the reaction is approximately 0.99:1 for 20 mM catalyst and 0.93:1 for 10 mM catalyst. The ratios for the production of N_2 versus hydrazine and ammonia are calculated as 0.5:1 and ~ 0.54:1 for 20 mM and 10 mM catalyst, respectively. Therefore, the N-N bond cleavage of hydrazine achieved mass balance within experimental error as proposed in Equation 4.

Table 6.4 Kinetic Results for Hydrazine to Ammonia Conversion with 20 mM (PCP)IrH_2 at 85 °C

Time (min)	$[N_2H_4]$,M	$[NH_3]$, M	Yield NH_3 vs. Reacted N_2H_4	$[N_2]$, M	Yield N_2 vs. Reacted N_2H_4	N_2/NH_3
0	0.100	0.000		0.000		
30	0.083	0.014	0.851	0.010	0.574	0.675
60	0.075	0.023	0.936	0.013	0.532	0.568
90	0.068	0.033	1.025	0.016	0.488	0.476
120	0.059	0.044	1.058	0.020	0.471	0.445
150	0.046	0.053	0.980	0.028	0.510	0.521
180	0.034	0.064	0.971	0.034	0.514	0.530
210	0.026	0.075	1.011	0.037	0.495	0.489
240	0.012	0.086	0.974	0.045	0.513	0.527
270	0.007	0.092	0.991	0.047	0.504	0.509
		Average	**0.993**		**0.503**	**0.508**

Table 6.5 Kinetic Results for Hydrazine to Ammonia Conversion with 10 mM (PCP)IrH_2 at 85 °C

Time (min)	$[N_2H_4]$,M	$[NH_3]$, M	Yield NH_3 vs. Reacted N_2H_4	$[N_2]$, M	Yield N_2 vs. Reacted N_2H_4	N_2/NH_3
0	0.1000	0.0000		0.0000		
30	0.0938	0.0047	0.758	0.0039	0.621	0.819
60	0.0856	0.0125	0.868	0.0082	0.566	0.652
90	0.0797	0.0172	0.847	0.0117	0.576	0.680
150	0.0703	0.0266	0.896	0.0164	0.552	0.617
210	0.0633	0.0328	0.894	0.0203	0.553	0.619
270	0.0551	0.0438	0.976	0.0230	0.512	0.525
330	0.0469	0.0516	0.972	0.0273	0.514	0.529
390	0.0399	0.0594	0.988	0.0304	0.506	0.512
530	0.0328	0.0657	0.978	0.0344	0.511	0.523
		Average	**0.927**		**0.536**	**0.554**

At 90 minutes, using 10 mM catalyst, 17 mM NH_3 is produced; doubling the concentration of catalyst to 20 mM yields approximately double the concentration of NH_3, 33 mM at this same time point. This trend continues throughout the reaction, indicating that it most likely exhibits first order dependence of catalyst. Graphing these sets of concentration data versus time gives a linear regression. The shape of the kinetic curve conforms to a zero-order regression with respect to concentration of hydrazine as well.

Figure 6.2 Conversion of Hydrazine to Ammonia Conversion at 85 °C Catalyzed with (PCP)IrH_2 ([(PCP)IrH_2]° = 20 mM) and its Representation by a Linear Regression

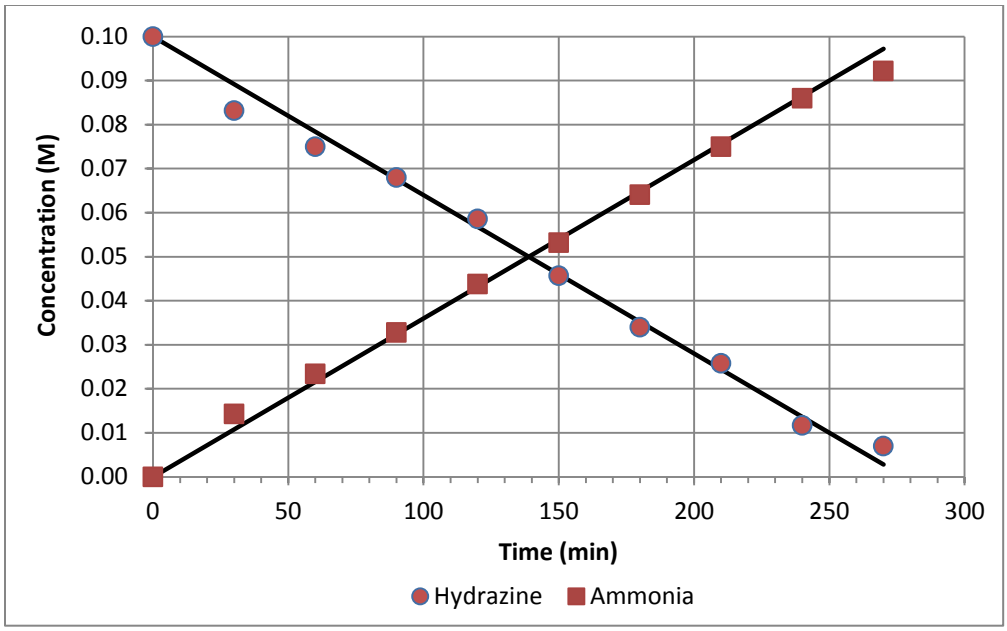

When the reaction is carried out at a lower [(PCP)IrH_2]° of 10 mM, plotting the experimental data showed that the rate of the reaction follows the proposed kinetic scheme only to conversion of ~50% and then gradually decreases (Figure 6.3). One possible explanation is gradual "self-poisoning" of the catalyst, through inhibition of ammonia and free hydrogen to form (PCP)IrH_4 and **6-3** at the end of the reaction. Earlier it was described that increasing the concentration of hydrazine to 0.4 M also slows down the reaction to 24 hours. Perhaps, the higher concentration of hydrazine allows for the production of a higher concentration of hydrogen and, since competitive binding between hydrogen and ammonia exists based on the thermodynamic reactions, it can be assumed all of these factors lead to "self-poisoning" of the catalyst and longer reaction times. Further studies are being conducted to confirm this explanation. Perhaps another explanation is that the reaction under hydrogen atmosphere is occurring via a different mechanism and therefore would not follow the kinetic scheme of this reaction. Currently, it can be concluded that the ideal reaction conditions are 20 mM catalyst and 0.1 M hydrazine.

Figure 6.3 Conversion of Hydrazine to Ammonia Conversion at 85 °C Catalyzed with $(PCP)IrH_2$ ($[(PCP)IrH_2]° = 10$ mM) and its Representation by a Linear Regression

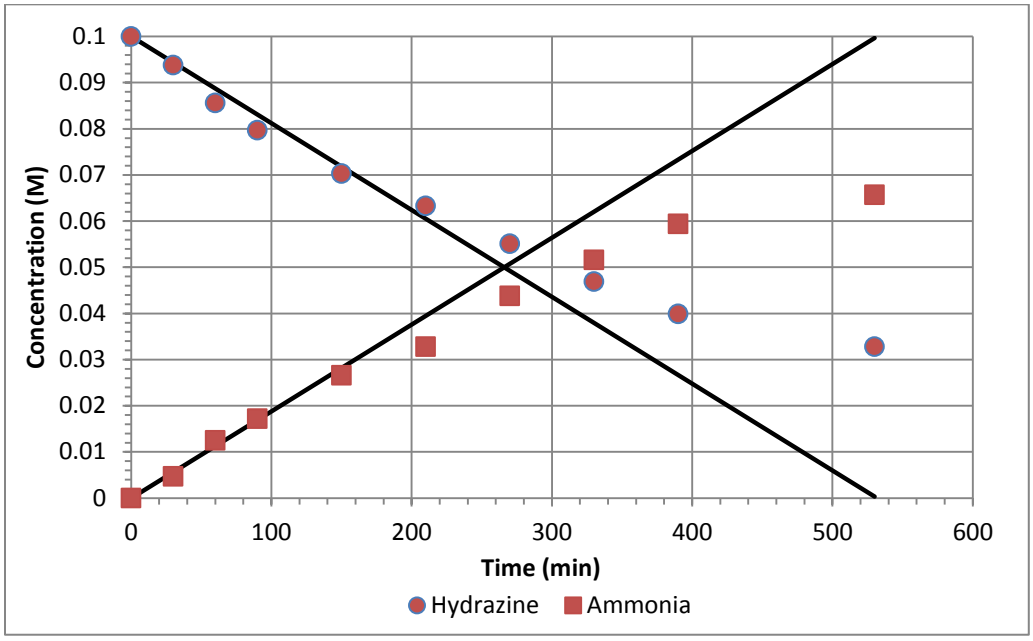

From calculated ratios, the experimental trends depicted by the regression curve, a first order rate law expression can be derived.

$$d[NH_3]/dt = - d[N_2H_4]/dt = k_1[(PCP)IrH_2)] \quad (5)$$

The only two experimentally observed iridium complexes in the reaction are **6-2a** and **6-3** (near completion). Any and all other iridium complexes are intermediates present in very small amounts and not observable by NMR spectroscopy. This experimental observation provides the basis for using the steady state approximation in kinetic analysis. Based on experimental observations, thermodynamic data, and kinetic data, a series of chemical equations can be proposed for a kinetic mechanism.

$$(PCP)IrH_2 + N_2H_4 \rightarrow (PCP)IrH_2(N_2H_4) \quad (6)$$

$$(PCP)IrH_2(N_2H_4) \xrightarrow{(k_1)} (PCP)IrH_2(NH) + NH_3 \quad (7)$$

$$(PCP)IrH_2(NH) + N_2H_4 \xrightarrow{(k_2)} (PCP)IrN_2H_4 + NH_3 \quad (8)$$

$$(PCP)IrN_2H_4 \xrightarrow{(k_3)} (PCP)Ir(H_2)(N_2) + H_2 \quad (9)$$

$$(PCP)Ir(H_2)(N_2) + N_2H_4 \xrightarrow{(k_4)} (PCP)IrH_2(N_2H_4) + N_2 \quad (10)$$

Equation 8 proceeds rapidly at room temperature as has been observed experimentally. It is practically irreversible as deemed by the thermodynamic experiments, therefore [**6-2a**]° ≈ [(PCP)IrH_2]°. After the transformation of hydrazine to ammonia is complete, the combined consumption of N_2H_4 in Equation 6 should include the loss of initial **6-2a** (10 or 20 mM) and the remaining free [N_2H_4]° = 100 - [**6-2a**]° = 100 - [(PCP)IrH_2]° mM. Decomposition of **6-2a** with expulsion of an NH_3 molecule leads to highly reactive catalytic intermediate, (PCP)IrH_2NH (Equation 7). This step is presumably the rate limiting step with the rate constant of k_1. Rapid transfer of protons again leads to loss of ammonia which can be released upon addition of N_2H_4 leading to experimentally observed complex **6-1** (Equation 8). Dehydrogenation of the hydrazine ligand, leads to (PCP)Ir(H_2)(N_2) (Equation 9). Ligand exchange in (PCP)Ir(H_2)(N_2) leads to the expulsion of N_2 and regeneration of the starting iridium complex (Equation 10). It has been demonstrated that (PCP)Ir(H_2)(N_2) is not easily isolated or observed experimentally and, computationally, the release of nitrogen from hydrogen has been determined as very accessible.

Kinetic analysis of the reaction scheme of Equations 6 through 10 is presented in the supplemental material. This kinetic analysis leads to determination of the rate determining step k_1 value for this reaction, the release of the first equivalent of ammonia (Equation 7). Four experiments were conducted at two catalyst concentrations, and the average first order rate constant was determined to be 9.4 x 10^{-3} min^{-1} (Table 3). Overall, the consumption rate of hydrazine and the formation rate of ammonia corresponding to Equation 4 (at least, at the early stages) are both zero-order reactions with respect to the hydrazine concentration and are first-order reactions with respect to the initial (PCP)IrH_2 concentration.

Table 6.6 Values of k_1, the Rate Constant for the Release of NH_3 from **2a** (Equation 7)

Experiment	[(PCP)IrH_2]°	k_1, min^{-1}
1	0.01	$9.8 \cdot 10^{-3}$
2	0.01	$9.4 \cdot 10^{-3}$
3	0.02	$9.4 \cdot 10^{-3}$
4	0.02	$9.0 \cdot 10^{-3}$

6.2.8 Discussion of Proposed Mechanism

A mechanism is proposed in accordance with the experimental results discussed above (Figure 6.4). The proposed mechanism starts with the formation of **6-2a** upon addition of hydrazine to (PCP)IrH_2. The first half of the mechanism is the hydrogenation of hydrazine to release two equivalents of NH_3 while

the second half of the mechanism is the dehydrogenation to form N_2 and H_2. The two halves of the reaction mechanism will be discussed in more detail below supported by DFT calculations (Figures 6.5 and 6.6 respectively).

Figure 6.4 Proposed Mechanism for the Catalytic Synthesis of Ammonia, Nitrogen and Hydrogen

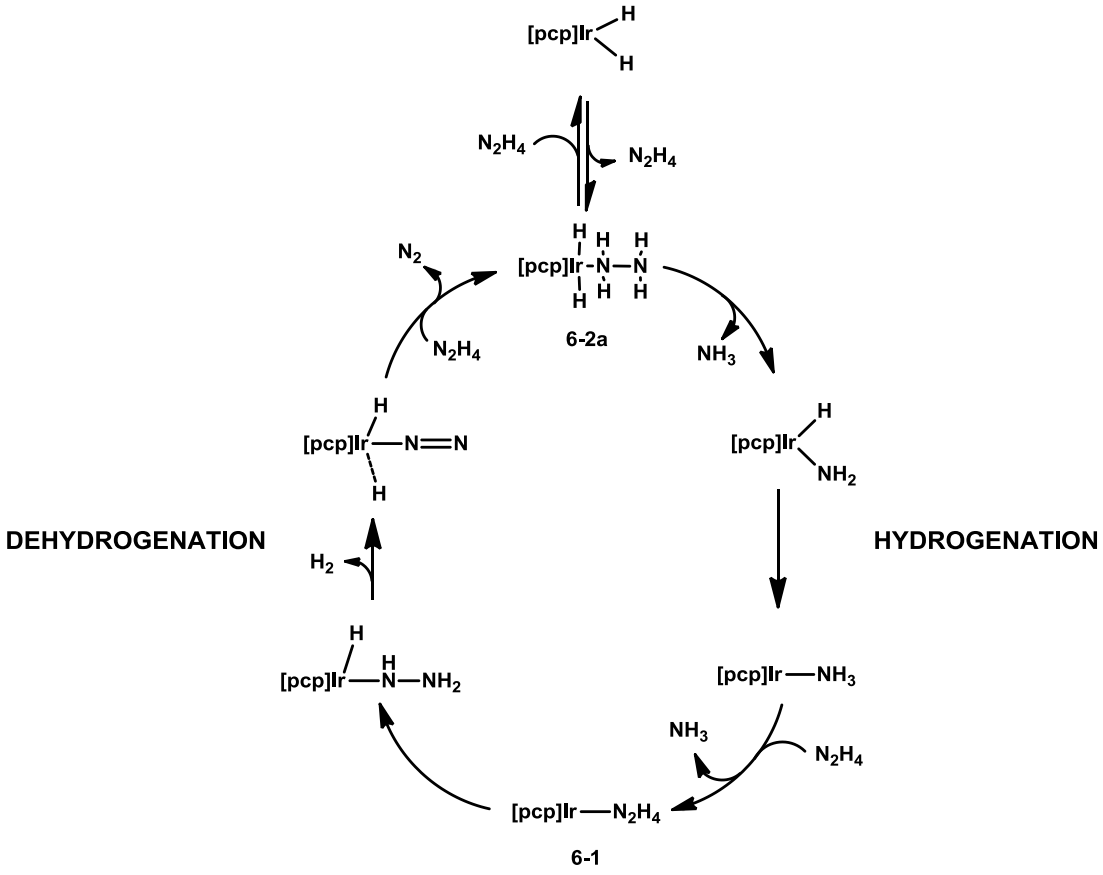

Figure 6.5 Proposed Pathway for the Hydrogenation of Hydrazine to Form Ammonia, Nitrogen and Hydrogen

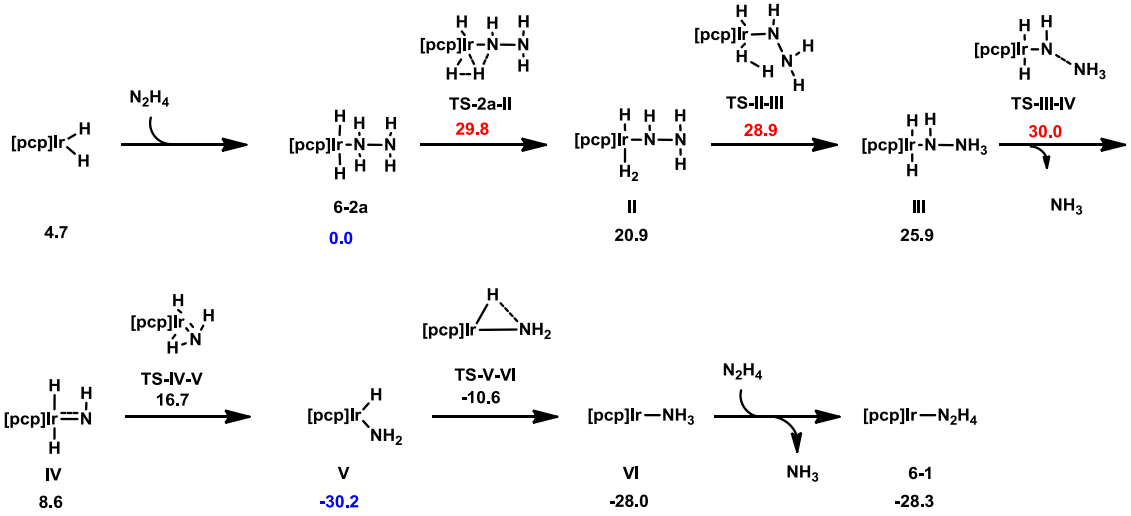

The hydrogenation pathway starts after addition of hydrazine to (PCP)IrH_2 to yield **6-2a**, calculated to be downhill by 4.7 kcal/mol. The following three steps detail possible rate determining steps. First, transfer of hydrogen from the α-N of hydrazine to an iridium hydride gives complex **II**. Subsequent transfer of hydrogen to the β-N gives **III**. The dihydrogen ligand has multiple degrees of freedom and can easily rotate, thereby either of the hydrogens can be involved in the transfer. Finally, release of the first equivalent of ammonia yields **IV**. The two hydrogen transfers and the N-N bond cleavage each have an energy barrier of approximately 30 kcal/mol. If release of ammonia is rate determining, then less sterically hindered (^{iPr4}PCP)Ir catalyst would be less likely to release NH_3 due to a high energy barrier or high stability of the four coordinate complex. The less sterically hindered catalyst presumably binds much more strongly to ammonia and therefore the reaction is much slower. As was observed experimentally, the (^{iPr4}PCP)Ir catalyst is much less active. Transfer of a hydrogen from the iridium center in **IV** yields **V**, which has been characterized at -30 ˚C.[23] Hydrogen transfer via **TS-V-VI** yields **VI**, which has also been characterized at room temperature (refer to Scheme 6.1). An energy difference of 2 kcal/mol and an energy of -11 kcal/mol for **TS-V-VI** are in accordance with previous experiments which have shown that **V** easily transitions to **VI**, as it is the thermodynamically preferred product. Neither **V** nor **VI** was observed during the transformation of hydrazine to ammonia. The release of ammonia from **VI** gives the second equivalent of ammonia allowing for addition of a second hydrazine molecule to the 14e$^-$ fragment to generate **6-1**.

This concludes the first half or hydrogenation portion of the catalytic cycle and leads to the dehydrogenation of hydrazine (Figure 6.6).

Figure 6.6 Proposed Pathway for the Dehydrogenation of Hydrazine to Form Nitrogen and Hydrogen

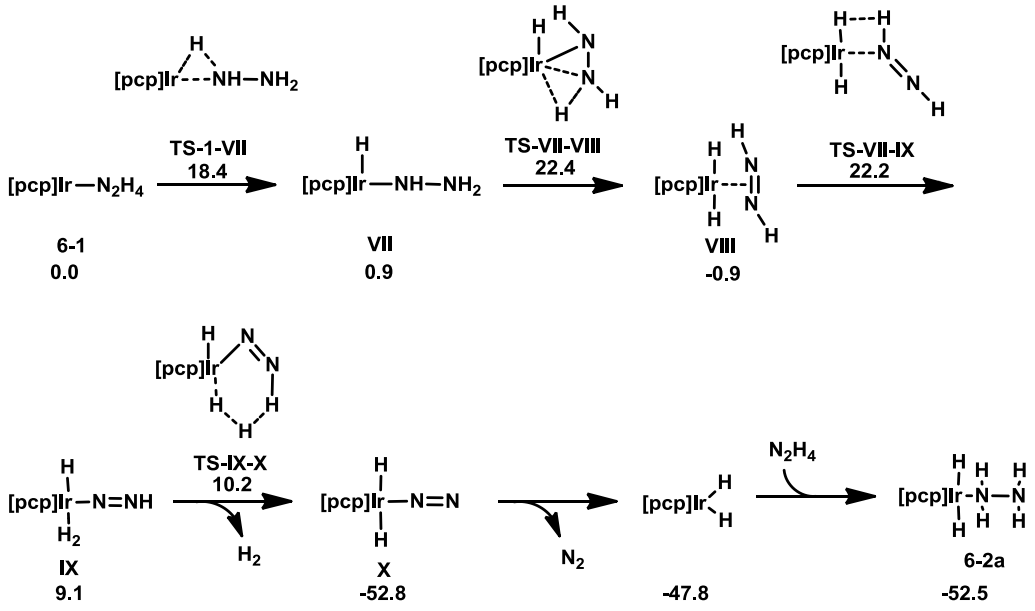

N-H activation and subsequent transfer of two hydrogens to the iridium center leads to a side-on diazene intermediate (**VIII**). Diazene intermediates have been cited in many references as a critical intermediate during the synthesis of ammonia from nitrogen and hydrogen.[34,66,67] Subsequent hydrogen transfers to the metal center from the diazene intermediate and loss of hydrogen gives the dihydride dinitrogen complex (**X**). Nitrogen release from **X** to give the dihydride complex and addition of a second molecule of hydrazine leads back to the start of the catalytic cycle. The reaction barrier for the dehydrogenation reaction is 22.4 kcal/mol and the reaction is exothermic as ΔG = -52.8 kcal/mol.

Overall, the process has been calculated to be extremely thermodynamically downhill, with ΔG = - 80.7 kcal/mol. The thermodynamic driving force for this reaction comes from entropic considerations ($2N_2H_4$ going to $2NH_3$, N_2, and H_2) and the formation of products that are more stable. The reverse reaction ($2NH_3$, N_2, and H_2 going to $2N_2H_4$) would require upwards of 111 kcal/mol. The overall reaction barrier is 30 kcal/mol. Only one other case of hydrogenative N-N bond cleavage has been reported for a pincer complex.[42] In this case, the hydrogen source is H_2, while, in the proposed mechanism discussed above for (PCP)IrH_2 (Figure 6.4), the source is hydrazine itself. This proposed mechanism also differs

from the proposed mechanism by Hartwig for the formation of ammonia via substituted hydrazine as there is no potential for C-H activation. As such, N-H activation of hydrazine can lead to N-N bond cleavage and evolution of NH_3.

6.2.9 Reaction with Hydrazine Sulfate, Azobenzene and Azo-tert-butane

Hydrazine sulfate is another source of hydrazine and is often easier to handle as it is a powder at room temperature. (PCP)IrH_2 was reacted with hydrazine sulfate and sodium *tert*-butoxide in *p*-xylene-d_{10} and no reaction was observed at room temperature as expected, yet upon heating at 100 ˚C for 20 hours, **6-3** is observed as the major product and free ammonia is observed by ^{1}H NMR spectroscopy.

Scheme 6.10 Reaction with Hydrazine Sulfate

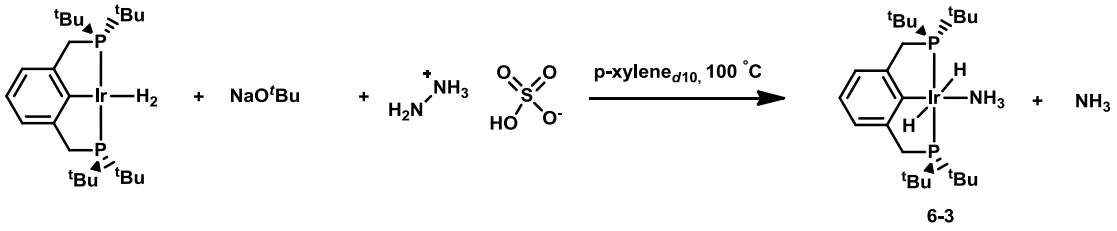

In attempts to isolate a diazene intermediate proposed in Figure 6.6, azobenzene was reacted with either the 14e$^-$ (PCP)Ir or (PCP)IrH_2 at room temperature, which generates two C-H activation product isomers in a 2:1 ratio (**6-5: 6-6**, Scheme 6.11). The isomer in which the C-H activated phenyl ring is trans to the hydride and the azo is trans to PCP aryl ring (**6-5**) is the major isomer. The ^{31}P NMR spectrum shows two signals at 55.7 ppm for the major isomer and 52.3 ppm for the minor isomer. The ^{1}H NMR spectrum shows two triplets in the hydride region at -9.4 ppm and -18.5 ppm, each integrating to one proton with respect to the integrated 36 ^{t}butyl protons. These isomers are similar to the final product for the addition of methylphenylhydrazine (MePhNNH_2) to the (PCP)Ir fragment isolated by Hartwig (Scheme 6.2), as well as other examples in the literature.[62,68] However, in these reported examples, C-H activation occurs first, followed by nitrogen coordination.

Scheme 6.11 Reaction with Azobenzene

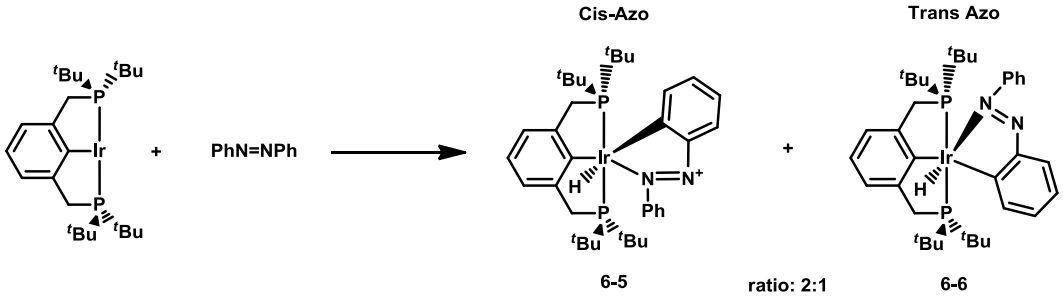

When present, C-H bonds will be activated by (PCP)Ir preferentially over the coordination of dinitrogen.[69] In the presence of N_2H_2 without any C-H aryl bonds, a diazene complex, either side-on or end-on, or the N-H activation of diazene would be preferential. In an attempt to eliminate any potential C-H activation of R substituents, (PCP)IrH_2 was reacted with azo-*tert*-butane, however no reaction was observed presumably due to the large steric hindrance of the bulky ^{t}butyl groups. Complexes **6-5** and **6-6** give some evidence that diazene can be activated and supported by a (PCP)Ir complex, but dissociation to nitrogen and hydrogen would be energetically downhill and so isolation of a non-substituted diazene complex would be unlikely.

6.3 Closing

Various (PCP)Ir pincer hydrazine complexes have been characterized. The main complex ((PCP)$IrH_2N_2H_4$) can undergo both dehydrogenation to form nitrogen and hydrogen as well as an N-N bond cleavage to form ammonia, nitrogen and hydrogen. The dehydrogenation reaction occurred under vacuum with a calculated ΔG of -42 kcal/mol. While the release of NH_3 is favored thermodynamically (ΔG = -80 kcal/mol), is only observed under catalytic conditions. Kinetically, the reaction indeed conforms to a zero-order reaction with respect to the concentration of hydrazine and first-order with respect to the initial (PCP)IrH_2 concentration, with a single kinetic parameter, k_1, characterizing concentrations of hydrazine and ammonia. DFT calculations support a mechanism in which the hydrogen transfer from hydrazine to iridium, and vice versa, is an important feature in both the hydrogenation and dehydrogenation pathways.

6.4 Experimental

General Methods

All reactions were performed under an argon atmosphere unless specified using standard Schlenck techniques or in an argon-filled glove box. C_6H_6, C_6D_6, and *p*-xylene-d_{10} were either dried over Na/K alloy and collected via vacuum transfer or stirred over activated alumina for 48 hours, filtered, and then stored over molecular sieves. Norbornene (NBE) was sublimed before use. Hydrazine was purchased from Aldrich as 1M solution in THF. NH_3 was purchased from Aldrich as 0.1 M solution in THF. All other substrates were degassed before entry to glovebox and used without further purification. ($^{t\text{Bu4}}$PCP)Ir(H)(Ph),[50] ($^{t\text{Bu4}}$PCP)IrH$_2$,[70] ($^{t\text{Bu4}}$PCP)IrHCl,[71] ($^{i\text{Pr4}}$PCP)IrH$_2$,[57] (POCOP)IrH$_2$,[40] and ($^{i\text{Pr4}}$PCOP)IrH$_2$[63] were synthesized according to literature. ^{1}H and ^{31}P NMR spectra were obtained from either a 400 or 500 MHz Varian instrument. The residual peak of the deuterated solvent was used as a reference for all ^{1}H NMR spectra and an internal capillary standard of PMe_3 in *p*-xylene-d_{10} (-62.4 ppm) was used to reference ^{31}P NMR chemical shifts.

(PCP)IrN$_2$H$_4$, 6-1

To a 0.5 mL *p*-xylene-d_{10} solution of 8.9 mg catalyst (15 μmol) in a J. Young NMR tube, 3 μL of 5M NBE in *p*-xylene-d_{10} stock solution (16 μmol) and 2.1 μL C_6H_6 (23.5 μmol) were added to generate (PCP)Ir(H)(Ph) *in situ*. To this mixture, 46 μL of 1M hydrazine in THF (46 μmol) was added to the solution. The solution changed to orange in color and formed the title complex *in situ*. **^{31}P NMR (*p*-xylene-d_{10}, 161.9 MHz):** δ 68.9 (s, (*PCP*)IrN$_2$H$_4$). **^{1}H NMR (*p*-xylene-d_{10}, 400 MHz):** δ 7.06 (d, J_{HH} = 7.2 Hz, 2H, Ar-*H*), 6.87 (t, J_{HH} = 7.2 Hz, 1H, Ar-*H*), 4.8 (bs, 2H, β-NH_2), 3.24 (t, 2H, α-NH_2), 2.95 (t, 4H, CH_2P), 1.34 (t, J_{PH} = 6.4 Hz, 36H, P^{t}Bu$_2$).

(PCP)IrH$_2$N$_2$H$_4$, 6-2a

To a solution of 5 mg (PCP)IrH$_2$ (8.5 μmol) in *p*-xylene, 46 μL of a 1M hydrazine in THF solution (46 μmol) was added in a J. Young NMR tube. The solution immediately changed color from dark red to pale yellow. The solvent was removed slowly under reduced pressure to give a pale yellow solid. The solid was redissolved in *p*-xylene-d_{10} and NMR spectroscopy showed quantitative conversion to the product. Crystals suitable for X-ray crystallography were grown from a pentane/*p*-xylene solution

containing excess hydrazine in THF. X-ray crystallography refinement and structure parameters are included in Tables 6.7 through 6.11. **^{31}P NMR (*p*-xylene-d_{10}, 161.9 MHz):** δ 66.2 (s, (*PCP*)Ir$H_2N_2H_4$). **^{1}H NMR (*p*-xylene-d_{10}, 400 MHz):** δ 6.83 (d, J_{HH} = 7.0 Hz, 2H, Ar-*H*), 6.75 (t, J_{HH} = 7.5 Hz, 1H, Ar-*H*), 3.81 (s, 2H, β-NH_2), 3.16 (t, J_{HH} = 3.2 Hz, 4H, CH_2P), 2.95 (t, J_{HH} = 3.6 Hz, 2H, α-NH_2), 1.32 (t, J_{PH} = 4.8 Hz, 36H, P^{t}Bu$_2$), -8.74 (t, J_{PH} = 11.6 Hz, 2H, Ir-H_2).

(PCP)IrHCl($H_2N_2H_2$), 6-2b

To a solution of 5.8 mg (PCP)IrHCl in C_6D_6, 46 μL of 1M hydrazine in THF solution (46 μmol) was added. The solution changed from orange to golden yellow. The product precipitates from solution as yellow solid within ten minutes. **^{31}P NMR (*p*-xylene-d_{10}, 161.9 MHz):** δ 50.3 (s, (*PCP*)IrHCl($H_2N_2H_2$)). **^{1}H NMR (*p*-xylene-d_{10}, 400 MHz):** δ 6.85 (t, 1H, Ar-*H*), 6.83 (d, 2H, Ar-*H*), 4.24 (bs, 2H, β-N*H*), 4.06 (bs, 2H, α-NH_2), 3.25 (d of vt, 2H, CH_2P), 3.13 (d of vt, 2H, CH_2P), 1.56 (t, J_{PH} = 6.2 Hz, 18H, P^{t}Bu$_2$), 1.50 (t, J_{PH} = 6.2 Hz, 18H, P^{t}Bu$_2$), -21.19 (bs, 1H, Ir-*H*).

(PCP)IrH_2PhHN_2H_2, 6-2c

To a solution of 5 mg (PCP)IrH_2 (8.5 μmol) in *p*-xylene, 1 μL Ph$HNNH_2$ (8.5 μmol) was added in a J. Young NMR tube. The solution immediately changed color from dark red to pale yellow. The solvent is removed slowly under reduced pressure to give a pale yellow solid. The solid was redissolved in *p*-xylene-d_{10} and NMR spectroscopy showed quantitative conversion to the product. **^{31}P NMR (*p*-xylene-d_{10}, 161.9 MHz):** δ 66.6 (s, (*PCP*)IrH_2PhHN_2H_2). **^{1}H NMR (*p*-xylene-d_{10}, 400 MHz):** δ 6.81 (d, 2H, Ar-*H*), 6.94 (t, J_{HH} = 9.6 Hz, 2H, *phenyl*NHNH_2), 6.81 (d, 2H, Ar-*H*), 6.78 (t, J_{HH} = 7.6 Hz, 1H, *phenyl*NHNH_2), 6.74 (t, 1H, Ar-*H*), 6.22 (d, J_{HH} = 7.6 Hz, 2H, *phenyl*NHNH_2), 5.20 (bs, 1H, β-N*H*), 3.42 (bs, 2H, α-NH_2), 3.17 (t, J_{HH} = 3.6 Hz, 4H, CH_2P), 1.35 (t, J_{PH} = 6 Hz, 36H, P^{t}Bu$_2$), -8.50 (t, J_{PH} = 14.8 Hz, 2H, Ir-H_2).

(PCP)IrHCl($PhHN_2H_2$), 6-2d

To a solution of 5.8 mg (PCP)IrHCl in C_6D_6, 0.9 μL Ph$HNNH_2$ was added. The solution changed from orange to golden yellow. The product precipitated from solution as yellow solid after the solution was allowed to sit for at least 30 minutes. **^{31}P NMR (*p*-xylene-d_{10}, 161.9 MHz):** δ 47.8 (s, (*PCP*)IrHCl($PhHN_2H_2$)). **^{1}H NMR (*p*-xylene-d_{10}, 400 MHz):** δ 7.14 (bs, 2H, *phenyl*NHNH_2), 6.68 (bt, 1H,

*phenyl*NHNH$_2$), 6.24 (bs, 2H, *phenyl*NHNH$_2$) 5.44 (bs, 1H, β-N*H*), 4.18 (bs, 2H, α-NH_2), 2.94 (bs, 4H, CH_2P^{t}Bu$_2$), 1.25 (t, J_{PH} = 6 Hz, 36H, P^{t}Bu$_2$), -22.06 (bs, 1H, Ir-*H*).

(PCP)IrH$_2$(NH$_3$), 6-3

To a solution of 5 mg (PCP)IrH$_2$ (8.5 μmol) in *p*-xylene-d_{10}, 90 μL of a 0.5 M NH$_3$ in THF solution (46 μmol) was added in a J. Young NMR tube. The solution immediately changed color from dark red to pale orange upon mixing. NMR spectroscopy showed quantitative conversion to the product. **^{31}P NMR (*p*-xylene-d_{10}, 161.9 MHz):** δ 67.2 (s, (*PCP*)IrH$_2$(NH$_3$)). **^{1}H NMR (*p*-xylene-d_{10}, 400 MHz):** δ 6.79 (d, J_{HH} = 7.5 Hz, 2H, Ar-*H*), 6.67 (t, J_{HH} = 7.3 Hz, 1H, Ar-*H*), 3.10 (t, J_{HH} = 3.5 Hz, 4H, CH_2P^{t}Bu$_2$), 2.2 (s, 3H, NH_3), 1.35 (t, J_{PH} = 5.8 Hz, 36H, P^{t}Bu$_2$), -8.75 (t, J_{PH} = 14.8 Hz, 2H, Ir-H_2).

(^{iPr4}PCP)IrH$_2$N$_2$H$_4$, 6-4

To a solution of 5 mg (^{iPr4}PCP)IrH$_2$ (8.5 μmol) in *p*-xylene, 46 μL of a 1M hydrazine in THF solution (46 μmol) was added in a J. Young NMR tube. The solution immediately changed color from dark red to pale yellow. The solvent is removed slowly under reduced pressure to give a pale yellow solid. The solid was redissolved in *p*-xylene-d_{10} and NMR spectroscopy showed quantitative conversion to the product. **^{31}P NMR (*p*-xylene-d_{10}, 161.9 MHz):** δ 53.8 (s, (^{iPr4}*PCP*)IrH$_2$N$_2$H$_4$). **^{1}H NMR (*p*-xylene-d_{10}, 400 MHz):** δ 6.86 (d, J_{HH} = 7.0 Hz, 2H, Ar-*H*), 6.80 (t, J_{HH} = 6.5 Hz, 1H, Ar-*H*), 3.70 (bs, 2H, β-NH$_2$), 3.03 (t, J_{HH} = 4.0 Hz, 4H, CH_2P), 2.99 (t, J_{HH} = 4.0 Hz, 2H, α-NH_2), 1.91 (m, 4H, PC*H*(CH$_3$)$_2$), 1.23 (qt, J_{PH} = 7.5 Hz, 12H, PCH(CH_3)$_2$), 1.11 (qt, J_{PH} = 6.0 Hz, 12H, PCH(CH_3)$_2$), -9.25 (t, J_{PH} = 16.0 Hz, 2H, Ir-H_2).

(PCP)Ir(H)(Azobenzene) cis and trans isomers, 6-5 and 6-6

Method 1: To a 0.5 mL *p*-xylene-d_{10} solution of 5.2 mg (PCP)IrH$_2$ (15 μmol) in a J. Young NMR tube, excess NBE was added, followed by addition of 4.1 mg azobenzene (23 μmol). *Method 2:* To a 0.5 mL *p*-xylene-d_{10} solution of 5.0 mg (PCP)IrH$_2$ (15 μmol) in a J. Young NMR tube 2.0 mg azobenzene (11 μmol) was added. In both methods, the solution changed from red to dark brown. Complexes **6-5** (Cis-Azo) and **6-6** (Trans-Azo) were obtained in a 2:1 ratio and characterized *in situ*. **^{31}P NMR (*p*-xylene-d_{10}, 161.9 MHz):** δ 55.8 (s, Cis-Azo), 52.3 (s, Trans-Azo). **^{1}H NMR (*p*-xylene-d_{10}, 400 MHz):** δ 8.74 (t, J_{HH} = 8 Hz, 2H, PCP aryl cis-azo), 8.63 (d, J_{HH} = 8 Hz, 1H, PCP aryl cis-azo), 7.69 (d, 1H, Ar-*H*), 7.3-7.1 (Ar-*H*), 7.92 (t, J_{HH} = 8 Hz, 2H, PCP aryl trans-azo), 3.38 (dt, J_{HH} = 4 Hz, J_{PH} = 16 Hz, 2H, trans-azo), 3.24 (dt,

J_{HH} = 4 Hz, J_{PH} = 16 Hz, 2H, cis-azo), 3.13 (dt, J_{HH} = 4 Hz, J_{PH} = 16 Hz, 2H, trans-azo), 3.05 (dt, J_{HH} = 4 Hz, J_{PH} = 16 Hz, , 2H cis-azo), 1.26 (t, J_{PH} = 6 Hz, 18H, P^{t}Bu, trans-azo), 1.18 (t, J_{PH} = 8 Hz, 18H, P^{t}Bu, cis-azo), 0.57 (t, J_{PH} = 6 Hz, 18H, P^{t}Bu, trans-azo), 0.52 (t, J_{PH} = 4 Hz, 18H, P^{t}Bu, cis-azo), -9.35 (t, J_{PH} = 20.0 Hz, 1H, Ir-H, cis-azo), -18.45 (t, J_{PH} = 20.0 Hz, 1H, Ir-H, trans-azo).

Low Temperature NMR spectroscopy

To a 0.4 mL mesitylene-d_{12} solution of 5.2 mg catalyst (~8.5 μmol) in a J. Young NMR tube, 1.5 mg NBE and C_6H_6 were added to generate (PCP)Ir(H)(Ph) in situ. The sample was cooled in a -45 ˚C glovebox freezer for ten minutes. The sample was removed from the freezer 46 μL hydrazine (46 μmol) was added immediately. Upon removal from an argon glove box, the sample was immediately frozen in a liquid nitrogen bath. The NMR instrument was pre-chilled and the sample was inserted into a -30 ˚C NMR instrument. Both ^{31}P and ^{1}H NMR spectra were obtained at -30,-20, -10, 0, 10 and 25 ˚C.

Catalytic Conversion of N_2H_4 to NH_3

To a 0.5 mL *p*-xylene-d_{10} solution of 5 mg catalyst (~8.5 μmol) in a J. Young NMR tube, 46 μL 1M hydrazine in THF (46 μmol) was added. The solution changed from dark red to yellow instantaneously. The solution was heated in a 100 ˚C oil bath. During heating, the solution changed from pale yellow to dark green and upon completion changed to red. Upon cooling and mixing, the red solution changed to a bright yellow. Reaction progress was monitored at different time intervals by NMR spectroscopy. Concentration of ammonia was determined via integration correlated to the known concentration of an internal PMe_3 capillary standard.

Catalytic Conversion of N_2H_4 to NH_3 under a hydrogen atmosphere

The catalyst was dissolved in 450 μL *p*-xylene-d_{10} and 50 μL 1 M hydrazine in THF solution (50 μmol) was then added. The solution was transferred to J. Young NMR tube and 1 atm hydrogen was added after the solution was degassed. The solution was heated in a 100 ˚C oven while the solution was mixed used a rotary motor. Reaction was monitored periodically by NMR spectroscopy. The concentration of ammonia was determined by integration of the proton NMR signal, calibrated by the known concentration of the PMe_3 capillary standard.

Exchange Equilibrium between N_2H_4 and PEt_3

To a 0.5 mL *p*-xylene-d_{10} solution of 5.6 mg (PCP)IrH_2 (9.5 μmol) in an NMR tube, 46 μL hydrazine (46 μmol) and 1.3 μL PEt_3 (8.8 μmol) were added. The NMR tube was sealed under an argon atmosphere and the solution was monitored by ^{31}P and ^{1}H NMR spectroscopy. The concentration of each species was determined by integration of each ^{31}P NMR shift or integration of each hydride shift in correlation to the known concentration of added species and to the known concentration of an internal standard. Characterization of (PCP)IrH_2PEt_3 has been previously published.[72]

Kinetics experiments

0.01 M or 0.02 M catalyst was dissolved in 450 μL *p*-xylene-d_{10} and 50 μL hydrazine in THF was added to the solution. The solution was transferred to J. Young NMR tube and heated in a 100 ˚C oven while mixed by a rotary motor. Reaction was monitored at different time intervals by NMR spectroscopy. The concentration of ammonia was determined by integration of the proton NMR signal, calibrated by the known concentration of the PMe_3 capillary standard.

Computational Details

DFT calculations were completed by Tian Zhou. All calculations used DFT methodologies as implemented by the Gaussian 09[73] computer program. All the data presented here results from calculations using the TPSS[74] set of functionals but M06[75] and PBE[76] functionals were also examined, giving similar results. The Hay-Wadt relativistic effective (small) core potential[77] and the LANL2TZ basis set[78] augmented by a diffuse d-type function (exponent = 0.07645)[79] was utilized for Ir atom, and all other atoms (P, N, C, and H) were treated with the 6-311G (d,p) basis sets.[80] All the geometries and potential energies were calculated for all the stationary points along the reaction paths by standard optimization procedures. Normal mode analysis was performed to further verify the nature of a particular stationary point (intermediate or transition state). The resulting set of vibrational frequencies was employed (without scaling) to determine zero-point energy corrections. Enthalpies (ΔH, $\Delta H^{\ddagger}$) and Gibbs free energies (ΔG, $\Delta G^{\ddagger}$; T = 298.15 K, P = 1 atm) were subsequently obtained from the potential energies (ΔE, $\Delta E^{\ddagger}$) using standard thermodynamic corrections.[81] In order to enhance computational stability and accuracy[82] in geometry optimization and normal calculations, an increased atomic grid sizes setting (grid = ultrafine option) was utilized.[83]

Table 6.7 Crystal Data and Structure Refinement for (PCP)$IrH_2(N_2H_4)$, **6-2a**

Identification code	5kf58a	
Empirical formula	C24 H49 Ir N2 P2	
Formula weight	619.79	
Temperature	100(2) K	
Wavelength	0.71073 Å	
Crystal system	Monoclinic	
Space group	P2(1)/c	
Unit cell dimensions	a = 12.3325(7) Å	α= 90°.
	b = 16.8277(9) Å	β= 106.853(1)°.
	c = 13.4798(7) Å	γ = 90°.
Volume	2677.3(3) $Å^3$	
Z	4	
Density (calculated)	1.538 Mg/m^3	
Absorption coefficient	5.119 mm^{-1}	
F(000)	1256	
Crystal size	0.21 x 0.03 x 0.01 mm^3	
Theta range for data collection	1.73 to 30.56°.	
Index ranges	-17<=h<=17, -23<=k<=24, -19<=l<=19	
Reflections collected	31294	
Independent reflections	8171 [R(int) = 0.0672]	
Completeness to theta = 30.56°	99.5 %	
Absorption correction	Semi-empirical from equivalents	
Max. and min. transmission	0.9506 and 0.4128	
Refinement method	Full-matrix least-squares on F^2	
Data / restraints / parameters	8171 / 11 / 305	
Goodness-of-fit on F^2	1.011	
Final R indices [I>2sigma(I)]	R1 = 0.0430, wR2 = 0.0807	
R indices (all data)	R1 = 0.0644, wR2 = 0.0872	
Largest diff. peak and hole	2.589 and -1.996 $e.Å^{-3}$	

Table 6.8 Atomic Coordinates (x 10^4) and Equivalent Isotropic Displacement Parameters ($Å^2$x 10^3) for (PCP)$IrH_2(N_2H_4)$, **6-2a.** U(eq) is defined as one third of the trace of the orthogonalized U^{ij} tensor.

	x	y	z	U(eq)
Ir(1)	3356(1)	3157(1)	2891(1)	9(1)
P(1)	5287(1)	3166(1)	3140(1)	11(1)
P(2)	1428(1)	3347(1)	2293(1)	11(1)
N(1)	3372(3)	2535(2)	4335(3)	14(1)
N(2A)	2920(4)	2961(3)	5068(4)	20(1)
N(2B)	3840(30)	2994(16)	5320(20)	20(1)
C(1)	3318(4)	3662(3)	1503(3)	14(1)
C(2)	4307(4)	3798(2)	1208(3)	12(1)
C(3)	4282(4)	4219(3)	309(3)	16(1)
C(4)	3262(4)	4478(3)	-355(3)	18(1)
C(5)	2268(4)	4278(3)	-150(3)	18(1)
C(6)	2285(4)	3862(3)	756(3)	15(1)
C(7)	5385(4)	3404(3)	1842(3)	15(1)
C(8)	1202(4)	3546(3)	911(3)	15(1)
C(9)	6145(4)	2211(3)	3465(4)	16(1)
C(10)	6491(4)	2053(3)	4636(4)	22(1)
C(11)	7214(4)	2197(3)	3096(4)	22(1)
C(12)	5393(4)	1519(3)	2914(4)	21(1)
C(13)	6109(4)	4004(3)	3963(3)	17(1)
C(14)	5915(4)	4002(3)	5032(4)	25(1)
C(15)	7384(4)	3997(3)	4090(4)	24(1)
C(16)	5615(4)	4777(3)	3404(4)	22(1)
C(17)	445(4)	2478(3)	2265(4)	16(1)
C(18)	268(4)	2371(3)	3341(4)	24(1)
C(19)	-723(4)	2534(3)	1442(4)	23(1)
C(20)	1023(4)	1722(3)	2005(4)	26(1)
C(21)	837(4)	4280(3)	2733(4)	20(1)
C(22)	1148(4)	4333(3)	3911(4)	26(1)
C(23)	-464(4)	4362(3)	2287(4)	26(1)
C(24)	1388(4)	4991(3)	2346(4)	26(1)

Table 6.9 Bond Lengths [Å] and Angles [°] for (PCP)IrH_2(N_2H_4), **6-2a**

Ir(1)-C(1)	2.043(4)	C(8)-H(8A)	0.9900
Ir(1)-N(1)	2.205(4)	C(8)-H(8B)	0.9900
Ir(1)-P(2)	2.3013(11)	C(9)-C(10)	1.535(7)
Ir(1)-P(1)	2.3072(11)	C(9)-C(12)	1.538(7)
Ir(1)-H(1)	1.596(10)	C(9)-C(11)	1.539(6)
Ir(1)-H(2)	1.595(10)	C(10)-H(10A)	0.9800
P(1)-C(7)	1.833(4)	C(10)-H(10B)	0.9800
P(1)-C(13)	1.897(4)	C(10)-H(10C)	0.9800
P(1)-C(9)	1.904(5)	C(11)-H(11A)	0.9800
P(2)-C(8)	1.833(4)	C(11)-H(11B)	0.9800
P(2)-C(17)	1.893(5)	C(11)-H(11C)	0.9800
P(2)-C(21)	1.897(5)	C(12)-H(12A)	0.9800
N(1)-N(2A)	1.456(6)	C(12)-H(12B)	0.9800
N(1)-N(2B)	1.50(3)	C(12)-H(12C)	0.9800
N(1)-H(1N1)	0.899(10)	C(13)-C(14)	1.528(6)
N(1)-H(1A)	0.897(10)	C(13)-C(15)	1.531(6)
N(1)-H(1B)	0.900(10)	C(13)-C(16)	1.538(7)
N(2A)-H(2A1)	0.901(10)	C(14)-H(14A)	0.9800
N(2A)-H(2A2)	0.907(10)	C(14)-H(14B)	0.9800
N(2B)-H(2B1)	0.907(10)	C(14)-H(14C)	0.9800
N(2B)-H(2B2)	0.900(10)	C(15)-H(15A)	0.9800
C(1)-C(2)	1.408(6)	C(15)-H(15B)	0.9800
C(1)-C(6)	1.416(6)	C(15)-H(15C)	0.9800
C(2)-C(3)	1.396(6)	C(16)-H(16A)	0.9800
C(2)-C(7)	1.510(6)	C(16)-H(16B)	0.9800
C(3)-C(4)	1.387(6)	C(16)-H(16C)	0.9800
C(3)-H(3)	0.9500	C(17)-C(18)	1.538(7)
C(4)-C(5)	1.375(6)	C(17)-C(19)	1.545(6)
C(4)-H(4)	0.9500	C(17)-C(20)	1.547(7)
C(5)-C(6)	1.402(6)	C(18)-H(18A)	0.9800
C(5)-H(5)	0.9500	C(18)-H(18B)	0.9800
C(6)-C(8)	1.508(6)	C(18)-H(18C)	0.9800
C(7)-H(7A)	0.9900	C(19)-H(19A)	0.9800
C(7)-H(7B)	0.9900	C(19)-H(19B)	0.9800

C(19)-H(19C)	0.9800	C(22)-H(22B)	0.9800
C(20)-H(20A)	0.9800	C(22)-H(22C)	0.9800
C(20)-H(20B)	0.9800	C(23)-H(23A)	0.9800
C(20)-H(20C)	0.9800	C(23)-H(23B)	0.9800
C(21)-C(22)	1.524(7)	C(23)-H(23C)	0.9800
C(21)-C(24)	1.541(7)	C(24)-H(24A)	0.9800
C(21)-C(23)	1.548(7)	C(24)-H(24B)	0.9800
C(22)-H(22A)	0.9800	C(24)-H(24C)	0.9800

C(1)-Ir(1)-N(1)	176.19(16)	N(2A)-N(1)-Ir(1)	117.3(3)
C(1)-Ir(1)-P(2)	82.78(13)	N(2B)-N(1)-Ir(1)	116.2(11)
N(1)-Ir(1)-P(2)	96.83(10)	N(2A)-N(1)-H(1N1)	107(4)
C(1)-Ir(1)-P(1)	83.06(13)	N(2B)-N(1)-H(1N1)	134(4)
N(1)-Ir(1)-P(1)	97.48(10)	Ir(1)-N(1)-H(1N1)	109(4)
P(2)-Ir(1)-P(1)	165.57(4)	N(2A)-N(1)-H(1A)	102(6)
C(1)-Ir(1)-H(1)	91.8(18)	Ir(1)-N(1)-H(1A)	103(6)
N(1)-Ir(1)-H(1)	92.0(18)	H(1N1)-N(1)-H(1A)	119(6)
P(2)-Ir(1)-H(1)	85.9(17)	N(2A)-N(1)-H(1B)	120(10)
P(1)-Ir(1)-H(1)	91.8(17)	N(2B)-N(1)-H(1B)	86(10)
C(1)-Ir(1)-H(2)	88.6(18)	Ir(1)-N(1)-H(1B)	113(10)
N(1)-Ir(1)-H(2)	87.6(18)	H(1N1)-N(1)-H(1B)	85(10)
P(2)-Ir(1)-H(2)	91.8(18)	N(1)-N(2A)-H(2A1)	96(3)
P(1)-Ir(1)-H(2)	90.6(18)	N(1)-N(2A)-H(2A2)	110(4)
H(1)-Ir(1)-H(2)	178(2)	H(2A1)-N(2A)-H(2A2)	109.0(16)
C(7)-P(1)-C(13)	102.9(2)	N(1)-N(2B)-H(2B1)	93(4)
C(7)-P(1)-C(9)	102.6(2)	N(1)-N(2B)-H(2B2)	121(10)
C(13)-P(1)-C(9)	109.1(2)	H(2B1)-N(2B)-H(2B2)	109.9(17)
C(7)-P(1)-Ir(1)	102.34(15)	C(2)-C(1)-C(6)	115.7(4)
C(13)-P(1)-Ir(1)	116.39(15)	C(2)-C(1)-Ir(1)	122.3(3)
C(9)-P(1)-Ir(1)	120.60(15)	C(6)-C(1)-Ir(1)	121.8(3)
C(8)-P(2)-C(17)	102.3(2)	C(3)-C(2)-C(1)	121.7(4)
C(8)-P(2)-C(21)	102.0(2)	C(3)-C(2)-C(7)	120.6(4)
C(17)-P(2)-C(21)	110.2(2)	C(1)-C(2)-C(7)	117.5(4)
C(8)-P(2)-Ir(1)	102.62(15)	C(4)-C(3)-C(2)	120.5(4)
C(17)-P(2)-Ir(1)	119.35(15)	C(4)-C(3)-H(3)	119.7
C(21)-P(2)-Ir(1)	117.20(15)	C(2)-C(3)-H(3)	119.7

C(5)-C(4)-C(3)	119.2(4)	C(9)-C(11)-H(11C)	109.5
C(5)-C(4)-H(4)	120.4	H(11A)-C(11)-H(11C)	109.5
C(3)-C(4)-H(4)	120.4	H(11B)-C(11)-H(11C)	109.5
C(4)-C(5)-C(6)	120.6(4)	C(9)-C(12)-H(12A)	109.5
C(4)-C(5)-H(5)	119.7	C(9)-C(12)-H(12B)	109.5
C(6)-C(5)-H(5)	119.7	H(12A)-C(12)-H(12B)	109.5
C(5)-C(6)-C(1)	121.4(4)	C(9)-C(12)-H(12C)	109.5
C(5)-C(6)-C(8)	120.4(4)	H(12A)-C(12)-H(12C)	109.5
C(1)-C(6)-C(8)	117.9(4)	H(12B)-C(12)-H(12C)	109.5
C(2)-C(7)-P(1)	110.2(3)	C(14)-C(13)-C(15)	109.4(4)
C(2)-C(7)-H(7A)	109.6	C(14)-C(13)-C(16)	108.4(4)
P(1)-C(7)-H(7A)	109.6	C(15)-C(13)-C(16)	108.0(4)
C(2)-C(7)-H(7B)	109.6	C(14)-C(13)-P(1)	110.2(3)
P(1)-C(7)-H(7B)	109.6	C(15)-C(13)-P(1)	114.6(3)
H(7A)-C(7)-H(7B)	108.1	C(16)-C(13)-P(1)	105.9(3)
C(6)-C(8)-P(2)	109.0(3)	C(13)-C(14)-H(14A)	109.5
C(6)-C(8)-H(8A)	109.9	C(13)-C(14)-H(14B)	109.5
P(2)-C(8)-H(8A)	109.9	H(14A)-C(14)-H(14B)	109.5
C(6)-C(8)-H(8B)	109.9	C(13)-C(14)-H(14C)	109.5
P(2)-C(8)-H(8B)	109.9	H(14A)-C(14)-H(14C)	109.5
H(8A)-C(8)-H(8B)	108.3	H(14B)-C(14)-H(14C)	109.5
C(10)-C(9)-C(12)	108.4(4)	C(13)-C(15)-H(15A)	109.5
C(10)-C(9)-C(11)	108.7(4)	C(13)-C(15)-H(15B)	109.5
C(12)-C(9)-C(11)	106.6(4)	H(15A)-C(15)-H(15B)	109.5
C(10)-C(9)-P(1)	110.6(3)	C(13)-C(15)-H(15C)	109.5
C(12)-C(9)-P(1)	108.1(3)	H(15A)-C(15)-H(15C)	109.5
C(11)-C(9)-P(1)	114.2(3)	H(15B)-C(15)-H(15C)	109.5
C(9)-C(10)-H(10A)	109.5	C(13)-C(16)-H(16A)	109.5
C(9)-C(10)-H(10B)	109.5	C(13)-C(16)-H(16B)	109.5
H(10A)-C(10)-H(10B)	109.5	H(16A)-C(16)-H(16B)	109.5
C(9)-C(10)-H(10C)	109.5	C(13)-C(16)-H(16C)	109.5
H(10A)-C(10)-H(10C)	109.5	H(16A)-C(16)-H(16C)	109.5
H(10B)-C(10)-H(10C)	109.5	H(16B)-C(16)-H(16C)	109.5
C(9)-C(11)-H(11A)	109.5	C(18)-C(17)-C(19)	109.1(4)
C(9)-C(11)-H(11B)	109.5	C(18)-C(17)-C(20)	108.5(4)
H(11A)-C(11)-H(11B)	109.5	C(19)-C(17)-C(20)	106.5(4)

C(18)-C(17)-P(2)	109.6(3)	C(24)-C(21)-P(2)	106.9(3)
C(19)-C(17)-P(2)	115.2(3)	C(23)-C(21)-P(2)	113.7(3)
C(20)-C(17)-P(2)	107.8(3)	C(21)-C(22)-H(22A)	109.5
C(17)-C(18)-H(18A)	109.5	C(21)-C(22)-H(22B)	109.5
C(17)-C(18)-H(18B)	109.5	H(22A)-C(22)-H(22B)	109.5
H(18A)-C(18)-H(18B)	109.5	C(21)-C(22)-H(22C)	109.5
C(17)-C(18)-H(18C)	109.5	H(22A)-C(22)-H(22C)	109.5
H(18A)-C(18)-H(18C)	109.5	H(22B)-C(22)-H(22C)	109.5
H(18B)-C(18)-H(18C)	109.5	C(21)-C(23)-H(23A)	109.5
C(17)-C(19)-H(19A)	109.5	C(21)-C(23)-H(23B)	109.5
C(17)-C(19)-H(19B)	109.5	H(23A)-C(23)-H(23B)	109.5
H(19A)-C(19)-H(19B)	109.5	C(21)-C(23)-H(23C)	109.5
C(17)-C(19)-H(19C)	109.5	H(23A)-C(23)-H(23C)	109.5
H(19A)-C(19)-H(19C)	109.5	H(23B)-C(23)-H(23C)	109.5
H(19B)-C(19)-H(19C)	109.5	C(21)-C(24)-H(24A)	109.5
C(17)-C(20)-H(20A)	109.5	C(21)-C(24)-H(24B)	109.5
C(17)-C(20)-H(20B)	109.5	H(24A)-C(24)-H(24B)	109.5
H(20A)-C(20)-H(20B)	109.5	C(21)-C(24)-H(24C)	109.5
C(17)-C(20)-H(20C)	109.5	H(24A)-C(24)-H(24C)	109.5
H(20A)-C(20)-H(20C)	109.5	H(24B)-C(24)-H(24C)	109.5
H(20B)-C(20)-H(20C)	109.5		
C(22)-C(21)-C(24)	107.7(4)		
C(22)-C(21)-C(23)	108.6(4)		
C(24)-C(21)-C(23)	107.9(4)		
C(22)-C(21)-P(2)	111.8(3)		

Table 6.10 Hydrogen Coordinates (x 10^4) and Isotropic Displacement Parameters ($Å^2$x 10 ^{3}) for (PCP)$IrH_2(N_2H_4)$, **6-2a**

	x	y	z	U(eq)
H(1)	3400(40)	4006(14)	3430(30)	20(13)
H(2)	3260(40)	2306(14)	2350(40)	23(14)
H(1N1)	2970(50)	2080(20)	4170(50)	60(20)
H(1A)	4110(20)	2510(40)	4680(70)	50
H(2A1)	3380(20)	2740(20)	5640(20)	24
H(2A2)	3080(50)	3487(10)	5060(40)	24
H(1B)	4000(200)	2210(190)	4600(400)	50
H(2B1)	3380(20)	2740(20)	5640(20)	24
H(2B2)	3700(200)	3522(19)	5300(200)	24
H(3)	4970	4329	152	20
H(4)	3250	4790	-946	21
H(5)	1563	4424	-625	22
H(7A)	6035	3764	1899	18
H(7B)	5515	2911	1493	18
H(8A)	976	3051	508	18
H(8B)	587	3941	664	18
H(10A)	5824	2096	4888	32
H(10B)	7058	2446	4992	32
H(10C)	6812	1518	4776	32
H(11A)	7612	1691	3293	34
H(11B)	7715	2636	3419	34
H(11C)	6998	2255	2340	34
H(12A)	5822	1021	3065	32
H(12B)	5157	1613	2164	32
H(12C)	4722	1482	3162	32
H(14A)	6225	3513	5399	37
H(14B)	5100	4030	4952	37
H(14C)	6294	4462	5430	37
H(15A)	7723	4493	4420	36
H(15B)	7510	3949	3408	36
H(15C)	7734	3545	4524	36

H(16A)	4791	4779	3274	33
H(16B)	5795	4812	2743	33
H(16C)	5945	5234	3838	33
H(18A)	-82	1853	3375	35
H(18B)	-228	2794	3458	35
H(18C)	1001	2399	3874	35
H(19A)	-1140	2037	1433	34
H(19B)	-616	2624	758	34
H(19C)	-1153	2977	1613	34
H(20A)	1705	1607	2575	39
H(20B)	1232	1808	1366	39
H(20C)	498	1272	1912	39
H(22A)	748	4782	4108	40
H(22B)	1967	4412	4194	40
H(22C)	929	3840	4189	40
H(23A)	-837	3960	2601	39
H(23B)	-682	4286	1534	39
H(23C)	-697	4893	2443	39
H(24A)	1160	5486	2613	40
H(24B)	1140	5002	1586	40
H(24C)	2214	4939	2591	40

Table 6.11 Torsion Angles [°] for (PCP)$IrH_2(N_2H_4)$, **6-2a**

C(1)-Ir(1)-P(1)-C(7)	-11.9(2)	C(1)-C(2)-C(3)-C(4)	-3.8(7)
N(1)-Ir(1)-P(1)-C(7)	164.31(19)	C(7)-C(2)-C(3)-C(4)	170.3(4)
P(2)-Ir(1)-P(1)-C(7)	-22.9(2)	C(2)-C(3)-C(4)-C(5)	-3.6(7)
C(1)-Ir(1)-P(1)-C(13)	99.4(2)	C(3)-C(4)-C(5)-C(6)	4.1(7)
N(1)-Ir(1)-P(1)-C(13)	-84.4(2)	C(4)-C(5)-C(6)-C(1)	2.6(7)
P(2)-Ir(1)-P(1)-C(13)	88.4(2)	C(4)-C(5)-C(6)-C(8)	-171.6(4)
C(1)-Ir(1)-P(1)-C(9)	-124.7(2)	C(2)-C(1)-C(6)-C(5)	-9.3(6)
N(1)-Ir(1)-P(1)-C(9)	51.5(2)	Ir(1)-C(1)-C(6)-C(5)	173.7(3)
P(2)-Ir(1)-P(1)-C(9)	-135.8(2)	C(2)-C(1)-C(6)-C(8)	165.0(4)
C(1)-Ir(1)-P(2)-C(8)	14.9(2)	Ir(1)-C(1)-C(6)-C(8)	-12.0(6)
N(1)-Ir(1)-P(2)-C(8)	-161.31(19)	C(3)-C(2)-C(7)-P(1)	163.0(3)
P(1)-Ir(1)-P(2)-C(8)	25.9(2)	C(1)-C(2)-C(7)-P(1)	-22.7(5)
C(1)-Ir(1)-P(2)-C(17)	126.9(2)	C(13)-P(1)-C(7)-C(2)	-100.1(3)
N(1)-Ir(1)-P(2)-C(17)	-49.2(2)	C(9)-P(1)-C(7)-C(2)	146.6(3)
P(1)-Ir(1)-P(2)-C(17)	138.0(2)	Ir(1)-P(1)-C(7)-C(2)	21.0(3)
C(1)-Ir(1)-P(2)-C(21)	-95.9(2)	C(5)-C(6)-C(8)-P(2)	-160.9(4)
N(1)-Ir(1)-P(2)-C(21)	87.9(2)	C(1)-C(6)-C(8)-P(2)	24.7(5)
P(1)-Ir(1)-P(2)-C(21)	-84.8(2)	C(17)-P(2)-C(8)-C(6)	-148.5(3)
C(1)-Ir(1)-N(1)-N(2A)	-144(2)	C(21)-P(2)-C(8)-C(6)	97.5(3)
P(2)-Ir(1)-N(1)-N(2A)	-59.7(3)	Ir(1)-P(2)-C(8)-C(6)	-24.3(3)
P(1)-Ir(1)-N(1)-N(2A)	118.5(3)	C(7)-P(1)-C(9)-C(10)	161.8(3)
C(1)-Ir(1)-N(1)-N(2B)	168(3)	C(13)-P(1)-C(9)-C(10)	53.2(4)
P(2)-Ir(1)-N(1)-N(2B)	-108.1(12)	Ir(1)-P(1)-C(9)-C(10)	-85.5(3)
P(1)-Ir(1)-N(1)-N(2B)	70.1(12)	C(7)-P(1)-C(9)-C(12)	-79.7(3)
N(1)-Ir(1)-C(1)-C(2)	-97(2)	C(13)-P(1)-C(9)-C(12)	171.7(3)
P(2)-Ir(1)-C(1)-C(2)	179.0(4)	Ir(1)-P(1)-C(9)-C(12)	33.0(4)
P(1)-Ir(1)-C(1)-C(2)	1.7(3)	C(7)-P(1)-C(9)-C(11)	38.8(4)
N(1)-Ir(1)-C(1)-C(6)	80(2)	C(13)-P(1)-C(9)-C(11)	-69.9(4)
P(2)-Ir(1)-C(1)-C(6)	-4.2(3)	Ir(1)-P(1)-C(9)-C(11)	151.5(3)
P(1)-Ir(1)-C(1)-C(6)	178.5(4)	C(7)-P(1)-C(13)-C(14)	168.3(3)
C(6)-C(1)-C(2)-C(3)	9.9(6)	C(9)-P(1)-C(13)-C(14)	-83.3(4)
Ir(1)-C(1)-C(2)-C(3)	-173.1(3)	Ir(1)-P(1)-C(13)-C(14)	57.3(4)
C(6)-C(1)-C(2)-C(7)	-164.3(4)	C(7)-P(1)-C(13)-C(15)	-67.8(4)
Ir(1)-C(1)-C(2)-C(7)	12.7(5)	C(9)-P(1)-C(13)-C(15)	40.6(4)

Ir(1)-P(1)-C(13)-C(15)	-178.8(3)	C(21)-P(2)-C(17)-C(20)	-174.6(3)
C(7)-P(1)-C(13)-C(16)	51.2(3)	Ir(1)-P(2)-C(17)-C(20)	-34.7(4)
C(9)-P(1)-C(13)-C(16)	159.6(3)	C(8)-P(2)-C(21)-C(22)	-168.2(4)
Ir(1)-P(1)-C(13)-C(16)	-59.8(3)	C(17)-P(2)-C(21)-C(22)	83.8(4)
C(8)-P(2)-C(17)-C(18)	-164.5(3)	Ir(1)-P(2)-C(21)-C(22)	-57.1(4)
C(21)-P(2)-C(17)-C(18)	-56.6(4)	C(8)-P(2)-C(21)-C(24)	-50.5(4)
Ir(1)-P(2)-C(17)-C(18)	83.3(3)	C(17)-P(2)-C(21)-C(24)	-158.6(3)
C(8)-P(2)-C(17)-C(19)	-41.1(4)	Ir(1)-P(2)-C(21)-C(24)	60.6(4)
C(21)-P(2)-C(17)-C(19)	66.7(4)	C(8)-P(2)-C(21)-C(23)	68.4(4)
Ir(1)-P(2)-C(17)-C(19)	-153.4(3)	C(17)-P(2)-C(21)-C(23)	-39.6(4)
C(8)-P(2)-C(17)-C(20)	77.6(4)	Ir(1)-P(2)-C(21)-C(23)	179.5(3)

Derivation of kinetic equations

Gross reaction:

$$2\ N_2H_4 \ \rightarrow \ 2\ NH_3 + N_2 + H_2 \quad (1)$$

Initial Reaction:

$$(PCP)Ir(H_2) + N_2H_4 \ \rightarrow \ (PCP)Ir(H_2)–N_2H_4 \quad (2)$$

Reaction Set:

$$PCPIr(H_2)–N_2H_4 \ \xrightarrow{(k_1)} \ (PCP)Ir(H_2)=NH + NH_3 \quad (3)$$

$$(PCP)Ir(H_2)=NH + N_2H_4 \ \xrightarrow{(k_2)} \ (PCP)Ir–N_2H_4 + NH_3 \quad (4)$$

$$(PCP)Ir–N_2H_4 \ \xrightarrow{(k_3)} \ (PCP)Ir(H_2)–N=N + H_2 \quad (5)$$

$$(PCP)Ir(H_2)–N=N + N_2H_4 \ \xrightarrow{(k_4)} \ (PCP)Ir(H_2)–N_2H_4 + N_2 \quad (6)$$

[Ir] balance:

$$[(PCP)Ir(H_2)N_2H_4] + [(PCP)Ir(H_2)NH_3] \ = \ [(PCP)Ir(H_2)]°.$$

Because $[(PCP)Ir(H_2)–NH_3] << [(PCP)Ir(H_2)–N_2H_4]$ during most of the reaction:

$$[(PCP)Ir(H_2)N_2H_4] \ \approx [(PCP)Ir(H_2)]° \text{ and } [N_2H_4]_{start} = [N_2H_4]° - [(PCP)Ir(H_2)]° \quad (7)$$

<u>The steady-state approach to kinetics of the multi-stage reaction (Reactions 3-6)</u>

Equations 1 and 4

$$d[(PCP)Ir(H_2)N_2H_4]/dt = -k_1\cdot[\ (PCP)Ir(H_2)N_2H_4] + k_4\cdot[(PCP)Ir(H_2)N_2][N_2H_4] \approx 0 \quad (8)$$

Since $[(PCP)Ir(H_2)N_2H_4] \ \approx \ [(PCP)Ir(H_2)]°$, then:

$$[(PCP)Ir(H_2)N_2] \ \approx \ k_1\cdot[(PCP)Ir(H_2)]°/(k_4\cdot[N_2H_4]) \quad (9)$$

Equations 3 and 4

$$d[(PCP)Ir(H_2)N_2]/dt \ = \ k_3\cdot[(PCP)IrN_2H_4] - k_4\cdot[(PCP)Ir(H_2)N_2]\cdot[N_2H_4] \ \approx \ 0 \quad (10)$$

$$[(PCP)IrN_2H_4] \ \approx \ k_4\cdot[(PCP)Ir(H_2)N_2]\ [N_2H_4]/k_3 \ =$$

Substitution of Equation 9

$$[(PCP)IrN_2H_4] \approx k_4\cdot k_1\cdot[(PCP)IrH_2]°/(k_4\cdot[N_2H_4])\ [N_2H_4]/k_3 \approx k_1\cdot[(PCP)IrH_2]°/k_3 \quad (11)$$

Equations 2 and 3

$$d[(PCP)IrN_2H_4]/dt \ = \ k_2\cdot[(PCP)Ir(H_2)NH]\ [N_2H_4] \ - \ k_3\cdot[(PCP)IrN_2H_4] \ \approx \ 0 \quad (12)$$

$$[(PCP)Ir(H_2)NH] \ \approx \ k_3\cdot[(PCP)IrN_2H_4]/(k_2\ [N_2H_4]) \quad (13)$$

Substituting of Equation 11

$$[(PCP)Ir(H_2)NH] \approx k_3 \cdot [k_1 \cdot [(PCP)IrH_2]^\circ / k_3] / (k_2 \cdot [N_2H_4]) \approx k_1 \cdot [(PCP)IrH_2]^\circ / (k_2 \cdot [N_2H_4]) \quad (14)$$

Consumption of hydrazine (Equations 4 and 6):

$$-d[N_2H_4]/dt = k_2 \cdot [(PCP)IrH_2NH] \cdot [N_2H_4] + k_4 \cdot [(PCP)Ir(H_2)N_2] \cdot [N_2H_4] =$$

$$k_2 \cdot k_1 \cdot [(PCP)IrH_2]^\circ / (k_2 \cdot [N_2H_4]) \cdot [N_2H_4] + k_4 \, k_1 \cdot [(PCP)Ir(H_2)]^\circ / (k_4 \cdot [N_2H_4]) \cdot [N_2H_4] =$$

$$2 \cdot k_1 \cdot [(PCP)Ir(H_2)]^\circ \quad (15)$$

$[N_2H_4]$

$$-\int d[N_2H_4] = 2 \cdot k_1 \cdot [(PCP)Ir(H_2)]^\circ \cdot t \quad (16)$$

$[N_2H_4]_{start}$

$$[N_2H_4] = [N_2H_4]_{start} - 2 \cdot k_1 \cdot [(PCP)IrH_2]^\circ \cdot t = [N_2H_4]^\circ - [(PCP)IrH_2]^\circ - 2 \cdot k_1 \cdot [(PCP)IrH_2]^\circ \cdot t \quad (17)$$

Hydrazine in a complex with $(PCP)Ir(H_2)$, $[(PCP)Ir(H_2)N_2H_4] \approx [(PCP)Ir(H_2)_2]^\circ$.

The total amount of hydrazine, both free and bound

$$[N_2H_4] + [(PCP)Ir(H_2)]^\circ \approx [N_2H_4]^\circ - 2 \cdot k_1 \cdot [(PCP)Ir(H_2)]^\circ \cdot t \quad (18)$$

Formation of ammonia (Equations 3 and 4):

$$d[NH_3]/dt = k_1 \cdot [(PCP)Ir(H_2)\text{–}N_2H_4] + k_2 \cdot [(PCP)Ir(H_2)\text{=}NH] \cdot [N_2H_4] =$$

$$k_1 \cdot [(PCP)Ir(H_2)]^\circ + k_1 \cdot [(PCP)Ir(H_2)]^\circ = 2 \cdot k_1 \cdot [(PCP)Ir(H_2)]^\circ \quad (19)$$

$[NH_3]$

$$\int d[NH_3] = [NH_3] = 2 \cdot k_1 \cdot [(PCP)Ir(H_2)]^\circ \cdot t \quad (20)$$

References

(1) Fryzuk, M. D.; Johnson, S. A. *Coord. Chem. Rev.* **2000**, *200-202*, 379.
(2) Shilov, A. E. *Russian Chemical Bulletin, Int. Ed.* **2003**, *52*, 2555.
(3) Allen, A. D.; Senoff, C. V. *Chem. Commun.* **1965**, 621.
(4) Senoff, C. V. *J. Chem. Educ.* **1990**, *67*, 368.
(5) Mackay, B. A.; Fryzuk, M. D. *Chem. Rev.* **2004**, *104*, 385.
(6) Pool, J. A.; Lobkovsky, E.; Chirik, P. J. *Nature (London, United Kingdom)* **2004**, *42*, 527.
(7) Hidai, M.; Mizobe, Y. *Chem. Rev.* **1995**, *95*, 1115.
(8) Ghosh, R.; Kanzelberger, M.; Emge, T. J.; Hall, G. S.; Goldman, A. S. *Organometallics* **2006**, *25*, 5668.
(9) Lee, D. W.; Kaska, W. C.; Jensen, C. M. *Organometallics* **1998**, *17*, 1.
(10) Van der Boom, M. E.; Liou, S.-Y.; Ben-David, Y.; Gozin, M.; Milstein, D. *J. Am. Chem. Soc.* **1998**, *120*, 13415.
(11) Liu, H. *Ammonia Synthesis Catalysts: Innovation and Practice*; World Scientific Publishing Co. Pte. Ltd. and Chemical Industry Press: Singapore, 2013.
(12) Schrock, R. R. *Accounts Chem. Res.* **2005**, *38*, 955.
(13) Barney, B. M.; Lee, H.-I.; Dos Santos, P. C.; Hoffman, B. M.; Dean, D. R.; Seefeldt, L. C. *Dalton Trans* **2006**, 2277.
(14) Chatt, J.; Dilworth, J. R.; Richards, R. L. *Chem. Rev.* **1978**, *78*, 589.
(15) Yandulov, D. V.; Schrock, R. R. *Science* **2003**, *301*, 76.
(16) Stephan, G. C.; Sivasankar, C.; Studt, F.; Tuczek, F. *Chem.-Eur. J.* **2008**, *14*, 644.
(17) Yandulov, D. V.; Schrock, R. R. *Inorg. Chem.* **2005**, *44*, 1103.
(18) Ertl, G. *Z. Anorg. Allg. Chem.* **2012**, 487.
(19) Umegaki, T.; Yan, J.-M.; Zhang, X.-B.; Shioyama, H.; Kuriyama, N. *International Journal of Hydrogen Energy* **2009**, *34*, 2303.
(20) Lu, Z.-H.; Xu, Q. *Functional Materials Letters* **2012**, *5*, 9 pages.
(21) *CRC Handbook of Chemistry and Physics*; 92nd ed.; Haynes W. M., Ed.; CRC Press: Boca Raton, FL, 2011-2012.
(22) Shilov, A. E. *Metal Complexes in Biomimetic Chemical Reactions: N_2 Fixation in Solution, Activation and Oxidation of Alkanes, Chemical Models of Photosynthesis*, 1997.
(23) Kanzelberger, M.; Zhang, X.; Emge, T. J.; Goldman, A. S.; Zhao, J.; Incarvito, C.; Hartwig, J. F. *J. Am. Chem. Soc.* **2003**, *125*, 13644.
(24) Morgan, E.; MacLean, D. F.; McDonald, R.; Turculet, L. *J. Am. Chem. Soc.* **2009**, *131*, 14234.
(25) Cartwright Sykes, A.; White, P.; Brookhart, M. *Organometallics* **2006**, *25*, 1664.
(26) Sykes, A. C., PhD Thesis, University of North Carolina at Chapel Hill, 2006.
(27) Gutsulyak, D. V.; Piers, W. F.; Borau-Garcia, J.; Parvez, M. *J. Am. Chem. Soc.* **2013**, *135*, 11776.
(28) Chang, Y.-H.; Nakajima, Y.; Tanaka, H.; Yoshizawa, K.; Ozawa, F. *Organometallics* **2013**, *33*, 715.
(29) Feller, M.; Diskin-Posner, Y.; Shimon, L. J. W.; Ben-Ari, E.; Milstein, D. *Organometallics* **2012**, *31*, 4083.
(30) Khaskin, E.; Iron, M. A.; Shimon, L. J. W.; Zhang, J.; Milstein, D. *J. Am. Chem. Soc.* **2010**, *132*, 8542.
(31) Gu, X.-Q.; Chen, W.; Morales-Morales, D.; Jensen, C. M. *J. Mol. Cat. A* **2002**, *189*, 119.
(32) Arashiba, K.; Miyake, Y.; Nishibayashi, Y. *Nature Chem.* **2011**, *3*, 120.
(33) Umehara, K.; Kuwata, S.; Ikariya, T. *J. Am. Chem. Soc.* **2013**, *135*, 6754.
(34) Rozenel, S. S.; Arnold, J. *Inorg. Chem.* **2012**, *91*, 9730.
(35) Pun, D.; Bradley, C. A.; Lobkovsky, E.; Keresztes, I.; Chirik, P. J. *J. Am. Chem. Soc.* **2008**, *130*, 14046.
(36) Bernskoetter, W. H.; Olmos, A. V.; Lobkovsky, E.; Chirik, P. J. *Organometallics* **2006**, *25*, 1021.
(37) Hanna, T. E.; Keresztes, I.; Lobkovsky, E.; Chirik, P. J. *Inorg. Chem.* **2007**, *46*, 1675.
(38) Chirik, P. J. *Dalton Trans. FIELD Full Journal Title:Dalton Transactions* **2007**, 16.

(39) Bernskoetter, W. H.; Pool, J. A.; Lobkovsky, E.; Chirik, P. J. *J. Am. Chem. Soc.* **2005**, *127*, 7901.
(40) Bernskoetter, W. H.; Lobkovsky, E.; Chirik, P. J. *J. Am. Chem. Soc.* **2005**, *127*, 14051.
(41) Pool, J. A.; Bernskoetter, W. H.; Chirik, P. J. *J. Am. Chem. Soc.* **2004**, *126*, 14326.
(42) Bart, S. C.; Bowman, A. C.; Lobkovsky, E.; Chirik, P. J. *J. Am. Chem. Soc.* **2007**, *129*, 7212.
(43) Fryzuk, M. D.; Love, J. B.; Rettig, S. J.; Young, V. G. *Science* **1997**, *275*, 1445.
(44) Nishibayashi, Y.; Iwai, S.; Hidai, M. *Science* **1998**, *279*, 540.
(45) Askevold, B.; Nieto, J. T.; Tussupbayev, S.; Diefenbach, M.; Herdtweck, E.; Holthausen, M. C.; Schneider, S. *Nature Chem.* **2011**, *3*, 532.
(46) Holscher, M.; Prechtl, M. H. G.; Leitner, W. *Chem.-Eur. J.* **2007**, *13*, 6636.
(47) Huang, Z.; Zhou, J.; Hartwig, J. F. *J. Am. Chem. Soc.* **2010**, *132*, 11458.
(48) Hydrazine is more reactive then THF at the temperatures cited and therefore no dehydrogenation of THF is observed by NMR.
(49) Gupta, M.; C. Kaska, W.; M. Jensen, C. *Chem. Commun.* **1997**, *0*, 461.
(50) Kanzelberger, M.; Singh, B.; Czerw, M.; Krogh-Jespersen, K.; Goldman, A. S. *J. Am. Chem. Soc.* **2000**, *122*, 11017.
(51) Collin, R. L.; Lipscomb, W. N. *Acta. Cryst.* **1951**, *4*, 10.
(52) Use or addition of polar solvents such as THF improves solubility only slightly.
(53) Field, L. D.; Li, H. L.; Dalgarno, S. J.; McIntosh, R. D. *Inorg. Chem.* **2013**, *52*, 1570.
(54) Birchall, T.; Jolly, W. L. *J. Am. Chem. Soc.* **1965**, *87*, 3007.
(55) Chang, Y.-H.; Chan, P.-M.; Tsai, Y.-F.; Lee, G.-H.; Hsu, H.-F. *Inorg. Chem.* **2014**, *53*, 664.
(56) Schrock, R. R.; Glassman, T. E.; Vale, M. G. *J. Am. Chem. Soc.* **1991**, *113*, 725.
(57) Liu, F.; Goldman, A. S. *Chem. Commun.* **1999**, 655.
(58) Göttker-Schnetmann, I.; White, P. S.; Brookhart, M. *Organometallics* **2004**, *23*, 1766.
(59) Vigalok, A.; Ben-David, Y.; Milstein, D. *Organometallics* **1996**, *15*, 1839.
(60) Poverenov, E.; Gandelman, M.; Shimon, L. J. W.; Rozenberg, H.; Ben-David, Y.; Milstein, D. *Organometallics* **2005**, *24*, 1082.
(61) Lindner, R.; Bosch, B. v. d.; Lutz, M.; Reek, J. N. H.; Vlugt, J. I. v. d. *Organometallics* **2011**, *30*, 499.
(62) Flores, J. A.; Haibach, M. C.; Goldman, A. S. In *245th ACS National Meeting&Exposition*; American Chemical Society: New Orleans, LA, United States, 2013, INOR-199.
(63) Ahuja, R.; Punji, B.; Findlater, M.; Supplee, C.; Schinski, W.; Brookhart, M.; Goldman, A. S. *Nature Chem.* **2011**, *3*, 167.
(64) (^{iPr4}PCOP)IrHCl was provided by A. Steffens as a previously prepared sample and therefore exact concentration of catalyst and volume of solvent is unknown.
(65) Calculated as $0.5\cdot(2\cdot[N_2H_4]° - 2\cdot[N_2H_4] - [NH_3])$
(66) Field, L. D.; Li, H. L.; Dalgarno, S. J.; McIntosh, R. D. *Inorg. Chem.* **2012**, *51*, 3733.
(67) Lukoyanov, D.; Dikanov, S. A.; Yang, Z.-Y.; Barney, B. M.; Samoilova, R. I.; Narasimhulu, K. V.; Dean, D. R.; Seefeldt, L. C.; Hoffman, B. R. *J Am Chem Soc* **2011**, *133*, 11655.
(68) Zhang, X.; Kanzelberger, M.; Emge, T. J.; Goldman, A. S. *J. Am. Chem. Soc.* **2004**, *126*, 13192.
(69) Laviska, D. A., PhD Thesis, Rutgers, The State University of New Jersey, 2013.
(70) *(a)* Gupta, M.; Hagen, C.; Flesher, R. J.; Kaska, W. C.; Jensen, C. M. *Chem. Commun.* **1996**, 2083-2084. (b) Gupta, M.; Hagen, C.; Kaska, W. C.; Cramer, R. E.; Jensen, C. M. *J. Am. Chem. Soc.* **1997**, 119, 840-841. (c) Gupta, M.; Kaska, W. C.; Jensen, C. M. *Chem. Commun.* ***1997****, 461-462.*
(71) Moulton, C. J.; Shaw, B. L. *J. Chem. Soc., Dalton Trans.* **1976**, 1020.
(72) Field, K. D.; Kundu, S.; Krogh-Jespersen, K.; Goldman, A. S.; American Chemical Society: 2012, INOR-1200.
(73) Frisch, M. J. T., G. W.; Schlegel, H. B.; Scuseria, G. E.; Robb, M. A.; Cheeseman, J. R.; Scalmani, G.; Barone, V.; Mennucci, B.; Petersson, G. A.; Nakatsuji, H.; Caricato, M.; Li, X.; Hratchian, H. P.; Izmaylov, A. F.; Bloino, J.; Zheng, G.; Sonnenberg, J. L.; Hada,

M.; Ehara, M.; Toyota, K.; Fukuda, R.; Hasegawa, J.; Ishida, M.; Nakajima, T.; Honda, Y.; Kitao, O.; Nakai, H.; Vreven, T.; Montgomery, Jr., J. A.; Peralta, J. E.; Ogliaro, F.; Bearpark, M.; Heyd, J. J.; Brothers, E.; Kudin, K. N.; Staroverov, V. N.; Kobayashi, R.; Normand, J.; Raghavachari, K.; Rendell, A.; Burant, J. C.; Iyengar, S. S.; Tomasi, J.; Cossi, M.; Rega, N.; Millam, N. J.; Klene, M.; Knox, J. E.; Cross, J. B.; Bakken, V.; Adamo, C.; Jaramillo, J.; Gomperts, R.; Stratmann, R. E.; Yazyev, O.; Austin, A. J.; Cammi, R.; Pomelli, C.; Ochterski, J. W.; Martin, R. L.; Morokuma, K.; Zakrzewski, V. G.; Voth, G. A.; Salvador, P.; Dannenberg, J. J.; Dapprich, S.; Daniels, A. D.; Farkas, Ö.; Foresman, J. B.; Ortiz, J. V.; Cioslowski, J.; Fox, D. J.; Gaussian, Inc.: Wallingford, CT, 2009.

(74) Tao, J. M.; Perdew, J. P.; Staroverov, V. N.; Scuseria, G. E. *Phys Rev. Lett.* **2003**, *91*.

(75) Zhao, C. Y.; Truhlar, D. G. *Theo. Chem. Acc.* **2008**, *120*, 215.

(76) Perdew, J. P.; Burke, K.; Ernzerhof, M. *Phys Rev. Lett.* **1996**, *77*, 3865.

(77) Hay, P. J.; Wadt, W. R. *J. Chem. Phys.* **1985**, *82*, 299.

(78) Roy, L. E.; Hay, P. J.; Martin, R. L. *J. Chem. Theory Comput.* **2008**, *4*, 1029.

(79) Value obtianed as one-half times the exponent of the outermost d-type function in the LANL2TZ basis set for iridium

(80) Krishnan, R.; Binkley, J. S.; Seeger, R.; Pople, J. A. *J. Chem. Phys.* **1980**, *72*, 650.

(81) McQuarrie, D. A. *Statistical Thermodynamics*; Harper and Row: New York, 1973.

(82) Wheeler, S. E.; Houk, K. N. *J. Chem. Theory Comput.* **2010**, *6*, 395.

(83) Frisch, Æ.; Frisch, M. J.; Clemente, F. R.; G. W. Trucks *Gaussian 09 User's Reference*, 147.